The ternary system U(VI) / humic acid / Opalinus Clay

DISSERTATION

zur Erlangung des akademischen Grades

Doctor rerum naturalium
(Dr. rer. nat.)

vorgelegt

der Fakultät Mathematik und Naturwissenschaften
der Technischen Universität Dresden

von

Diplom-Chemikerin Claudia Joseph

geboren am 09.10.1981 in Meißen

Eingereicht am 07.06.2013

Die Dissertation wurde in der Zeit von November 2006 bis April 2010 am Helmholtz-Zentrum Dresden-Rossendorf, Institut für Ressourcenökologie angefertigt.

Betreuer:
Prof. Dr. Gert Bernhard

Gutachter:
Prof. Dr. Jörg Steinbach
Prof. Dr. Christian Ekberg

Tag der Verteidigung: 23.07.2013

CONTENTS

LIST OF ABBREVIATIONS AND SYMBOLS ____ IX

SUMMARY ____ XIII

ZUSAMMENFASSUNG ____ XVII

1 INTRODUCTION AND OBJECTIVES ____ 1

2 CLAY MINERALS AND NATURAL CLAY ROCK ____ 7

2.1 Characteristics of clay 7

2.2 The clay mineral kaolinite 11

2.3 The natural clay rock Opalinus Clay 13

2.3.1 The system Opalinus Clay / Opalinus Clay pore water 20

2.3.2 Characterization of Opalinus Clay suspensions as a function of pH 22

3 URANIUM AND HUMIC SUBSTANCES ____ 27

3.1 Uranium in the environment and in nuclear waste 27

3.2 The characteristics of humic substances 30

4 SORPTION OF U(VI) AND HUMIC ACID ONTO CLAY ____ 37

4.1 Description of sorption processes 37

4.2 Sorption of actinides onto clay minerals and clay rocks 40

4.3 The system U(VI) / humic acid / kaolinite 42

4.3.1 Speciation of U(VI) at pH 7.6 in dependence on background electrolyte 42

4.3.2 Sorption of U(VI) and humic acid at pH 7.6 in dependence on background electrolyte 44

4.4 The system U(VI) / humic acid / Opalinus Clay in Opalinus Clay pore water 47

4.4.1 Aqueous U(VI) speciation modeling 47

4.4.2 U(VI) sorption as a function of S/L ratio 48

4.4.3 U(VI) and humic acid sorption as a function of time 49

4.4.4 Sorption isotherms of U(VI) and humic acid 49

4.4.5 Sorption of U(VI) in the presence of humic acid 54

4.4.6 Influence of CO_2 55

4.4.7 U(VI) speciation in the system determined by TRLFS under cryogenic conditions 56

4.4.8 U(VI) sorption onto Opalinus Clay studied with EXAFS spectroscopy 57

4.5 The system U(VI) / humic acid / Opalinus Clay in 0.1 mol/L $NaClO_4$ 60

4.5.1 Aqueous U(VI) and humic acid speciation modeling 60

4.5.2 pH-dependent U(VI) sorption in the absence of humic acid 62

4.5.3 pH-dependent U(VI) sorption in the presence of humic acid 63

4.5.4 pH-dependent humic acid sorption in the presence of U(VI) 64

4.6 Conclusions for the sorption of U(VI) and humic acid onto Opalinus Clay 65

5 DIFFUSION OF U(VI) AND HUMIC ACID IN OPALINUS CLAY 69
5.1 Principles of molecular diffusion 69
5.2 Diffusion of radionuclides through clay minerals and clay rocks 70
5.3 Experimental set-up 71
5.4 Filter diffusion parameters 73
5.5 Through-diffusion of HTO in dependence on temperature 74
5.6 Diffusion of U(VI) and humic acid in Opalinus Clay 75
5.6.1 Aqueous U(VI) and humic acid speciation in Opalinus Clay pore water 75
5.6.2 Study of the U(VI) speciation in Opalinus Clay pore water at 60 °C 78
5.6.3 Diffusion of U(VI) and humic acid in Opalinus Clay at 25 °C 81
5.6.4 Diffusion of U(VI) and humic acid in Opalinus Clay at 60 °C 84
5.7 Conclusions for the diffusion of U(VI) and humic acid in Opalinus Clay 87
6 OUTLOOK 91
7 EXPERIMENTAL DETAILS 93
7.1 Materials, methods, and solutions 93
7.1.1 Kaolinite 93
7.1.2 Opalinus Clay 93
7.1.3 Background electrolytes 93
7.1.4 Acids and bases 94
7.1.5 UO_2^{2+} stock solutions 94
7.1.6 Humic acid stock solutions 94
7.1.7 pH measurements 96
7.1.8 E_h determination 96
7.1.9 Liquid scintillation counting 96
7.2 Clay characterization 97
7.2.1 Element analysis 97
7.2.2 Cation exchange capacity 97
7.2.3 Specific surface area 98
7.2.4 Carbon fractions 98
7.2.5 Particle size distribution 98
7.2.6 Infrared spectroscopy 98
7.2.7 X-ray diffraction 98
7.2.8 Mössbauer spectroscopy 99
7.2.9 Leaching experiments in Opalinus Clay pore water at pH 7.6 99
7.2.10 Leaching experiments in 0.1 mol/L $NaClO_4$ in dependence on pH 100
7.2.11 Photon correlation spectroscopy 100
7.2.12 Zeta potential measurements 100
7.3 Characterization of U(VI) and HA solutions 101
7.3.1 Solvent extraction 101
7.3.2 TRLFS measurements under cryogenic conditions 101

7.3.3 Characterization of the diffusion reservoir solutions at 25 and 60 °C ... 104

7.4 Sorption experiments ... 105

7.4.1 General procedure ... 105
7.4.2 Influence of background electrolyte ... 107
7.4.3 S/L ratio dependence ... 107
7.4.4 Kinetic sorption experiments ... 107
7.4.5 U(VI) and humic acid sorption isotherms ... 107
7.4.6 Influence of humic acid and CO_2 on the U(VI) sorption ... 108
7.4.7 Influence of pH ... 108
7.4.8 EXAFS measurements ... 108

7.5 Diffusion experiments ... 112

7.6 Modeling ... 113

7.6.1 Speciation calculations with EQ3/6 ... 113
7.6.2 Modeling of diffusion processes using COMSOL Multiphysics 3.5a ... 113

8 REFERENCES ... 117

LIST OF FIGURES ... 137

LIST OF TABLES ... 141

LIST OF ABBREVIATIONS AND SYMBOLS

AAS	atomic absorption spectroscopy
ATR	attenuated total reflection
b.d.	below detection limit
BET	Brunauer, Emmett, and Teller
BGR	German Federal Institute of Geosciences and Natural Resources
CEC	cation exchange capacity
CNM	metal ion charge neutralization model
EXAFS	extended X-ray absorption fine-structure
f	fixed parameter during fitting procedure
FT–IR	Fourier transform – infrared
HA	humic acids
IAEA	International Atomic Energy Agency
IC	ion chromatography
ICCD	intensified charge-coupled device
ICP–MS	inductively coupled plasma – mass spectrometry
IEP	isoelectric point
LC	loading capacity
LIFS	laser-induced fluorescence spectroscopy
LSC	liquid scintillation counting
n.a.	not analyzed
Nd:YAG	neodymium-doped yttrium aluminum garnet
NEA	Nuclear Energy Agency
n.g.	not given
NICCA	consistent nonideal competitive adsorption
OECD	Organization for Economic Co-operation and Development
OPA	Opalinus Clay
p.a.	“pro analysi” = for analysis, reagent of high purity
PCS	photon correlation spectroscopy
PEC	proton exchange capacity
PP	polypropylene
pzc	point of zero charge
SCM	surface complexation model
SEM–EDX	scanning electron microscopy with energy dispersive X-ray detector
S/L	solid-to-liquid ratio

TC	total carbon
TIC	total inorganic carbon
TOC	total organic carbon
TRLFS	time-resolved laser-induced fluorescence spectroscopy
TTA	thenoyltrifluoroacetone
UV-vis	ultraviolet-visible
XAS	X-ray absorption spectroscopy
XANES	X-ray absorption near-edge structure
XRD	X-ray diffraction
ZPNC	zero point of net charge

α	rock capacity factor
a_{eq}	amount of a substance sorbed on the solid phase in µg/kg
a_m	amount of a substance sorbed on a solid in maximum (saturation of the solid) in µg/kg
a.u.	arbitrary unit
b	Langmuir sorption coefficient in m^3/µg
c	tracer concentration in the mobile phase in mol/m^3
c_{eq}	equilibrium concentration of the substance in solution in µg/m^3
cmol/kg	centimols per 1 kg
Da	Dalton
D_a	apparent diffusion coefficient in m^2/s
D_e	effective diffusion coefficient in m^2/s
D_f	effective diffusion coefficient of the filters in m^2/s
D_w	diffusion coefficient in bulk water in m^2/s
$\delta(k)$	total phase-shift
ε	diffusion-accessible porosity
E_a	activation energy in kJ/mol
E_h	redox potential
E_x	energy of the X-ray photon
E_0	absorption edge energy
eV	electronvolt
F	number of free variables
$f(k)$	backscattering amplitude
$\hbar$	reduced Planck constant
I	ionic strength

I_t	true ionic strength
$I(t)$	total luminescence intensity at time t
I_0	luminescence intensity of the luminescent compound at $t = 0$
J	diffusive flux in mol/(m^2·s)
k	wave number of the photo-electron
K_d	distribution coefficient in m^3/kg
k_F	Freundlich coefficient in m^3/kg
L	sample thickness
m	electron mass
meq/100 g	milli-equivalents per 100 g
N	number of neighbor atoms
μ	absorption coefficient
$\mu_0(E)$	smooth background function
$\Delta\mu_0$	jump of the absorption coefficient at the absorption edge
n_F	Freundlich exponent
P	number of data points
R	distance to the neighboring atom; gas constant, 8.314 J/(mol·K)
ρ	dry bulk density in kg/m^3
S_0^2	amplitude reduction factor
σ^2	disorder in neighbor distance, Debye-Waller factor
t	time
T	temperature
τ	luminescence lifetime
$T_{1/2}$	half-life
wt.%	weight percent
x	spatial coordinate in m
$\chi(E)$, $\chi(k)$	EXAFS fine-structure function
χ_{red}^2	reduced chi-squared value
ζ	zeta potential

Summary

The storage of nuclear waste in deep geological formations is discussed worldwide as the main strategy for nuclear waste management. To ensure the confinement of the nuclear waste, a multiple barrier system which consists of engineered, geo-engineered, and geological barriers will be applied. Thereby, in Germany the definition of the isolating rock zone represents an important safety function indicator.

Clay rock is internationally investigated as potential host rock for a repository and represents a part of the geological barrier. In the present work, the natural clay rock Opalinus Clay from the Mont Terri rock laboratory, Switzerland, was studied.

In Germany, the direct disposal of the spent nuclear fuel without the reprocessing of the spent fuel is preferred. In case of water ingress, radionuclides can be released from the nuclear waste repository into its surroundings, namely the host rock of the repository. Humic acids, ubiquitous in nature, can be found associated with the inorganic components in natural clay rock (1.5×10^{-3} wt.% in Opalinus Clay). They can be released under certain conditions. Due to their variety of functional groups, humic acids are very strong complexing agents for metal ions. They have inherent redox abilities and a colloidal conformation in solution. Because of these characteristics, humic acids can affect the mobility of metal ions such as actinides. Furthermore, in the near-field of a repository elevated temperatures have to be considered due to the heat production resulting from the radioactive decay of the various radionuclides in the nuclear waste.

This work focuses on the interaction of uranium, as main component of spent nuclear fuel, with Opalinus Clay and studies the influence of humic acid and elevated temperature on this interaction. For investigation of the retention behavior of the clay and the mobility of U(VI) in the system, batch sorption and diffusion experiments were performed. To clarify which U(VI) and humic acid species were present under the applied conditions, aqueous speciation modeling was used. Additionally, the U(VI) speciation in solution and on the clay surface was investigated by spectroscopic methods.

Prior to the investigation of the ternary system U(VI) / humic acid / clay, the applied batches of Opalinus Clay were characterized (e.g., specific surface area, carbon content, cation exchange capacity, elemental composition, particle size distribution). Leaching studies with Opalinus Clay in synthetic Opalinus Clay pore water (pH 7.6, I_t = 0.34 mol/L) and in $NaClO_4$ (pH 3 – 10, I = 0.1 mol/L) were performed to identify the competing ions and their concentrations in the background electrolytes. These data were used to calculate the U(VI) and humic acid speciation in solution. Calcium and

carbonate ions are present under pore water conditions as well as in 0.1 mol/L $NaClO_4$ from pH 7 to 8.5, due to dissolution of calcite (mineral fraction in Opalinus Clay). Thus, the U(VI) speciation is dominated by the aquatic $Ca_2UO_2(CO_3)_3$ complex. In the case of pore water, $Ca_2UO_2(CO_3)_3$(aq) is also the dominant U(VI) species in the presence of humic acid, which was corroborated by time-resolved laser-induced fluorescence spectroscopic measurements. A significantly changed speciation was found in 0.1 mol/L $NaClO_4$ in the presence of humic acid. At pH > 7, the negatively charged $UO_2(CO_3)_2HA(II)^{4-}$ complex determines the U(VI) speciation, thus repressing the $Ca_2UO_2(CO_3)_3$(aq) complex. In addition, the speciation of humic acid is influenced from ions leached out from Opalinus Clay. The CaHA(II) complex is the dominating humic acid species in solution.

Batch sorption experiments in 0.1 mol/L $NaClO_4$ showed that Opalinus Clay has the strongest retardation effect on U(VI) in the pH range from pH 4.5 to 7. However, under environmentally relevant conditions (pH > 7), the sorption of U(VI) onto Opalinus Clay is very weak. Under pore water conditions, a distribution coefficient (K_d) of 0.0222 ± 0.0004 m^3/kg was determined, which was shown to be independent of solid-to-liquid ratios ≥ 60 g/L. In addition, in pore water, the U(VI) sorption onto Opalinus Clay is not influenced by humic acid, which is supported by the speciation results. Extended X-ray absorption fine-structure investigations confirmed this batch sorption result.

The U(VI) diffusion experiments performed in pore water at 25 °C with Opalinus Clay bore core samples confirmed the K_d value obtained by batch sorption experiments. In the diffusion experiments at 60 °C, a change in the U(VI) speciation occurred. Beside $Ca_2UO_2(CO_3)_3$(aq), a colloidal U(VI) species was formed. Almost equivalent apparent diffusion coefficient (D_a) values were determined for the diffusion of the aqueous U(VI) species at 25 and 60 °C through Opalinus Clay. Thus, based on the investigations in the present study the breakthrough of U(VI) through Opalinus Clay is expected to be independent of the temperature and should occur nearly at the same time. Modeling calculations showed that it would take about 10 years until a detectable amount of ^{233}U(VI) (1×10^{-9} mol/L) migrates through an 11 mm thick Opalinus Clay sample.

Two distinct humic acid size fractions – a large- and a small-sized colloid fraction – diffused through the Opalinus Clay samples. Within three months, the high molecular size humic acid colloids migrated only about 500 µm into the clay, whereas the low molecular size fraction diffused through the entire Opalinus Clay samples and were consequently detected in the receiving reservoirs. These findings demonstrate a filtration effect of the compacted clay. The diffusion experiments revealed that the effect of humic acid on U(VI) diffusion is negligible and, under the studied conditions, independent of temperature.

The obtained results contribute to data bases used for modeling of interaction and migration processes in uranium / clay rock systems. Thus, the collected sorption and diffusion data are not only relevant for safety assessment of nuclear waste repositories but also for any clay-containing system present in the environment, where the geochemical interaction with uranium contaminated water plays a role.

Concerning the suitability of Opalinus Clay as host rock for a nuclear waste repository, it can be concluded, that Opalinus Clay has a relatively high retardation potential for U(VI). In case of water ingress U(VI) as part of the nuclear waste is released into the clay formation. Under near-neutral pH conditions, it will be complexed by calcium and carbonate ions leached out from Opalinus Clay, whereby $Ca_2UO_2(CO_3)_3(aq)$ is formed. This complex is only weakly retarded by sorption onto the clay, which can contribute to an enhanced mobility of U(VI) in the host rock. However, the U(VI) migration through the clay rock is governed by molecular diffusion. This decelerates the migration of $Ca_2UO_2(CO_3)_3(aq)$ through Opalinus Clay and thus it represents the decisive retardation process in the investigated system. Additionally, under environmentally relevant conditions, humic acid has no significant influence on U(VI) / Opalinus Clay interaction even at an elevated temperature of 60 °C. This was shown by speciation, sorption, as well as diffusion experiments.

Zusammenfassung

Eine weltweit diskutierte Strategie zum Umgang mit radioaktiven Abfällen ist deren Endlagerung in tiefen geologischen Formationen. Zur Abschirmung der Umwelt vor den schädlichen Einflüssen des radioaktiven Abfalls soll ein Multibarrierensystem bestehend aus technischen, geotechnischen und geologischen Barrieren im Endlager dienen. Dabei ist in Deutschland die Definition des einschlusswirksamen Gebirgsbereichs ein wichtiger sicherheitstechnischer Indikator.

Tongestein wird als potentielles Endlagerwirtsgestein und Teil der geologischen Barriere international erforscht. In der vorliegenden Arbeit wurde das natürliche Tongestein Opalinuston aus dem Mont Terri Felslabor, Schweiz, untersucht.

In Deutschland wird die direkte Endlagerung des abgebrannten Kernbrennstoffes ohne Wiederaufarbeitung des Brennstoffs favorisiert. Bei Wassereinbruch können Radionuklide aus dem Abfall in die Umgebung des Endlagers freigesetzt werden, d. h. sie können in Kontakt mit dem Wirtsgestein kommen. Ubiquitär in der Natur vorkommende Huminsäuren können mit den anorganischen Komponenten des natürlichen Tongesteins vergesellschaftet sein (1.5×10^{-3} Gew.-% in Opalinuston). Unter bestimmten Bedingungen können die Huminsäuren freigesetzt werden. Ihre Struktur enthält eine Vielzahl von funktionellen Gruppen, was sie zu starken Komplexbildnern für Metallionen macht. Sie besitzen Redoxeigenschaften und bilden in Lösung eine kolloidale Konformation aus. Aufgrund dieser Charakteristika können sie die Mobilität von Metallionen wie den Actinoiden beeinflussen. Weiterhin sind im Nahfeld eines Endlagers erhöhte Temperaturen zu erwarten, welche aus der Wärmefreisetzung beim radioaktiven Zerfall der verschiedenen Radionuklide im radioaktiven Abfall resultieren.

Die vorliegende Studie konzentriert sich auf die Untersuchung der Wechselwirkung von Uran, als Hauptkomponente des endgelagerten abgebrannten Kernbrennstoffs, mit Opalinuston und untersucht dabei den Einfluss von Huminsäure und erhöhter Temperatur. Um das Rückhaltevermögen des Tongesteins gegenüber U(VI) und die U(VI)-Mobilität im System zu ermitteln, wurden Sorptions- und Diffusionsversuche durchgeführt. Zur Klärung, welche U(VI)- und Huminsäurespezies unter den untersuchten Bedingungen vorliegen, wurde die aquatische Speziation berechnet. Zusätzlich wurde die U(VI)-Speziation in Lösung und an der Tonoberfläche mit spektroskopischen Methoden untersucht.

Vor der Untersuchung des ternären Systems U(VI) / Huminsäure / Ton wurden die eingesetzten Opalinuston-Chargen charakterisiert (z. B. spezifische Oberfläche, Kohlenstoffgehalt, Kationenaustauschkapazität, elementare Zusammensetzung,

Partikelgrößenverteilung). Anschließend wurden Auslaugungsversuche mit Opalinuston in synthetischem Opalinustonporenwasser (pH 7.6, I_t = 0.34 mol/L) und in $NaClO_4$ (pH 3 – 10, I = 0.1 mol/L) durchgeführt, um relevante Konkurrenzionen zu identifizieren und deren Konzentration in den Hintergrundelektrolyten zu bestimmen. Die erhaltenen Daten wurden zur Berechnung der U(VI)- und Huminsäurespeziation in Lösung verwendet. Unter Porenwasserbedingungen sowie in 0.1 mol/L $NaClO_4$ von pH 7 bis 8.5 liegen, durch die Auflösung von Calcit (Mineralphase im Opalinuston), Calcium- und Carbonationen in Lösung vor. Dadurch wird die U(VI)-Speziation von dem aquatischen $Ca_2UO_2(CO_3)_3$-Komplex dominiert. Im Falle des Porenwassers ist $Ca_2UO_2(CO_3)_3(aq)$ auch in Gegenwart von Huminsäure die dominierende U(VI)-Spezies. Dies wurde durch zeitaufgelöste laserinduzierte fluoreszenzspektroskopische Messungen nachgewiesen. Eine signifikante Änderung der U(VI)-Speziation tritt in 0.1 mol/L $NaClO_4$ in Gegenwart von Huminsäure auf. Bei pH > 7 bestimmt der negativ geladene $UO_2(CO_3)_2HA(II)^{4-}$-Komplex die U(VI)-Speziation, wobei der Anteil von $Ca_2UO_2(CO_3)_3(aq)$ zurückgedrängt wird. Auch die Huminsäurespeziation wird durch die vom Opalinuston ausgelaugten Ionen beeinflusst. So ist der CaHA(II)-Komplex die dominierende Huminsäurespezies in Lösung.

Sorptionsversuche in 0.1 mol/L $NaClO_4$ zeigten, dass Opalinuston gegenüber U(VI) den stärksten Retardationseffekt im pH-Bereich 4.5 bis 7 aufweist. Unter umweltrelevanten Bedingungen hingegen (pH > 7) ist die U(VI)-Sorption an Opalinuston sehr schwach. Unter Porenwasserbedingungen wurde ein Verteilungskoeffizient (K_d) von 0.0222 ± 0.0004 m^3/kg ermittelt, der von Fest-Flüssig-Verhältnissen ≥ 60 g/L unabhängig ist. Außerdem wird die U(VI)-Sorption an Opalinuston in Porenwasser nicht von Huminsäure beeinflusst. Dies wird durch die Ergebnisse aus den Speziationsrechnungen unterstützt. Röntgenabsorptionsspektroskopische Untersuchungen bestätigten ebenfalls dieses Sorptionsergebnis.

Die U(VI)-Diffusionsexperimente in Porenwasser bei 25 °C unter Verwendung von Opalinustonbohrkernstücken bestätigten den K_d-Wert der Sorptionsexperimente. In den Diffusionsexperimenten bei 60 °C trat eine Änderung in der U(VI)-Speziation auf. Neben $Ca_2UO_2(CO_3)_3(aq)$ wurde eine kolloidale U(VI)-Spezies gebildet. Für die Diffusion der aquatischen U(VI)-Spezies durch Opalinuston bei 25 und 60 °C wurden annähernd gleiche scheinbare (apparente) Diffusionskoeffizienten (D_a) bestimmt. Das bedeutet, der Durchbruch von U(VI) durch Opalinuston ist unabhängig von den hier untersuchten Temperaturen und wird deshalb etwa zum gleichen Zeitpunkt erwartet. Modellierungen zeigten, dass es etwa zehn Jahre dauern würde, bis eine detektierbare Menge an ^{233}U(VI) (1×10^{-9} mol/L) durch ein 11 mm-dickes Opalinustonbohrkernstück migrieren würde.

Zwei verschiedene Huminsäuregrößenfraktionen diffundierten durch die Opalinustonproben – eine große und eine kleine kolloidale Größenfraktion. Innerhalb von drei Monaten migrierten die hochmolekularen Huminsäurekolloide nur 500 µm in den Ton, während die niedermolekularen Huminsäurekolloide durch die gesamten Opalinustonproben diffundierten und dadurch im Auffangreservoir detektiert werden konnten. Diese Resultate demonstrieren den Filtrationseffekt des Tongesteins. Die Diffusionsversuche zeigten, dass der Einfluss von Huminsäure auf die U(VI)-Diffusion, unabhängig von der in dieser Arbeit verwendeten Temperatur, vernachlässigbar ist.

Die erhaltenen Ergebnisse tragen zu Datenbanken bei, die für die Modellierung von Wechselwirkungs- und Migrationsprozessen in Uran / Tongestein-Systemen genutzt werden. Das bedeutet, die gesammelten Sorptions- und Diffusionsdaten sind nicht nur für den Langzeitsicherheitsnachweis eines Endlagers für radioaktive Abfälle von Relevanz, sondern auch für jedes tonhaltige System in der Umwelt, bei dem die geochemische Wechselwirkung mit urankontaminierten Wässern eine Rolle spielt.

Bezüglich der Eignung von Opalinuston als Wirtsgestein für ein Endlager radioaktiver Abfälle lässt sich schlussfolgern, dass Opalinuston ein relativ hohes Retardationspotential bezüglich U(VI) aufweist. Wenn U(VI) als Bestandteil des radioaktiven Abfalls bei Wassereinbruch im Endlager in die Umgebung freigesetzt wird, wird es unter umweltrelevanten Bedingungen von Calcium- und Carbonationen, welche aus dem Opalinuston herausgelöst werden, komplexiert. Dabei bildet sich $Ca_2UO_2(CO_3)_3(aq)$. Dieser Komplex wird nur schwach durch Sorption am Tongestein zurückgehalten, was zu einer erhöhten U(VI)-Mobilität im Wirtsgestein führen kann. Im untersuchten System wird die U(VI)-Migration durch das Tongestein jedoch durch molekulare Diffusion bestimmt. Sie verzögert die Migration von $Ca_2UO_2(CO_3)_3(aq)$ durch Opalinuston und stellt somit den maßgeblichen Retardationsprozess im System dar. Huminsäure hat keinen signifikanten Einfluss auf die U(VI) / Opalinuston-Wechselwirkung, sogar bei einer erhöhten Temperatur von 60 °C. Dies wurde mittels Speziationsmodellierungen sowie durch Sorptions- und Diffusionsversuche gezeigt.

1 Introduction and objectives

The energy production by nuclear fission of heavy elements such as uranium represents an attractive alternative to the combustion of the resources oil, coal, and gas. Currently, 437 nuclear power plants are operating in 30 countries worldwide (IAEA, 2012). After the nuclear power plant incident of Fukushima Daiichi in 2011, Germany decided to abandon the energy production by nuclear power (BGBl, 2011). The nine German nuclear power plants still in operation will be shut down until 2022. Main problem of the nuclear energy production is the high radiotoxicity of the applied and spent nuclear fuels. On the one hand, during the operation of a nuclear power plant the consequences for the population are disastrous in case of an incident (see Chernobyl 1986, Fukushima Daiichi 2011). On the other hand, if nuclear power is used for energy production, the resulting nuclear waste has to be isolated to ensure long-term safety of people and the protection of the environment. The main strategy concerning nuclear waste management that is discussed worldwide is the final storage in deep geological formations. In this context, the detailed investigation of the radionuclide interaction with the geo- and biosphere is needed to clarify how the radionuclides can be retarded if they are mobilized. Such observations become relevant not only for the installation and operation of nuclear waste repositories, but also for the optimization of uranium mining, the remediation of uranium mines, the recovery of uranium from deposits, and after a nuclear incident.

The individual processes of nuclear fuel production and waste management are comprised in the nuclear fuel cycle. The two major types of fuel cycle are the once-through and the closed fuel cycle (NEA, 2006). In the once-through cycle, the spent nuclear fuel is disposed directly in form of reactor fuel elements, where the fuel is embedded in fuel rods made of stainless steel or zirconium alloy. This is the present German concept of nuclear waste management. In the closed fuel cycle, the spent nuclear fuel is reprocessed, which means that the unused fissile material (uranium, plutonium) is recovered and reused. Currently, this fuel cycle is preferred by several countries (e.g., China, France, India, Japan, United Kingdom, and Russian Federation). The high-level waste which remains after reprocessing consists of the fission products and minor actinides. These are often present in liquid form and have to be transformed into solids for disposal (normally by vitrification).

During safety assessment of nuclear waste repositories scenarios which represent the compilation and arrangement of safety relevant features, events, and processes are described (e.g., Mazurek et al., 2003). Irrespective of which nuclear fuel cycle is preferred, radionuclides with long half-lives ($T_{1/2}$), but also high radiotoxicity (e.g., ^{239}Pu)

Tab. 1: Selection of radionuclides with long half-lives contained in high-level nuclear waste (Jörg et al., 2010; Magill et al., 2006).

Radionuclide	$T_{1/2}$
^{232}Th	1.405×10^{10} a
^{238}U	4.468×10^{9} a
^{235}U	7.038×10^{8} a
^{129}I	1.57×10^{7} a
^{247}Cm	1.56×10^{7} a
^{237}Np	2.144×10^{6} a
^{242}Pu	3.75×10^{5} a
^{79}Se	3.27×10^{5} a
^{99}Tc	2.1×10^{5} a

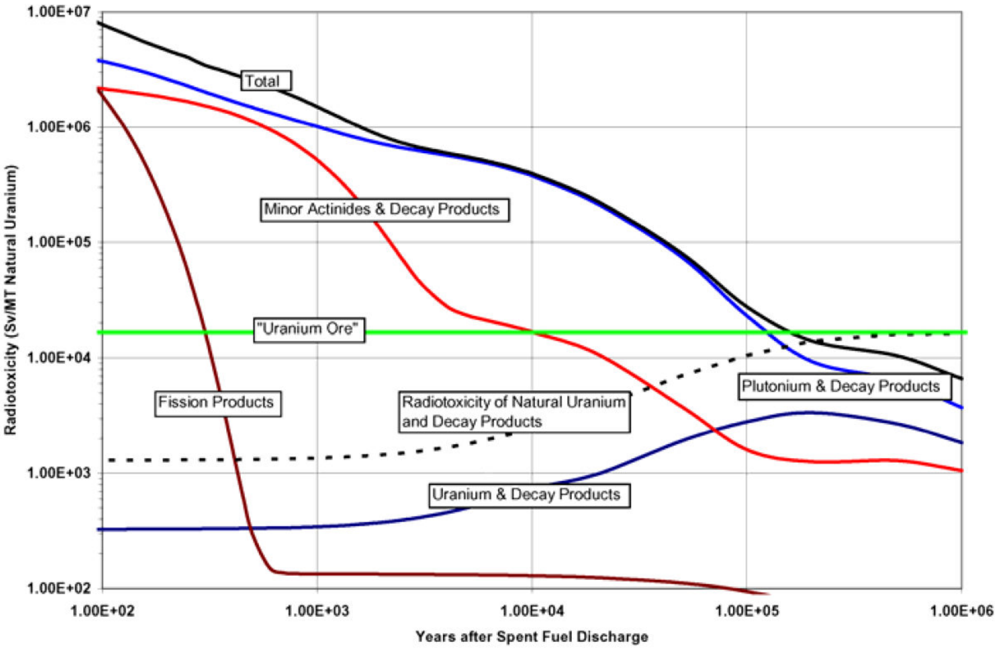

Fig. 1: Radiotoxicity evolution in time and its components ((OECD/NEA, 2006); Fig. 1.2).

deserve special attention (**Tab. 1**, **Fig. 1**). Safety case analyses have to be performed to assess whether or not radionuclides could be mobilized and released into the surroundings of the repository. Thus, the retardation ability of the repository barriers toward radionuclides needed to be determined. In particular, it has to be considered that the prevention of the radionuclides entry in the ecosphere needs to be maintained until their radioactivity is decayed to the natural radiotoxicity level (limit proposed by Germany: about one million years). For this, knowledge of the bio- and geochemical interaction processes of the radionuclides, such as sorption, diffusion, surface precipitation or the behavior of solid solutions, is necessary.

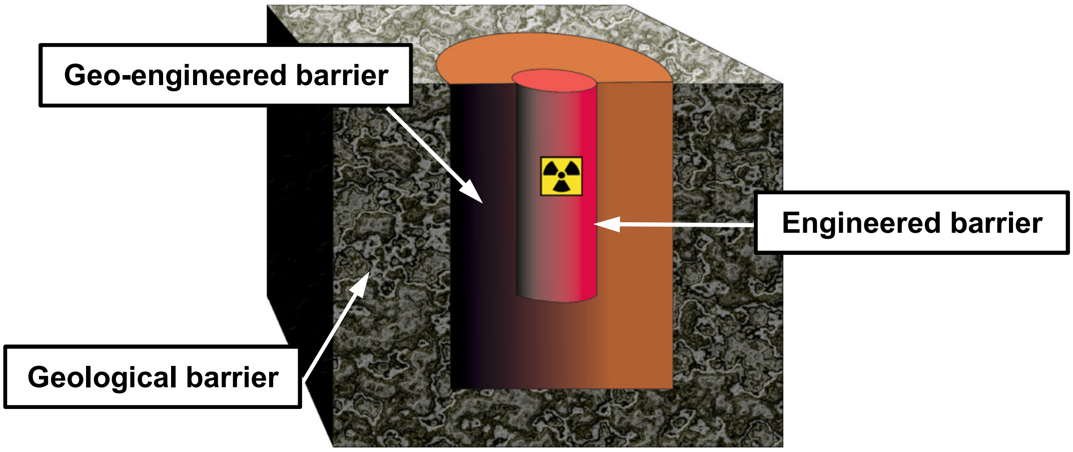

Fig. 2: Multiple barrier system of a nuclear waste repository (based on BfS, 2012).

For shielding of the nuclear waste, a multiple barrier system which consists of engineered, geo-engineered, and geological barriers (**Fig. 2**) will be applied. All barriers have the function to hinder water ingress and the release of radionuclides in the geo- and biosphere. The engineered barrier is represented by the conditioned (solidified, preferably water-insoluble) waste, which is placed in containers. Several geo-engineered barriers (backfill material such as bentonite, dam system, borehole plugs) are applied to stabilize and close the repository. The geological barrier consists of the host rock, in which the nuclear waste repository is installed, and the overburden with the aquifer system. In Germany, an important safety function indicator for safety assessment of a repository is the definition of the so-called isolating rock zone (BMU, 2010; Noseck et al., 2012). It describes an area, where the nuclear waste is contained and, at best, only minimal quantities of the radioactive material are released. Along with the engineered barriers, the isolating rock zone ensures the containment of the nuclear waste.

Possible host rocks for nuclear waste repositories, which are investigated worldwide, are salt domes (Germany, USA), clay rock (France, Switzerland, Belgium), and granite rock (Sweden, Finland, Canada). In Germany, there are regions for all three potential host rocks. Thus, for each host rock a separate study was prepared by the Federal Institute of Geosciences and Natural Resources (BGR) in Hanover: salt formations (Kockel and Krull, 1995), clay formations (Hoth et al., 2007), crystalline formations (Bräuer et al., 1994). Therein, the corresponding formations in Germany were described and evaluated for their suitability for further investigations as possible disposal site. The crystalline formations are not favored as disposal sites in Germany, because of their inappropriate geologic situation (heavily fissured) in comparison to salt and clay rock. A salt dome as host rock for a nuclear waste repository for high-level waste was investigated intensively during the last decades (Gorleben (Klinge et al., 2002)) and a wide data base was created. In the year 2000, a ten years moratorium concerning the investigations at Gorleben was adopted by the German government to intensify the investigations on clay and, consequently, to form coequal data bases for both host rocks. In April 2013, the German government reached a final agreement concerning the draft bill of the German site selection law. It is planned to adopt the bill in July 2013. Furthermore, the German government decided to create a 24-member enquete commission that will work out the criteria for the selection of a repository of nuclear waste until 2015. From 2015 on, the search for and selection of a disposal site for high-level waste is scheduled. It is planned to start the construction of a high-level waste repository in Germany in 2031.

In the clay study from Hoth et al. (2007), all German clay rock formations with the required depth and thickness were described (Jurassic formation, Lower Cretaceous formation, Tertiary formation). After considering further geological restrictions, e.g., earthquake zones or presence of aquifers used for drinking water, suitable areas of clay rock formations were identified in the North German Cretaceous formation and in the North and South German Jurassic formation (**Fig. 3**). The South German Jurassic formation is called Opalinus Clay which extends to Switzerland. There, the clay rock is intensively studied as host rock for a nuclear waste repository in the Mont Terri rock laboratory (Nagra, 2002).

In a nuclear waste repository hosted by clay rock, radioactive decay of the actinides and their fission products will result in elevated temperatures of up to 100 °C close to the waste containers (Brasser et al., 2008). In the case of Opalinus Clay, in dependence on the drilling depth, the inherent temperature of the host rock formation varies between 30 and 60 °C. Exclusively in the near-field of a repository, heat production by the waste canisters will result in higher temperatures over time periods up to $10^4 – 10^5$ years (Johnson et al., 2002). For safety assessment the temperature effect on the speciation of the radionuclides and their sorption and diffusion properties must be clarified.

Furthermore, it has to be considered that in natural clay rock organic matter is strongly associated with mineral constituents. Organic compounds such as small organic molecules (Courdouan et al., 2007), but also complex macromolecules such as humic substances (Claret et al., 2003) can be released from the clay under certain conditions. Humic material can also be found in soils and sediments in the surroundings of a repository. Because of their variety of functional groups, humic substances show a pronounced ability for complex formation. In addition, they are known for their inherent redox properties (Schmeide and Bernhard, 2009) and for their ability to form stable colloids (Artinger et al., 2002). Thus, they can move through the aquifer system in the

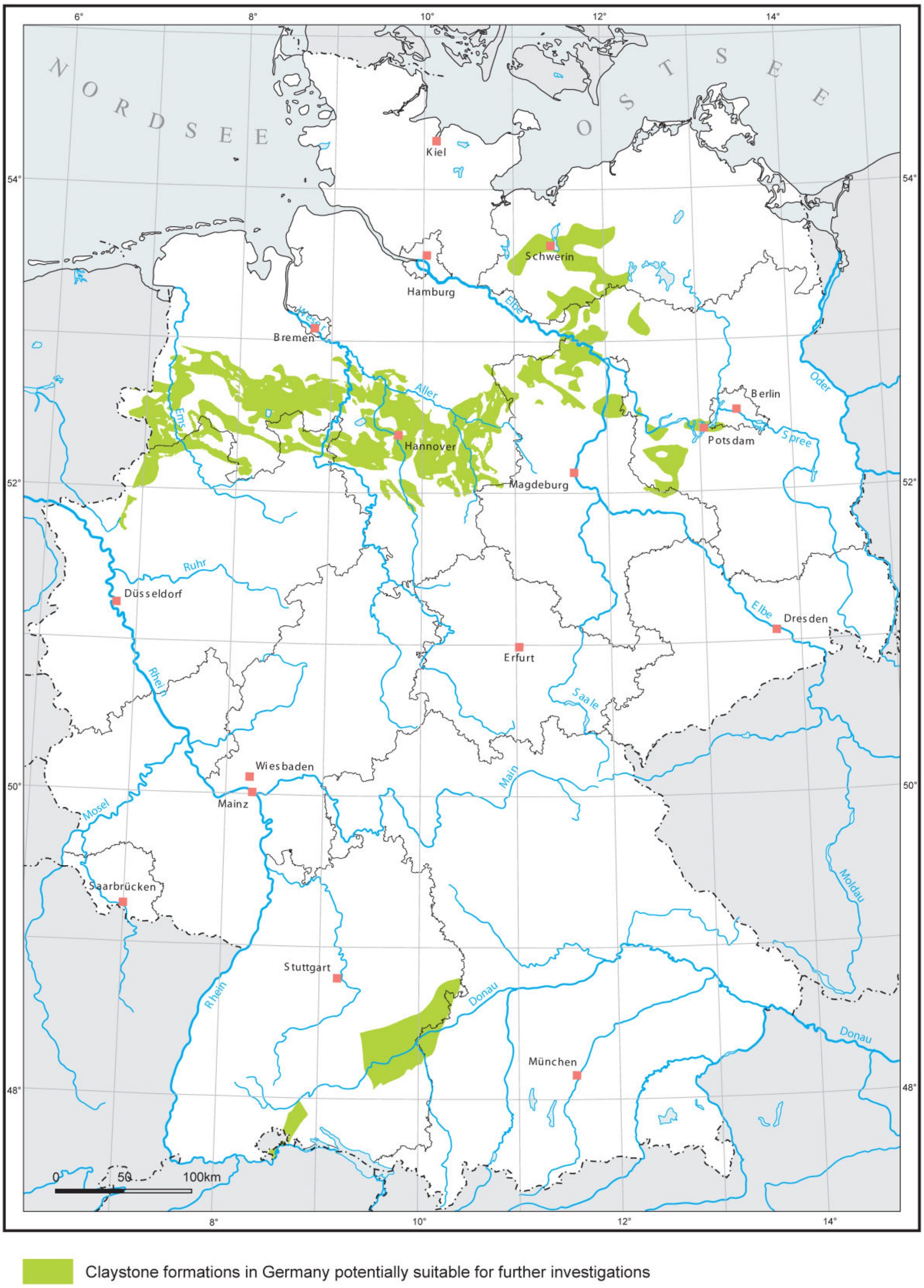
N O R D S E E
O S T S E E
Kiel
Hamburg
Schwerin
Bremen
Weser
Elbe
Aller
Ems
Hannover
Berlin
Oder
Potsdam
Spree
Magdeburg
Ruhr
Düsseldorf
Elbe
Dresden
Erfurt
Rhein
Saale
Wiesbaden
Mainz
Main
Mosel
Saarbrücken
Moldau
Stuttgart
Donau
Rhein
Donau
München
0
50
100km
6°
8°
10°
12°
14°
54°
52°
50°
48°
🟩 Claystone formations in Germany potentially suitable for further investigations

Fig. 3: Clay rock formations in Germany potentially suitable for further investigations as nuclear waste disposal site ((Hoth et al., 2007); Fig. 4.30).

surroundings of a repository as it was demonstrated for Gorleben (Schäfer et al., 2005). Therefore, humic substances can influence the speciation and migration of actinides in a repository.

This work contributes to the investigations of natural clay as host rock for a nuclear waste repository in Germany. As, so far, no disposal site in Germany for a nuclear waste repository for high-level waste in clay rock is determined; there is no possibility to obtain German reference clay. However, thanks to international cooperation and the BGR, Opalinus Clay from the Mont Terri rock laboratory, Switzerland has been obtained and was used as natural clay in the described experiments.

The general objective of this work was to estimate the retention ability of Opalinus Clay concerning U(VI). To validate the influence of organic matter on the U(VI) interaction with the clay, humic acid was added to the system. To study the effect of an elevated temperature on the system, experiments at 60 °C were carried out. Sorption and diffusion experiments were performed to determine parameters such as distribution coefficients, K_d, and diffusion coefficients, D_e. To clarify which U(VI) species are present in solution in the U(VI) / humic acid / Opalinus Clay system, speciation calculations were used, whereby especially the influence of competing ions present in dependence on the background electrolyte were studied. In addition, the U(VI) speciation in solution and on the clay surface was investigated by spectroscopic methods.

Within this work, methods and techniques for geochemical investigations of clay rock were tested and optimized. If once there is a site-specific decision concerning German clay, this knowledge can be easily transferred. The parameters determined in this work shall contribute to the data base used for modeling of geochemical interaction processes, which can be applied for safety assessment of nuclear waste repositories as well as for uranium mining or remediation scenarios.

2 Clay minerals and natural clay rock

2.1 Characteristics of clay

Clays are present in soils and geological formations. Regardless of environment, clay minerals are always formed due to interaction of aqueous solutions with rocks. These solutions may have a wide range of temperatures and ionic strengths. Thus, composition and crystal structure of clay minerals depend mainly on the local conditions (temperature, electrolyte, rock). Clay minerals are formed or transformed by alteration processes or by direct precipitation from solutions (Velde and Meunier, 2008).

Bailey (1980) defined clays as fine-grained phyllosilicates and specified the nomenclature of the clay structures and the phyllosilicate classification. The following description of clay structures and clay properties is based on Jasmund and Lagaly (1993) and Velde and Meunier (2008).

The structure of phyllosilicates can be described as superposed atomic planes oriented parallel to the (001) face (Miller index). Thereby, clays are distinguished by the occupation of their planes with cations and anions and the connection of their planes with each other. Planes are classified as sheets and layers.

Sheets are composed of a cationic plane which is enclosed by two planes of anions. Tetrahedral sheets consist of linked SiO_4^{4-} or AlO_4^{5-} tetrahedra which form a two-dimensional lattice with hexagonal cavities (**Fig. 4a**). Octahedral sheets are composed of O^{2-} or OH^- octahedra with Al^{3+}, Fe^{3+}, Fe^{2+}, or Mg^{2+} as central cation. The octahedra are connected by sharing six vertices forming a lattice of hexagonal symmetry (**Fig. 4b**). Trioctahedral sheets consist of octahedra which are all occupied by a divalent central cation. In dioctahedral sheets one third of the octahedra positions remain vacant. The central cations are trivalent.

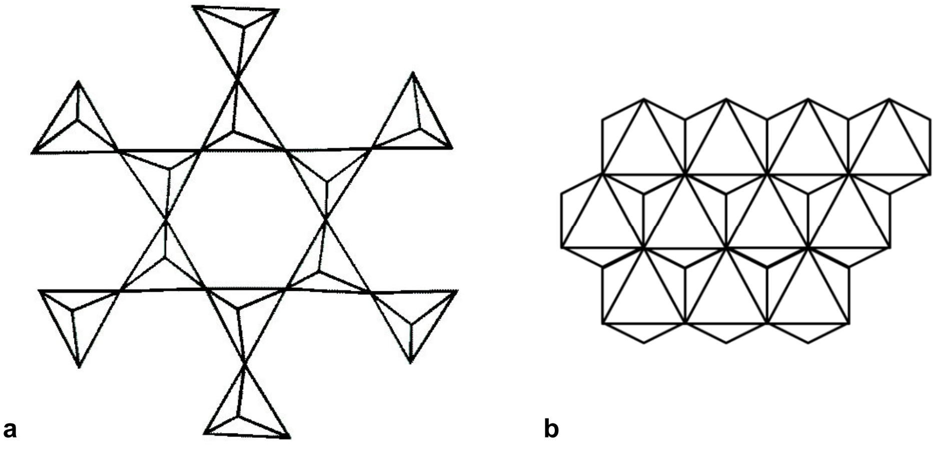

Fig. 4: Tetrahedral sheet with hexagonal cavities (**a**) and trioctahedral sheet (**b**). Only the oxygen framework is shown, central cations were omitted (based on Jasmund and Lagaly, 1993).

Layers describe how the sheets are linked to each other. Two layer structures (1:1) consist of a tetrahedral sheet which is bound to an octahedral sheet (**Fig. 5a**). The charge of the cations is compensated by the negative charge of the anions forming the framework. The uncharged layers interact via hydrogen bonds and van der Waals forces. One representative of this layer type is the clay mineral kaolinite. In three layer structures (2:1) the octahedral sheet is enclosed by two tetrahedral sheets (**Fig. 5b**). The structure can be uncharged, e.g., in the case of talc and pyrophyllite. The negative charge can also be in excess, for instance, due to substitutions in the octahedral sheet (dioctahedral: $R^{3+} \rightarrow R^{2+}$; trioctahedral: $R^{2+} \rightarrow R^{+}$). This charge is compensated by interlayer cations. Their position in the layers depends on the charge they have to compensate. High negative charges are compensated by cations which lost their bound water. They connect covalently to the layers in the ditrigonal cavities of the tetrahedral sheets (e.g., K^+ in illites). Low negative charges are compensated by cations which are still coordinated by some water molecules. They are located in the interlayer space between the tetrahedral sheets (e.g., Ca^{2+} in smectites). Furthermore, an additional sheet with an excess of positive charge can be present (2:1:1) for charge compensation (e.g., Mg^{2+} in chlorites). In this sheet, the cations are coordinated to OH^- groups which only electrostatically interact with the tetrahedral sheets of the 2:1 layer. Furthermore, there is a special group of 2:1 clay minerals whose crystal structure is comparable to that of fibers. Their structure consists of discontinuous octahedral and tetrahedral sheets, which are periodically inversed (e.g., sepiolite).

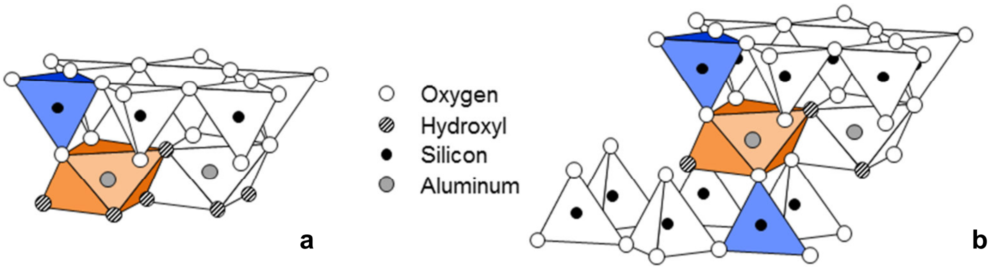

Fig. 5: Layer structures of phyllosilicates: 1:1 layer (**a**) and 2:1 layer (**b**) (based on Jasmund and Lagaly, 1993).

In soils and geological formations mixed layer clay minerals are manifold and widespread. They seem to be intermediate states between two structures and can be grouped into dioctahedral (e.g., illite / smectite) and trioctahedral species (e.g., biotite / vermiculite). Their structures can be regular (e.g., chlorite / smectite) or irregular (e.g., illite / smectite).

The high variability in composition known for phyllosilicates is a result of ionic substitutions which can take place in the tetrahedral ($Si^{4+} \leftrightarrow Al^{3+}$), octahedral ($Al^{3+} \leftrightarrow Fe^{3+}$) as well as interlayer sheets ($Ca^{2+} \leftrightarrow Sr^{2+}$). Primarily, phyllosilicates are classified by their layer type. Within the layer type, they are divided in groups and subgroups. **Tab. 2** summarizes the chemical composition of the phyllosilicates that are used in this work or that are present as a fraction of Opalinus Clay.

Tab. 2: Overview of phyllosilicates with their corresponding composition (Velde and Meunier, 2008) applied in this work and present in Opalinus Clay.

Phyllosilicates	**Composition**	
1:1 layer clay		
Kaolinite	$\mathrm{Si_4O_{10}Al_4(OH)_8}$	
2:1 layer clay		
Illite	$\mathrm{[Si_{4-x}Al_x]O_{10}[Al_{2-y}(Fe^{2+},Mg)_y](OH)_2K_{x+y}}$	$-0.3 < x < -0.7$; $-0.2 < y < -0.6$
Montmorillonite *	$\mathrm{Si_4O_{10}[(Al,Fe^{3+}{}_{2-y})Mg_y](OH)_2K_y}$	$-0.3 < y < -0.6$
2:1:1 layer clay		
Chlorite	$\mathrm{[Si_{4-x}Al_x]O_{10}[(Fe^{2+},Mg)_{3-y-z},(Al,Fe^{3+})_y,}$ $\mathrm{<>_z](OH)_2AlMg_2(OH)_6}$ **	$-0.3 < x < -1.0$; $0 < y + 2z < -0.7$

* Most popular representative for the smectite phyllosilicate group; smectite is contained in Opalinus Clay as mixed layer with illite.

** <> = vacancies

Ions can interact with clay at the basal and edge surfaces as well as in the interlayers by sorption and exchange reactions. The external basal surfaces (001) are formed by tetrahedral sheets. Their hexagonal cavities have basic character. The strength of these Lewis bases depends on the cation substitutions in the tetrahedral and octahedral sheets. Their charge is described as the pH-independent “permanent charge” of clay minerals. Sorption of metal ions at these charged sites takes place by exchange of bound cations and is determined by electrostatic interaction.

The edge surfaces of phyllosilicates consist of interrupted Si–O, R^{2+}–OH, or R^{3+}–OH bonds. The charge of the sites varies with pH and is described as “variable charge” of clays. Protonation of the sites at low pH values leads to Lewis acids, deprotonation at high pH values to Lewis bases. The charged sites are able to act as an adsorbent for several cations and anions from the surrounding solution; thereby, the interaction is based on covalent bonds and van der Waals forces.

Weakly bound cations in external and internal surfaces (interlayers) can be exchanged with other cations. The number of positive charges available for exchange is defined as cation exchange capacity (CEC). CEC is expressed in milli-equivalents per 100 g (meq/100 g) or more recently in centimols per 1 kg (cmol/kg). Both the variable and the permanent charge contribute to the CEC. In the case of 1:1 layer clays, the CEC is influenced mainly by the variable charge at the clay edges. The smaller the crystal size, the bigger is the external surface. Due to the influence of variable charge, the CEC is pH-dependent and thus usually determined at pH 7 at room temperature. In 2:1 layer clays the CEC is mainly dependent on the permanent charge, which influences the bond of the charge compensating cations in the interlayers of the tetrahedral sheets. If the charge is too high, cations are irreversibly bound to the interlayer space and cannot be exchanged. Thus, the CEC for illites is smaller than for smectites and the variable charge becomes more important for illites.

The basal surfaces of 2:1 layer clays are considered to be negatively charged. Cations attached to the surfaces can be interpreted as an electrical double layer (model of Gouy (1910) and Chapman (1913)). The bonding energy of sorbing cations is the highest close to the surface. It decreases with increasing distance to the charged surface. Simultaneously, the number of anions increases. In the concept of Stern (1924), close to the surface of the clay layer, the electric potential of the ions is considered to decrease linearly with increasing distance up to a critical point. The thickness of this so-called “Stern layer” depends on the radius of the ions in the layer. After the Stern layer, a diffuse layer with an exponential decrease of electric potential follows (Gouy-Chapman). The “isoelectric point” (IEP) is attributed to the pH where the charge on the plane separating the Stern layer from the diffuse layer is zero (Gillman and Uehara, 1980). The IEP can be determined by zeta potential measurements.

In addition to the IEP, the “point of zero charge” (pzc) is also used to describe charge neutrality at solid-solution interfaces. In general, the pzc is the pH value where the surface charge is zero. Gillman and Uehara (1980) defined various terms for pzc: The zero point of net charge (ZPNC) describes the pH where the total net surface charge is zero. That means, the sorption of cations and anions from an indifferent electrolyte is equal. The ZPNC can be determined by ion sorption measurements. pH_0 is attributed to the pH value where the variable net surface charge is zero. At this point, the sorption of H^+ and OH^- is in balance. pH_0 can be determined by potentiometric titration; it is marked by the intersection of the titration curves at different electrolyte concentrations. Specific sorption of cations and anions lowers and raises the pH_0, respectively. pH_0 is equal to the IEP, if there is no specific sorption of other ions at the surface. In this study, pzc is applied in the meaning of pH_0. At pH values > pzc, the negative charge dominates the surfaces and a good cation sorption can be observed. At pH values < pzc, the positive charge becomes dominant. There, a sorption of anions is possible as well as a low cation sorption.

Due to their porous structure the internal surface of clays is several times higher than their external surface. The size of the internal surface is often used to distinguish between different adsorbents since there, sorption processes predominantly take place. The standard method to determine the internal surface size, the so-called specific surface area, is the analysis of the gas sorption isotherm after the model of Brunauer, Emmett and Teller (Brunauer et al., 1938), also called BET method. The BET model assumes the sorption of molecules in multilayers on energetically homogeneous surfaces excluding any interaction between the sorbing molecules. For measurement, inert gases such as N_2 are used.

Clay minerals are used in a wide range of applications. Their ability to form a ceramic material after firing leads to their use for pottery items such as kaolinite for porcelain. In soils, they are the most active mineral constituent by being responsible for cation exchange and providing a surface for micro-organic interaction (Parker and Rae, 1998). Colloidal clay minerals are known to influence the distribution of trace elements in ecosystems (Parker and Rae, 1998).

Clays are characterized by a good retention behavior toward various heavy metals. This property leads to their application as barriers in landfills (Roehl, 1997) and is also an important factor regarding their suitability as host rock for a nuclear waste repository (BGR, 2007).

Phyllosilicates with 2:1 layer structure are able to swell if cations with bound water molecules are incorporated in the clay interlayers. This effective sealing characteristic is especially pronounced in case of montmorillonite (Parker and Rae, 1998). The resulting low hydraulic conductivity is one of the main characteristics plead also for the application of clay as host rock and backfill material in nuclear waste repositories.

This work focuses on kaolinite, as representative for the clay minerals, and the natural clay rock Opalinus Clay. Their characteristics are discussed in detail in the following sections.

2.2 The clay mineral kaolinite

Kaolinite can be assigned to the clay sub-group of kaolins. Minerals from this sub-group are formed preferably during the dissolution of feldspars dominated silicate rocks either under hydrothermal conditions (hydrothermal kaolins) or during weathering under tropic conditions (residual kaolins). Kaolinite belongs to sedimentary kaolins, which can be described as transformed residual kaolin (Jasmund and Lagaly, 1993). Deposits of kaolinite can be found, for instance, in the People's Republic of China, Central and Western Europe, Brazil, and in the south-east of the United States (Jasmund and Lagaly, 1993).

In this study, Georgia kaolinite, batch KGa-1b (Pruett and Webb, 1993), obtained from the Clay Mineral Society was used for experiments. Its elementary composition was already investigated by Křepelová et al. (2006) and Pruett and Webb (1993) (cf. **Tab. 3**), resulting in comparable values. This clay batch contains some impurities (e.g., TiO_2) since pure kaolinite (structure described in section **2.1**) cannot be found in nature. These impurities provide additional binding sites for sorbing compounds such as U(VI). However, their weight fractions in the clay mineral are negligible, thus having no significant effect on sorption. In KGa-1b, uranium was found in traces of 3.69 ppm (Křepelová et al., 2006) and 1.96 ppm (Pruett and Webb, 1993), respectively. The total organic carbon (TOC) amounted to 231 ppm (Pruett and Webb, 1993).

Tab. 3: Composition of kaolinite batch KGa-1b.

Compound	Data from Pruett and Webb (1993) / wt.%	Data from Křepelová et al. (2006) * / wt.%
Al_2O_3	39.1	42.98
SiO_2	45.2	47.85
TiO_2	1.64	1.45
Fe_2O_3	0.21	0.27
CaO	0.02	< 0.06
K_2O	0.02	0.01

* Error: ± 10 wt.%

For characterization of the clay structure X-ray diffraction (XRD) and Fourier transform – infrared (FT–IR) spectroscopy were applied (Chipera and Bish, 2001; Křepelová, 2007; Madejová and Komadel, 2001). The diffractograms measured for different size fractions showed clearly reflections of kaolinite but also of anatase (TiO_2) (Křepelová, 2007). In the IR spectrum of kaolinite, bands could be assigned to several hydroxyl group and Si–O vibrations (Křepelová, 2007).

The particle size distribution indicated the presence of two main fractions, 57.8 % of the particles were < 2 µm and 32.0 % were < 0.5 µm (Pruett and Webb, 1993). The specific surface area of kaolinite was determined to be in the range from 11.7 to 11.8 m^2/g (Křepelová, 2007; Pruett and Webb, 1993) using N_2-BET. Its CEC amounted to 1.83 meq/100 g (Křepelová et al., 2006).

Redden et al. (1998) described the difficulty of modeling the pzc of kaolinite since several binding sites are present at basal siloxane and gibbsite-like surfaces as well as at the edge surfaces. They modeled two pzc values for kaolinite, 6.0 at the gibbsite-like surface and 8.0 at the edge surfaces. The values were in agreement with the modeling results of Wieland and Stumm (1992) who published values of 5.9 for the basal surface and 7.5 for the edges. However, using potentiometric titration experimentally determined pzc values were also reported in the literature, for instance, 4.5 (Motta and Miranda, 1989) and ~ 5.5 (Huertas et al., 1998).

To determine the IEP of KGa-1b zeta potential measurements of kaolinite suspensions were performed as described in section **7.2.11**. The results are depicted in **Fig. 6**.

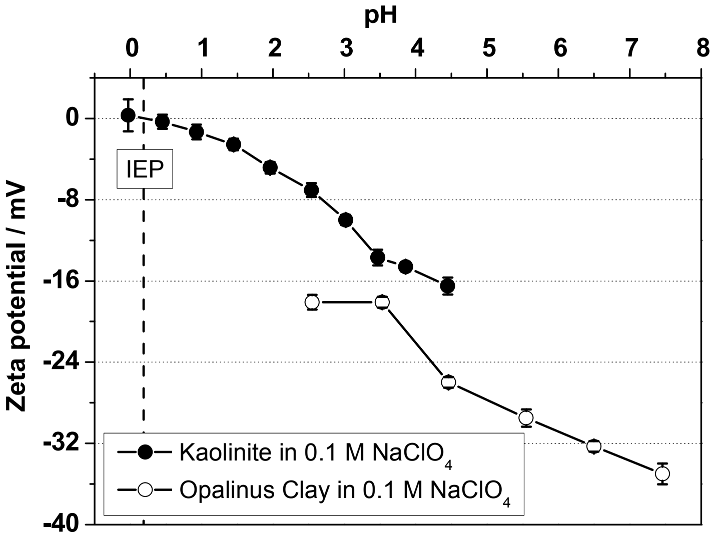

Fig. 6: Zeta potential of kaolinite and Opalinus Clay in 0.1 mol/L $NaClO_4$ (solid-to-liquid ratio (S/L) = 0.1 g/L) as a function of pH.

With decreasing pH from pH 4.5 to 0, an increase of the zeta potential of kaolinite suspensions from –16.5 mV to 0.32 mV was observed. The pH at which the experimental data intersects the x-axis at ζ = 0 mV is defined as IEP. In this study, the IEP was determined to be 0.2. Vane and Zang (1997) measured the zeta potential for Georgia kaolinite in 0.01 mol/L KCl in a wide pH range. They found ζ values between 0.7 mV at pH 2 and –54 mV at pH 10, leading to an IEP of about 2. The difference to the measured value of this study can be attributed to differences in ionic strength and background electrolyte.

In this work, kaolinite was used as reference clay for U(VI) sorption studies. Thereby, the influence of the background electrolyte and humic acid was investigated. The U(VI) and humic acid sorption on kaolinite was already comprehensively studied in previous experiments (Křepelová et al., 2006; Sachs and Bernhard, 2008). These data can be compared to the sorption characteristics obtained under the conditions applied in this study. Furthermore, kaolinite represents a mineral fraction of Opalinus Clay, on which the present study is mainly focused.

2.3 The natural clay rock Opalinus Clay

In nature, clay minerals in geological formations are associated with the surrounding rock minerals. This so-called mineral cement can be either quartz, calcite, or / and iron minerals. The clay minerals can also appear as aggregates with organic matter (Kaufhold et al., 2003).

For this study, Opalinus Clay (OPA) from the Mont Terri rock laboratory, Switzerland was used. OPA is a fine-grained sedimentary clay rock formed in a shallow sea about 180 million years ago. Its name originates from an ammonite species which is the most common fossil found in this formation, *Leioceras opalinum* (**Fig. 7**). The heterogeneous clay rock consists of several layers of partially calcareous, mica-rich, and silty clay minerals, in which lenses and laminaes of calcareous sandstone or silt, beds of limestone, concretions of pyrite, siderite, and limestone as well as ammonites are embedded (Nagra, 2002).

Fig. 7: Shells of *Leioceras opalinum* – index fossil of OPA (picture size: 10 cm; Nagra, 2002).

OPA was one of the clay rocks chosen to be investigated as potential host rock for a nuclear waste repository in Switzerland. In Mont Terri, OPA occurs with a maximum overburden of about 300 m and a thickness of about 150 m (Pearson et al., 2003). Since 1996, questions concerning the construction and the safety of a repository are investigated in the rock laboratory. To solve these questions long-term experiments are performed, for instance, concerning the dimension and properties of the excavation disturbed zone, thermal influences on the host rock, water and gas transport, diffusion, and interaction of OPA with (geo-)engineered barriers (Nagra, 2002).

Generally, the OPA formation is subdivided into five lithological sub-units with ‘sandy’, ‘shaly’, and ‘calcareous-sandy’ facies. **Tab. 4** presents the mineralogy of OPA shaly and sandy facies as average of nine and four samples, respectively (Pearson et al., 2003). Sandy facies are characterized by a higher quartz fraction than shaly facies. On the other hand, shaly facies contain more calcite than sandy facies.

Tab. 4: Mineralogy of OPA shaly and sandy facies (average of nine and four samples) (Pearson et al., 2003).

Mineral	Shaly facies / wt.%	Sandy facies / wt.%
Clay minerals	58 – 76	45 – 70
– Illite	16 – 40	15 – 35
– Illite / smectite mixed layer	5 – 20	5 – 20
– Chlorite	4 – 20	4.4 – 15
– Kaolinite	15 – 33	13 – 35
Quartz	6 – 24	16 – 32
Calcite	5 – 28	7 – 17
Siderite	1 – 4	1.1 – 3
Albite	0.6 – 2.2	0.8 – 2.2
K-feldspar	1 – 3.1	2.5 – 5
Dolomite / ankerite	0.2 – 2	0.3 – 2
Pyrite	0.6 – 2	0.7 – 3.2
Organic carbon	< 0.1 – 1.5	0.2 – 0.5

In the present study, sorption and diffusion experiments with U(VI) were carried out with three different OPA batches. The batches BHE-24/1 and BLT-11/01 were crushed and homogenized under aerobic and anaerobic conditions, respectively. They were used for sorption experiments under aerobic and anaerobic conditions. Both batches can be assigned to the shaly fraction of OPA. From bore core BLT-14 pristine OPA samples were used for diffusion experiments. This batch belongs to the sandy fraction of OPA.

The three OPA batches were characterized in detail. This was necessary, since, due to the heterogeneity of the natural clay rock, there can be differences between the individual OPA batches. The characterization ensured that the applied OPA samples had properties typical for Mont Terri OPA. Thereby, the determined values had to be in the published range of values (Nagra, 2002; Pearson et al., 2003), otherwise the samples were discarded. Thus, the sorption and diffusion results obtained in this study for U(VI) and humic acid could be compared to values already published for Mont Terri OPA samples and different interacting compounds.

For the OPA samples used in the diffusion experiments, specific diffusion characteristics (e.g., transport porosity) were important. These were determined by tritiated water (HTO) diffusion experiments and thus they are discussed separately in section **5**.

The determined properties for the two batches used in sorption experiments are summarized in **Tab. 5**. Both batches show relatively similar characteristics. The specific surface areas are in agreement with published data (Pearson et al., 2003). Pearson et al. (2003) illustrated that a N_2-BET value of 37 m^2/g corresponds to an average pore size of 3.9 nm and a clay porosity of 16.8 %. Since only external surfaces are determined, the determination of the specific surface area with N_2-BET does not represent a suitable method in the case of OPA. This is due to the nonpolar structure of N_2 which hinders the molecules to penetrate into the smectite interlayers (Nagra, 2002). Thus, Pearson et al. (2003) measured the total surface area using Keeling's hygroscopicity method (Keeling, 1958), where the total uptake of water by a dried clay sample was determined in an atmosphere with constant humidity. Values between 112 and 147 m^2/g for OPA were obtained which are about three times higher than the N_2-BET values.

Tab. 5: Main characteristics of OPA batches BHE-24/1 and BLT-11/01.

Batch	**BHE-24/1**	**BLT-11/01**	**Pearson et al. (2003)**
Grain size / µm	< 500	< 200	
N_2-BET / m^2/g	41.3 ± 0.5	38.8 ± 0.3	
TOC / wt.%	1.09 ± 0.06	0.96 ± 0.02	
TC * / wt.%	2.49 ± 0.02	1.87 ± 0.01	
CEC / meq/100 g	10.26 ± 0.52	12.89 ± 0.14	
Main components ** / wt.%			
SiO_2	39.04 ± 3.90	36.37 ± 3.64	30.0 – 53.12
Al_2O_3	17.91 ± 1.79	20.08 ± 2.01	16.7 – 19.7
Fe_2O_3	6.53 ± 0.65	6.04 ± 0.60	5.62 – 6.23
CaO	5.42 ± 0.11	3.16 ± 0.06	2.96 – 16.2
K_2O	3.47 ± 0.35	3.61 ± 0.36	2.2 – 2.92
MgO	2.32 ± 0.05	2.33 ± 0.05	1.7 – 2.47
U content / ppm	2.83 ± 0.28	2.93 ± 0.29	2.4 – 2.5

* TC = total carbon

** only compounds > 1 wt.% are shown

The determined TOC values are in agreement with the values shown in **Tab. 4** for shaly facies. Pearson et al. (2003) found that 0.15 % of TOC of OPA can be attributed to humic material. The rest was assigned to kerogen and uncharacterized organic matter.

Compared to the published TC values between 2.28 and 4.5 wt.% (Pearson et al., 2003) for shaly facies, the measured TC value of BLT-11/01 is slightly lower. Such a value is normally attributed to the calcareous-sandy facies of OPA, which are reported to have a TC value of about 1.02 wt.% (Pearson et al., 2003), rather than the shaly facies. This small discrepancy can be attributed to the heterogeneity of OPA.

The determined CEC values are comparable to the values published by Nagra (2002). They range from 11.1 meq/100 g (Ni-ethylenediamine method; Pearson et al., 2003) to 16.0 meq/100 g (Co-hexamine method; Blanc et al., 2001).

The main component compositions of both investigated OPA batches are in good agreement with the values that Pearson et al. (2003) found for shaly facies. Only potassium shows slightly higher values in this study. Elements which are only present in traces in the used OPA batches are summarized in **Tab. 6**.

Tab. 6: Trace elements in OPA batches BHE-24/1 and BLT-11/01 (in ppm).

Element	BHE-24/1	BLT-11/01	Element	BHE-24/1	BLT-11/01	Element	BHE-24/1	BLT-11/01
Li	190	190	Ga	30	30	Y	20	20
Na	3200	3200	Rb	120	120	La	40	40
P	81	82	Sr	230	230	Ce	80	80
Mn	400	400	Ba	300	300	Zr	130	130
Co	30	30	Tl	1	1	Nb	18	18
Ni	70	70	Pb	30	30	Cs	8	8
Cu	30	30	Ti	5000	5000	Th	14	14
Zn	100	100						

The particle size distribution of batch BHE-24/1 is shown in **Fig. 8**. In this batch, the particle sizes are widely spread. The smallest particles have a size of about 0.5 µm, the biggest particle sizes amount to about 30 µm. 90 % of the particles are < 13 µm, 50 % are < 4 µm.

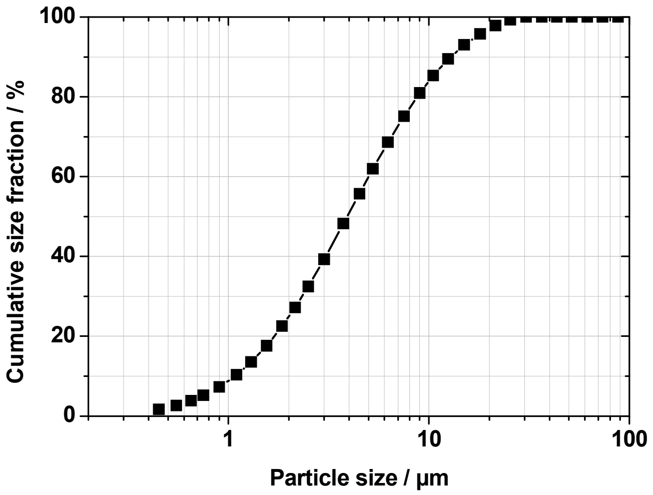

Fig. 8: Particle size distribution of OPA batch BHE-24/1.

In **Fig. 9**, the IR spectra of some mineral components of OPA are compared to the IR spectrum of OPA (batch BHE-24/1). Spectral contributions of kaolinite, illite, illite / smectite mixed layer, quartz, and calcite were clearly identified in the IR spectrum of OPA. The main spectral features are summarized in **Tab. 7**. The interpretation of the vibration bands was based on Madejová and Komadel (2001) for the clay minerals as well as for quartz and Andersen and Brečević (1991) for calcite.

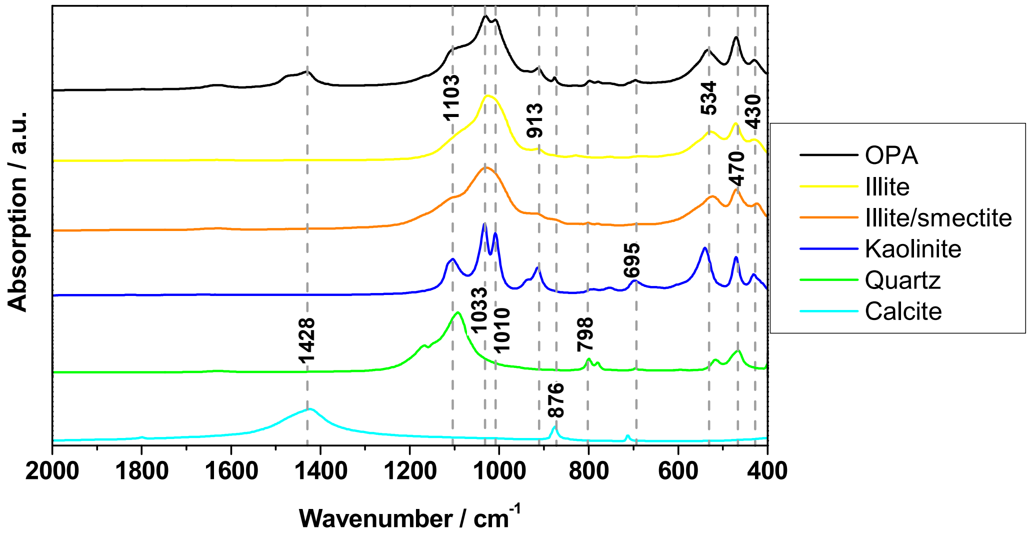

Fig. 9: IR spectra of some mineral components of OPA compared to the IR spectrum of OPA batch BHE-24/1. The spectra are shifted along the y-axis.

Tab. 7: Assignments of the IR bands of OPA batch BHE-24/1.

Position / cm^{-1}	**Mineral**	**Assignment**
1428	Calcite	asymmetric C–O stretching
1103	Kaolinite	perpendicular Si–O stretching
1033 / 1010	Kaolinite	in plane Si–O stretching
913	Kaolinite	OH deformation of inner OH groups
876	Calcite	CO_3 out-of-plane deformation
798	Quartz	Si–O stretching
695	Kaolinite	Si–O_2 perpendicular
534	Illite, illite / smectite	Al–O–Si deformation
470	Illite, illite / smectite, kaolinite, quartz	Si–O–Si deformation
430	Illite, kaolinite	Si–O deformation

Fig. 10 shows the IR spectra of the batches BHE-24/1 and BLT-11/01. The comparison of the spectra demonstrates that there are negligible spectroscopic differences between the batches.

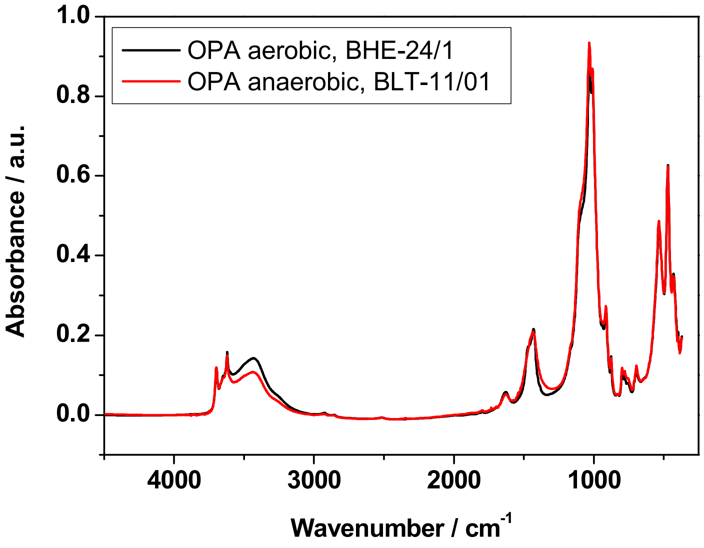

Fig. 10: IR spectra of OPA batches applied for sorption experiments.

The two OPA batches were additionally characterized by XRD. The corresponding diffractograms are shown in **Fig. 11**. The XRD patterns of illite, kaolinite, quartz, and calcite were identified in the diffractograms of both batches.

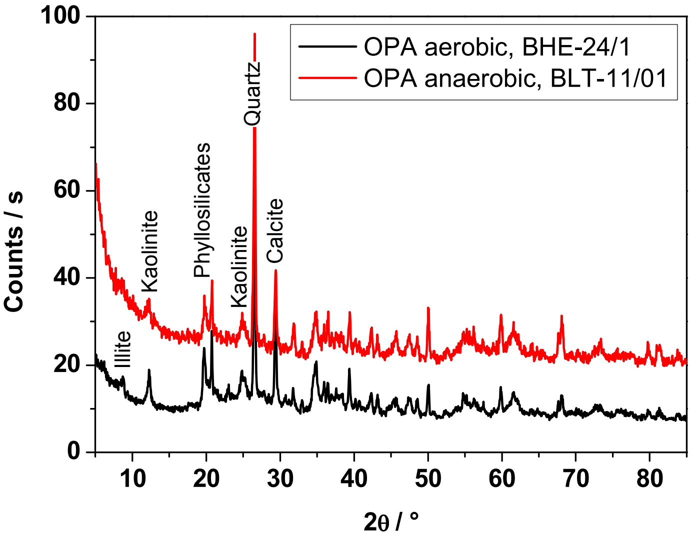

Fig. 11: X-ray diffractograms of the OPA batches BHE-24/1 and BLT-11/01. The diffractograms are shifted along the y-axis.

Based on these investigations, it can be assumed that the OPA batches applied in the sorption experiments under aerobic and anaerobic conditions were comparable.

2.3.1 The system Opalinus Clay / Opalinus Clay pore water

Several million years ago, OPA sediments were deposited and compacted due to sedimentation of further minerals on OPA. The porosity was reduced and the so-called pore water was released to a large extent (Nagra, 2002). Since this time, the composition of the pore water remaining in the clay has changed slowly but steadily. During the last 40 million years, the salinity of the pore water decreased. Nowadays, it amounts to two third of the sea water salinity (Nagra, 2002).

The *in situ* composition of OPA pore water was investigated with leaching experiments in the Mont Terri rock laboratory and by extraction analysis of hermetically sealed bore cores (Pearson et al., 2003). Due to the heterogeneity of the clay and different measurement artifacts, a variability of the data was observed. Modeling was applied to define site-specific reference pore water. The associated modeling data base is described in detail in Pearson et al. (2003). The composition of reference pore water was shown to be consistent with field data. Thus, it can be applied in speciation calculations, sorption, and diffusion experiments.

Courdouan et al. (2007) used synthetic pore water for the extraction of dissolved organic matter from OPA. Only a small fraction of TOC was extractable (< 0.38 %). From this, 36 % were low molecular weight organic acids (< 500 Da) such as acetic acid, lactic acid, and formic acid.

The fact that there is organic matter still preserved in OPA after such a long time period points to constant reducing conditions in this geochemical system (Nagra, 2002). However, the *in situ* determination of the redox potential of pore water was not possible so far due to the strong influence of oxygen impurities during measurement (Pearson et al., 2003). In consideration of the redox-active elements, the redox potential of OPA was modeled. Based on the rock composition, the major redox-active elements in OPA are Fe, Mn, and S. Fe is present as Fe(II) in pyrite and siderite, or as Fe(III) in the case of nonredox-active phyllosilicates such as chlorite. Mn can be found as Mn(II) in the carbonates. S is mainly present in its reduced form in pyrite or as SO_4^{2-} in celestite which can be found in the veins of undisturbed OPA and as traces in the OPA bulk formation (Pearson et al., 2003). In theory, the organic carbon fraction could also be oxidized, but it is supposed to be a very slow reaction. Thus, its contribution was neglected (Nagra, 2002). Pearson et al. (2003) obtained a redox potential of –200 mV for OPA. Fernández et al. (2007) concluded that the redox potential is controlled by the SO_4^{2-} / pyrite or pyrite / Fe(III) redox couples and reported a value of –196 mV at pH 7.6.

In this study, OPA pore water (hereafter referred to as “pore water”) was synthesized according to the model of Pearson (1998) (pH 7.6; cf. **Tab. 8**). Based on the ionic basis species of the elements contained in pore water an ionic strength of 0.39 mol/L can be calculated (Lehmann et al., 1996). However, this value does not reflect the natural conditions, because there, the ions are present in various complexed species (e.g., aqueous metal carbonato or metal hydroxo complexes). Thus, using the speciation code EQ3/6 (Wolery, 1992), the true ionic strength (I_t) of 0.36 mol/L was recalculated for pore water (cf. **Tab. 8**). Synthetic pore water was applied for U(VI) and humic acid sorption experiments under aerobic and anaerobic conditions as well as for diffusion experiments under anaerobic conditions in this work. In particular, under anaerobic conditions the oxidation state of uranium was checked, since the OPA / pore water system could be able to reduce the applied U(VI) to U(IV) (cf. section **4.4.1**, **Fig. 22**).

Tab. 8: Composition of pore water: modeled by Pearson (1998) (pore water$_{\text{theor}}$), prepared for the experiments (pore water$_{\text{exp}}$), and ions leached out from OPA during 7 days contact time with pore water (pore water$_{\text{exp7d}}$) (Δleached$_{\text{7d}}$ = difference between pore water$_{\text{exp}}$ and pore water$_{\text{exp7d}}$).

Element / Ion	**Pore water$_{\text{theor}}$ / mol/L**	**Pore water$_{\text{exp}}$ / mol/L**	**Pore water$_{\text{exp7d}}$ / mol/L**	**Δleached$_{\text{7d}}$ / mol/L**
Na	2.4×10^{-1}	n.a. *	n.a. *	n.a. *
K	1.6×10^{-3}	$(2.3 \pm 0.2)\times10^{-3}$	$(2.2 \pm 0.2)\times10^{-3}$	$-(0.1 \pm 0.5)\times10^{-3}$
Mg	1.7×10^{-2}	$(1.6 \pm 0.03)\times10^{-2}$	$(1.63 \pm 0.03)\times10^{-2}$	$(0.03 \pm 0.06)\times10^{-2}$
Ca	2.6×10^{-2}	$(2.5 \pm 0.05)\times10^{-2}$	$(2.7 \pm 0.05)\times10^{-2}$	$(0.2 \pm 0.1)\times10^{-2}$
Sr	5.1×10^{-4}	$(4.9 \pm 0.5)\times10^{-4}$	$(5.0 \pm 0.5)\times10^{-4}$	$(0.1 \pm 1.0)\times10^{-4}$
Al	-	b.d. **	$(1.6 \pm 0.2)\times10^{-7}$	-
Si	-	b.d. **	$(7.7 \pm 0.8)\times10^{-5}$	-
U	-	b.d. **	$(5.3 \pm 0.5)\times10^{-9}$	-
Cl^-	3.0×10^{-1}	$(2.88 \pm 0.3)\times10^{-1}$	$(2.81 \pm 0.3)\times10^{-1}$	$-(0.06 \pm 0.57)\times10^{-1}$
SO_4^{2-}	1.4×10^{-2}	$(1.4 \pm 0.04)\times10^{-2}$	$(1.5 \pm 0.04)\times10^{-2}$	$(0.11 \pm 0.09)\times10^{-2}$
CO_3^{2-}/HCO_3^-	4.8×10^{-4}	$(4.0 \pm 0.1)\times10^{-4}$	$(7.4 \pm 0.2)\times10^{-4}$	$(3.4 \pm 0.3)\times10^{-4}$
I_t	0.36	0.37	0.34	-

* n.a. = not analyzed

** b.d. = below detection limit

In order to determine the ions released from OPA into the pore water in dependence on time and to clarify when the system is in equilibrium, a leaching experiment was conducted. The results of these studies are published in Joseph et al. (2011).

The experiment showed that the concentrations of ions in the suspension filtrates were in equilibrium after 7 days. Thus, this time was chosen as optimal pre-equilibration time for the U(VI) and humic acid sorption experiments discussed in section **4.4**.

The initial ion composition of pore water in the experiment (pore water$_{\text{exp}}$) and the ions leached out during 7 days contact time of OPA with pore water (Δleached$_{\text{7d}}$) are shown in **Tab. 8**. It can be seen that the leaching of the alkaline and earth alkaline metal ions (except for calcium) can be neglected since the experimental errors of the concentrations measured after 7 days are larger than the values themselves. Obviously, aluminum and silicon ions leached out due to dissolution processes of clay minerals and quartz in OPA. Since the pore water was prepared in perfluoroalkoxy bottles, the measured silicon cannot be released from glass bottles. Sulfate and carbonate ions are also released. They originate from pyrite oxidation and different carbonate minerals in the clay. The increase of the calcium and carbonate concentration in solution indicates the dissolution of the calcite fraction of OPA.

On the basis of the composition of pore water$_{\text{exp}}$ and under consideration of the final concentrations of Ca, Al, Si, SO_4^{2-}, and CO_3^{2-} an I_t of 0.34 mol/L was calculated for the pore water used in these experiments.

After the leaching experiment, the remaining OPA was studied by XRD. Compared to the diffractogram of untreated OPA (cf. **Fig. 11**), additional patterns were detected in the resulting diffractogram of the leached out clay (**Fig. 12**). These could be attributed to NaCl, which is the main salt component in pore water. No further changes were observed in the diffractogram of the leached out OPA sample. Thus, it can be concluded that the mineral structure of OPA does not change due to contact with pore water. This verifies that pore water indeed is close to equilibrium with OPA.

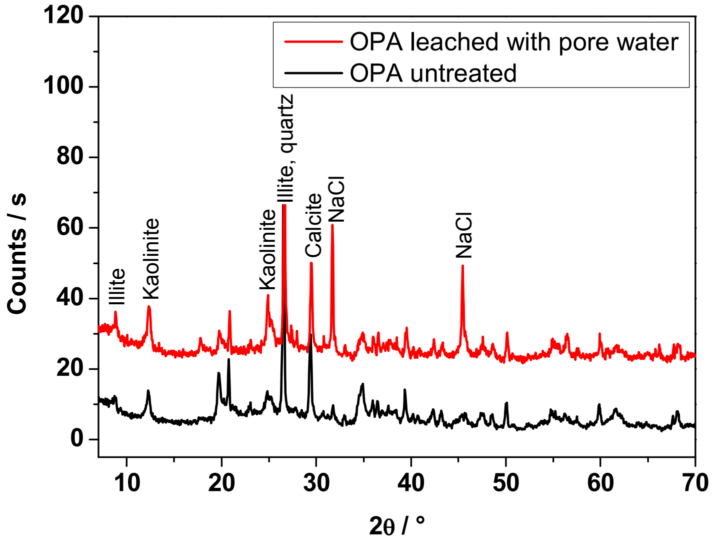

Fig. 12: X-ray diffractogram of OPA (BHE-24/1) untreated and leached out with pore water. The diffractograms are shifted along the y-axis.

2.3.2 *Characterization of Opalinus Clay suspensions as a function of pH*

Based on the OPA / pore water investigations, questions arise how the clay rock behaves and which ions dissolve in water at pH values different from pH 7.6. In a nuclear waste repository, partial areas in the host rock could be contacted with fluid having a lower or higher pH value than pore water, for instance due to microbial processes (pH 6.7; Wersin et al., 2010) or due to leaching of concrete from the geo-engineered barriers (pH > 12.5; Bradbury and Baeyens, 2004). Thus, leaching studies with OPA were performed in a wide pH range. The characteristics of OPA before and after contact with 0.1 mol/L $NaClO_4$ and the dissolved ions found in solution were investigated in dependence on pH. Under natural conditions, the S/L ratio of clay rock and water is much larger than the ratio of 4 g/L that is applied in these experiments. Furthermore, the background electrolyte has an ionic strength that is two or three times larger (cf. section **2.3.1**) than the ionic strength used in these experiments. However, these investigations were fundamental for further studies, where the U(VI) and humic acid sorption onto OPA in dependence on pH were investigated by batch sorption experiments (cf. section **4.5**) and surface complexation modeling. The results of these studies are published in Joseph et al. (2013, accepted).

Zeta potential measurements showed that with decreasing pH from pH 7.5 to 2.5, the zeta potential of OPA suspensions increased from –35 mV to –18.1 mV (cf. **Fig. 6**). The continual negative ζ values imply that the charge of the OPA particles at the plane between Stern and diffuse layer is negative throughout the studied pH range. The negative (permanent) charge is dominating the basal surfaces of the clay minerals and could not be compensated.

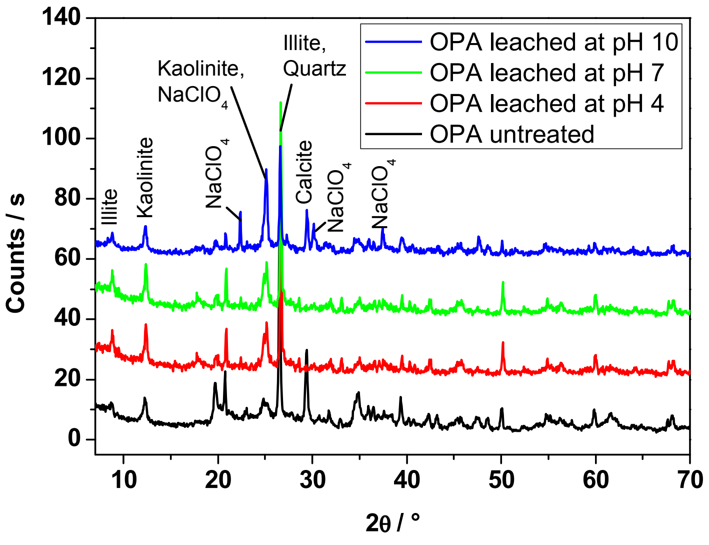

Fig. 13: X-ray diffractograms of untreated OPA (batch BHE-24/1) and OPA leached out with 0.1 mol/L $NaClO_4$ at pH 4, 7, and 10. The diffractograms are shifted along the y-axis for clarity.

OPA samples which were leached at pH 4, 7, or 10 for 90 days were studied by XRD. Compared to the diffractogram of untreated OPA, additional patterns were detected in the resulting diffractograms (cf. **Fig. 13**). These were attributed to the background electrolyte $NaClO_4$. As expected for pH 4 and 7, the calcite pattern did not appear in the diffractograms obtained from the pH-equilibrated samples because of acid addition. The calcite fraction was leached out after 90 days. Further changes in the diffractograms were not observed. Secondary mineral phases could not be detected.

The samples used for XRD measurements were also investigated by Mössbauer spectroscopy. The contents of Fe(II) and Fe(III) in aerobic untreated and pH-equilibrated OPA samples are shown in **Tab. 9**. According to those data, about 45 % of Fe(II) originally contained in anaerobic OPA is already oxidized to Fe(III) in OPA crushed and stored under aerobic conditions. Further oxidation took place due to contact with the aqueous solution. This effect was observed for all pH values studied. Therefore, it can be assumed that about 50 % of the iron in the OPA samples used for the pH-dependent sorption experiments (cf. section **4.5**) are still present as Fe(II). Presumably, ferrihydrite is formed during this oxidative process. Ferrihydrite is thermodynamically unstable and acts as a precursor for more crystalline minerals such as hematite and goethite (Cornell and Schwertmann, 2003).

Tab. 9: Results of Mössbauer spectroscopy and N_2-BET measurements (error: 2σ).

Sample	**Fe(II) / %**	**Fe(III) / %**	**N_2-BET / m^2/g**
Untreated OPA	55.1 ± 4.0	44.9 ± 2.4	41.3 ± 0.5 *
pH 4	47.5 ± 5.6	52.5 ± 4.0	47.1 ± 0.6
pH 7	49.5 ± 4.2	50.5 ± 3.0	48.0 ± 0.5
pH 10	48.2 ± 8.8	51.8 ± 6.4	41.5 ± 0.5

* (Joseph et al., 2011)

As expected, the results of the N_2-BET measurements of the samples show a small increase of the specific surface area at pH 4 and 7 (**Tab. 9**). This is due to dissolution of carbonate containing minerals such as calcite under acid conditions, thereby, leaving a slightly more porous OPA.

Filtrates of suspensions of OPA obtained between pH 3 and 10 were analyzed for leached out ions. Furthermore, they were checked for the presence of colloids by photon correlation spectroscopy (PCS). No colloids were detected in any sample. However, a relatively high particle concentration would be needed to detect very small particles of about 1 nm in diameter. Thus, the presence of a low amount of very small colloids cannot be completely excluded.

In **Fig. 14**, the concentrations of ions leached out of OPA are shown for Ca, Mg, Sr, Si, Al, Fe, and SO_4^{2-} as a function of pH. At pH 3, the calcium concentration is about seven times higher than the magnesium concentration. Strontium is only present in traces since it is only contained in OPA as accessory mineral in form of celestite ($SrSO_4$) (0.02 - 0.06 wt.%, Pearson et al., 2003).

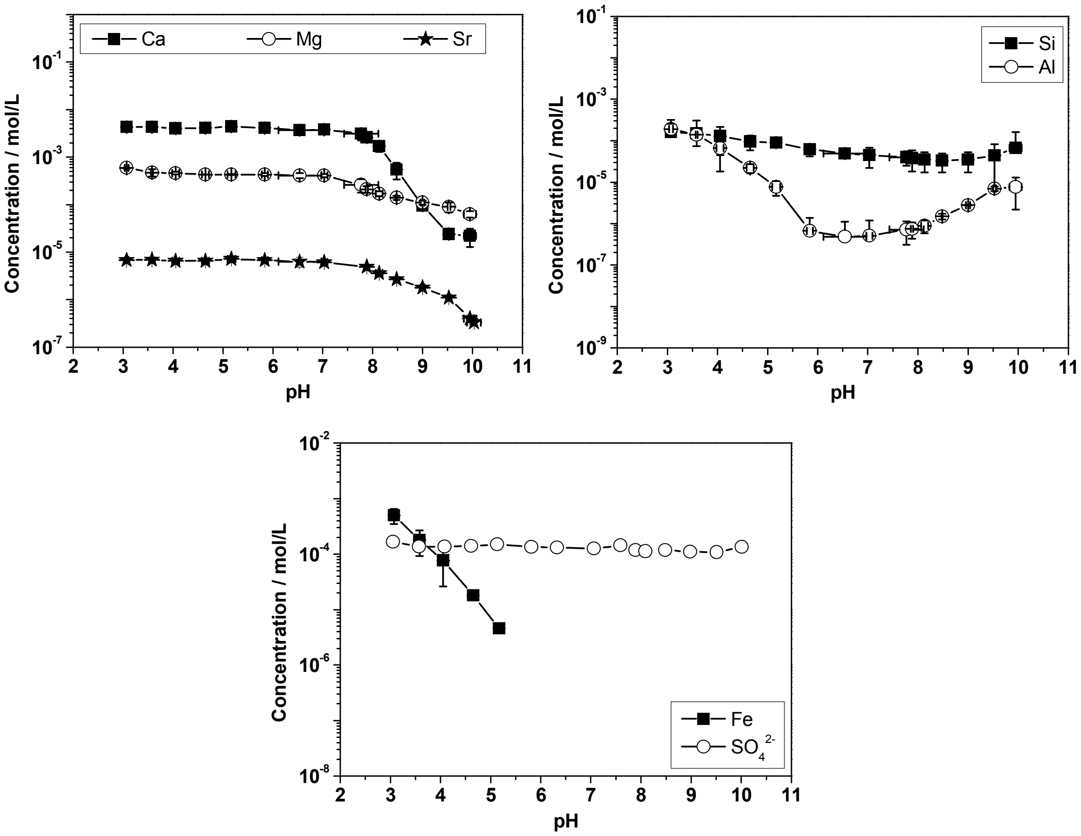

Fig. 14: Concentrations of Ca, Mg, Sr, Si, Al, Fe, and SO_4^{2-} in OPA suspensions contacted with 0.1 mol/L $NaClO_4$ (S/L = 4 g/L) as a function of pH.

The influence of pH on the clay mineral and quartz fractions of OPA is illustrated by the aluminum and silicon concentrations in solution. Especially at very low and very high pH values, dissolution of these minerals can be observed. Only at pH ≤ 5, iron is detected in solution, which results from dissolution of pyrite, siderite, and chlorite as well as of the formed Fe(III) mineral fraction of OPA. The sulfate concentration in solution originates from pyrite oxidation.

The pH-dependent concentrations of competing ions in solution lead to a pH-dependent ionic strength. The resulting I_t was calculated for each adjusted pH value based on the experimentally determined composition of the background electrolyte including the competing ions K, Mg, Ca, Sr, Al, Si, Fe, F^-, Cl^-, and SO_4^{2-} as well as the total inorganic carbon (TIC). In the pH range from pH 3 to 9, I_t amounts to 0.11 mol/L in average. Above pH 9, I_t increases to 0.21 mol/L at pH 10 due to elevated CO_2 intake from the atmosphere.

3 Uranium and humic substances

3.1 Uranium in the environment and in nuclear waste

Uranium was discovered by M. H. Klaproth in 1789 (Klaproth, 1789). Its most important isotopes are ^{238}U, ^{235}U, ^{234}U, and ^{233}U. The following compilation about the origin and properties of these isotopes is taken from Lieser (1980). ^{238}U is the main isotope in natural uranium (99.274 %). It is the parent nuclide of the radium decay series, where it decays by emission of alpha particles to ^{234}Th. ^{235}U can be found in nature with a percentage of 0.720 %. This parent nuclide of the actinium decay series is an alpha particle emitter, which decays to ^{231}Th. Both ^{238}U and ^{235}U have very long half-lives (cf. **Tab. 1**), thus being primordial. ^{234}U as daughter nuclide of ^{238}U represents the third natural uranium isotope (0.005 %). With a half-life of 2.455×10^5 a, it decays to ^{230}Th by emission of alpha particles. The radium and actinium decay chains end with stable isotopes of lead. ^{233}U is no longer present in nature. Nowadays, it is produced by neutron absorption of ^{232}Th, where firstly ^{233}Th is formed, which decays to ^{233}Pa and ^{233}U, respectively in a series by emission of one electron. ^{233}U belongs to the neptunium decay series. It is an alpha emitter and decays to ^{229}Th with a half-life of 1.592×10^5 a.

The electron configuration of the element uranium is [Rn] $5f^3$ $6d^1$ $7s^2$ (Cordfunke, 1969). It can exist in the oxidation states U(III), U(IV), U(V), and U(VI). Under acidic conditions, the trivalent and tetravalent oxidation states appear as simple hydrated ions, U^{3+} and U^{4+}, while the higher oxidation states form oxygenated species in solution called uranyl ions, UO_2^+ and UO_2^{2+} (Katz et al., 1986). Under environmentally relevant conditions the oxidation states U(IV) ([Rn] $5f^2$ $6d^0$ $7s^0$) and U(VI) ([Rn] $5f^0$ $6d^0$ $7s^0$) are most important (Silva and Nitsche, 1995). Thereby, U(IV) species appear mostly as relatively insoluble and immobile, while U(VI) species are predominantly more soluble and mobile (Fauth et al., 1985; Silva and Nitsche, 1995).

Uranium minerals found in nature are divided in reduced species containing U(IV) and oxidized species containing U(VI) (Burns, 1999). In addition, mixed-valence minerals (U(IV)-U(VI)) and at least one U(V) mineral (Burns and Finch, 1999) are described. Uranium deposits are dominated by reduced uranium minerals. The most important minerals for uranium mining are uraninite with the nominal composition UO_{2+x} (Finch and Murakami, 1999) and its botryoidal variety pitchblende (Fayek et al., 1997). Further economically interesting reduced uranium minerals are coffinite ($USiO_4\cdot n\ H_2O$) and brannerite ($(U,Ca,Y,Ce)(Ti,Fe)_2O_6$) (Finch and Murakami, 1999; WNA, 2012). Compared to reduced uranium minerals, a higher number of oxidized uranium species is known. They are formed by oxidative dissolution of uraninite caused by weathering processes (e.g., autunite $Ca[(UO_2)(PO_4)]_2\cdot10-12\ H_2O$, carnotite $K_2(UO_2)_2(V_2O_8)\cdot3\ H_2O$, liebigite $Ca_2(UO_2)(CO_3)_3{\cdot}11\ H_2O$) (Finch and Murakami, 1999).

The mined uranium is predominantly converted to UO_2, which is applied as nuclear fuel for energy production in fission reactors. The most important nuclear fuels are the uranium isotopes ^{233}U and ^{235}U as well as the plutonium isotope ^{239}Pu, since their nuclei are instable and can be easily split by absorption of slow (thermal) neutrons (Lieser, 1980). The artificial fissile isotopes ^{233}U and ^{239}Pu are produced by nuclear reactions in breeder reactors (Lieser, 1980). ^{235}U is the only natural fissile isotope. However, its fraction in natural uranium is too small to sustain a nuclear chain reaction (cf. **Fig. 15a**). Thus, it has to be enriched before its application as nuclear fuel. For this, technologies such as gaseous diffusion or centrifugation are used (Villani, 1979).

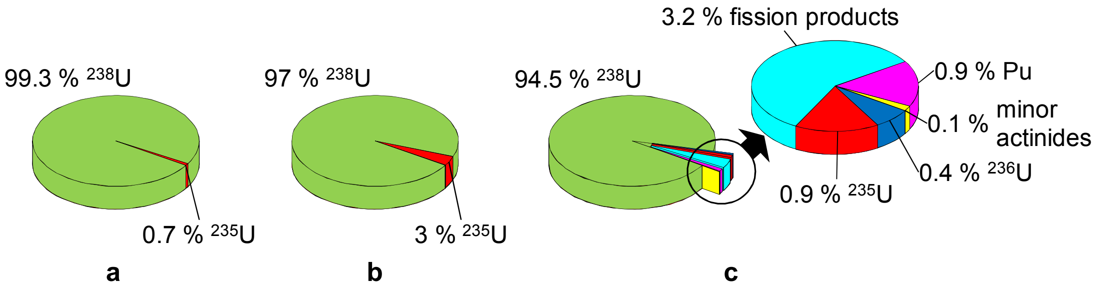

Fig. 15: Chemical composition of natural uranium (**a**), low-enriched uranium (**b**), and spent nuclear fuel (**c**) (values based on Volkmer, 2007).

During the enrichment procedure a depleted and an enriched uranium stream are yielded (NEA, 2006). Depleted uranium has a ^{235}U content of about 0.3 % (NEA, 2006). Due to its characteristics, depleted uranium is used, for instance, as X-ray radiation shielding in medicine and industry, armor-piercing ammunition, and defensive tank armor (Bleise et al., 2003). Enriched uranium is classified into different grades. In highly-enriched uranium the ^{235}U fraction is higher than 20 % (NEA, 2006). It is applied, for instance, for nuclear weapons, as propulsion of submarines, and as fuel for research reactors (Breivik, 2008). If the ^{235}U fraction is enriched to at least 90 %, the uranium is called weapons-grade (Breivik, 2008; Cochran and Paine, 1995). Low-enriched uranium contains less than 20 % ^{235}U. It is predominantly applied as nuclear fuel in the most commercially used nuclear reactors where a ^{235}U content of less than 5 % is required (cf. **Fig. 15b**).

The composition of spent nuclear fuel (**Fig. 15c**) shows that uranium with its isotopes ^{238}U, ^{235}U, and ^{236}U still represents the main component of the fuel after using in a nuclear power plant. The second largest fraction is presented by the fission products, which mainly consists of lanthanides (70 %), technetium (10 %), noble gases (7 %), and cesium (4 %) (Lieser, 1980). Due to neutron absorptions and decay reactions of ^{238}U, plutonium isotopes and minor actinides – such as isotopes of neptunium, americium, and curium – are also part of the spent nuclear fuel. They are the radionuclides with the highest long-term radiotoxicity (Lieser, 1980; OECD/NEA, 2006) and highest thermal output (Brasser et al., 2008) in the spent fuel.

Since the once-through nuclear fuel cycle is preferred in Germany (cf. section **1**), the spent nuclear fuel will be disposed directly. Consequently, uranium will be a large fraction of high-level nuclear waste stored in a nuclear waste repository. In case of water ingress in a repository, uranium (and other radionuclides) can be mobilized. In dependence on the present conditions, uranium may form soluble U(VI) species with the available surrounding anions, e.g., carbonate. For example, in **Fig. 16**, the U(VI) speciation under aerobic conditions in 0.1 mol/L NaCl as a function of pH is shown.

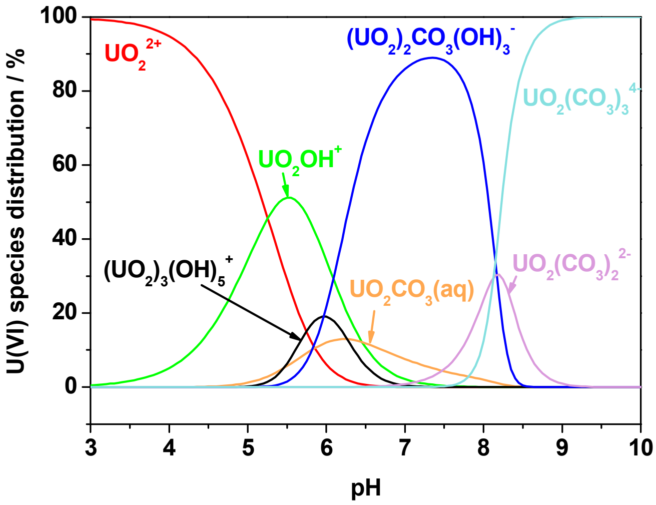

Fig. 16: Speciation of U(VI) as a function of pH in 0.1 mol/L NaCl ([U(VI)] = 1×10^{-6} mol/L; $pCO_2 = 10^{-3.5}$ atm). Only species > 5 % are shown.

The formed uranium species can migrate through the host rock as far as they reach the aquifer system. Further anthropogenic sources of uranium in near-surface groundwater are phosphate fertilizers (Birke et al., 2009) and dissolved depleted uranium ammunition (Schimmack et al., 2007), that was used by the US air force in Gulf War (1991), Bosnia-Herzegovina (1995), and Kosovo (1999) and which is still distributed in the environment. From the groundwater, uranium species can be transported into the biosphere, where they can enter the food chain.

The long-lived uranium isotopes are both radiotoxic and chemotoxic (Bleise et al., 2003; Burkart, 1991). The alpha particles emitted from the uranium isotopes have only little penetrating power (4 cm in air, 50 µm in soft tissue) and thus are unable to move deeply in human skin. However, if once uranium is incorporated, the alpha particles have a harming effect on the cells. Thus, uranium is considered as internal radiation hazard (Bleise et al., 2003), which delivers a much higher radiation dose after entering the body (Burnham, 2001).

To identify and characterize dissolved or solid uranium species, primarily spectroscopic techniques such as time-resolved laser-induced fluorescence spectroscopy (TRLFS) (Brachmann, 1997), attenuated total reflection FT–IR (ATR FT–IR) spectroscopy (Müller et al., 2008), X-ray absorption spectroscopy (XAS) involving X-ray absorption near-edge structure (XANES) and extended X-ray absorption fine-structure (EXAFS) measurements (Nitsche, 1995), and ultraviolet-visible (UV-vis) spectroscopy (Moll et al., 2003) are applied.

As shown above, the contact of uranium with soil components can have different reasons. In the present work, the investigation of the uranium interaction with OPA and kaolinite shall expand the knowledge about uranium sorption and migration behavior in a potential nuclear waste repository situated in clay rock. However, the results are also relevant for the above mentioned interaction scenarios of uranium with soil, since clay is an important soil component.

For experiments, solutions of depleted uranium were applied. In addition, ^{233}U solutions were used exclusively or in a mixture with depleted uranium solutions. Within the performed sorption and diffusion experiments, the interpretation of the behavior of uranium under different conditions was mainly based on the analysis of the uranium concentration in solution. For this, inductively coupled plasma – mass spectrometry (ICP–MS; ^{238}U) and liquid scintillation counting (LSC; ^{233}U) were applied. ^{233}U was used since it allows the simultaneous determination of the uranium and humic acid concentration in solution with LSC without any high preparative effort. By this means, the analysis of small sample volumes (≤ 250 µL) without further dilution and a high sample throughput were possible. Furthermore, TRLFS and EXAFS studies were performed to investigate uranium species in solution or sorbed onto OPA.

3.2 The characteristics of humic substances

Humic substances represent an important family of organic compounds occurring in soils, waters, and sediments. In natural clay, they are strongly associated with the mineral components. However, they can be released under certain conditions as shown for Callovo-Oxfordian Clay from Meuse/Haute Marne, France treated with an alkaline solution (Claret et al., 2003). OPA from Mont Terri contains about 1.5×10^{-3} wt.% humic material (Pearson et al., 2003).

Humic substances have no definite structure since these macromolecular biopolymers are compounds of plant, animal, and microbial origin which were highly transformed by biological and chemical processes (Hayes, 1998). Their composition and structure depends on the origin and age of the material. Generally, their structure is described as a hydrophobic framework of aromatic rings linked by more flexible carbon chains equipped with different functional groups (e.g., carboxyl, hydroxyl, amine) (Davies and Ghabbour, 1998). The resulting carbon skeleton contains micropores of various sizes which can be occupied by inorganic ions as well as small organic compounds (Schulten and Leinweber, 1996). One example of a schematic structure of humic substances is shown in **Fig. 17**.

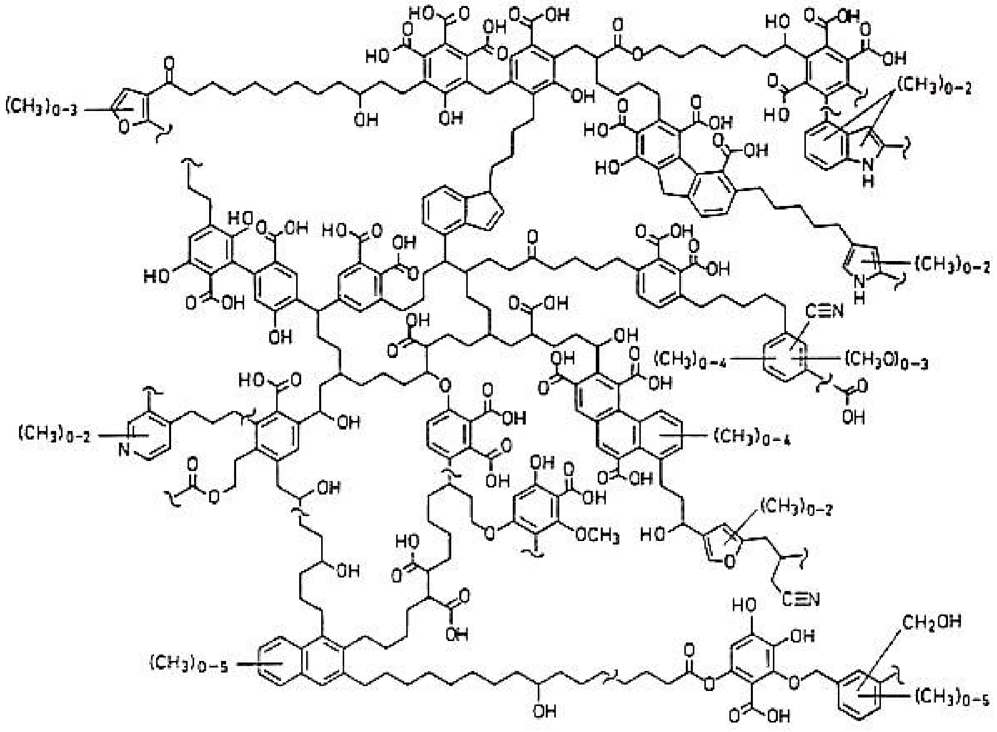

Fig. 17: Hypothetical structure of humic substances adopted from Schulten and Schnitzer (1993); Fig. 1.

Due to their diversity, humic substances are classified by their aqueous solubility, which mainly depends on their molecular weight and their functionality (Davies and Ghabbour, 1998). Separation and purification procedures of humic substances are based on this important property. Humic substances are grouped into fulvic acids, humic acids, and humins.

Fulvic acids have the lowest molecular weight of all humic substances, ranging from 500 to 2000 Da (von Wandruszka, 2000). They are soluble and consequently mobile at all pH values.

Humic acids (HA) are highly functionalized compounds. They are soluble over a wide pH range but not under acidic conditions. Their typical molecular weights extend a range from 2 to 1300 kDa (von Wandruszka, 2000).

Humins have the highest molecular weight of all humic substances. They have a dominating aromatic character and are insoluble at all pH values.

Humic substances are generally composed of 38 – 65 % C, 31 – 55 % O, 3.4 – 5.7 % H, 0.3 – 3.4 % N, 0.2 – 4.6 % S, and 0 – 0.6 % P (Suffet and MacCarthy, 1989). Thereby, the heterogeneity in elemental composition is pronounced stronger in HA than in fulvic acids (Gaffney et al., 1996). The dominating functional groups are carboxyl, phenolic, hydroxyl, ketonic, and quinone groups (Stevenson, 1985). Fulvic acids contain more carboxyl, phenolic, and ketonic groups than HA and have more aliphatic than aromatic character (Stevenson, 1985). Thus, they are well soluble in aqueous solutions. HA are more aromatic and become insoluble when the carboxyl groups are protonated at low pH values. This diversity of functionalities in the structure allows humic substances to bind both hydrophilic and hydrophobic species (Gaffney et al., 1996).

The conformation of humic substances is still unclear. Generally, two concepts can be found in literature (Pédrot et al., 2010; von Wandruszka, 2000). On the one hand, humic substances are described as macromolecular polyelectrolytes that can form molecular aggregates. On the other hand, humic substances are regarded as supramolecular assemblies of small molecules without macromolecular character. The individual compounds are connected by weak attraction forces (van der Waals forces, electrostatic forces, hydrogen bonds). Pédrot et al. (2010) preferred the second concept as they observed supramolecular associations of small molecules in their experiments. However, they were not able to exclude the presence of macromolecules in the bulk dissolved organic matter. Irrespective of the size distribution of the humic substance molecules, it is known that their amphiphilic character, in particular in case of HA, leads to intra- and intermolecular aggregation of the molecules to so-called pseudomicelles (von Wandruszka, 2000). The molecules fold and coil in a manner that hydrophilic functional groups are situated outward and more hydrophobic parts of the structure are placed in the center of the pseudomicelle (cf. **Fig. 18**).

Pseudomicelles are colloidal particles (Guetzloff and Rice, 1996). Thereby, the size of colloids ranges from 1 nm to 1 µm. The hydrophilic character on the colloidal surface results from various electrical charges, which originate from several acidic and basic groups (e.g., carboxyl, phenolic, and amine). They influence the conformation by repulsion and attraction effects of equal or opposed charged sites, which leads to expansion or coiling of the molecules (Hayes, 1998). The charge and consequently, the conformation of humic substances can be affected by variation of humic substance concentration, pH value, and ionic strength (Gaffney et al., 1996; Pédrot et al., 2010). Thereby, the influence of the pH value is stronger than the effect of the ionic strength (Pédrot et al., 2010). Under environmental conditions (low humic substance and electrolyte concentration, neutral pH), humic substances form linear polyelectrolytes (Gaffney et al., 1996).

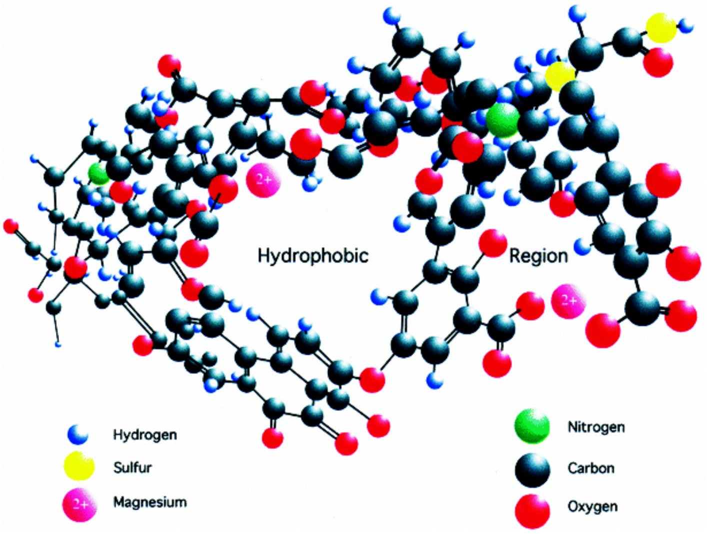

Fig. 18: Humic acid pseudomicelle (adopted from von Wandruszka (2000); Fig. 2).

To characterize humic substances and to distinguish between the various types, several methods can be used. For determination of the size distribution of the humic substance aggregates various fractionation techniques are available such as ultrafiltration (Pédrot et al., 2010) or gel permeation chromatography (Kim et al., 1990). Spectroscopic methods provide information about certain structural features of humic substances but not of the total structure, for instance, UV-vis spectroscopy, FT–IR spectroscopy, and ^{13}C-nuclear magnetic resonance spectroscopy (Bortiatynski et al., 1996; Chen et al., 1977; MacCarthy and Rice, 1985). The acidity of humic substances, which mainly originates from the carboxyl and phenolic groups, is characterized by the proton exchange capacity (PEC). Using direct titration, the PEC can be calculated (Kim et al., 1990). The resulting value is often slightly higher than the amount of carboxyl groups but significantly smaller than the total proton exchange capacity, which is determined by reaction with $Ba(OH)_2$ (Stevenson, 1982). It was suggested that the PEC determines mainly the carboxyl group capacity of a humic substance; however, a small fraction of weak acidic groups is also included (Kim et al., 1991).

The wide variety of functional groups explains the strong complexation ability of humic substances with inorganic as well as organic compounds. Since this study is focused on uranium and clay minerals, only the interaction of humic substances with metal ions will be discussed further. The complex formation of natural HA was already investigated for actinides such as Th(IV) (Beneš, 2009), U(VI) (Czerwinski et al., 1994; Montavon et al., 2000; Sachs et al., 2007a; Steudtner et al., 2011a), Np(IV) (Schmeide et al., 2005), Np(V) (Seibert et al., 2001), Pu(III) (Mahajan et al., 1989; Schmeide et al., 2006), Pu(IV) (Szabó et al., 2010), Am(III) (Czerwinski et al., 1996; Morgenstern et al., 2000; Sakuragi et al., 2004), and Cm(III) (Czerwinski et al., 1996; Morgenstern et al., 2000). Methods such as ultrafiltration (Czerwinski et al., 1996), anion exchange (Montavon et al., 2000), TRLFS (Sachs et al., 2007a), ATR FT–IR spectroscopy (Steudtner et al., 2011a), or UV-vis spectroscopy (Seibert et al., 2001) were used to determine stability constants of the actinide HA complexes. A large binding heterogeneity for metal ions is observed due to the wide variation in HA functionality, which makes it difficult to determine HA complexation constants. To solve this problem, several models for the description of metal ion binding to HA were developed and reported in literature such as the metal ion charge neutralization model (CNM) of Kim and Czerwinski (1996), the Humic Ion-Binding Model VI of Tipping (1998), or the consistent nonideal competitive adsorption (NICCA)-Donnan model of Kinniburgh et al. (1999).

Primarily, functional groups such as carboxyl, hydroxyl, phenolic, and ketonic groups are responsible for metal ion complexation (Stevenson, 1985). Thereby, carboxyl groups are dominating. However, nitrogen- and sulfur-containing groups can be also involved in complex formation (Khwaja et al., 2006; Stevenson, 1985). To determine their specific contribution to complexation, HA can be synthesized from amino acids and carbohydrates based on the melanoidin concept (Pompe et al., 1996). The resulting compounds behave similar to natural HA (Pompe et al., 1996; Pompe et al., 1998), but with the advantage that their functionality can be defined by the preparation procedure. For instance, this method was applied to investigate the role of sulfur functionalities in HA on the complexation of U(VI) (Sachs et al., 2010). Another concept to investigate the specific contribution of the humic substance functional groups is the application of small organic model ligands for complexation studies. These model ligands represent building blocks of humic substances. Recently, it was shown by this means that sulfur and nitrogen functionalities play only a subordinate role in U(VI) complexation by HA compared to carboxyl groups (Kremleva et al., 2012; Raditzky et al., 2010).

Beside their complexation ability, humic substances are known for their inherent redox properties, which were already investigated for the actinides uranium, neptunium, and plutonium (Marquardt et al., 2004; Sachs and Bernhard, 2011; Schmeide and Bernhard, 2009; Schmeide et al., 2012).

HA colloids are mobile and thus can be transported through surface and groundwater as it was already shown for HA leached out of soil in the surroundings of the potential German nuclear waste disposal site Gorleben (Artinger et al., 2000). Along with their complexation and redox properties HA may influence the migration of metal ions in geological environments as shown for U(VI) in quartz sand (Artinger et al., 2002; Mibus et al., 2007b), U(VI) in compacted kaolinite (Sachs et al., 2007b), and Eu(III) in sedimentary rock (Seida et al., 2010). Thus, the presence of humic substances is an important influencing factor with regard to the interaction of actinides with clay minerals and clay rocks. This should be considered in the safety assessment of a nuclear waste repository.

In this study, the influence of HA on the sorption of U(VI) on kaolinite and OPA as well as the influence of HA on the migration of U(VI) in OPA was investigated (cf. sections **4** and **5**). For this, the in-house synthesized ^{14}C-labeled and unlabeled HA type M42 were used. Their characteristics are described in section **7.1.6** of this work. The ^{14}C-labeling resulted in beta particle emitting HA molecules, which then could be easily analyzed by LSC, simultaneously with the alpha particle emitter ^{233}U (cf. section **7.1.9**). Additionally, the ^{14}C-labeling enabled the performance and interpretation of experiments under environmentally relevant HA concentrations (Pompe et al., 2000a).

4 Sorption of U(VI) and humic acid onto clay

4.1 Description of sorption processes

In the case of water ingress in a nuclear waste repository, radionuclides are released. The dissolved radionuclides can interact with the different solid phases present within the repository and its surroundings. For safety case assessment, the processes occurring at the surface of the solids are of particular scientific interest. Therefore, sorption represents one of the fundamental surface phenomena which significantly influences the mobility of the radionuclides.

Adsorption describes the concentration or agglomeration of compounds at the boundary of two phases, e.g., liquid / solid, gas / solid. In general, physisorption and chemisorption are distinguished. Physisorption describes the physical process where the substance is mainly bound to the surface by van der Waals forces (dipole-dipole interaction, London dispersion force, Debye (induced dipole) force). Energies for this interaction do not reach values > 50 kJ/mol (Kümmel and Worch, 1990). For chemisorption a chemical reaction between compound and surface is postulated with interaction energies ranging from 60 to 450 kJ/mol (Kümmel and Worch, 1990). Usually, a covalent bond is formed.

“Adsorption” is distinguished from “absorption”. The latter means the migration of a substance from one phase into the bulk of another by diffusion. Adsorption and absorption processes can occur simultaneously. In such a case, the shorter term “sorption” is used (Ościk, 1982). This term is also applied in the present study, since adsorption and absorption were not distinguished in the performed experiments.

Primarily, sorption isotherms are used to describe sorption processes occurring in the two phase system liquid / solid, such as those studied in the present work. So far, no universally applicable isotherm equation is available, which describes the sorption behavior adequately in each case. Thus, for each investigated system a series of equations has to be tested for their adaptability. The isotherms are classified with regard to the number of parameters they contain. In this study, only examples of one and two parameter isotherms shall be discussed closer. In general, isotherms describe the relation of the amount of a substance sorbed on the solid phase in equilibrium, a_{eq} [µg/kg], to the equilibrium concentration of the substance in solution, c_{eq} [µg/m^3], at a constant temperature, T (Kümmel and Worch, 1990). The simplest sorption isotherm is represented by the linear isotherm after Henry (1803) (**Eq. 1**). This equation contains only one new parameter, K_d [m^3/kg], the distribution coefficient (or Henry’s sorption constant) and is only valid at low substrate concentrations.

$$a_{eq} = K_d \cdot c_{eq} \qquad \textbf{Eq. 1}$$

The most commonly used two parameter isotherms are the equations found by Freundlich (1906) (**Eq. 2**) and Langmuir (1918) (**Eq. 3**).

$$a_{eq} = k_F \cdot c_{eq}^{n_F} \qquad \textbf{Eq. 2}$$

$$a_{eq} = \frac{a_m \cdot b \cdot c_{eq}}{1 + b \cdot c_{eq}} \qquad \textbf{Eq. 3}$$

The two new parameters of the empirically found Freundlich isotherm are denoted as Freundlich coefficient, k_F [m^3/kg], and Freundlich exponent, n_F [–]. These parameters depend on the nature of the dissolved substance and the temperature (Freundlich, 1906). Usually, the Freundlich isotherm is applied to describe sorption in the medium concentration range (Kümmel and Worch, 1990) on heterogeneous surfaces (Moore et al., 1986).

The Langmuir isotherm contains two new parameters, a_m and b. Here, b [m^3/µg] is the Langmuir sorption coefficient (Vodrážka, 1979). a_m [µg/kg] means the amount of substance which can sorb onto the solid in maximum ($b \cdot c_{eq} >> 1$) (Kümmel and Worch, 1990). Thus, in contrast to the Freundlich isotherm the saturation state is taken into consideration in the Langmuir equation. Additionally, for the Langmuir isotherm the following assumptions were made: (i) sorption occurs on a regular plane surface consisting of only one kind of sorption sites; (ii) molecules are sorbing in a monomolecular layer on the solid and each sorption site is occupied by only one molecule; (iii) no interaction occurs between the individual sorbed molecules (Langmuir, 1918; Moore et al., 1986). At low concentrations ($b \cdot c_{eq} << 1$), the Langmuir equation becomes the Henry isotherm with $a_m \cdot b = K_d$.

Normally, the adjustable parameters of the isotherms are determined by linear regression. There are at least three different ways to linearize the Langmuir isotherm (Kinniburgh, 1986). The linearized form of the Freundlich isotherm is represented in **Eq. 4** (Vodrážka, 1979).

$$\log\left(a_{eq}\right) = \log\left(k_F\right) + n_F \cdot \log\left(c_{eq}\right) \qquad \textbf{Eq. 4}$$

If $n_F = 1$, the Freundlich isotherm becomes the Henry isotherm. Then, k_F is equal to K_d.

There are different data bases of K_d values (Bradbury et al., 2010; Jung et al., 2001; Tachi et al., 2011), where data for the sorption of various radionuclides onto different solids are collected. However, several factors that influence the sorption affinity are often not considered in such data bases, e.g., S/L ratio, pH, and temperature. In previous studies, different methods were used to consider several influencing factors. Payne et al. (2011) was able to compare the sorption of U(VI) onto different geological materials by normalization of the respective K_d values with the specific surface areas of the materials. Samper et al. (2010) and Lu et al. (2012) developed variable-K_d models, which consider the dependence of K_d on ionic strength and initial substrate concentration as well as on the pH.

Complementary to the K_d concept, sorption processes can be described theoretically by surface complexation models (SCM) (Stumm, 1992). In such models the sorption of aqueous species is interpreted as chemical reactions on specific mineral surface binding sites, whereby sorbed surface species result. In general, data bases are created, which combine protonation constants of surface binding sites found on the respective mineral and substance-dependent complexation constants of the formed surface species. Several types of SCM are known. They can be distinguished with regard to their description of surface protonation reactions and their electrostatic terms, e.g., constant capacitance model (Schindler and Gamsjäger, 1972; Stumm et al., 1970; Stumm et al., 1976; Stumm et al., 1980), generalized two-layer model (Dzombak and Morel, 1990), or triple layer model (Davis et al., 1978). However, in all models solid surface binding sites ($\equiv$X–OH) are the essential components.

Two modeling approaches are used to describe sorption by SCM, the “generalized composite” approach and the “component additivity” approach (Davis et al., 1998). The generalized composite approach simulates sorption using generic surface binding sites. The surface complexation model parameters (variety of binding site types, chemical reactions) are varied in such way that they fit the experimental data. Only little information about the system is required. However, the approach is always specific for the investigated system. For instance, it was used to model the U(VI) sorption onto Hanford sediment (Um et al., 2007) or the sorption of rare earth elements onto basaltic rock (Tertre et al., 2008). The component additivity approach predicts sorption using unique surface binding sites for each sorbing substance. Thereby, known surface complexation data for simple systems are collected and combined in one data base to describe mineralogically complex systems. In this context, “blind prediction” sorption modeling describes a methodology to model unknown systems without performing specific experiments, which should be the most prominent goal of thermodynamic data bases. The validation of such predictions by independent experiments provides insight into the correctness, completeness, and significance of the species and reactions building up the model in use. In case of discrepancies between model and experiment, it shows the gaps in the data base, where further experiments are needed. Previously, this approach was applied to describe the U(VI) sorption on granite (Nebelung and Brendler, 2010) and OPA (Joseph et al., 2013, accepted).

In the present study, batch sorption experiments were performed to investigate the influence of the background electrolyte, the S/L ratio, HA, and pH on U(VI) sorption onto OPA and kaolinite. Sorption isotherms were determined to calculate K_d values for the U(VI) and HA sorption onto OPA. The findings provide a first hint of the retention strength of OPA toward U(VI) and the factors that influence the mobility of U(VI) in the system. The determined K_d values will be compared with the results obtained by diffusion experiments discussed in section **5**.

4.2 Sorption of actinides onto clay minerals and clay rocks

Clay-containing soils and sediments as well as clay rocks have a complex mineralogy as already discussed in section **2.3**. To understand and correctly quantify the contribution of the clay fraction on actinide interaction in such heterogeneous systems, batch sorption experiments with pure clay minerals such as kaolinite (Křepelová et al., 2006; Sachs and Bernhard, 2008; Schmeide and Bernhard, 2010), montmorillonite (Bradbury and Baeyens, 2006; Chisholm-Brause et al., 2001; Kowal-Fouchard et al., 2004), and illite (Bradbury and Baeyens, 2009) were performed in previous studies. These pure clay minerals can also be found in natural clay rocks. Since pure clay minerals have a definite composition, the possible interaction processes are easier to elucidate and to model. Furthermore, inert background electrolytes such as sodium chloride (Kornilovich et al., 2000; Redden et al., 1998), sodium nitrate (Thompson et al., 1998), or sodium perchlorate (Bradbury and Baeyens, 2006; Kowal-Fouchard et al., 2004; Křepelová et al., 2006; Sachs and Bernhard, 2008; Schmeide and Bernhard, 2010) were used in these experiments. Thus, an influence of competing ions had not to be considered.

To approach natural conditions, organic matter was added to these binary systems. For instance, the sorption of Eu(III), Th(IV), Np(IV), Np(V), and U(VI) onto pure clay minerals in the absence and presence of HA (Křepelová et al., 2006; Schmeide and Bernhard, 2010) or fulvic acid (Kornilovich et al., 2000) was investigated. It was observed that the metal ion sorption onto clay minerals is strongly affected by the presence of humic substances, since they increased or decreased the metal ion sorption depending on pH (Křepelová et al., 2006; Schmeide and Bernhard, 2010) or humic substance concentration (Kornilovich et al., 2000; Křepelová et al., 2006).

Clay and HA are negatively charged under environmental conditions. Both can interact with positively charged metal ions, which neutralize the charges (Stevenson, 1985). Thus, clays, or minerals in general, humic material, and metal ions can form associates. A schematic description of such a ternary system and its various interaction processes is given in **Fig. 19**.

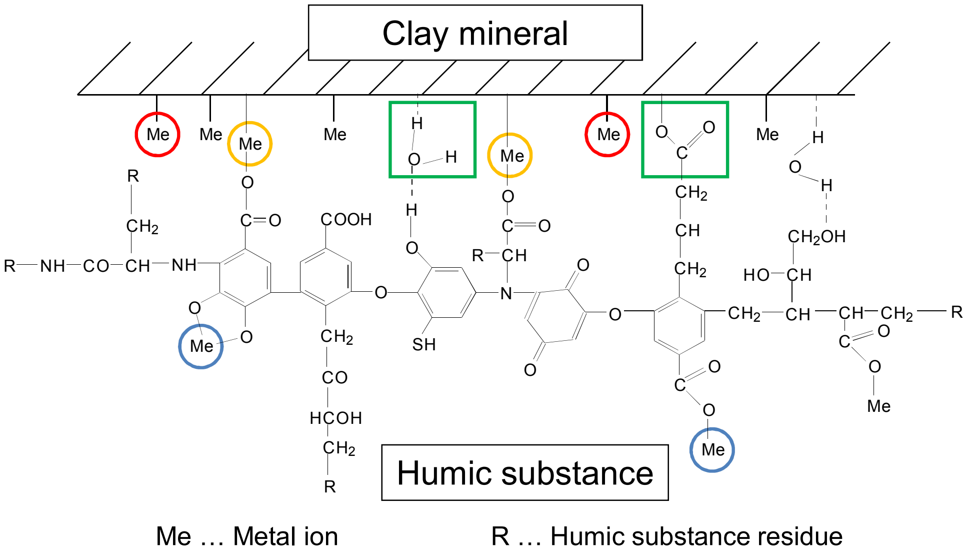

Fig. 19: The ternary system metal ion / humic substance / clay mineral: (red) metal ions can sorb onto the clay surface; (yellow) sorbed metal ions can serve as bridging compound between clay and humic material; (green) the humic substance can sorb directly on the clay surface; (blue) humic substances can complex metal ions via a variety of functional groups (adopted from Sachs et al., 2009; Fig. 3; based on Stevenson, 1985).

Currently, sorption studies are extended from pure clay minerals to complex natural clay rocks, which are discussed as possible host rock for nuclear waste disposal sites. In Europe, these are, e.g., OPA from Mont Terri, Switzerland (Fröhlich et al., 2011; Hartmann et al., 2008; Joseph et al., 2011; Schott et al., 2012; Wu et al., 2009), Callovo-Oxfordian Clay from Meuse/Haute Marne, France (Hartmann et al., 2008), Boom Clay from Mol, Belgium (Hart et al., 1994), and Boda Claystone from Mecsek, Hungary (Mell et al., 2006). In natural clay rocks, complex salt solutions, the so-called pore water, occur as background electrolyte as described already for OPA in section **2.3.1**. Pore water contains ions which can act as competing reactants in sorption studies. So far, only a few studies used pore water as background electrolyte for sorption experiments (Fröhlich et al., 2012; Joseph et al., 2011; Schott et al., 2012; Wu et al., 2009).

The pH-dependent sorption of actinides or lanthanides on natural clay rocks, especially OPA, was rarely studied. This is not surprising since natural clay is usually in equilibrium with its pore water. However, the intention to investigate the pH-dependent sorption using an inert background electrolyte is that the results can be compared to known systems of pure clay minerals to assess the individual contributions of the various minerals to the observed overall sorption behavior. The interaction of U(VI), Eu(III), and Cm(III) with OPA and Callovo-Oxfordian Clay in 0.1 mol/L $NaClO_4$ was investigated by Hartmann et al. (2008) by batch sorption and spectroscopic experiments as well as by geochemical calculations. They found that the clay minerals in the clay rock act as main sorbents for tri- and hexavalent actinides. Lippold and Lippmann-Pipke

(2009) studied the Tb(III) sorption onto OPA and the influence of HA on this interaction. By comparing their results with model data, they observed a few nonlinearities which were ascribed to the presence of competing ions originating from the clay (calcium, magnesium, aluminum, iron). Fröhlich et al. (2011) investigated the Np(V) sorption onto OPA as a function of pH, Np(V) concentration, solid-to-liquid ratio, and partial pressure of CO_2 in saturated calcite solution. They assumed that, in dependence on pH and Np(V) concentration, Np(V) is sorbed onto different OPA surface binding sites.

In the following sections the sorption experiments performed in the present study are discussed in detail.

Section **4.3** presents the results for the U(VI) sorption onto the pure clay mineral kaolinite at pH 7.6. Therein, the influence of HA and background electrolyte was studied.

In literature, sorption studies are dominating which focusing on the binary systems actinide / clay at $I \leq 0.1$ mol/L. However, so far, no studies are known which investigate ternary systems actinide / humic substance / clay at a higher ionic strength, where a more complex chemistry is expected. Thus, in section **4.4**, results are presented concerning the U(VI) sorption onto OPA in the absence and presence of HA using synthetic OPA pore water (pH 7.6) as background electrolyte. The competing ions, originating from the pore water, can control the speciation of U(VI) and HA by forming soluble or insoluble species or occupying important binding sites. The examination of the pore water effects was coupled with sorption and spectroscopic experiments to verify the results of speciation calculations.

In section **4.5**, sorption experiments with the ternary system U(VI) / HA / OPA are described in dependence on pH using an inert background electrolyte (0.1 mol/L $NaClO_4$). Within these experiments, it was clarified to which extent U(VI) can be mobilized by HA in dependence on pH. Going beyond the findings of Lippold and Lippmann-Pipke (2009) it was investigated which ions leached out of the clay (cf. section **2.3.2**) are actually interacting with U(VI) and HA.

4.3 The system U(VI) / humic acid / kaolinite

4.3.1 Speciation of U(VI) at pH 7.6 in dependence on background electrolyte

In dependence on the experimental conditions, different U(VI) and HA species are present in solution. Based on the OECD/NEA data base (Guillaumont et al., 2003), the U(VI) and HA species distribution was calculated using the speciation code EQ3/6 (Wolery, 1992). HA complexation constants were included in calculations based on the CNM. A detailed description of the computations is given in section **7.6.1.**

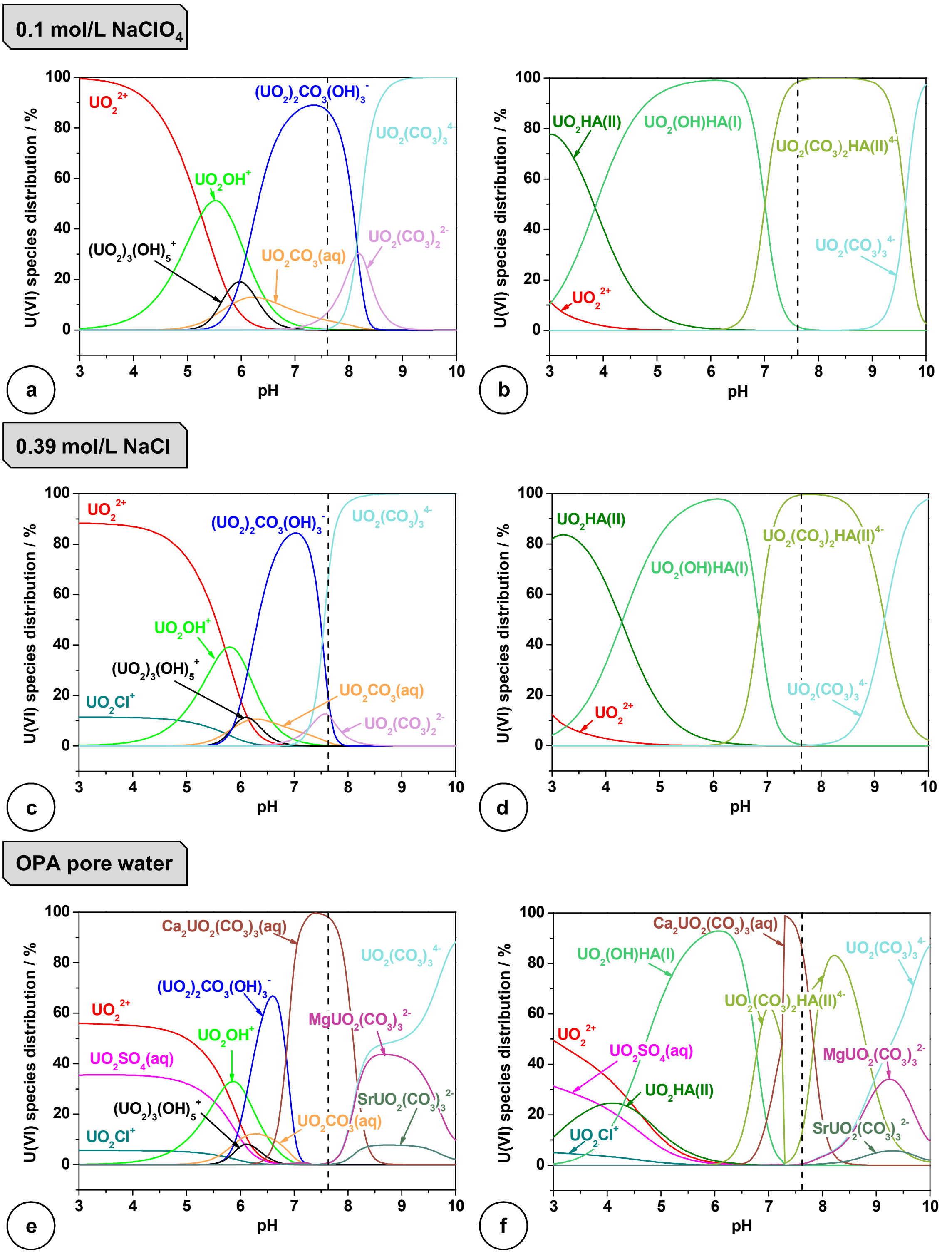

Fig. 20: Speciation of U(VI) as a function of pH in 0.1 mol/L $NaClO_4$ (**a, b**), 0.39 mol/L NaCl (**c, d**), and OPA pore water (**e, f**) both in the absence (**a, c, e**) and presence (**b, d, f**) of HA ([U(VI)] = 1×10^{-6} mol/L; [HA] = 50 mg/L). Only species > 5 % are shown.

In **Fig. 20**, the speciation of U(VI) (1×10^{-6} mol/L) is shown in dependence on the background electrolyte (0.1 mol/L $NaClO_4$, 0.39 mol/L NaCl, OPA pore water) and in the absence and presence of 50 mg HA/L, respectively. Oxidizing aerobic conditions were assumed in the calculations (room temperature, E_h = 800 mV, $pCO_2 = 10^{-3.5}$ atm). The following discussion is focused on pH 7.6, since sorption experiments onto kaolinite with different background electrolytes (cf. section **4.3.2**) as well as sorption and diffusion studies with OPA in pore water (cf. section **4.4** and **5.6**) were performed at this pH value.

In 0.1 mol/L $NaClO_4$ in the absence of HA, the U(VI) speciation at pH 7.6 is dominated by $(UO_2)_2CO_3(OH)_3^-$ (87 %) (**Fig. 20a**). In the presence of HA (**Fig. 20b**), the so far established U(VI)-HA complexes, $UO_2HA(II)$ (Czerwinski et al., 1994), $UO_2(OH)HA(I)$ (Zeh et al., 1997), and $UO_2(CO_3)_2HA(II)^{4-}$ (Steudtner et al., 2011a) are formed in dependence on pH in different fractions. At pH 7.6, $UO_2(CO_3)_2HA(II)^{4-}$ dominates the U(VI) speciation to almost 100 %.

To approximate pore water conditions, 0.39 mol/L NaCl was used as background electrolyte, because the stoichiometric ionic strength of pore water is 0.39 mol/L and NaCl represents its main component (cf. **Tab. 20**). In the absence of HA, the U(VI) speciation at pH 7.6 is mainly comprised of $UO_2(CO_3)_3^{4-}$ (59 %), $(UO_2)_2CO_3(OH)_3^-$ (26 %), and $UO_2(CO_3)_2^{2-}$ (13 %) (**Fig. 20c**). In the presence of HA, the U(VI) speciation is again dominated by $UO_2(CO_3)_2HA(II)^{4-}$ at pH 7.6 (**Fig. 20d**).

Fig. 20e,f show the speciation of U(VI) in the absence and presence of HA in pore water as a function of pH. Since the concentration of ions is a function of pH, the pore water composition (cf. **Tab. 8**) is only valid at pH 7.6. Thus, **Fig. 20e,f** give an exact picture only at pH 7.6. The changing carbonate concentrations and the dissolution of calcite as a function of pH, however, have been considered in aqueous speciation modeling.

In pore water at pH 7.6, the U(VI) speciation is clearly dominated by $Ca_2UO_2(CO_3)_3(aq)$ (Bernhard et al., 2001) (**Fig. 20e**), indicating a significant influence of calcium and carbonate ions present due to dissolution of calcite. Other charged alkaline earth carbonato complexes with U(VI) are reported in the literature, $CaUO_2(CO_3)_3^{2-}$ (Bernhard et al., 2001), $SrUO_2(CO_3)_3^{2-}$ (Dong and Brooks, 2006), and $MgUO_2(CO_3)_3^{2-}$ (Dong and Brooks, 2006). Their presence was considered in the calculations; however, their influence was found to be negligible at pH 7.6 and thus they are not considered in further discussions. In the presence of HA (**Fig. 20f**), again, the $Ca_2UO_2(CO_3)_3(aq)$ complex is the dominant species at pH 7.6 (88 %). The $UO_2(CO_3)_2HA(II)^{4-}$ complex is formed with a fraction of 11 %. That means that the presence of HA has only a small effect on the speciation of U(VI) in pore water.

4.3.2 Sorption of U(VI) and humic acid at pH 7.6 in dependence on background electrolyte

In order to determine the influence of the applied background electrolyte on the U(VI) and HA sorption, batch sorption experiments with kaolinite were carried out using

0.1 mol/L $NaClO_4$, 0.39 mol/L NaCl, and pore water. The U(VI) sorption was investigated in the absence and presence of HA and the HA sorption was examined in the absence and presence of U(VI). The results were interpreted using the U(VI) speciation calculations shown in section **4.3.1**.

In **Tab. 10**, the results of the U(VI) sorption experiments with kaolinite are given.

Tab. 10: U(VI) sorbed onto kaolinite in dependence on background electrolyte in the absence and presence of HA (S/L = 4 g/L, pH 7.6) in comparison to literature data.

Background electrolyte	**0.01 mol/L $NaClO_4$ ***	**0.1 mol/L $NaClO_4$**	**0.39 mol/L NaCl**	**OPA pore water**
[U(VI)] = 1×10^{-6} mol/L	~ 98 %	(88.4 ± 1.1) %	(85.1 ± 1.5) %	(42.4 ± 4.2) %
[U(VI)] = 1×10^{-6} mol/L + [HA] = 10 mg/L	~ 90 %	(87.2 ± 1.7) %	(85.4 ± 2.2) %	(36.0 ± 1.9) %
[U(VI)] = 1×10^{-6} mol/L + [HA] = 50 mg/L	~ 65 %	(38.8 ± 4.6) %	(53.1 ± 1.4) %	(30.7 ± 2.8) %

* At pH 7.5 (Křepelová et al., 2006).

The U(VI) sorption onto kaolinite decreased slightly with increasing ionic strength of the inert background electrolyte, ranging from 0.01 mol/L $NaClO_4$ to 0.39 mol/L NaCl. The decrease can be attributed to the increasing concentration of $UO_2(CO_3)_3^{4-}$ in U(VI) speciation at pH 7.6 with increasing ionic strength (cf. **Fig. 20a,c**). This U(VI) species sorbs only weakly onto kaolinite compared to $(UO_2)_2CO_3(OH)_3^-$, which dominates the U(VI) speciation in 0.1 mol/L $NaClO_4$ (cf. **Fig. 20a**). This effect was slightly compensated by the fact that the samples of the 0.39 mol/L experiments had a final pH of 7.5, where the U(VI) speciation is composed of $UO_2(CO_3)_3^{4-}$ (36 %), $(UO_2)_2CO_3(OH)_3^-$ (48 %), and $UO_2(CO_3)_2^{2-}$ (12 %). Thus, the fraction of $UO_2(CO_3)_3^{4-}$ was in fact lower than for pH 7.6. In pore water, the amount of sorbed U(VI) decreased further. This is due to the formation of the neutral $Ca_2UO_2(CO_3)_3$(aq) complex, which seems to sorb only weakly onto the clay possibly due to its neutral character.

The presence of 10 mg HA/L had no significant effect on U(VI) sorption in all investigated systems. However, at concentrations of 50 mg HA/L the U(VI) sorption decreased significantly in all sorption experiments. This is due to the formation of $UO_2(CO_3)_2HA(II)^{4-}$, which leads to a mobilization of U(VI) (**Fig. 20b,d,f**).

The U(VI) sorption onto kaolinite in the presence of 10 mg HA/L was diminished with increasing ionic strength of the inert background electrolyte. At the presence of 50 mg HA/L the opposite effect was observed for the investigated systems. The U(VI) sorption increased from *I* = 0.1 mol/L to *I* = 0.39 mol/L. The U(VI) speciation in the presence of 50 mg HA/L (cf. **Fig. 20b,d**) cannot explain this increase. In 0.1 mol/L $NaClO_4$ and 0.39 mol/L NaCl, $UO_2(CO_3)_2HA(II)^{4-}$ is always dominating the U(VI) speciation at pH 7.6. However, as described in section **3.2**, the HA conformation is influenced by ionic strength. The higher the salinity of the background electrolyte the better the negative charges on the HA macromolecules are screened. This leads to coiling of HA. Thus, it is assumed that more coiled HA molecules were present in 0.39 mol/L NaCl solution than in 0.1 mol/L $NaClO_4$. Consequently, a higher amount of HA could sorb onto the kaolinite surface in 0.39 mol/L NaCl than in 0.1 mol/L $NaClO_4$.

The sorbed amounts of HA onto kaolinite in the absence and presence of U(VI) in dependence on background electrolyte are summarized in **Tab. 11**.

Tab. 11: HA sorbed onto kaolinite in dependence on background electrolyte in the absence and presence of U(VI) (S/L = 4 g/L, pH 7.6) in comparison to literature data.

Background electrolyte	0.01 mol/L $NaClO_4$ *	0.1 mol/L $NaClO_4$	0.39 mol/L NaCl	OPA pore water
[HA] = 10 mg/L	~ 23 %	(72.1 ± 4.2) %	(74.0 ± 5.7) %	(68.9 ± 5.4) %
[HA] = 50 mg/L	~ 10 %	(17.2 ± 1.6) %	(28.3 ± 1.5) %	(33.8 ± 1.5) %
[HA] = 10 mg/L + [U(VI)] = 1×10^{-6} mol/L	~ 50 %	(72.4 ± 3.5) %	(74.3 ± 6.0) %	(74.5 ± 4.8) %
[HA] = 50 mg/L + [U(VI)] = 1×10^{-6} mol/L	-	(19.7 ± 1.2) %	(30.6 ± 1.5) %	(37.6 ± 1.4) %

* At pH 7.5 (Křepelová et al., 2006).

At 10 mg HA/L and in the absence of U(VI), the increase of the ionic strength from 0.01 mol/L to 0.1 mol/L leads to an increase of HA sorption. As discussed above, this can be attributed to screening of the negatively charged side chains of the HA molecules. Such a behavior was already described in the literature (Křepelová et al., 2006; Kretzschmar et al., 1997; Murphy et al., 1992). However, an additional increase of the ionic strength to 0.39 mol/L or the application of pore water in the sorption experiments did not increase the HA sorption further.

In all investigated systems, the percentage HA sorption decreased with increasing HA concentration. This effect reduced with increasing ionic strength, presumably, again due to neutralization of the negative HA charges by cations.

Except for 0.01 mol/L $NaClO_4$, U(VI) had no influence on HA sorption at both investigated HA concentrations in any investigated system. Křepelová et al. (2006) explained the behavior in 0.01 mol/L $NaClO_4$ with the possible association of U(VI) with HA on the kaolinite surface (cf. **Fig. 19**). This process is expected to be strongest in the pH range where the U(VI) sorption on kaolinite is increased, a range which includes pH 7.5. However, with regard to the U(VI) speciation shown in **Fig. 20**, it can be concluded that U(VI) is quantitatively bound to HA at higher salinities. The formed $UO_2(CO_3)_2HA(II)^{4-}$ complex represents only a minor fraction in HA speciation (about 1 %) and thus does not affect HA sorption.

4.4 The system U(VI) / humic acid / Opalinus Clay in Opalinus Clay pore water

Selected contents of this section are published in Joseph et al. (2011).

4.4.1 Aqueous U(VI) speciation modeling

The U(VI) speciation in the absence and presence of HA in pore water as a function of pH is shown in **Fig. 21**. In contrast to the U(VI) speciation modeling in OPA pore water discussed in section **4.3.1**, the ions leached out of OPA at pH 7.6 (cf. **Tab. 8**) are considered in these calculations. In the absence of HA (cf. **Fig. 21a**), this consideration affects the U(VI) speciation only at low pH values. The $UO_2SiO(OH)_3^+$ complex is formed due to silicon that was leached out of OPA. Further remarkable changes cannot be observed. However, since the ion concentrations in the background electrolyte were determined at pH 7.6 in the leaching experiment (cf. **Tab. 8**), **Fig. 21** gives an exact picture only for pH 7.6. There, the $Ca_2UO_2(CO_3)_3(aq)$ complex is still the dominating species in the absence and presence of HA, even under consideration of the ions leached out of OPA. In the presence of HA, the fractions of the dominating species changed slightly to 76 % $Ca_2UO_2(CO_3)_3(aq)$ and 22 % $UO_2(CO_3)_2HA(II)^{4-}$, respectively.

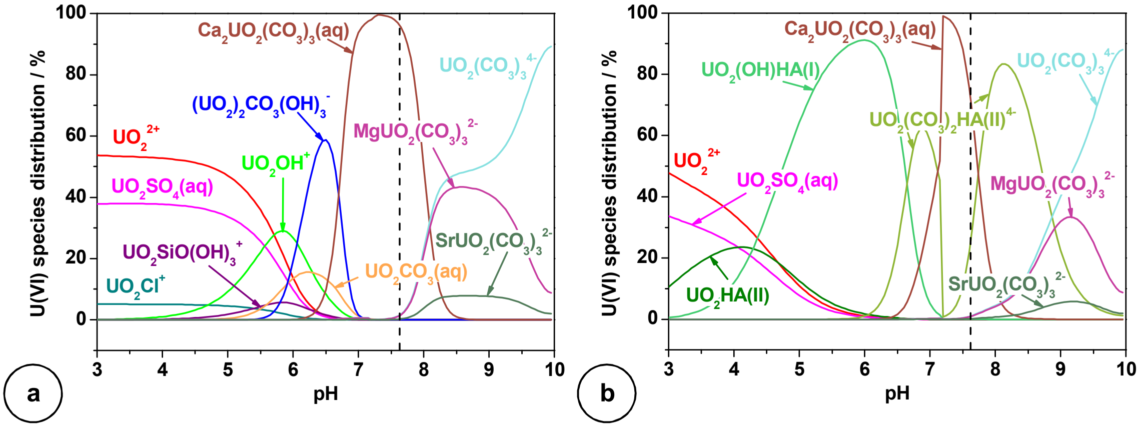

Fig. 21: Speciation of U(VI) as a function of pH in pore water in the (**a**) absence and (**b**) presence of HA under consideration of the ions leached out from OPA ($[U(VI)] = 1\times10^{-6}$ mol/L; [HA] = 50 mg/L). Only species > 5 % are shown.

Because of the large effect of the calcium ions on the U(VI) speciation, their influence on the HA speciation was also studied. The results from the speciation modeling show that at pH 7.6 the calcium humate complex, CaHA(II), clearly dominates the HA speciation with a fraction of about 75 % (not shown). It can be concluded that HA binding sites are nearly saturated with calcium ions in pore water. Due to the presence of the neutral $Ca_2UO_2(CO_3)_3(aq)$ complex in solution, an interaction of U(VI) with HA is only subordinate.

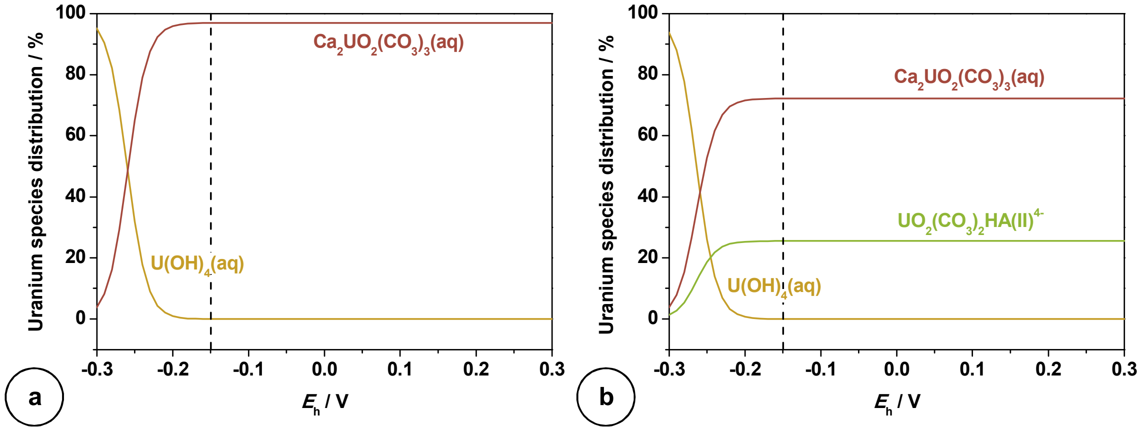

Fig. 22: Speciation of uranium as a function of E_h in pore water in the absence (**a**) and presence (**b**) of HA under consideration of the ions leached out from OPA ([U(VI)] = 1×10^{-6} mol/L; [HA] = 50 mg/L, pH 7.6). Only species > 5 % are shown.

In **Fig. 22**, the uranium speciation for pore water conditions is depicted in the absence and presence of HA as a function of the redox potential, E_h. Irrespective of HA presence, redox potentials of $E_h < -150$ mV are required of the surrounding chemical system to reduce $Ca_2UO_2(CO_3)_3$(aq) to a U(IV) species. This relatively high stability of the complex against reduction was already described by Brooks et al. (2003). They designated $Ca_2UO_2(CO_3)_3$(aq) as a less energetically favorable electron acceptor. As explained in section **2.3.1**, the modeled redox potential of the surrounding OPA / pore water system amounts to –200 mV. Consequently, U(VI) should be reduced to U(IV) under anaerobic conditions.

4.4.2 U(VI) sorption as a function of S/L ratio

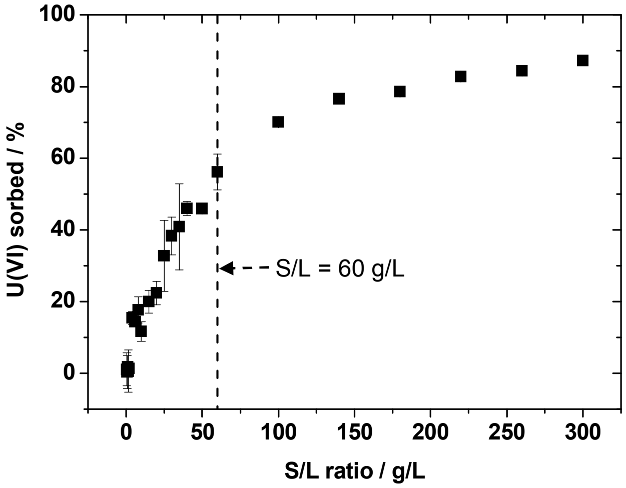

Fig. 23: U(VI) sorbed onto OPA as a function of S/L ratio ([U(VI)] = 1×10^{-6} mol/L; pore water).

The U(VI) sorption onto OPA as a function of the S/L ratio is shown in **Fig. 23**. An S/L ratio of 60 g/L was chosen for the following sorption studies. Under these conditions, about 50 % of U(VI) are sorbed onto OPA, an adequate amount for the interpretation of the sorption results.

4.4.3 U(VI) and humic acid sorption as a function of time

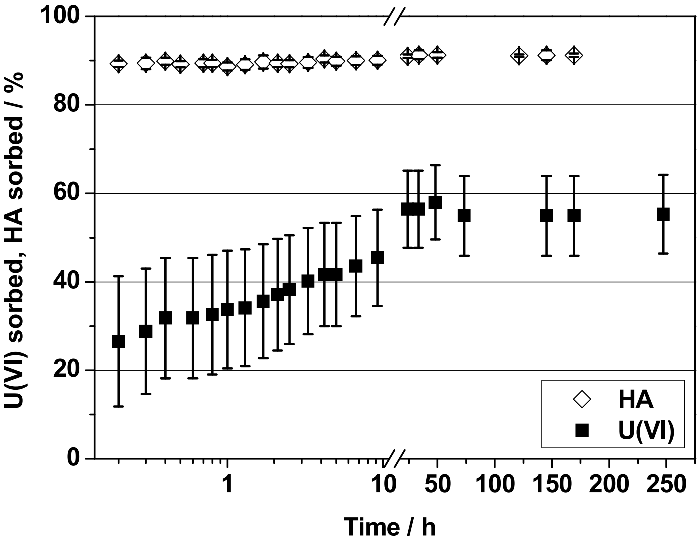

Fig. 24: U(VI) and HA sorbed onto OPA as a function of time ([U(VI)] = 1×10^{-6} mol/L; [HA] = 10 mg/L; S/L = 60 g/L; pore water).

The U(VI) and HA sorption onto OPA as a function of time is shown in **Fig. 24**. It is evident that HA reached sorption equilibrium very fast (within 1 h) with an average amount of sorbed HA of 91.2 ± 0.1 %. Thus, 1 day was considered to be sufficient to achieve the sorption equilibrium between HA and OPA. For U(VI), a much slower sorption kinetic was observed. The U(VI) sorption equilibrium was reached within 24 h with an average sorption of 55.0 ± 0.2 %. After that, the amount of sorbed U(VI) remained roughly stable for the investigated time of 247 h. Based on these results, an equilibration time of 3 days was chosen for the sorption experiments with U(VI).

4.4.4 Sorption isotherms of U(VI) and humic acid

The U(VI) and HA sorption results obtained by varying the U(VI) or HA concentration at constant S/L ratio are depicted in **Fig. 25** and **Fig. 26**. The data were fitted using the Freundlich isotherm (cf. section **4.1**, **Eq. 2** and **Eq. 4**), which is a common procedure as shown in other sorption studies, e.g., for neptunium (Altenhein-Haese et al., 1994; Mincher et al., 2003), uranium (Altenhein-Haese et al., 1994; Hull et al., 2004), and plutonium (Altenhein-Haese et al., 1994; Zuo et al., 2010). The Langmuir isotherm was also tested; however, it was less suitable to fit the sorption results.

The Freundlich sorption isotherm for the HA sorption onto OPA in pore water is shown in **Fig. 25**.

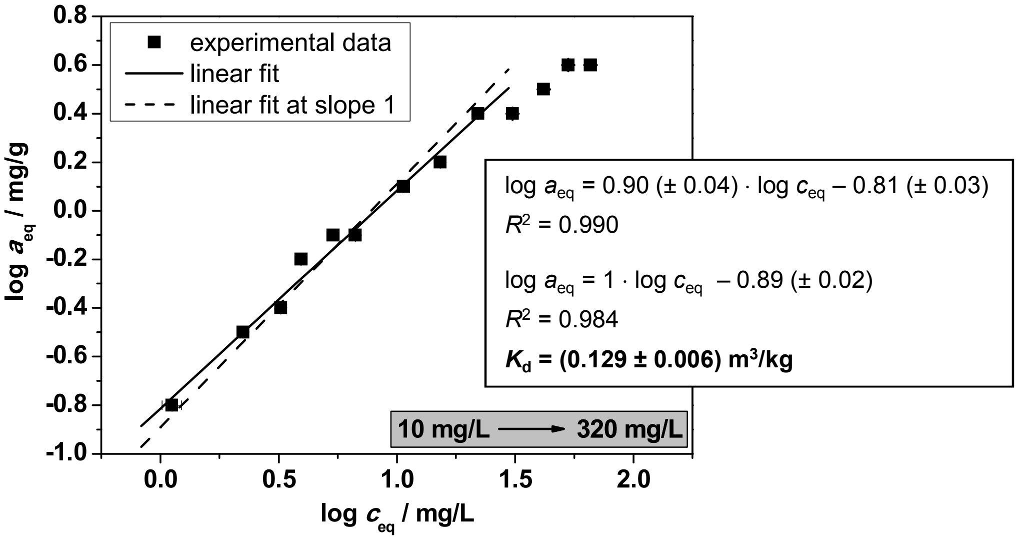

Fig. 25: Freundlich isotherm of the HA sorption onto OPA with varying HA concentration ([HA] = 10 – 320 mg/L; S/L = 60 g/L; pore water).

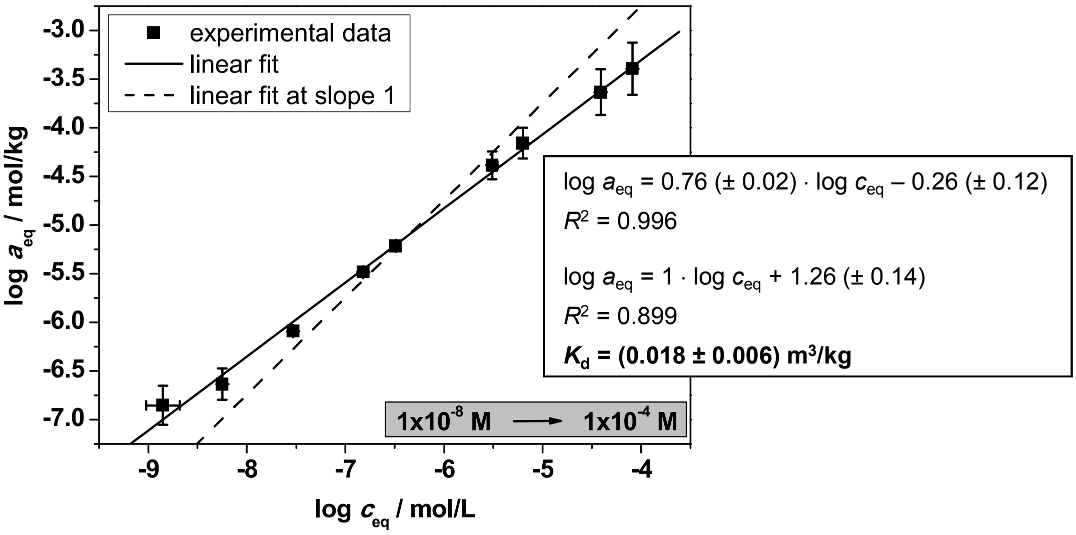

Fig. 26: Freundlich isotherm of the U(VI) sorption onto OPA with varying U(VI) concentration ([U(VI)] = 1×10^{-8} – 1×10^{-4} mol/L; S/L = 60 g/L; pore water).

With initial HA concentrations between 10 and 160 mg/L, the amount of sorbed HA increased linearly. At higher initial HA concentrations (> 160 mg/L) the slope of the sorbed amount of HA slightly decreased indicating that saturation of binding sites for HA sorption was reached. Since the Freundlich isotherm definition excludes the saturation range (cf. section **4.1**), the K_d value of sorbed HA onto OPA was determined for the range 10 – 160 mg HA/L. It amounts to 0.129 ± 0.006 m³/kg.

In pore water, CaHA(II) is the dominant HA species in solution (cf. section **4.4.1**). Previously, the influence of calcium ions on the HA sorption onto various clay minerals, such as kaolinite (Saada et al., 2003) and montmorillonite (Majzik and Tombacz, 2007; Sutton and Sposito, 2006), was investigated. An increased HA sorption was observed, when calcium ions were present in solution (Saada et al., 2003). Sutton and Sposito (2006) simulated the HA sorption onto Ca-montmorillonite. They observed differences in the sorption behavior when Ca-saturated HA were used instead of pure HA. The protonated HA existing under acidic conditions interacted mainly with the clay mineral by hydrogen bonds. The Ca-saturated HA preferred to sorb via cation bridges. But also a few water bridges and indirect hydrogen bonds mediated by water molecules were formed. For the present study, it cannot be estimated which mineral phase of OPA acts as the main sorbent for CaHA(II) because of the heterogeneity of OPA. However, it can be assumed that cation bridges originating mainly from calcium also play an important role in the sorption process.

In **Fig. 26**, the sorption isotherm for the U(VI) sorption onto OPA is presented. Using the Freundlich equation and a fixed slope of 1, a K_d value of 0.018 ± 0.006 m^3/kg was determined. Experiments with an S/L ratio of 4 g/L were also performed (not shown). There, a K_d value of 0.065 ± 0.025 m^3/kg was determined using U(VI) concentrations of $1\times10^{-8} - 5\times10^{-7}$ mol/L. Amayri et al. (2008) determined for the U(VI) sorption onto OPA a K_d value of 0.03 ± 0.01 m^3/kg using an S/L ratio of 15 g/L and U(VI) concentrations of $1\times10^{-8} - 1\times10^{-4}$ mol/L. They determined a Freundlich coefficient of $n_F = 1.21$, pointing to a nonlinear sorption. For the U(VI) sorption onto OPA presented in this study, a nonlinear sorption behavior was observed, too, but in contrast to Amayri et al. (2008), n_F values of 0.76 (S/L = 60 g/L) and 0.64 (S/L = 4 g/L) were determined. Thus, two different interaction behaviors for the U(VI) sorption onto OPA were observed in the literature and in the present study. These can be attributed to the different U(VI) concentrations and S/L ratios in the experiments.

To extrapolate from laboratory experiments to real field conditions, it is necessary to assume that the K_d values are independent of S/L ratios. Comparing the results presented here and in the study of Amayri et al. (2008), it is obvious that the determined K_d values depend on the S/L ratio used in the experiments. Phillippi et al. (2007) investigated the phenomenon of K_d–S/L ratio dependence in detail by modeling the sorption in the system U(VI) / carbonate / Fe(III)-coated sand. They observed that the U(VI) sorption in the absence of carbonate and the carbonate sorption in the absence of U(VI) were independent of the S/L ratio. In the ternary system, however, a dependence on the S/L ratio was observed. The effect was also described by Zheng et al. (2003), who investigated the U(VI) sorption onto two soils containing different amounts of calcium carbonate. With increasing U(VI) concentration the U(VI) sorption decreased. They concluded that this behavior was an artifact due to calcite dissolution. They proposed that high S/L ratios should be used for determining K_d values in calcareous soils. Then, the complete calcite dissolution can be avoided and the calcite saturation of the solution is maintained. To verify this assumption, for this study an additional Freundlich sorption isotherm was calculated using the data of the U(VI) sorption onto OPA as a function of S/L ratio (cf. **Fig. 23**). The results are depicted as K_d vs. S/L ratio in **Fig. 27**.

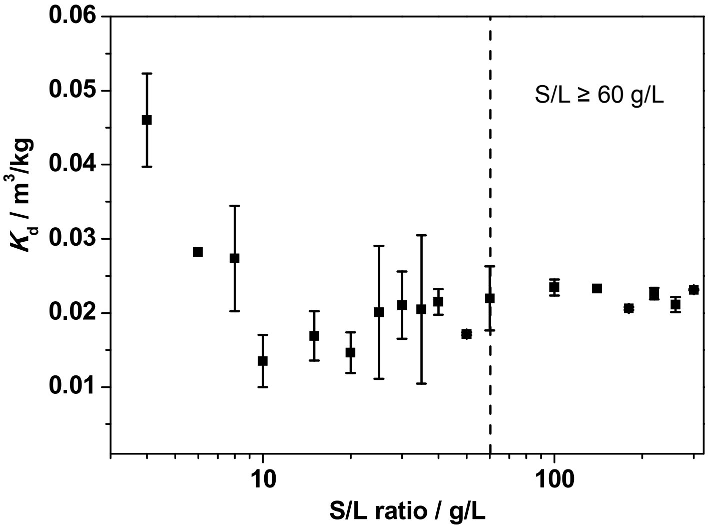

Fig. 27: K_d values of the U(VI) sorption onto OPA as a function of S/L ratio ([U(VI)] = 1×10^{-6} mol/L; S/L = 4 – 300 g/L; pore water).

Therefore, it can be concluded that for an initial U(VI) concentration of 1×10^{-6} mol/L, a K_d value, that is independent of S/L ratio, can only be obtained for S/L ratios ≥ 60 g/L. The respective Freundlich isotherm shows the highest linearity of all discussed isotherms in this study (n_F = 0.997; not shown). The resulting K_d value amounts to 0.0222 ± 0.0004 m^3/kg and is representative for the investigated system U(VI) / OPA / pore water. Since this K_d value is independent of S/L for S/L ≥ 60 g/L, it can be used to predict the sorption behavior of U(VI) onto OPA, which is relevant for performance assessment of OPA as a host rock for a nuclear waste repository.

The obtained K_d value of 0.0222 ± 0.0004 m^3/kg indicates a weak sorption affinity of U(VI) toward OPA, obviously due to the predominant formation of the $Ca_2UO_2(CO_3)_3(aq)$ complex in solution.

Wu et al. (2009) determined a K_d value of 0.025 ± 0.005 m^3/kg for Np(V) sorption onto OPA by batch sorption experiments. This is very close to the U(VI) value determined in the present work, implying similar sorption affinities for U(VI) and Np(V) toward OPA. This is in contrast to results obtained for U(VI) and Np(V) sorption onto pure clay minerals such as kaolinite (Křepelová et al., 2006; Schmeide and Bernhard, 2010), where at pH 7.5 98 % of U(VI), but only 24.5 % of Np(V) sorbed. This difference can be attributed to the absence of $Ca_2UO_2(CO_3)_3(aq)$ in those systems. Only little is known about the interaction of this complex with other minerals. Fox et al. (2006)

investigated the U(VI) sorption onto ferrihydrite and quartz in the presence of different calcium concentrations in solution. Under conditions where the $Ca_2UO_2(CO_3)_3(aq)$ species is predominating in the U(VI) speciation, a decreasing U(VI) sorption onto both minerals was observed with increasing calcium concentration. Meleshyn et al. (2009) studied the influence of this complex on the U(VI) sorption onto Ca- and Na-bentonites using $NaNO_3$ or $Ca(NO_3)_2$ as background electrolytes. Under near-neutral pH conditions, $Ca_2UO_2(CO_3)_3(aq)$ dominates the U(VI) speciation in $Ca(NO_3)_2$, whereas $(UO_2)_2CO_3(OH)_3^-$ is the predominant species in $NaNO_3$. In $Ca(NO_3)_2$, a lower U(VI) sorption was observed than in $NaNO_3$. Using $NaNO_3$ as background electrolyte, the U(VI) sorption onto Ca-bentonite was lower compared to the U(VI) sorption onto Na-bentonite. This was also attributed to the formation of $Ca_2UO_2(CO_3)_3(aq)$ due to leaching of calcium ions.

The low U(VI) sorption affinity toward OPA cannot exclusively be attributed to the formed $Ca_2UO_2(CO_3)_3(aq)$ complex. Bradbury and Baeyens (Personal communication, 2010) investigated U(VI) sorption onto Na-illite as principal sorbing mineral phase in OPA rock (16 – 40 wt.%, cf. shaly facies **Tab. 4**). The experimental data were described by a two site protolysis nonelectrostatic surface complexation and cation exchange sorption model. The modeling results were used to predict sorption isotherms measured onto OPA, whereby Bradbury and Baeyens (Personal communication, 2010) observed an overestimation of the U(VI) sorption isotherm. After addition of the complexation constant of the so-called “nonsorbing U(VI) species” $Ca_2UO_2(CO_3)_3(aq)$ to the model, the resulting model underestimated the experimental data. It was concluded that illite is not a suitable model to predict the sorption behavior of U(VI) onto OPA. Other U(VI) species-sorbing mineral phases have to be present in OPA. Hartmann et al. (2008) studied the U(VI) sorption onto OPA from Benken, Switzerland, in 0.1 mol/L $NaClO_4$ by batch and spectroscopic experiments as a function of pH. A significant decrease of the U(VI) sorption at pH 6.5 – 9.0 was observed. To reproduce the experimental data, model calculations were performed. They demonstrated that calculated and experimental data show a divergence, which was reduced when $Ca_2UO_2(CO_3)_3(aq)$ was included as nonsorbing species in the calculations. They concluded that this complex prevents U(VI) sorption onto OPA significantly. But they still ascertained a difference between calculations and experiments and assumed that $Ca_2UO_2(CO_3)_3(aq)$ sorbs to some extent to the minerals surface. This assumption is confirmed in the present study. The U(VI) sorption onto the clay mineral kaolinite in pore water (S/L = 4 g/L) was studied under identical experimental conditions such as described in this section (cf. section **4.3.2**). The results showed that the specifically sorbed amount of U(VI) onto kaolinite is higher ((42.4 ± 4.2) % = (2.2 ± 0.2) $\mu g/m^2$, cf. **Tab. 10**) than onto OPA ((0.045 ± 0.003) $\mu g/m^2$, cf. section **4.4.5**, **Tab. 12**). Based on these results, it can be concluded, that kaolinite as a main fraction in OPA (15 – 33 wt.%, cf. **Tab. 4**) is not a sufficient model for description of the available binding sites, too. Zheng et al. (2003) investigated the U(VI) sorption in natural geologic settings, in detail, onto two soils (pH 5 and pH 8) containing different concentrations of calcium carbonate. They showed that at high calcium carbonate concentrations at pH 8 the U(VI) sorption onto the soil was lower, which was attributed to the increased formation of $Ca_2UO_2(CO_3)_3(aq)$. They modeled their results using two different surface complexation models, a ferrihydrite model and a ferrihydrite and clay model. With the first model the sorption data at pH 8 were fitted very well, supporting ferrihydrite as main sorbent fraction in the soil. With the second model nearly identical results were obtained. Zheng et al. (2003) concluded that under these conditions U(VI) sorption onto clay minerals is relatively weak compared to U(VI) sorption onto ferrihydrite. OPA contains about 1.6 – 6 wt.% iron-containing mineral phases (cf. **Tab. 4**), namely pyrite and siderite. Whether these phases are the main sorbents for $Ca_2UO_2(CO_3)_3(aq)$ in OPA is unknown up to now. However, Joseph et al. (2013, accepted) could show – based on the current state of thermodynamic data for surface complexation modeling – that beside illite and montmorillonite, Fe(III) minerals formed in the system also represent important binding sites for U(VI) in OPA.

4.4.5 Sorption of U(VI) in the presence of humic acid

OPA contains about 1 wt.% organic carbon (cf. section **2.3**). Only a small portion of the TOC (about 0.15 wt.%) consists of humic material (Pearson et al., 2003), that means a fraction of about 1.5×10^{-3} wt.% of OPA. In the present experiments, a HA concentration of 50 mg HA/L in maximum was used. Under consideration that HA type M42 contains (56.1 ± 0.3) wt.% carbon (cf. **Tab. 21**), at an S/L ratio of 60 g clay/L a TOC of 0.05 wt.% results. That means the experiments were performed in 30-fold excess.

The results of the U(VI) sorption onto OPA in the absence and presence of HA are summarized in **Tab. 12**. Since different OPA batches were used in the experiments under ambient atmosphere and inert gas conditions, the sorption results were normalized to the specific surface area (cf. **Tab. 5**). For the experiments performed under ambient atmosphere **Tab. 12** shows that the U(VI) sorption is not influenced by HA. These results are in agreement with the U(VI) speciation results, where the presence of HA had no effect on the U(VI) speciation at pH 7.6 (cf. **Fig. 21**). In contrast to this, Křepelová et al. (2006) showed that the presence of HA decreased the U(VI) sorption onto kaolinite at pH 7.5 in 0.1 mol/L $NaClO_4$. This effect increased with increasing HA concentration and was attributed to the formation of dissolved U(VI) humate complexes. However, in the presence of calcium ions, the formation of U(VI)

Tab. 12: U(VI) and HA sorption onto OPA under ambient atmosphere (pCO_2 = $10^{-3.5}$ atm) or inert gas conditions (N_2-box) (S/L = 60 g/L; pore water).

	U(VI) sorbed / µg/m^2		**HA sorbed / µg/m^2**	
	CO_2	**N_2**	**CO_2**	**N_2**
[U(VI)] = 1×10^{-6} mol/L	0.045 ± 0.003	0.046 ± 0.002	-	-
[U(VI)] = 1×10^{-6} mol/L + [HA] = 10 mg/L	0.044 ± 0.003	0.047 ± 0.001	3.5 ± 0.2	3.9 ± 0.1
[U(VI)] = 1×10^{-6} mol/L + [HA] = 50 mg/L	0.045 ± 0.002	0.049 ± 0.002	17.6 ± 0.6	19.5 ± 0.4
[HA] = 10 mg/L	-	-	3.5 ± 0.3	3.9 ± 0.1
[HA] = 50 mg/L	-	-	17.6 ± 0.5	19.3 ± 0.4

humate complexes is repressed, as verified by the present data.

Furthermore, **Tab. 12** presents the HA sorption onto OPA. With increasing HA concentration, the sorbed amount of HA onto OPA increased. At both HA concentrations used, no influence of U(VI) on the HA sorption can be observed. This corresponds to the HA speciation results and can be attributed to the saturation of HA binding sites by calcium ions. Kornilovich et al. (2000) and Křepelová et al. (2008) proposed for the sorption of metal ions onto clay minerals in the presence of humic substances that the metal ion can be located between the solid phase and the humic substance (cf. **Fig. 19**). In the quaternary system U(VI) / HA / OPA / pore water studied here, it is assumed that the place of the metal ion is occupied by calcium, but not by U(VI). U(VI) and HA did not affect each other in the sorption process.

Finally, it was tested by means of solvent extraction whether the added U(VI) is reduced to U(IV) in the systems OPA / pore water or HA / OPA / pore water. U(IV) could not be detected in the extracts. Thus, a reduction of U(VI) by OPA or by HA can be excluded under ambient atmosphere conditions.

4.4.6 Influence of CO_2

In addition to the sorption experiments performed under ambient conditions with OPA batch BHE-24/1, the U(VI) sorption onto OPA was investigated under inert gas atmosphere using OPA batch BLT-11/01. The results are also shown in **Tab. 12**.

Since pore water was used as background electrolyte, the U(VI) and HA species distributions do not change under inert gas conditions, they are independent of the surrounding atmosphere. $Ca_2UO_2(CO_3)_3(aq)$ is still dominating the U(VI) speciation and CaHA(II) is still the determining species of the HA speciation. As expected, the amounts of sorbed U(VI) and HA onto OPA obtained under inert gas conditions agree well with the results obtained under ambient atmosphere. Small differences can be attributed to the different OPA batches applied in the respective sorption experiments.

It can be concluded that CO_2 from the surrounding gas atmosphere has no significant influence on the U(VI) and HA sorption in the OPA / pore water system.

The reduction of U(VI) to U(IV) in the systems OPA / pore water and HA / OPA / pore water was investigated by solvent extraction under inert gas conditions. U(IV) was not detected in the extracts. However, the possible formation of an insoluble U(IV) species on the clay surface cannot be excluded completely. For this, the surface had to be investigated closer, for example, by XAS (XANES).

4.4.7 U(VI) speciation in the system determined by TRLFS under cryogenic conditions

TRLFS measurements were performed at 153 K to spectroscopically identify the U(VI) species present in solution under aerobic conditions before and after sorption onto OPA (cf. section **4.4.5**). Experimental details can be found in section **7.3.1.** The results are shown in **Tab. 13**.

Tab. 13: Luminescence properties of the measured U(VI) species (λ_{ex} = 410 nm).

Sample	**Main luminescence emission bands / nm ***
Pore water	
[U(VI)] = 1×10^{-6} mol/L	485.0, 501.6, 522.8, 545.4, 571.3
Filtered supernatant after sorption	
$[U(VI)]_0 = 1\times10^{-6}$ mol/L	485.1, 502.1, 523.2, 545.2, 571.1
$[U(VI)]_0 = 1\times10^{-6}$ mol/L + $[HA]_0$ = 10 mg/L	485.4, 501.9, 522.9, 545.6, 571.9
$[U(VI)]_0 = 1\times10^{-6}$ mol/L + $[HA]_0$ = 50 mg/L	485.8, 502.6, 523.9, 546.6, 569.5

* Error: ± 0.3 nm

The main luminescence emission bands of the U(VI) species present in pore water and in the filtrates of the respective sorption samples in the absence and presence of HA are very similar. This indicates the presence of the same U(VI) species in all solutions. Except for the first emission band, the measured peak positions are almost identical to those published by Wang et al. (2004) and Bernhard and Geipel (2007) for $Ca_2UO_2(CO_3)_3(aq)$. As shown in Bernhard and Geipel (2007), the main luminescence emission bands of $UO_2(CO_3)_3^{4-}$ shifted on average by about 3.5 nm toward lower wavelengths at 100 K compared to the $Ca_2UO_2(CO_3)_3(aq)$. For measurements at cryogenic temperatures of about 6 K, Wang et al. (2004) showed the main luminescence emission bands of different uranyl carbonato species. These bands differ from the corresponding bands of the free uranyl ion by a blue shift of several nanometers (average values: $Ca_2UO_2(CO_3)_3(aq)$: 15 nm; $UO_2CO_3(aq)$: 19 nm; $UO_2(CO_3)_3^{4-}$: 19 nm; $UO_2(CO_3)_2^{2-}$: 21 nm; $(UO_2)_2(OH)_3CO_3^-$: 23 nm). The shift of the luminescence emission bands as compared to the free uranyl ion (not shown) that is found in the present study amounts to 15 nm on average and can be assigned to the blue shift obtained for $Ca_2UO_2(CO_3)_3$(aq). The presence of other uranyl carbonato species can be excluded since then the shift would have to be at least 4 nm higher than the measured shift.

For $Ca_2UO_2(CO_3)_3$(aq) a luminescence lifetime of about 1 ms is reported (Bernhard and Geipel, 2007; Wang et al., 2004). The lifetimes of the U(VI) species in pore water and in the filtrates of the sorption samples in the absence and presence of HA also approximate 1 ms, which further indicates the presence of $Ca_2UO_2(CO_3)_3$(aq). This means that the calculated U(VI) speciation given in section **4.4.1** is confirmed by TRLFS measurements.

4.4.8 U(VI) sorption onto Opalinus Clay studied with EXAFS spectroscopy

EXAFS samples were prepared to investigate the influence of HA (10 mg/L) on U(VI) sorption onto OPA. The experimental details of EXAFS measurements and sample preparation are described in section **7.4.8**. The investigated EXAFS samples with their sorbed amounts of U(VI) and HA are given in **Tab. 14**.

Tab. 14: OPA samples prepared for EXAFS measurements with their sorbed amounts of U(VI) and HA, ([U(VI)] = 1×10^{-4} mol/L; [HA] = 10 mg/L; S/L = 20 g/L; pore water; $pCO_2 = 10^{-3.5}$ atm) and results of the first fit of the EXAFS spectra. The multiple scattering path $MS_{U=O}$ was taken into consideration as explained in the text (cf. section **7.4.8**). Asymptotic standard deviations are given in parentheses.

EXAFS notation	U(VI) sorbed / µg/m^2	HA sorbed / µg/m^2	Shells	N	R / Å	σ^2 / Å^2	ΔE_0 / eV	χ_{red}^2
U9-40	3.5 ± 0.3	10.6 ± 0.4	U–O$_{ax}$	2.3(3)	1.798(5)	0.002(1)	4(1)	1.09
			U–O$_{eq}$	3.5(8)	2.44(1)	0.006(3)		
U9-41	1.55 ± 0.95	-	U–O$_{ax}$	2 f *	1.806(4)	0.0020(4)	5.0(8)	0.71
			U–O$_{eq}$	4.4(7)	2.43(1)	0.010(2)		

* f … This parameter was fixed during fitting procedure.

A blank clay sample without U(VI) and HA was prepared to determine the amount of ions leached out of OPA (cf. **Tab. 15**). Based on these data the main U(VI) species in solution were calculated using EQ3/6. The U(VI) speciation in pore water in the absence and presence of HA is clearly dominated by the $Ca_2UO_2(CO_3)_3$(aq) complex with fractions of 98 % and 94 %, respectively. Consequently, the respective U(VI) sorption is very low in both samples investigated. In solution of sample U9-40, the $UO_2(CO_3)_2HA(II)^{4-}$ complex is only formed with a fraction of about 4 %. However, the amount of sorbed U(VI) in the presence of HA is more than twice as high as in the absence of HA. Thus, HA seems to increase the U(VI) sorption onto OPA. This is in

Tab. 15: Ions leached out from OPA during 13 days contact time with pore water (pore water$_{exp13d}$); S/L = 20 g/L.

Element / Ion	Pore water$_{exp13d}$ / mol/L
Na	2.4×10^{-1}
K	2.2×10^{-3}
Mg	1.6×10^{-2}
Ca	2.5×10^{-2}
Sr	4.9×10^{-4}
Al	1.7×10^{-7}
Si	4.3×10^{-5}
Cl^-	2.9×10^{-1}
SO_4^{2-}	1.4×10^{-2}
CO_3^{2-} / HCO_3^-	7.2×10^{-4}

contrast to the findings presented in section **4.4.5** (cf. **Tab. 12**), where HA had no significant effect on the U(VI) sorption onto OPA. This discrepancy can be explained by the 100-fold higher U(VI) concentration used to prepare the EXAFS samples compared to the U(VI) concentration used in the batch experiments in section **4.4.5**. Presumably, at this high U(VI) concentration the suitable U(VI) binding sites onto OPA are already saturated and the remaining U(VI) interacts with sorbed HA.

The number of neighbor atoms, *N*, the distance to the neighboring atom, *R*, and the disorder in the neighbor distance, σ^2, also known as Debye-Waller factor, were fitted only for the oxygen atoms. With this, contributions of the axial and equatorial oxygen coordination shells of uranyl as well as the multiple scattering path of the axial oxygen atoms U–O$_{ax1}$–U–O$_{ax2}$ (MS$_{U=O}$) (Hudson et al., 1995) were considered. **Tab. 14** summarizes the obtained structural parameters from this first fit. Furthermore, the threshold energy, ΔE_0, and the reduced chi-squared value of the fit, χ_{red}^2, are given.

The data show that there are always two axial and up to five equatorial oxygen atoms coordinated around U(VI). The distance of U–O$_{ax}$ was determined to be about 1.80 Å. For the distance of U–O$_{eq}$ values of about 2.43 and 2.44 Å were obtained. Since the equatorial oxygen atoms are associated with binding sites on the clay surface mainly provided by Al-, Si-, and Fe-containing minerals or are coordinated by ions present in solution (hydroxyl, carbonate, HA), the U–O$_{eq}$ distance in this first fit points toward a possible binding species bound to the equatorial oxygen atoms.

Fig. 28 presents the EXAFS spectra and the corresponding Fourier transforms of the samples U9-40 and U9-41. Due to the low U(VI) sorption, the $\chi(k)$ functions of sample U9-40 and U9-41 are very noisy at higher *k* values. However, both EXAFS spectra show similar oscillations, the Fourier transforms display comparable peaks. The fitted

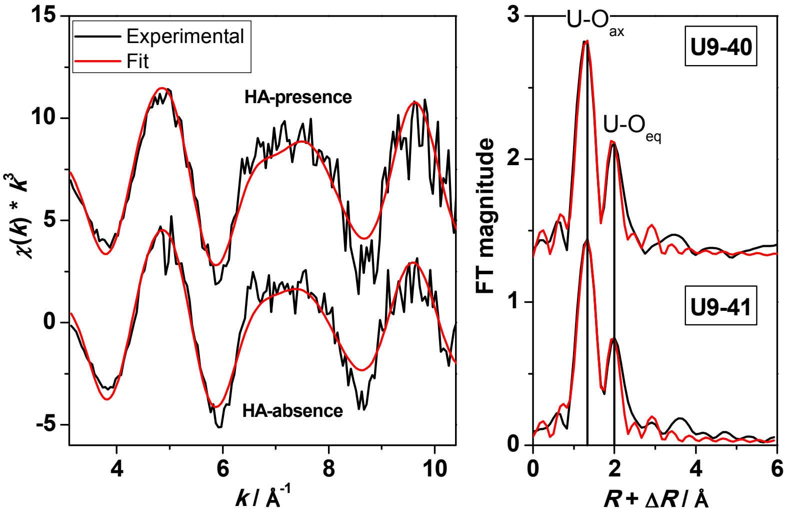

Fig. 28: Uranium L_{III}-edge k^3-weighted EXAFS spectra and their corresponding Fourier transforms of samples U9-40 and U9-41 for the U(VI) sorption onto OPA in pore water in the presence (U9-40) and absence (U9-41) of HA. The spectra are shifted along the y-axis for clarity.

structural parameters of sample U9-40 and U9-41 are similar, too (cf. **Tab. 14**). Consequently, an influence of HA on the formed U(VI) surface complex onto OPA under pore water conditions can be excluded based on EXAFS analysis. This is in agreement with the results obtained for the U(VI) sorption onto kaolinite (Křepelová et al., 2008). Therein, no influence of HA on the structural EXAFS parameters was observed, too.

The determined U–O_{eq} distances of 2.43 Å and 2.44 Å point to carbon bound to the equatorial oxygen atoms. These U–O_{eq} distances were already reported in the literature for the Ca^{2+} / UO_2^{2+} / CO_3^{2-} system (Bernhard et al., 2001). There, six equatorial oxygen atoms were coordinated to UO_2^{2+}. In the present study, for the equatorial oxygen atoms lower coordination numbers of 3.5 and 4.4 were obtained by fitting the EXAFS spectra. This leads to the assumption that $Ca_2UO_2(CO_3)_3(aq)$ possibly sorbs onto OPA by loss of at least one bidentate carbonate coordination as proposed by Foerstendorf et al. (2012) for ternary uranyl carbonate surface complexes formed onto ferrihydrite. However, at the current stage of data analysis, it cannot be clarified which mineral phase of OPA serves as U(VI) sorbent under these conditions.

In both samples, the FT peak at *R* + Δ*R* ~ 3.6 Å indicates the presence of a U–U interaction (Bargar et al., 2000; Szabó et al., 2000). Thus, the formation of a solid U(VI) species cannot be ruled out. However, this peak could be also attributed to a U–C–O multiple scattering path (Szabó et al., 2000).

4.5 The system U(VI) / humic acid / Opalinus Clay in 0.1 mol/L $NaClO_4$

The results of this section are published in Joseph et al. (2013, accepted).

4.5.1 Aqueous U(VI) and humic acid speciation modeling

In connection with the pH-dependent OPA leaching experiments discussed in section **2.3.2**, the U(VI) speciation in the absence and presence of HA is shown as a function of pH in **Fig. 29**. These speciation calculations are in contrast to the U(VI) species distributions shown in **Fig. 20a,b** since in **Fig. 29** the concentration of ions leached out from OPA, which were determined at specific pH values (cf. **Fig. 14**), was considered. Thus, the U(VI) speciation was calculated only for these pH values (shown as points in **Fig. 29**). The lines were drawn for visual reasons.

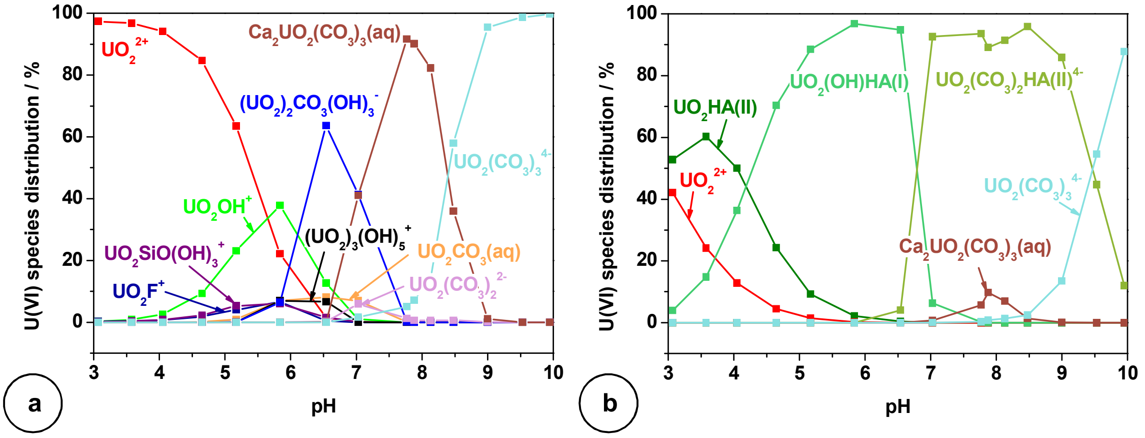

Fig. 29: Speciation of U(VI) as a function of pH in 0.1 mol/L $NaClO_4$ in the (**a**) absence and (**b**) presence of HA under consideration of the ions leached out from OPA ([U(VI)] = 1×10^{-6} mol/L; [HA] = 50 mg/L; $pCO_2 = 10^{-3.5}$ atm). Only species > 5 % are shown.

In the absence of HA at pH < 5.5, the U(VI) speciation is dominated by the free uranyl ion. At pH > 6, the uranyl carbonato species $(UO_2)_2CO_3(OH)_3^-$, $Ca_2UO_2(CO_3)_3(aq)$, and $UO_2(CO_3)_3^{4-}$ are dominant due to the presence of carbonate in solution. The presence of $Ca_2UO_2(CO_3)_3(aq)$ demonstrates the large influence of calcium on the U(VI) speciation, since it is leached out of OPA and competes with U(VI). Other charged uranyl alkaline earth carbonato complexes were modeled to be negligible in the investigated pH range.

The presence of HA affects the U(VI) speciation significantly (**Fig. 29b**). At low pH values (pH 3 – 4), $UO_2HA(II)$ dominates the speciation. $UO_2(OH)HA(I)$ is the prevailing species in solution in the pH range from pH 4.2 to 6.7. Due to the presence of carbonate in solution at pH > 6, $UO_2(CO_3)_2HA(II)^{4-}$ is formed. $UO_2(CO_3)_2HA(II)^{4-}$ prevents significantly the formation of $Ca_2UO_2(CO_3)_3(aq)$ which is formed only in a very small amount in the pH range from pH 7 to 9.

The HA speciation, depicted in **Fig. 30**, shows that in the whole pH range the U(VI) humate complexes play only a subordinate role compared to the humate complex formed with calcium leached out of OPA. CaHA(II) dominates the HA speciation in the pH range from pH 3 to about 8.5.

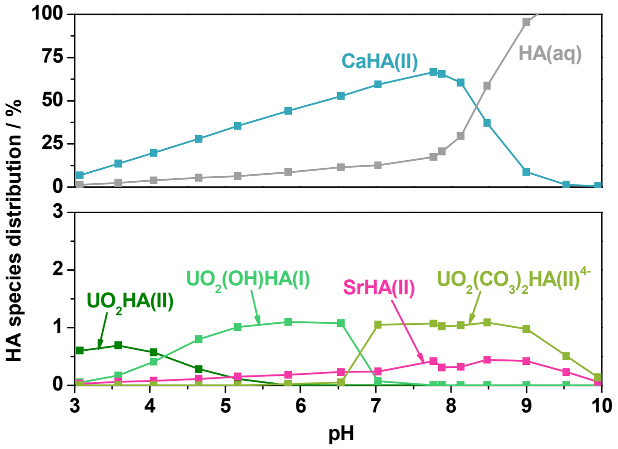

Fig. 30: Speciation of HA as a function of pH in 0.1 mol/L $NaClO_4$ in the presence of U(VI) under consideration of the ions leached out from OPA ([U(VI)] = 1×10^{-6} mol/L; [HA] = 50 mg/L; $p\mathrm{CO_2} = 10^{-3.5}$ atm).

Certain amounts of magnesium, aluminum, and iron are also found in solution. However, complexation data for humate complexes with these ions based on CNM are not available in the literature. In few studies, conditional stability constants for such complexes were determined (Lippold et al., 2005; Pandey et al., 2000; Tipping et al., 2002). For the speciation calculations performed in the present study based on CNM, pH- and ionic strength-independent complex formation constants and respective pH-dependent loading capacities (LC, cf. section **7.6.1**) are required. Especially in the case of iron and aluminum, different hydrolyzed species are present in solution in dependence on pH. Thus, different humate complexes can be expected, similar to U(VI) humate complexes. Although there are only few complexation data available, it is known that the interaction of aluminum with HA is stronger than that of calcium or magnesium (Beck et al., 2004), but much weaker than that of iron (Lippold et al., 2007). Iron competes strongly with UO_2^{2+} for the complexation with HA (Teterin et al., 2001). Tochiyama et al. (2004) demonstrated that Fe(III) forms stronger complexes with HA than with Fe(II). The oxidation state of the dissolved iron in the investigated system is not known. However, several redox processes can take place. On the one hand, atmospheric oxygen can oxidize the mineralogically bound Fe(II) in OPA. On the other hand, HA has reducing properties (Reiller, 2005; Sachs and Bernhard, 2011; Schmeide and Bernhard, 2009; Schmeide et al., 2012) and could potentially reduce the Fe(III) present in solution. Since these experiments were performed under aerobic conditions, it is assumed that Fe(III) is the dominating oxidation state in solution. At low pH values, HA precipitates to a certain extent due to protonation of the HA carboxyl groups. In the presence of metal ions this effect is increased due to additional screening of the negative charge of HA by these ions. Therefore, one can expect that at pH 3, where increased concentrations of aluminum and iron are present in solution (cf. **Fig. 14**), no aquatic but rather solid complexes of HA with aluminum and iron are formed (Lippold et al., 2007).

Based on this discussion, a sequence of U(VI) and the competing ions present in solution arranged by their interaction strength with HA can be assumed as follows: Fe(III) > Al(III) ≥ U(VI) > Sr(II) > Ca(II) > Mg(II). However, since the calcium concentration in solution is about two orders of magnitude higher than the concentrations of the other ions (cf. **Fig. 14**), the HA speciation will still be dominated by CaHA(II) over a wide pH range, even after inclusion of the still unknown complexation data of various magnesium, aluminum and iron humate complexes based on CNM to the EQ3/6 data base. The higher complexation constants of Fe(III), Al(III), U(VI), and Sr(II) cannot compensate their low concentrations as shown by the various U(VI) humate complexes and CaHA(II) (cf. **Fig. 30**).

4.5.2 pH-dependent U(VI) sorption in the absence of humic acid

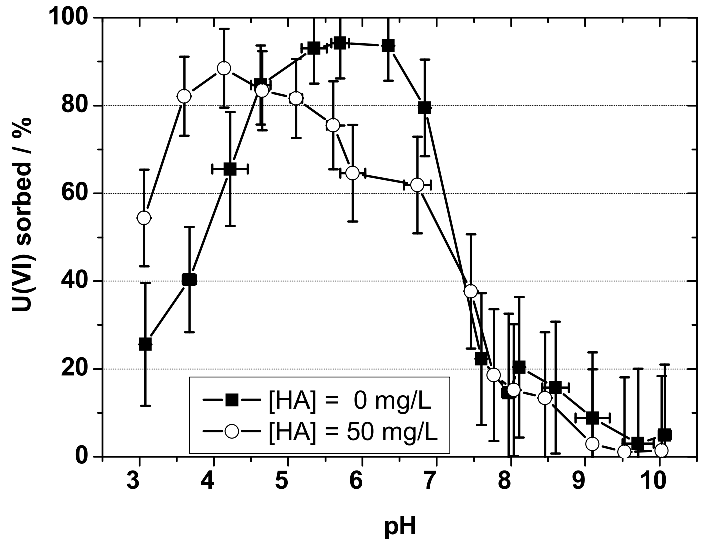

Fig. 31: U(VI) sorption onto OPA in the absence and presence of HA as a function of pH ([U(VI)] = 1×10^{-6} mol/L; [HA] = 0 or 50 mg/L; S/L = 4 g/L; $I = I_t$; $p\mathrm{CO_2} = 10^{-3.5}$ atm). Error bars: 2σ.

The U(VI) sorption onto OPA as a function of pH is shown in **Fig. 31**. In the absence of HA, the U(VI) sorption increased from about 20 % at pH 3 to about 95 % at pH 5.5. The comparison to the respective U(VI) speciation in **Fig. 29a** shows that the strongest

U(VI) sorption occurs when UO_2OH^+ and $(UO_2)_2CO_3(OH)_3^-$ are the dominating U(VI) species in solution. Above pH 7, a strong decrease of the U(VI) sorption was observed. This is due to the formation of $Ca_2UO_2(CO_3)_3(aq)$, which is known to sorb only weakly onto OPA (Joseph et al., 2011). In the pH range from pH 8.5 to 10, the U(VI) sorption decreased further to about 5 % at pH 10. Here, the highly negatively charged $UO_2(CO_3)_3^{4-}$ complex becomes the dominant species in solution.

Compared to the U(VI) sorption onto kaolinite (Křepelová et al., 2006), the U(VI) sorption curve is shifted to lower pH values in the case of OPA. This could be interpreted with the fact that the mineral phases that dominate the sorption have lower pzc values than kaolinite. Otherwise, the various mineral phases of OPA have other surface binding sites than kaolinite, which can form stronger surface complexes with U(VI). Thus, no distinct statement about the surface charge can be made.

However, at pH values > 8.5, it can be expected that the surface of OPA is predominantly negatively charged. Thus, the negligible sorption of $UO_2(CO_3)_3^{4-}$ can be attributed to electrostatic repulsion effects. In the pH range, where the neutral $Ca_2UO_2(CO_3)_3(aq)$ complex is the dominant species in solution, a low but compared to $UO_2(CO_3)_3^{4-}$ increased U(VI) sorption is observed. One reason could be that the neutral complex is not as much electrostatically repulsed as the negatively charged species. Otherwise, the dissolved calcium ions possibly screen the negatively charged surface by charge neutralization.

4.5.3 pH-dependent U(VI) sorption in the presence of humic acid

The presence of HA influences the U(VI) sorption onto OPA significantly (**Fig. 31**). Between pH 3 and 4.5, the U(VI) sorption is higher than in the absence of HA. This is due to the sorption of HA onto OPA which provides additional binding sites for U(VI). Furthermore, a partial precipitation of HA (~ 70 % at pH 3, cf. **Fig. 32**) occurs which is caused by charge neutralization of the negatively charged HA functional groups by the cations present in solution (including protons). That means, a part of U(VI) precipitates as HA complex. Additionally, a subsequent U(VI) sorption onto precipitated HA could be possible. The two last processes lead to an overestimation of the U(VI) sorption onto OPA. Such an influence of HA was already described for the U(VI) sorption on kaolinite (Křepelová et al., 2006; Sachs and Bernhard, 2008), cypris clay (Beneš et al., 1998), phyllite (Schmeide et al., 2000), and bentonite (Ren et al., 2010).

Between pH 4.5 and 7.5, the U(VI) sorption is decreased compared to the HA-free system. This is due to the formation of $UO_2(OH)HA(I)$. Thus, the presence of HA leads to a mobilization of U(VI) in the near-neutral pH range which was also observed for kaolinite (Křepelová et al., 2006; Sachs and Bernhard, 2008).

At pH values > 7.5, HA seems to have no effect on the U(VI) sorption onto OPA. In section **4.4.5**, it was already shown for the system U(VI) / HA / OPA / pore water that the U(VI) sorption onto OPA at pH 7.6 is not influenced by HA due to the presence of $Ca_2UO_2(CO_3)_3(aq)$. The present study shows that there is also no influence of HA on the U(VI) sorption at a lower ionic strength, which also could be attributed to the presence of the $Ca_2UO_2(CO_3)_3(aq)$ complex in solution (cf. **Fig. 29b**). However, from pH 7 to 10 the U(VI) speciation in the presence of HA is clearly dominated by $UO_2(CO_3)_2HA(II)^{4-}$ and $UO_2(CO_3)_3^{4-}$ (cf. **Fig. 29b**). Both complexes are negatively charged and are repulsed by a negatively charged clay surface resulting in a very low U(VI) sorption. Therefore, the different contributions of $Ca_2UO_2(CO_3)_3(aq)$, $UO_2(CO_3)_2HA(II)^{4-}$, and $UO_2(CO_3)_3^{4-}$ to the U(VI) sorption or mobilization cannot be clarified at the current state of knowledge.

The observed U(VI) sorption behavior is in contrast to the U(VI) sorption on kaolinite (Sachs and Bernhard, 2008), cypris clay (Beneš et al., 1998), and phyllite (Schmeide et al., 2000), where an additional U(VI) mobilization by HA was observed. However, it is in agreement with the observations made for the U(VI) sorption onto muscovite (Schmeide et al., 2000).

4.5.4 pH-dependent humic acid sorption in the presence of U(VI)

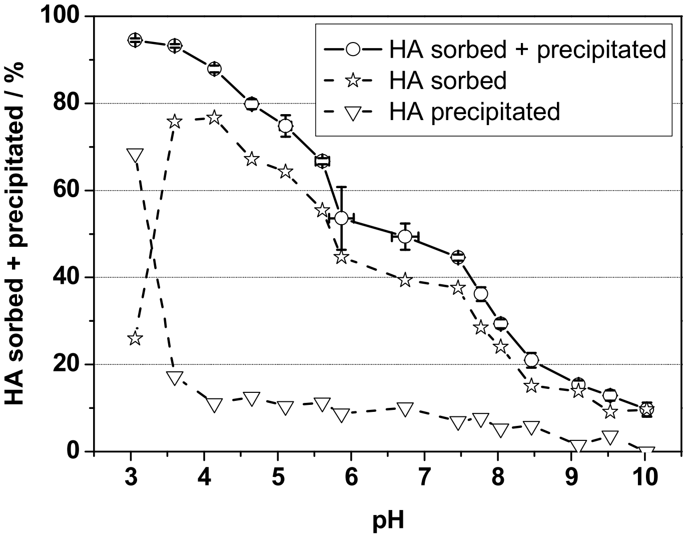

Fig. 32: HA sorption onto OPA in the presence of U(VI) as a function of pH ([HA] = 50 mg/L; [U(VI)] = 1×10^{-6} mol/L; S/L = 4 g/L; $I = I_t$; $pCO_2 = 10^{-3.5}$ atm). Error bars: 2σ.

To support the discussion of the previous section, the HA sorption onto OPA in the presence of U(VI) was investigated. The results are shown in **Fig. 32**. The high amount of HA removed from solution at pH 3 (nearly 95 %) points rather to a precipitation than to a sorption, because the negatively charged functional groups of the HA are protonated as well as complexed by several metal ions present in solution. For quantification of this effect, the amount of precipitated HA was determined by pH-dependent blank solutions without OPA but containing U(VI) and HA. The amount of HA sorbed was calculated as the difference of the total HA amount associated with OPA and the amount of precipitated HA. The results reveal an overlap of HA sorption and precipitation, which is especially pronounced at pH 3.

With increasing pH, a decrease of the HA sorption onto OPA was observed. Due to deprotonation of functional groups of HA with increasing pH, HA becomes more negatively charged. Furthermore, the OPA surface charge is more negative with increasing pH. Thus, due to electrostatic repulsion effects, the HA sorption decreased with pH. Such sorption behavior is typical for HA and was already described for several systems (Křepelová et al., 2006; Niu et al., 2009; Sachs and Bernhard, 2008; Schmeide et al., 2000).

The HA sorption onto OPA in 0.1 mol/L $NaClO_4$ as a function of pH was investigated by Lippold and Lippmann-Pipke (2009) and compared to the HA sorption onto illite and montmorillonite (S/L = 5 g/L, [HA] = 5 mg/L, pH 3 – 6). They observed the lowest HA sorption for OPA, which was explained with the presence of nonargillaceous constituents in OPA. In the present work, a 10-fold higher HA concentration was used. However, the huge influence of nonargillaceous OPA constituents can be confirmed. As shown in section **4.5.1**, calcium from the calcite mineral fraction is dissolved and complexed by HA. CaHA(II) dominates the HA speciation over a wide pH range.

4.6 Conclusions for the sorption of U(VI) and humic acid onto Opalinus Clay

U(VI) sorption onto OPA was studied by batch sorption experiments in synthetic OPA pore water at pH 7.6 and in 0.1 mol/L $NaClO_4$ as a function of pH both in the absence and in the presence of HA and under consideration of the OPA leached out ions.

For the experiments in pore water, it was demonstrated that U(VI) sorption onto OPA is very weak. A K_d value of 0.0222 ± 0.0004 m^3/kg was determined, which was shown to be independent of S/L ratios ≥ 60 g/L. Thus, this K_d value can be used to predict U(VI) sorption at real field conditions. The K_d value determined for U(VI) is close to that obtained for the Np(V) sorption onto OPA (0.025 ± 0.005 m^3/kg) (Wu et al., 2009). This shows that both actinides have nearly the same sorption affinity toward OPA in the OPA / pore water system. The U(VI) sorption onto kaolinite, which represents a mineral fraction of OPA, was determined to be about fifty times higher than onto OPA under pore water conditions. This leads to the conclusion that different mineral phases present in OPA seem to inhibit the U(VI) sorption.

Due to dissolution of calcite in OPA, calcium ions are present in the pore water and form the aquatic $Ca_2UO_2(CO_3)_3$ complex with U(VI). This complex dominates the U(VI) speciation under pore water conditions. HA was added to the system to investigate the influence of organic matter on the U(VI) sorption onto OPA. Since under these conditions $Ca_2UO_2(CO_3)_3$(aq) dominates still the U(VI) species distribution, the U(VI) sorption onto OPA is not influenced by HA. EXAFS investigations confirmed the batch sorption result. The U(VI) speciation in pore water in the absence and presence of HA was verified analytically by TRLFS measurements.

The speciation of HA in the pore water system is also influenced by the presence of dissolved calcium ions. The cations saturate the binding sites of HA almost completely. Thus, the HA speciation is dominated by CaHA(II), which inhibits the interaction of HA with U(VI).

Batch sorption experiments in 0.1 mol/L $NaClO_4$ showed that OPA has the strongest retardation effect on U(VI) in the pH range from pH 4.5 to 7. However, to approach natural conditions the observations made at pH > 7 are important. There, the U(VI) speciation is affected by the dissolved competing ions. Calcium and carbonate ions, which are formed by calcite dissolution, determine the U(VI) speciation. From pH 7 to 8.5, the $Ca_2UO_2(CO_3)_3$(aq) complex dominates the U(VI) speciation in solution. In the presence of this weakly sorbing complex, the U(VI) sorption onto OPA decreases strongly between pH 7 and 8.

The competing ions leached out from OPA also influence the HA speciation. Over a wide pH range, the CaHA(II) complex is the dominating HA species in solution. The presence of HA influences the U(VI) sorption significantly. In the acidic pH range, an increase of the U(VI) immobilization is observed. Under slightly acidic to near-neutral pH conditions, the U(VI) sorption is decreased due to mobilization of U(VI) by HA in form of the $UO_2(OH)$HA(I) complex. At pH > 7, the negatively charged $UO_2(CO_3)_2HA(II)^{4-}$ complex determines the U(VI) speciation. Although $UO_2(CO_3)_2HA(II)^{4-}$ represses $Ca_2UO_2(CO_3)_3$(aq), the amount of sorbed U(VI) onto OPA is not influenced by this complex. The different contributions of $Ca_2UO_2(CO_3)_3$(aq) and $UO_2(CO_3)_2HA(II)^{4-}$ to the U(VI) sorption or mobilization cannot be clarified at the current state of knowledge.

With regard to the sorption capability of complex clay formations, it is not sufficient to investigate the sorption and retention properties of pure clay minerals such as kaolinite (cf. section **4.3**) or illite toward actinides. Beside the clay minerals as sorbents the calcite fraction and all other calcium-containing minerals play also an important role, because they determine the background electrolyte composition, which in turn significantly affects the U(VI) and HA speciation and thus U(VI) sorption.

Concerning a nuclear waste repository, where OPA is intended to be used as part of the geological barrier, the following can be concluded. If U(VI) as part of the nuclear waste is released into the clay formation in the case of water ingress, it will be complexed by calcium and carbonate ions leached out from OPA, whereby $Ca_2UO_2(CO_3)_3(aq)$ is formed. This complex is only weakly retarded by sorption onto the clay, which can contribute to an enhanced mobility of U(VI) in the host rock. HA shows no significant influence on the U(VI) sorption behavior. Thus, the decisive retardation process seems to be the U(VI) migration through the clay rock that is governed by molecular diffusion.

Advanced studies are performed to approach further real field conditions by studying the diffusion of U(VI) in intact OPA rock cores (cf. section **5**).

5 Diffusion of U(VI) and humic acid in Opalinus Clay

The results of this section are published in Joseph et al. (2013).

5.1 Principles of molecular diffusion

The theoretical background of molecular diffusion has been described previously in detail (Van Loon et al., 2003; Van Loon and Soler, 2004). Thus, only a short summary will be given in this section.

The diffusive flux J [mol/(m^2·s)] of a solute is given by Fick's first law:

$$J = -D_e \cdot \frac{\partial c}{\partial x} \qquad \textbf{Eq. 5}$$

where the effective diffusion coefficient D_e [m^2/s] is multiplied by minus concentration gradient. c [mol/m^3] means the tracer concentration in the mobile phase and x [m] denotes the spatial coordinate. The change of concentration with time, t [s], is expressed by Fick's second law:

$$\frac{\partial c}{\partial t} = D_a \cdot \frac{\partial^2 c}{\partial x^2} \qquad \textbf{Eq. 6}$$

D_a [m^2/s] represents the apparent diffusion coefficient.

Both diffusion coefficients are linked by the rock capacity factor α [–] according to:

$$D_a = \frac{D_e}{\alpha} \qquad \textbf{Eq. 7}$$

The rock capacity factor α is defined as:

$$\alpha = \varepsilon + \rho \cdot K_d \qquad \textbf{Eq. 8}$$

where ε [–] is the diffusion-accessible porosity, ρ [kg/m^3] the dry bulk density and K_d [m^3/kg] the sorption distribution coefficient. For nonsorbing tracers such as tritiated water (HTO) with $K_d = 0$ it is assumed that α is equal to ε. The parameter D_e represents a measure for the solute flux through the clay. D_a accounts additionally for the tracer interaction with the clay.

In the present study, molecular diffusion was assumed for the migration of the used radionuclides through the OPA bore core samples. Thereby, the diffusion of HTO, ^{233}U(VI), and ^{14}C-labeled HA in OPA was studied at 25 and 60 °C under anaerobic conditions. Investigations at 60 °C were performed since the radioactive decay of the various radionuclides present in the nuclear waste will result in elevated temperatures of up to 100 °C close to the waste containers in a repository hosted by natural clay rock (Brasser et al., 2008). From HTO diffusion experiments, values for the diffusion-accessible porosity of the respective clay samples were determined (cf. section **5.5**). The U(VI) diffusion was investigated in the absence and presence of HA (cf. sections **5.6.3** and **5.6.4**). The speciation of U(VI) at elevated temperatures is only known for hydroxides and halide complexes (Grenthe et al., 1992; Guillaumont et al., 2003); however, for the present system, where alkaline earth ions and carbonate are present in solution, there are no data available. Thus, laser-induced fluorescence spectroscopy (LIFS), photon correlation spectroscopy (PCS), and scanning electron microscopy with energy dispersive X-ray detector (SEM–EDX) were applied to study the U(VI) speciation at 60 °C (cf. section **5.6.2**).

5.2 Diffusion of radionuclides through clay minerals and clay rocks

For safety assessment of potential host rocks for nuclear waste repositories, a profound knowledge of the migration behavior of accidentally released radionuclides in natural clay formations is required, also at elevated temperatures. So far, the diffusion studies in the case of OPA were mainly focused on experiments at room temperature with tracers such as HTO, $^{36}Cl^-$, $^{125}I^-$ (Van Loon et al., 2003), or $^{134}Cs^+$ (Jakob et al., 2009). Appelo et al. (2010) investigated the multicomponent diffusion in OPA for a variety of tracers (HTO, $^{22}Na^+$, $^{134}Cs^+$, $^{85}Sr^{2+}$, $^{36}Cl^-$, Br^-, and I^-). However, only few studies are known that focus on the diffusion properties of actinides in OPA. For instance, Wu et al. (2009) investigated the diffusion and sorption of Np(V) in / onto OPA and Bauer et al. (2006) studied the Pu diffusion in OPA. Bauer et al. (2006) observed an inhomogeneous Pu diffusion with no preferential pathway through the clay and determined that Pu mainly occurs as Pu(V) under these conditions. Alonso et al. (2009) were able to determine diffusion coefficients for U(VI), Re(VII), and Eu(III) already after a few days of diffusion in OPA (Mont Terri) by Rutherford backscattering spectrometry micro-scale profiling. No actinide diffusion studies in natural heterogeneous clays at elevated temperatures can be found in the literature. The first diffusion studies at elevated temperatures focused on conservative tracers and mainly on simple clay minerals. For instance, González-Sánchez et al. (2008) investigated the HTO diffusion through compacted clay minerals, namely illite, montmorillonite, and kaolinite, at different temperatures and ionic strengths. The effect of temperature on the diffusion of Na^+ (Kozaki et al., 1998; Liu et al., 2003), Cs^+ (Kozaki et al., 1996), Sr^{2+} (Kozaki et al., 1997), Cl^- (Kozaki et al., 2001), and Np(V) (Kozai et al., 2001) was studied for sodium montmorillonite. Thereby, an influence of the dry density and added sand fraction on activation energies was determined. Malikova et al. (2004) used molecular dynamics and Monte Carlo simulations to study the effect of temperature on the diffusion of Na^+ and Cs^+ in montmorillonite. Concerning natural clays, Van Loon et al. (2005) investigated OPA at higher temperatures and determined the activation energies of the self-diffusion of HTO, $^{22}Na^+$, and $^{36}Cl^-$. Recently, Savoye et al. (2011) determined the effective diffusion coefficients of HTO, $^{36}Cl^-$, $^{22}Na^+$, and $^{137}Cs^+$ through Callovo-Oxfordian Clay at 21 and 80 °C. Sodium bentonite was studied by Suzuki et al. (2004), who focused on the effect of anisotropy and temperature on diffusion of heavy water (HDO). Sato and Yui (1997) used sodium bentonite to investigate the diffusion of $^{59}Ni^{2+}$ in dependence on temperature and bentonite density.

The influence of HA on the migration of metal ions in geologic environments was investigated for U(VI) in quartz sand (Mibus et al., 2007b), for U(VI) in compacted kaolinite (Sachs et al., 2007b), and for Eu(III) in sedimentary rock (Seida et al., 2010).

5.3 Experimental set-up

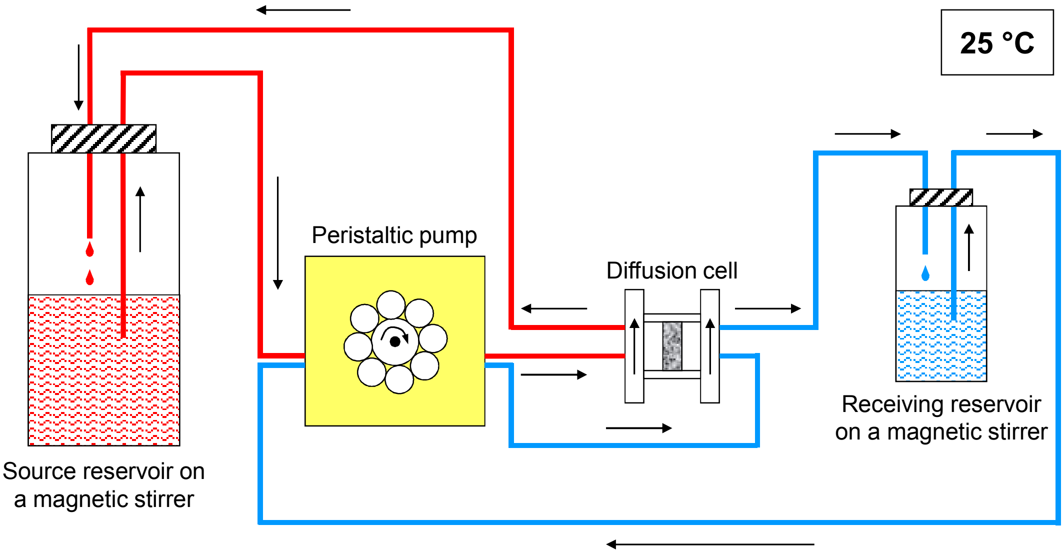
25 °C
Peristaltic pump
Diffusion cell
Receiving reservoir on a magnetic stirrer
Source reservoir on a magnetic stirrer

Fig. 33: Experimental set-up for the diffusion experiment at 25 °C (based on Van Loon et al. (2003)).

The details of the diffusion cells applied in the experiments were described by Van Loon et al. (2003). Four identical diffusion cells were used for the experiments; two cells were conditioned at 25 °C and the other two at 60 °C. Each OPA bore core sample was placed in the cells between two stainless steel filter plates (characteristics shown in section **7.6.2**, **Tab. 23**; 316L, pore diameter: 0.01 mm; MOTT industrial division, Farmington, USA).

The experimental set-up used for the diffusion experiments at 25 °C was given previously (Van Loon et al., 2003) and is shown in **Fig. 33**. The experiments were performed under anaerobic conditions (N_2). Each diffusion cell was coupled with a peristaltic pump (mod. Ecoline, Ismatec, IDEX Health & Science, Glattbrugg, Switzerland) and a source and receiving reservoir filled with 200 mL and 20 mL synthetic OPA pore water, respectively. 250 mL and 25 mL glass bottles (Duran®, Wertheim/Main, Germany) served as reservoirs. The solutions were circulating through the end plates of the cells, where they contacted the OPA samples.

For the diffusion experiments at 60 °C, the experimental set-up was changed slightly (**Fig. 34**). The diffusion cells were placed in a temperature-controlled laboratory sand-bath (mod. ST-72, Harry Gestigkeit GmbH, Düsseldorf, Germany) and the reservoirs were stirred and heated on top of a magnetic stirrer with integrated heating function (mod. MR 3002, Heidolph Instruments, Schwabach, Germany).

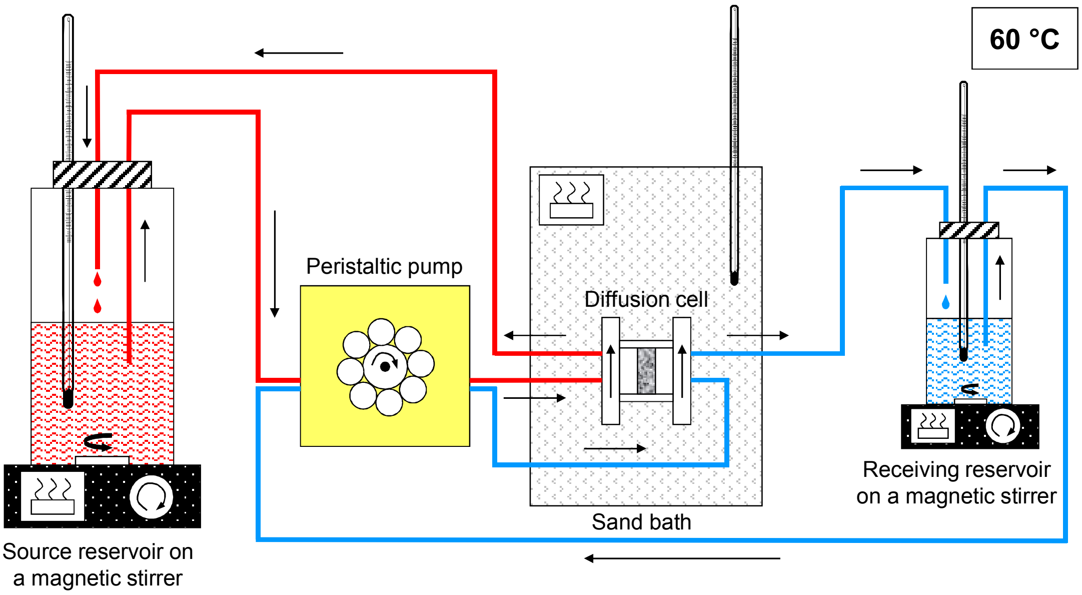
60 °C
Peristaltic pump
Diffusion cell
Sand bath
Source reservoir on a magnetic stirrer
Receiving reservoir on a magnetic stirrer

Fig. 34: Experimental set-up for the diffusion experiment at 60 °C (based on Van Loon et al. (2003)).

At first, HTO through- and out-diffusion experiments were performed as described by Van Loon et al. (2003) with all four diffusion cells – two cells at 25 °C, two cells at 60 °C – in order to determine values for the porosity of the clay samples ([HTO] = 1000 Bq/mL). After that, the ^{233}U(VI) in-diffusion in the absence and presence of ^{14}C-HA was studied. Using two diffusion cells the ^{233}U(VI) diffusion at 25 °C (cell 1) and 60 °C (cell 3) was investigated. The simultaneous diffusion of ^{233}U(VI) and ^{14}C-HA was studied (cell 2 at 25 °C and cell 4 at 60 °C) under the exclusion of light to minimize possible light-induced HA degradation processes ([^{233}U(VI)] = 1×10^{-6} mol/L, [^{14}C-HA] = 10 mg/L).

After three months, the diffusion experiments were stopped and the U(VI) and HA diffusion profiles were determined. Based on these profiles, diffusion parameters were determined as described in section **7.6.2** using COMSOL Multiphysics 3.5a (2008).

5.4 Filter diffusion parameters

For fitting the clay diffusion parameters, the diffusion characteristics of the adjacent stainless steel filter plates for HTO, U(VI), and HA have to be included in the model (cf. section **7.6.2**) because they can influence the retardation and migration of the tracer. In case of HTO, the filter K_d value was assumed to be 0. The corresponding filter D_e value, D_f, was taken from Glaus et al. (2008) and amounts to 2.3×10^{-10} m^2/s at 25 °C.

The temperature dependence of molecular diffusion can be described by the Arrhenius equation (Eisenberg and Kauzmann, 1969). With a known D_e value at a defined temperature (T_1), D_e at temperature T_2 can be calculated as follows:

$$D_e^{T_2} = D_e^{T_1} \cdot \exp\left\{\frac{E_a}{R} \cdot \left(\frac{1}{T_1} - \frac{1}{T_2}\right)\right\} \qquad \textbf{Eq. 9}$$

where E_a is the activation energy [kJ/mol] and R is the gas constant, 8.314 J/(mol·K). Using the E_a value of bulk water, i.e. E_a = 18 kJ/mol (Van Loon and Soler, 2004), D_f of HTO at 60 °C was determined to be 4.93×10^{-10} m^2/s.

Unlike HTO, for ^{233}U(VI) and ^{14}C-HA an interaction of the tracers with the filters can be assumed. The respective filter K_d values were obtained by sorption (25 °C) and extraction experiments (60 °C). For the sorption experiments, fresh filter plates were contacted with solutions of 1×10^{-6} mol/L ^{233}U(VI) or 10 mg/L ^{14}C-HA in pore water. After 2, 5, and 7 days, aliquots of the sample solutions were analyzed by LSC. The sorption of ^{233}U(VI) and ^{14}C-HA onto the filter plates was in equilibrium almost after 2 days. K_d values were determined with 7×10^{-5} m^3/kg and 1×10^{-4} m^3/kg for ^{233}U(VI) and ^{14}C-HA, respectively. At 60 °C, a sorption equilibrium of ^{233}U(VI) and ^{14}C-HA onto fresh filter plates was not reached within 28 days. Therefore, after finishing the clay diffusion experiment ^{233}U(VI) and ^{14}C-HA were extracted from the filter plates used in diffusion cells 3 and 4 with 1 mol/L HNO_3 and 2 mol/L NaOH, respectively. After shaking 5 days, the extracts were analyzed by LSC. The resulting K_d values amount to K_d(U(VI)) = 5×10^{-3} m^3/kg and K_d(HA) = 3.4×10^{-3} m^3/kg.

D_f values of U(VI) and HA were taken from the literature. If the diffusion coefficient of a certain species in bulk water, D_w [m^2/s], is known, D_f can be estimated by $D_f = D_w/10$ (Glaus et al., 2008). At 25 °C, D_f of $Ca_2UO_2(CO_3)_3$(aq), the dominating U(VI) species in pore water (cf. section **4.4.1**), was assumed to be 4.6×10^{-11} m^2/s based on the corresponding D_w from Kerisit and Liu (2010). During fitting routine this value had to be decreased slightly to 3.5×10^{-11} m^2/s. For HA, different D_w values at 25 °C were published depending on the origin and molecular size of HA (Mibus et al., 2007a; Morris et al., 1999). In this study, published D_w values for calcium humate complexes (Nebbioso and Piccolo, 2009) were applied and D_f was averaged to 1.3×10^{-11} m^2/s.

Using **Eq. 9** and E_a for bulk water, the applied D_f values at 60 °C were D_f(U(VI)) = 7.65×10^{-11} m^2/s and D_f(HA) = 2.84×10^{-11} m^2/s.

5.5 Through-diffusion of HTO in dependence on temperature

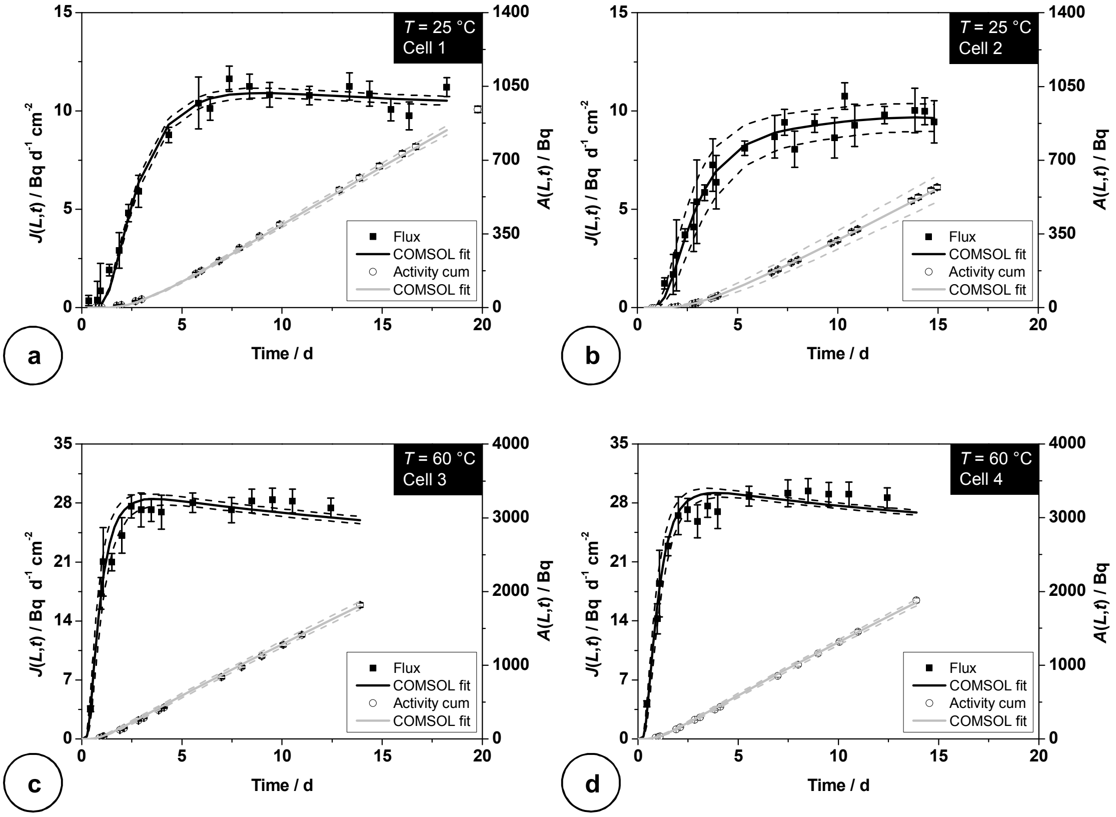

Fig. 35: Evolution of flux ($J(L,t)$) and cumulated diffused activity ($A(L,t)$) as a function of time in the HTO through-diffusion experiments at 25 °C (cells 1 and 2, **a + b**) and 60 °C (cells 3 and 4, **c + d**).

In **Fig. 35**, the time-dependent evolution of the diffusive flux and the cumulated diffused HTO activity in the receiving reservoirs are shown for 25 °C (**Fig. 35a,b**) and 60 °C (**Fig. 35c,d**), respectively. The diffusion parameter values obtained from these results are summarized in **Tab. 16**. For both temperatures the values are in relatively good agreement with literature data given by Van Loon and Soler (2004) for shaly facies OPA samples. The small differences can be explained by the fact that sandy facies OPA samples were used in the current experiments and that, in contrast to Van Loon and Soler (2004), the diffusion parameters of HTO in the adjacent filter plates were considered during COMSOL modeling. The ε values obtained by HTO diffusion experiments were incorporated in the ^{233}U(VI) and ^{14}C-HA diffusion model.

Tab. 16: Diffusion parameters of HTO in OPA determined by through-diffusion experiments at 25 and 60 °C.

	25 °C **Cell 1**	**Cell 2**	**60 °C** **Cell 3**	**Cell 4**
$[HTO]_0$ / Bq/mL	999 ± 8	1027 ± 4	1021 ± 4	1022 ± 11
V_0 / $\times 10^{-6}$ m^3 *	201.62	202.48	200.57	201.22
D_e / $\times 10^{-11}$ m^2/s	1.48 ± 0.03	1.26 ± 0.09	3.86 ± 0.07	3.98 ± 0.05
ε	0.16 ± 0.01	0.15 ± 0.01	0.16 ± 0.02	0.18 ± 0.02
$[HTO]_0$ / Bq/mL **	1217 ± 83		~ 1200 ± 90	
D_e / $\times 10^{-11}$ m^2/s **	1.21 ± 0.08		3.67 ± 0.22 / 3.93 ± 0.24	
ε **	0.09 ± 0.02		0.12 ± 0.01 / 0.19 ± 0.02	

* Initial volume of the source reservoir.

** Values from Van Loon and Soler (2004) measured at 23 °C (5 MPa) and at 65 °C (3 MPa).

5.6 Diffusion of U(VI) and humic acid in Opalinus Clay

5.6.1 Aqueous U(VI) and humic acid speciation in Opalinus Clay pore water

For the interpretation of the U(VI) diffusion results, information about the U(VI) and HA species present in solution at the beginning and end of the experiment is needed. The experiments were performed under anaerobic conditions in pore water at 25 and 60 °C. At the beginning of the diffusion experiment (at 25 °C), the $Ca_2UO_2(CO_3)_3(aq)$ complex dominates the speciation in the source reservoir solutions. The diffusion experiments were carried out for three months. After that, the U(VI) speciation was recalculated on the basis of the ion concentrations of Na, K, Sr, Al, Si, Ca, Mg, Ba, Mn, Cl^-, SO_4^{2-}, and CO_3^{2-}, the concentrations of $^{233}U(VI)$ and ^{14}C-HA, the pH, and E_h measured in the source reservoir solutions.

The results, summarized in **Tab. 17**, show that at the end of the diffusion experiments at 25 °C, $Ca_2UO_2(CO_3)_3(aq)$ is still the dominating species in all reservoir solutions. This is also true in the presence of HA, as shown for cell 2. At 60 °C, a calculation of the U(VI) speciation in pore water was not feasible due to the lack of thermodynamic data.

Initially, no silicon was present in the synthetic pore water (cf. pore $water_{theor}$, **Tab. 8**). However, due to OPA dissolution, silicon was found in the background electrolyte at the end of the diffusion experiments (cf. **Tab. 17**). The silicon concentration was also considered in subsequent speciation calculations but had no significant influence on the U(VI) speciation.

The oxidation state of uranium in the source reservoir solutions was investigated by solvent extraction (cf. section **7.3.1**). The uranium in the reservoir solutions at 25 and

Tab. 17: Characterization of the source reservoir solutions at 25 and 60 °C at the end of the ^{233}U(VI) and ^{14}C-HA diffusion experiments as well as U(VI) speciation in the reservoirs calculated for these conditions.

	25 °C		**60 °C**	
	Cell 1	**Cell 2**	**Cell 3**	**Cell 4**
[^{233}U(VI)] / mol/L	1.05×10^{-6}	9.30×10^{-7}	5.96×10^{-7}	5.00×10^{-7}
[^{14}C-HA] / mg/L	-	8.9	-	7.0
T / °C	23.3	23.3	61.5	59.2
pH	8.75	8.60	7.92	7.66
***E*$_h$** / mV	300	240	140	30
[Na] / mol/L	2.5×10^{-1}	2.3×10^{-1}	1.4×10^{-1}	1.4×10^{-1}
[K] / mol/L	2.1×10^{-3}	1.9×10^{-3}	1.8×10^{-3}	1.9×10^{-3}
[Mg] / mol/L	1.7×10^{-2}	1.7×10^{-2}	1.6×10^{-2}	1.6×10^{-2}
[Ca] / mol/L	2.4×10^{-2}	2.4×10^{-2}	2.5×10^{-2}	2.4×10^{-2}
[Sr] / mol/L	5.0×10^{-4}	5.0×10^{-4}	5.1×10^{-4}	5.1×10^{-4}
[Ba] / mol/L	7.2×10^{-8}	7.2×10^{-8}	2.3×10^{-7}	2.5×10^{-7}
[Al] / mol/L	7.8×10^{-7}	4.8×10^{-7}	1.1×10^{-6}	5.6×10^{-6}
[Si] / mol/L	8.2×10^{-5}	4.2×10^{-5}	6.5×10^{-4}	1.6×10^{-3}
[Mn] / mol/L	7.9×10^{-7}	8.0×10^{-7}	2.8×10^{-6}	2.6×10^{-6}
[Cl^-] / mol/L	3.0×10^{-1}	3.0×10^{-1}	3.0×10^{-1}	3.0×10^{-1}
[SO_4^{2-}] / mol/L	1.3×10^{-2}	1.4×10^{-2}	1.5×10^{-2}	1.5×10^{-2}
[CO_3^{2-} / HCO_3^-] / mol/L	3.6×10^{-4}	4.2×10^{-4}	3.2×10^{-4}	2.8×10^{-4}
U(VI) speciation (aqueous species accounting for 99 % or more)				
- **$Ca_2UO_2(CO_3)_3(aq)$**	97.87 %	97.14 %	not known	
- **$UO_2(CO_3)_3^{4-}$**	0.83 %	0.85 %		
- **$MgUO_2(CO_3)_3^{2-}$**	0.74 %	0.76 %		
- **$UO_2(CO_3)_2HA(II)^{4-}$**	-	0.70 %		

60 °C remained U(VI); no U(IV) was detected. This is not surprising since the measured *E*$_h$ values in the source solutions were too high for U(IV) to be formed (cf. **Tab. 17**, **Fig. 22**).

In **Fig. 36**, the particle size distributions of ^{14}C-HA colloids in the presence of ^{233}U(VI) are shown for the source reservoir solutions of cells 2 and 4 at the beginning and the end of the diffusion experiments. At 25 °C, before the diffusion experiment was started, the HA colloids present in the source reservoir solution showed a wide size distribution, where HA colloids < 100 kDa were clearly predominant. Furthermore, **Fig. 36a** shows that no interaction occurred between ^{14}C-HA and ^{233}U(VI). Since then, the particle size distribution should show the same pattern for ^{14}C-HA and ^{233}U(VI). In this study, ^{233}U(VI)

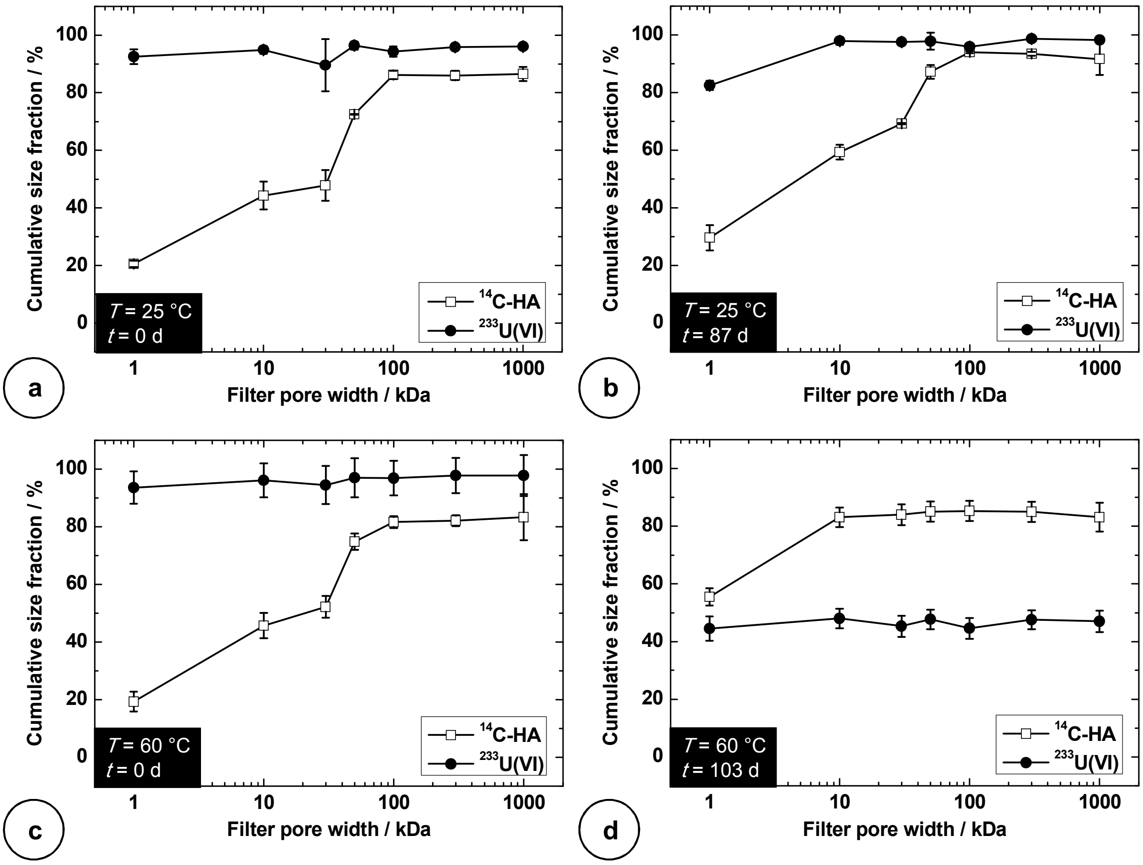

Fig. 36: Particle size distribution of ^{14}C-HA colloids in the presence of ^{233}U(VI) in the source reservoir solutions at 25 °C (cell 2; **a + b**) and 60 °C (cell 4; **c + d**) at the beginning (**a + c**) and the end (**b + d**) of the diffusion experiments. Percentage distribution refers to the respective concentration of ^{233}U(VI) and ^{14}C-HA in the unfiltered solution at the beginning and the end of the diffusion experiments.

passed all particle size filters without any significant hindrance, unlike HA. Thus, a diffusing U(VI)-HA species can be excluded. Within three months (**Fig. 36b**), HA degradation processes occurred to some extent. The fraction of HA colloids < 100 kDa was slightly increased. However, there was still no significant interaction observable between ^{14}C-HA and ^{233}U(VI), even after 87 days. This observation confirms the results of the speciation calculations shown in **Tab. 17**, where the fraction of $UO_2(CO_3)_2HA(II)^{4-}$ amounts to < 1 %.

At 60 °C, the particle size distribution of ^{14}C-HA and ^{233}U(VI) at the beginning of the investigations (**Fig. 36c**) was similar to that at 25 °C (**Fig. 36a**). However, the particle size distribution obtained after three months shows that the HA degradation at 60 °C was stronger than at 25 °C, since the fraction of HA colloids < 100 kDa was increased (**Fig. 36d**). This result is quite surprising because the opposite effect (i.e. condensation of humic material to larger polyaromatic structures) is reported in the literature (Kolokassidou et al., 2007). An interaction between ^{14}C-HA and ^{233}U(VI), which would yield a similar particle size distribution, could not be detected. At 60 °C, only about 50 %

of the uranium in the solution at the end of the diffusion experiment occurred as aqueous U(VI) species, which passed the filters. However, about 50 % of U(VI) were found to be retained on the various particle size filters (**Fig. 36d**), that means, U(VI) particles must have a size > 1000 kDa. These results indicate a change of the U(VI) speciation at 60 °C. Presumably, U(VI) formed colloids in pore water at 60 °C. These were not able to pass the used particle size filters. To investigate the U(VI) speciation at 60 °C, additional spectroscopic investigations were performed, as discussed in section **5.6.2**.

The solutions in the receiving reservoirs of cells 2 and 4 were analyzed regularly for tracers and their particle size distribution. No ^{233}U(VI) was detected in these reservoirs. At the end of the diffusion experiment at 25 °C, diffused HA colloids (< 1 kDa) were detected in the receiving reservoir of cell 2. At 60 °C, the solution in the receiving reservoir of cell 4 turned yellow already after one week, which is an indication of the presence of HA. About 25 days after starting the diffusion experiment, small HA colloids (< 1 kDa) could clearly be detected in the receiving reservoir solution. A further characterization of the diffused ^{14}C-containing molecules could not be performed due to their very low concentration (25 °C: 7.3×10^{-3} mg/L; 60 °C: 6.4×10^{-2} mg/L). However, since the color of the solution changed, it can be excluded that the detected diffused ^{14}C is CO_3^{2-}, which is a potential degradation product of HA. A filtration effect of clay was also observed by Sachs et al. (2007b) for the HA diffusion through compacted kaolinite.

5.6.2 Study of the U(VI) speciation in Opalinus Clay pore water at 60 °C

At 60 °C, the U(VI) species present in the source reservoir solution are not known. Thus, an experiment was performed to investigate this system in more detail. U(VI) (1×10^{-4} mol/L) was equilibrated in pore water (pH 7.6) at 60 °C (cf. section **7.3.3**). Periodically, samples were analyzed by LIFS.

The measured luminescence spectra of U(VI) in pore water are shown in **Fig. 37** as a function of equilibration time. The U(VI) luminescence spectrum obtained after 3 days is characterized by four emission bands with maxima at 467.0, 484.9, 504.7, and 527.2 nm. Since the $Ca_2UO_2(CO_3)_3$(aq) complex dominates the U(VI) speciation at 25 °C, this complex was assumed to be present at 60 °C as well. Therefore, a $Ca_2UO_2(CO_3)_3$(aq) model solution was prepared as described in Bernhard et al. (2001) and investigated by LIFS at different temperatures for comparison. The positions of the main bands of the respective luminescence spectra did not change with temperature (not shown). The emission bands of the spectrum obtained at 65 °C were in excellent agreement with the spectrum of U(VI) in the pore water after 3 days. With proceeding equilibration of U(VI) in pore water at 60 °C, a small shift of the U(VI) emission bands to

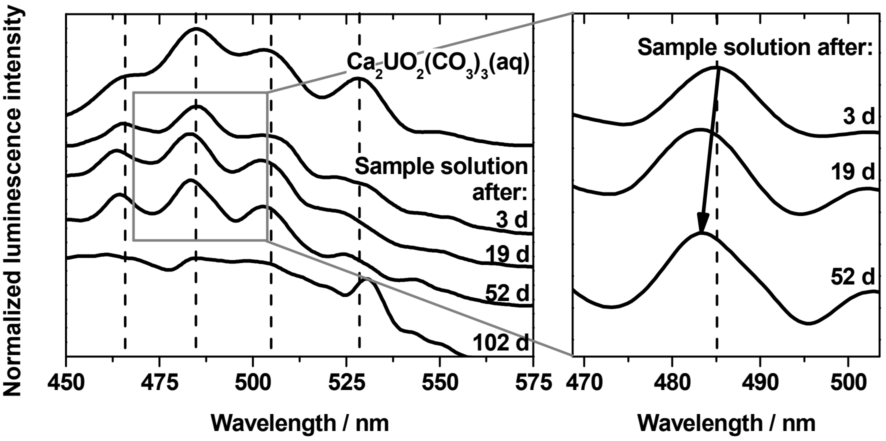

Fig. 37: Luminescence spectra of U(VI) ($[U(VI)]_0 = 1\times10^{-4}$ mol/L) in pore water at 60 °C as a function of equilibration time. For clarity, the spectra were normalized to a maximum intensity of 1 and shifted along the y-axis. As reference, the luminescence spectrum of $Ca_2UO_2(CO_3)_3(aq)$ at 65 °C is shown. The spectra were smoothed by Fast Fourier Transform filtering.

lower wavelengths was detected. At the end of the experiment (102 days), only a low intensity of the original U(VI) emission bands, but a strong band at 532 nm was observed. The variations in the emission band positions can be an indication for the slow transformation of the aqueous U(VI) species, $Ca_2UO_2(CO_3)_3(aq)$, to a colloidal U(VI) species. Consequently, the concentration of $Ca_2UO_2(CO_3)_3(aq)$ in solution decreased. Bernhard et al. (2001) described a similar small difference in the main emission bands and attributed it to the presence of both aqueous and solid species. The possible existence of a colloidal species is also verified by the distinct band at 532 nm, which results from the backscattering of the excitative laser beam (excitation wavelength: 266 nm) from the surface of the dispersed solid species. All three changes – shift in band positions, decrease of the luminescence intensity, and backscattering of the laser pulse at 532 nm – observed in the U(VI) / pore water system over time are clear indications of the formation of a colloidal U(VI) species.

The U(VI) samples with pore water were additionally analyzed by PCS. After 3 days, the scattered light intensity of the sample was equal to the count rate measured for Membrapure water (Membrapure Astacus, Bodenheim, Germany). That means that initially no colloids were present in the sample solution. After 102 days, the scattered light intensity was a 1000-fold higher in the sample. This indicates the formation of colloids. Additionally, the PCS showed a wide particle size distribution, no distinct particle size could be defined.

The colloidal phase of the sample after 102 days of equilibration was separated from solution by filtration (cf. section **7.3.3**) and analyzed by SEM–EDX. An image of the particles and their respective EDX spectra are shown in **Fig. 38**.

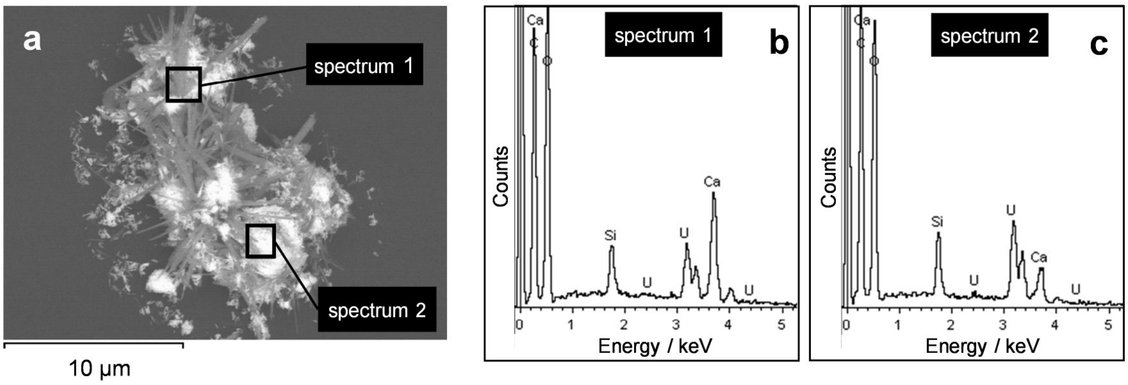

Fig. 38: (**a**) SEM image of the separated particles sputtered with carbon, (**b, c**) EDX spectra measured at the spots indicated by the boxes in (**a**) ($[U(VI)]_0 = 1\times10^{-4}$ mol/L; pore water).

The separated particles visible on the SEM image in **Fig. 38a** show a high heterogeneity. That was to be expected since different salts can precipitate in OPA pore water when heated up to 60 °C, especially after pH adjustment with Na_2CO_3. As shown in literature, various salts have a lower solubility at 60 °C than at 25 °C. In dependence on their specific solubility restrictions, precipitates of $SrCO_3$ (Busenberg et al., 1984), $CaCO_3$ (Brečević and Nielsen, 1989; Wolf et al., 1989), $MgCO_3$ (Königsberger et al., 1999), $SrSO_4$ (Reardon and Armstrong, 1987), and $CaSO_4$ (Power et al., 1966) can be expected. Since calcium and carbonate ions have relatively high solution concentrations in the U(VI) / pore water system, $CaCO_3$ particles are assumed to dominate the investigated colloids. Additionally, a small quantity of a U(VI) colloidal species is expected to be formed.

After analysis of the respective EDX spectra the following mean element fractions were obtained: Ca (7.1 mol%), Si (2.6 mol%), U (3.1 mol%), C (38.6 mol%), and O (48.6 mol%). The high content of C and O in the particles originates partially from the applied polycarbonate membranes for filtering of the solution. Additionally, the carbon used for sputtering artificially increased the carbon fraction of the investigated particles. Alternatively, the filter section could be sputtered with gold. However, this was not feasible since the resulting gold signals would overlap the signals of uranium in the EDX spectrum. Sulfur was not detected by EDX; it would show a signal at 2.3 keV. That means that colloids consisting of sulfate were not formed within the duration of the experiment.

As visible in the SEM image, it is not possible to distinguish between the different colloidal species which are formed upon heating of the solution. However, based on the EDX results, it is possible to limit the presumably formed colloidal U(VI) species to $CaUO_4$, uranophane $Ca(UO_2)_2SiO_3(OH)_2\cdot5\ H_2O$, and liebigite $Ca_2UO_2(CO_3)_3\cdot11\ H_2O$. It should be noted that an unknown colloidal U(VI) species can be formed during the experiment as well, since the U(VI) speciation at elevated temperatures is still unresolved. In contrast to the possible formation of U(VI) colloids, U(VI) can sorb onto inorganic colloids such as $CaCO_3$ particles and thus be transported in OPA.

Since there was no clay added to the solution, the origin of silicon in the EDX spectra has to be attributed to the glass bottle used in the experiment. Compared to the source reservoir solution of cell 3 at the end of the diffusion experiment, where silicon was additionally leached out of the OPA sample ([Si] = 6.5×10^{-4} mol/L), less silicon was found in the solution of this experiment without OPA ([Si] = 2.4×10^{-4} mol/L). Whether silicon contributes to the formed colloidal U(VI) species or not, cannot be clarified so far.

5.6.3 Diffusion of U(VI) and humic acid in Opalinus Clay at 25 °C

The experiments were conducted for three months. Within this time span, no ^{233}U(VI) could be detected in the receiving reservoirs of cells 1 and 2. However, as discussed in section **5.6.1**, diffused HA colloids were found.

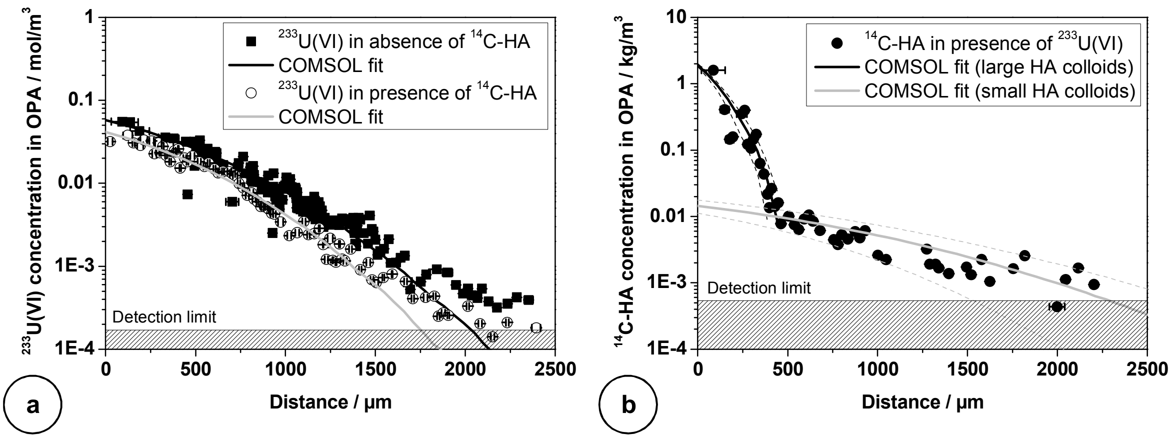

Fig. 39: Concentration profiles of ^{233}U(VI) in the absence (filled symbols) and presence (open symbols) of ^{14}C-HA (**a**) and of ^{14}C-HA in the presence of ^{233}U(VI) (**b**) in OPA at 25 °C.

In **Fig. 39a**, the ^{233}U(VI) diffusion profiles determined in the absence and presence of HA are shown. The comparison of the two data sets leads to the conclusion that in the presence of HA, ^{233}U(VI) penetrates the clay less deeply than in the absence of HA. A similar reduced metal ion diffusion in the presence of HA was already described by Seida et al. (2010) for the Eu(III) diffusion in sedimentary rock and by Mibus and Sachs (2006) for the U(VI) diffusion in compacted kaolinite.

Based on the ^{233}U(VI) distribution profiles in the samples and the additional information about the temporal evolution of the tracer concentration in the source reservoir, both parameters D_e and K_d can be adjusted individually. Their values are summarized in **Tab. 18**. The K_d value for U(VI) determined from the present diffusion studies agrees well with the K_d value determined by means of batch sorption experiments using crushed OPA material (cf. section **4.4.4**). In contrast, Wu et al. (2009) determined a larger K_d value for the Np(V) / OPA system by diffusion experiments (K_d = 0.1 ± 0.01 m^3/kg) than by batch sorption measurements (K_d = 0.025 ± 0.005 m^3/kg). The authors concluded that Np(V) was partially reduced to Np(IV) during the diffusion experiment. Since the K_d values determined for the U(VI) / OPA system by batch sorption and diffusion experiments are comparable, a reduction of U(VI) to U(IV) during the diffusion experiment can be excluded. This was also verified by solvent extraction experiments of source reservoir solution (cf. section **5.6.1**).

Tab. 18: Values for the ^{233}U(VI) and ^{14}C-HA diffusion parameters obtained at 25 °C.

	U(VI) in the absence of HA	**U(VI) in the presence of HA**		
	^{233}U(VI)	**^{233}U(VI)**	**HA**	
			large colloids	**small colloids**
[^{233}U(VI)]$_0$ / mol/L	1.07×10^{-6}	9.98×10^{-7}		
[^{14}C-HA]$_0$ / mg/L	-		10.1	3 *
V_0 / $\times 10^{-6}$ m^3	202.18		167.71	
t / d	89		87	
ρ / kg/m^3	2424		2392	
ε **	0.16 ± 0.01		0.15 ± 0.01	
α	61 ± 7	48 ± 7	309 ± 45	5 ± 1.2
D_e / $\times 10^{-12}$ m^2/s	1.9 ± 0.4	1.2 ± 0.3	0.65 ± 0.25	0.4 ± 0.25
D_a / $\times 10^{-14}$ m^2/s	3.1 ± 0.3	2.5 ± 0.3	0.21 ± 0.05	8 ± 3
K_d / m^3/kg	0.025 ± 0.003	0.020 ± 0.003	0.129 ± 0.018	0.002 ± 0.0005
K_d / m^3/kg ***	0.0222 ± 0.0004		0.129 ± 0.006	

* Based on c_0 and the fact, that about 30 % of HA colloids are < 1 kD (cf. **Fig. 36b**).

** Determined by HTO through-diffusion.

*** Determined by sorption experiments (cf. section **4.4.4**).

In comparison to Np(V) (Wu et al., 2009), the K_d of U(VI) determined by diffusion is one order of magnitude smaller, which implicates a weaker interaction of U(VI) with OPA compared to that of Np(V) – or of Np(IV) after reduction – with OPA. This is in contrast to the findings of Křepelová et al. (2006) and Schmeide and Bernhard (2010), who investigated U(VI) and Np(V) sorption on kaolinite. At pH 8, the K_d value of U(VI) was about one order of magnitude higher than the K_d of Np(V) ($[An]_0 = 1 \times 10^{-5}$ mol/L, I = 0.01 mol/L $NaClO_4$, $pCO_2 = 10^{-3.5}$ atm). The reason for these results was the absence of calcite and pyrite in the kaolinite model systems. In the diffusion studies with the complex clay rock OPA, these mineral constituents determine the U(VI) speciation (calcite) and Np oxidation state (pyrite) and lead to the reverse result.

The D_e value for the Np(V) diffusion in OPA amounts to $(6.9 \pm 1.1) \times 10^{-12}$ m^2/s (Wu et al., 2009). The D_e of U(VI) shown in **Tab. 18** is smaller. That means that if the same concentration gradient in diffusion experiments with Np(V) and U(VI) is applied, U(VI) would diffuse with a smaller flux through OPA than Np(V). However, the comparison of the D_a values which additionally consider the interaction of the actinides with OPA shows that the Np(V) diffusion in OPA, with a value of $D_a = (2.8 \pm 0.4) \times 10^{-14}$ m^2/s, is in the same range as that for U(VI). This leads to the conclusion that the migration of both actinides through OPA is similar.

The ε values for U(VI) and HA are expected to be smaller than that for HTO due to steric hindrance. However, the ε values of HTO were used for modeling. Since sorption of U(VI) onto inner surfaces of OPA is dominant, possible uncertainties regarding transport-relevant porosity are secondary (see also **Eq. 8** in this context).

A comparison of the K_d as well as D_e values determined for U(VI) in the absence and presence of HA shows that based on the experimental uncertainties, HA does not have a significant effect on U(VI) diffusion through compacted water-saturated OPA. Therefore, a major influence of diffusing $UO_2(CO_3)_2HA(II)^{4-}$ (cf. **Tab. 17**) was not observed. In section **4.4**, the U(VI) / HA / OPA / pore water system was investigated by means of batch sorption experiments. There, no influence of HA on the U(VI) interaction with OPA was observed, too. This result is confirmed by the diffusion experiments with intact OPA bore core samples.

In **Fig. 39b**, the diffusion profile measured for HA in OPA at 25 °C is shown. The profile indicates the presence of two size fractions of HA colloids, which are assigned to (i) a high molecular size HA colloid fraction (large HA colloids) and (ii) a low molecular size HA colloid fraction (small HA colloids). Within three months, the larger colloids diffused only about 500 µm into the OPA bore core due to restriction in the available pore space and due to strong sorption onto the OPA surface. However, the smaller HA colloid fraction showed a weaker sorption affinity toward OPA and diffused through the entire OPA sample and therefore, could be detected in the receiving reservoir. For both HA size fractions, the values for the diffusion parameters are presented in **Tab. 18**.

In comparison to the HA diffusion through compacted kaolinite ($D_a = 2.2 \times 10^{-12}$ m^2/s, pH 7, $\rho = 1670$ kg/m^3; (Sachs et al., 2007b)), the HA diffusion through OPA is much slower, which is due to the higher dry bulk density of OPA providing less pore space for diffusion. In section **4.4.4**, the K_d value of HA with OPA was determined by batch sorption experiments (cf. **Tab. 18**). This result is in very good agreement with the K_d value fitted for the large HA colloid fraction in the present diffusion experiment.

5.6.4 Diffusion of U(VI) and humic acid in Opalinus Clay at 60 °C

Similar to the experiments at 25 °C, no ^{233}U(VI) (cells 3 and 4) could be detected in the receiving reservoirs at 60 °C. However, small HA colloids (cell 4) were detected.

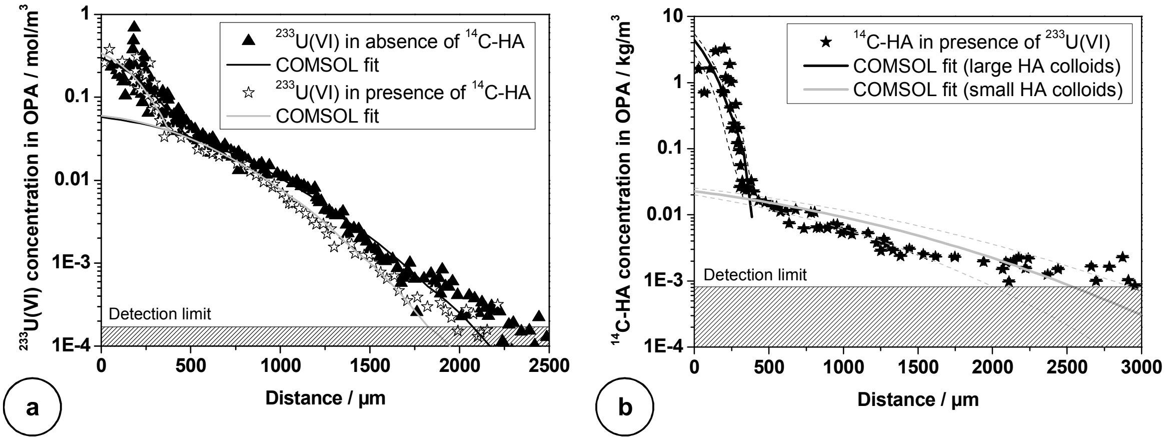

Fig. 40: Concentration profiles of ^{233}U(VI) in the absence (filled symbols) and presence (open symbols) of ^{14}C-HA (**a**) and of ^{14}C-HA in the presence of ^{233}U(VI) (**b**) in OPA at 60 °C.

Fitting the ^{233}U(VI) diffusion profiles, it became obvious that at least two different U(VI) species are involved in the diffusion process (**Fig. 40a**), which is indicated by two profiles. Based on the observations made with LIFS measurements and considering the PCS and SEM–EDX results, these two species were attributed to a diffusing colloidal and a diffusing aqueous U(VI) species ($Ca_2UO_2(CO_3)_3$(aq)). The colloidal U(VI) species was restricted in its migration and diffused only about 500 µm into the OPA sample. This is indicated by the intersection of the first profile with the second profile. The aqueous U(VI) species was more mobile (about sixfold D_a of the colloidal species; cf. **Tab. 19**) and could be detected up to a diffusion distance of about 2.5 mm.

As shown by LIFS studies, the amount of the colloidal U(VI) species increases and the concentration of $Ca_2UO_2(CO_3)_3$(aq) in solution decreases with time (cf. **Fig. 37**). Although the colloidal U(VI) species is unknown so far, it can be concluded, that both U(VI) species and thus also their respective diffusion profiles are dependent on each other. The colloidal U(VI) species is thermodynamically more stable than the aqueous U(VI) species. One can imagine that if the source reservoir solution was equilibrated more than three months at 60 °C, the fraction of the colloidal U(VI) species would increase further.

In comparison to the ^{233}U(VI) diffusion at 25 °C, the interaction of ^{233}U(VI) with OPA is stronger for both U(VI) species at 60 °C. The fitted K_d value for the colloidal U(VI) species is one order of magnitude larger than that at 25 °C. Several studies investigated the interaction of metal ions with mineral surfaces in dependence on temperature. For instance, an increased sorption at elevated temperatures was observed for Ni(II) and

Tab. 19: Values for the ^{233}U(VI) and ^{14}C-HA diffusion parameters obtained at 60 °C.

	U(VI) in the absence of HA		**U(VI) in the presence of HA**			
	^{233}U(VI)		**^{233}U(VI)**		**HA**	
	colloidal	**aqueous**	**colloidal**	**aqueous**	**large colloids**	**small colloids**
[^{233}U(VI)]$_0$ / mol/L	1.00×10^{-6}		9.94×10^{-7}			
[^{14}C-HA]$_0$ / mg/L	-				9.91	5.95 *
V_0 / $\times10^{-6}$ m^3	202.02		221.67			
t / d	102		103			
ρ / kg/m^3	2421		2404			
ε **	0.16 ± 0.02		0.18 ± 0.02			
α	605 ± 122	109 ± 12	722 ± 120	120 ± 12	962 ± 481	3.8 ± 0.5
D_e / $\times10^{-12}$ m^2/s	3 ± 1	3 ± 0.5	2.2 ± 0.8	2.5 ± 0.5	1.2 ± 0.8	0.35 ± 0.15
D_a / $\times10^{-14}$ m^2/s	0.50 ± 0.07	2.8 ± 0.2	0.30 ± 0.07	2.1 ± 0.2	0.12 ± 0.02	9 ± 2
K_d / m^3/kg	0.25 ± 0.05	0.045 ± 0.005	0.30 ± 0.05	0.050 ± 0.005	0.4 ± 0.2	0.0015 ± 0.0002

* Based on c_0 and the fact, that about 60 % of HA colloids are < 1 kD (cf. **Fig. 36d**).

** Determined by HTO through-diffusion.

Ln(III) onto montmorillonite (Tertre et al., 2005) as well as for Np(V), U(VI), and Eu(III) onto OPA (Fröhlich et al., 2012; Schmeide and Joseph, 2012; Schott et al., 2012).

With increasing temperature an increase of D_e is observed. Using **Eq. 9**, the activation energy, E_a, for the diffusion of U(VI) in OPA is estimated to be 10 kJ/mol. Such a value seems to be low when compared to E_a values for HTO with 21.1 ± 1.6 kJ/mol, for Na^+ with 21.0 ± 3.5 kJ/mol, and for Cl^- with 19.4 ± 1.5 kJ/mol (Van Loon et al., 2005). That means that the migration of U(VI) into OPA is less influenced by temperature than the diffusion of HTO, Na^+, or Cl^-. However, the calculated activation energy is based only on two temperatures and therefore, represents a preliminary result. Further temperature-dependent measurements are necessary to verify this value. In the future, the knowledge of the verified E_a for U(VI) in OPA will allow the calculation of D_e values as a function of temperature.

The D_e values of the colloidal and aqueous U(VI) species are equal. This is surprising because D_e is inversely proportional to the particle diameter according to the Stokes-Einstein equation. Therefore, a smaller D_e value of the colloidal U(VI) species would be expected due to its larger size. Based on the absence of structural evidence, the possible presence of preferential diffusion paths was neglected. A possible reason for the equal D_e values could be that diffusion as well as filtration effects play a role in the migration of the colloids through OPA as described by Voegelin and Kretzschmar (2002). Presumably, this can affect the determined values for the colloidal transport parameters. In order to adequately describe the aquatic / colloid system, the transport model should also account for the key aspects of an appropriate filtration theory. However, such an issue was far beyond the goals of the current study. For simplicity reason and due to lack of appropriate data, colloid formation in the sample was neglected in the model.

The D_a values for the U(VI) diffusion in OPA at 25 and 60 °C (aqueous U(VI) species) are almost equal within the experimental error. Obviously, the migration of aqueous U(VI) species through OPA is similar at both investigated temperatures. The breakthrough of U(VI) through OPA at 25 and 60 °C can be expected at roughly the same time.

The ^{233}U(VI) diffusion profiles at 60 °C in the absence and presence of HA are shown in **Fig. 40a**. The differences between both profiles are slightly smaller compared to the profiles obtained at 25 °C. Indeed, the corresponding diffusion parameter values support this observation (**Tab. 19**). The comparison of the U(VI) diffusion parameters of both U(VI) species in the absence and presence of HA shows that the K_d values are slightly increased and that the D_e values are slightly decreased in the presence of HA. However, within the experimental uncertainties, no significant influence of HA on the

U(VI) diffusion at 60 °C can be observed. That means that HA have no significant influence on the U(VI) migration through OPA independent of the temperature investigated in the present study. It can be concluded that small diffusing HA colloids merely have a minor potential for complexing and transporting U(VI).

Fig. 40b depicts the HA diffusion through OPA at 60 °C. The profile is very similar to that shown in **Fig. 39b**. Once more, the presence of several diffusing HA size fractions can be deduced. Close to the OPA / source reservoir boundary, the data of the large HA colloid fraction obtained at 60 °C scatter over a much wider range compared to the profile at 25 °C, making the fitting procedure more difficult. Presumably, this scattering results from the HA degradation process (cf. **Fig. 36**), which takes place during the diffusion experiment and is increased at elevated temperatures. It can be assumed that the present HA molecules as well as their degradation products show different sorption and diffusion properties resulting in a more complex HA diffusion profile in OPA. However, to be comparable with the diffusion results obtained at 25 °C, the fit of the profile was restricted to the contributions of only two HA size fractions.

The experimentally obtained K_d values indicate a somewhat stronger interaction of the large-sized HA fraction with OPA at 60 °C than at 25 °C. For the small-sized HA fraction such an influence of temperature on K_d was not detected. Due to large uncertainties, no effect of temperature on D_e for both HA fractions could be observed. However, the earlier detection of HA in the receiving reservoir at 60 °C compared to the experimental findings at 25 °C points toward a higher D_e value for the HA diffusion (small HA colloids) at 60 °C.

5.7 Conclusions for the diffusion of U(VI) and humic acid in Opalinus Clay

Diffusion experiments with ^{233}U(VI) in pristine samples of consolidated OPA were carried out under anaerobic conditions. The influence of both HA and elevated temperatures on the ^{233}U(VI) diffusion was investigated.

Speciation calculations showed that $Ca_2UO_2(CO_3)_3(aq)$ is the dominating U(VI) species in the source reservoir solution and therefore, the main diffusing U(VI) species at 25 °C during the whole diffusion experiment.

The ^{233}U(VI) and ^{14}C-HA diffusion profiles obtained from diffusion experiments were fitted. At 25 °C, K_d values were obtained for U(VI) (K_d = 0.025 ± 0.003 m^3/kg) and HA (large-sized HA colloids; K_d = 0.129 ± 0.018 m^3/kg) which are in very good agreement with K_d values determined by batch sorption experiments using crushed OPA material (cf. section **4.4.4**).

At 60 °C, LIFS and PCS studies showed that beside the aqueous species – identified as $Ca_2UO_2(CO_3)_3(aq)$ – a colloidal species is formed in solution with time.

SEM–EDX investigations showed that the colloidal species can contain U, C, O, Ca, and possibly Si, which points to the formation of dispersed solid uranium compounds such as $CaUO_4$, uranophane $Ca(UO_2)_2SiO_3(OH)_2 \cdot 5\ H_2O$, or liebigite $Ca_2UO_2(CO_3)_3 \cdot 11\ H_2O$. Otherwise, an unknown colloidal uranium species might have formed or U(VI) might be sorbed onto inorganic colloidal particles. Further investigations using XRD and EXAFS spectroscopy are necessary to identify the U(VI) species.

At 60 °C, diffusion profiles of two U(VI) species were observed in agreement with the speciation studies. These species could be attributed to a colloidal and an aqueous U(VI) species. The colloidal U(VI) species showed a higher affinity to OPA illustrated by an increased K_d value. Due to this and a restricted pore space available for transport, this species diffused only about 500 µm into OPA. Unlike the colloidal U(VI) species, the aqueous U(VI) species showed a weaker interaction with OPA. A deeper penetration into the clay was observed. However, compared to U(VI) at 25 °C, both U(VI) species showed higher K_d and D_e values. Based on D_e at 25 and 60 °C, a preliminary activation energy E_a of about 10 kJ/mol was estimated for the diffusion of U(VI) in OPA. Nearly equivalent D_a values were determined for the diffusion of the aqueous U(VI) species in OPA at 25 and 60 °C. Therefore, the breakthrough of U(VI) through OPA is expected to be independent of the temperatures investigated in the present study and should occur at nearly the same time. Modeling calculations were performed based on the best fit values of the diffusion parameters obtained at 25 and 60 °C. In **Fig. 41**, the modeled evolution of the ^{233}U(VI) concentration in the respective receiving reservoirs is presented as a function of time. The results demonstrate that at 25 and 60 °C U(VI) would need about 9 and 14.5 years, respectively, to migrate through an 11 mm thick OPA sample.

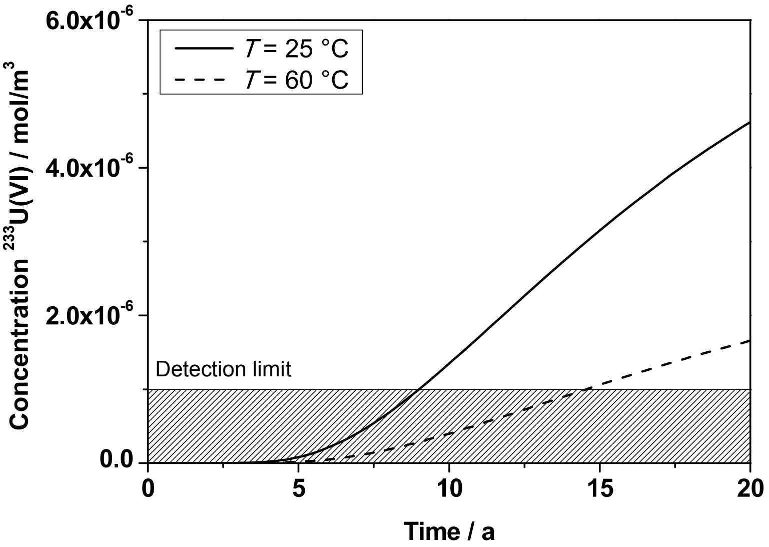

Fig. 41: Modeled evolution of the ^{233}U(VI) concentration in the receiving reservoir as a function of time at 25 and 60 °C.

For HA, a wide particle size distribution was determined in the source reservoir solution. Within the three months duration of the diffusion experiment, a degradation process was observed which became stronger at higher temperatures.

The diffusion results for HA at 25 and 60 °C showed that two distinct HA size fractions – a large- and a small-sized colloid fraction – were diffusing through the OPA samples. Within three months, the high molecular size HA colloids migrated only about 500 µm into the clay, whereas the low molecular size HA colloids diffused through the entire OPA samples (thickness: 11 mm) and consequently, were detected in the receiving reservoir. These findings demonstrate a filtration effect of the compacted clay. For the large HA colloid fraction, an increased K_d value was determined at 60 °C compared to that at 25 °C. The diffusion experiments revealed that the effect of HA on ^{233}U(VI) diffusion is negligible at both temperatures.

Regarding the suitability of OPA as host rock for a future nuclear waste repository, the diffusion experiments showed that OPA has a good retardation potential for U(VI) both at 25 and 60 °C. Although, in the case of water ingress, the U(VI) released from the nuclear waste will form weakly sorbing and consequently, mobile $Ca_2UO_2(CO_3)_3$(aq), the molecular diffusion process through OPA will retard the migration of $Ca_2UO_2(CO_3)_3$(aq). Thereby, the U(VI) diffusion behavior through OPA is comparable to that of Np(IV,V). Humic substances, being ubiquitous in soils and sediments and showing good complexation abilities for cations, have a negligible influence on the U(VI) migration through OPA even at elevated temperatures.

6 Outlook

The interpretation of the batch sorption experiments in this study revealed that there is still a lack of knowledge concerning the U(VI)-sorbing mineral phases of OPA in dependence on pH. Future work in the U(VI) / OPA system should focus on the determination of their specific contributions, especially, of the iron-containing minerals (pyrite, siderite, and their oxidation products). In addition, there are still open questions concerning the formed U(VI) surface complexes. In particular, the U(VI) surface complexes which are present under near-neutral pH conditions, where $Ca_2UO_2(CO_3)_3$(aq) determines the U(VI) speciation, should be identified. To answer these questions, batch sorption experiments with U(VI) are suggested, where individual noncalcareous mineral phases of OPA mixed with calcite act as sorbent. Thereby, calcite should be added to the system to influence the U(VI) speciation under near-neutral pH conditions. The formed U(VI) surface complexes should be characterized by potentiometric titration in connection with surface complexation modeling and suitable spectroscopic techniques (e.g., ATR FT–IR spectroscopy, EXAFS spectroscopy).

Furthermore, studies in the U(VI) / pore water system at higher temperatures should be extended. For instance, diffusion experiments at further elevated temperatures should be performed to validate the activation energy for the U(VI) diffusion through OPA determined in this study. Since the detailed U(VI) speciation in dependence on temperature is still unclear, the speciation studies at higher temperatures started in the present work should be intensified using calorimetry and spectroscopic methods such as TRLFS. The investigation of the U(VI) speciation at 60 °C showed that, in addition to $Ca_2UO_2(CO_3)_3$(aq), U(VI) was present as colloidal species. The nature and structure of this formed solid U(VI) species should be clarified, for instance by EXAFS spectroscopy or XRD.

7 Experimental details

7.1 Materials, methods, and solutions

7.1.1 Kaolinite

Georgia kaolinite, batch KGa-1b (Pruett and Webb, 1993), was obtained from the Clay Mineral Society.

7.1.2 Opalinus Clay

Three different bore cores of OPA from the Mont Terri rock laboratory, Switzerland were used (BHE-24/1, BLT-11/01, BLT-14). Bore cores BHE-24/1 and BLT-11/01 were taken by the BGR using air as drilling medium (Bossart and Thury, 2008) in September 2003. Bore core BLT-14 was extracted using the conservative single core technique in 2006/2007. Batch BHE-24/1 (bore core location coordinates: x: 2'579'354 – 381; y: 1'247'613 – 642; z: 513 – 516 in the Swiss LV95 coordinate system) was taken at a depth of 3.3 to 3.56 m. Bore core BLT-11/01 (x: 2'579'390.931; y: 1'247'630.298; z: 512.889) and bore core BLT-14 (x: 2'579'336.109; y: 1'247'711.127; z: 517.274) were taken at a depth of 3.06 – 3.07 m and 0.25 – 0.5 m, respectively. All bore cores were stored under argon atmosphere.

The preparation of the crushed and intact OPA bore core samples was performed at the Karlsruhe Institute of Technology – Institute for Nuclear Waste Disposal. For this, only the inner part of the bore cores was used for sample preparation.

7.1.3 Background electrolytes

Tab. 20: Composition for 1 L of synthetic OPA pore water (Pearson, 1998).

Salt	Amount / g	Company *
NaCl	12.38	Merck, Darmstadt, Germany
KCl	0.12	Merck
$MgCl_2 \cdot 6\ H_2O$	3.457	Merck
$CaCl_2 \cdot 2\ H_2O$	3.793	Acros Organics, Geel, Belgium
$SrCl_2 \cdot 6\ H_2O$	0.136	Fluka, St. Gallen, Switzerland
Na_2SO_4	2.00	Merck
$NaHCO_3$	0.04	Merck

* All reagents were of *p.a.* purity grade.

The OPA pore water was synthesized in this study according to the model of Pearson (1998) (pH 7.6; I_t = 0.36 mol/L, cf. **Tab. 8** and **Tab. 20**) in Milli-Q water (18 MΩ; mod. Milli-RO/Milli-Q-System, Millipore, Schwalbach, Germany).

Solutions of 0.1 mol/L $NaClO_4$ and 0.39 mol/L NaCl were prepared by dissolution of $NaClO_4 \cdot H_2O$ (*p.a.*, Merck) and NaCl, respectively, in Milli-Q water.

7.1.4 Acids and bases

HNO_3 (*p.a.*), HCl (*suprapur*), and HF (*suprapur*) for element analysis were obtained from Merck. For pH adjustment, diluted HCl (*p.a.*, Merck), $HClO_4$ (*p.a.*, Merck), and NaOH (*p.a.*, Roth, Karlsruhe, Germany) solutions were used. For pH-dependent studies in 0.1 mol/L $NaClO_4$ and 0.39 mol/L NaCl at pH values > 7, calculated amounts of 1 mol/L $NaHCO_3$ were added to accelerate equilibration with atmospheric CO_2. The resulting HCO_3^- concentration at pH 7.5 was smaller (2.15×10^{-4} mol/L) than under pore water conditions (4.8×10^{-4} mol/L (Pearson, 1998)).

7.1.5 UO_2^{2+} stock solutions

For sorption experiments, different $^{238}UO_2(ClO_4)_2$ stock solutions (5×10^{-4} mol/L in 0.005 mol/L $HClO_4$; for EXAFS: 5×10^{-2} mol/L in 0.5 mol/L $HClO_4$) were used. Furthermore, ^{233}U was used as tracer. For that, a solution of $^{233}UO_2(NO_3)_2$ was acquired (Eckert & Ziegler, Valencia, CA, USA), which was transformed into a $^{233}UO_2(ClO_4)_2$ solution by letting $^{233}UO_2(NO_3)_2$ dry up and adding the threefold molar quantity of 0.01 mol/L $NaHCO_3$ to form $^{233}UO_2(CO_3)_3^{4-}$ as precursor. After that, a surplus of 0.1 mol/L $HClO_4$ was added and $^{233}UO_2(ClO_4)_2$ was formed. The specific activity of the ^{233}U stock solution was determined with LSC (mod. TriCarb 3100 TR, Perkin Elmer, Freiburg, Germany) using Ultima Gold™ (Perkin Elmer) as scintillation cocktail. It amounts to 8.4 kBq/mL ($[^{233}U] = 1.02\times10^{-4}$ mol/L).

For sorption experiments with kaolinite and diffusion experiments with OPA, two aliquots of $^{233}UO_2(NO_3)_2$ were transformed to $^{233}UO_2Cl_2$ as described before but adding 0.1 mol/L HCl instead of $HClO_4$. The specific activity of the resulting two $^{233}U(VI)$ stock solutions amounted to 11.93 kBq/mL ($[^{233}U] = 1.44\times10^{-4}$ mol/L, sorption) and 15.2 kBq/mL ($[^{233}U] = 1.8\times10^{-4}$ mol/L, diffusion), respectively.

7.1.6 Humic acid stock solutions

In all studies, synthetic HA type M42 was applied, which represents a HA-like melanoidin from xylose and glutamic acid. It shows an elemental composition and functional group content comparable to those of most natural HA (Pompe et al., 2000a).

Three different HA batches were used, the unlabeled HA batch M145 and the two ^{14}C-labeled synthetic HA batches, M180A and R2/06A (due to scarcity of M180A).

HA type M42 was prepared as described for the unlabeled HA (Pompe et al., 2000a; Sachs et al., 2004), but using a mixture of ^{14}C-labeled and unlabeled glutamic acid as reaction partners. Some characteristics of the HA applied in this study are summarized in **Tab. 21** and compared to the properties of natural HA. The detailed description of the synthesis and characterization of HA type M42 can be found in Pompe et al. (1998) and Sachs et al. (2004).

Tab. 21: Characteristics of the HA applied in this study (Pompe et al., 1998; Sachs et al., 2004) and from natural HA (Stevenson, 1985; Suffet and MacCarthy, 1989).

HA type	**natural**	**synthetic M42**		
Elemental composition / wt.%				
C	38 – 65	56.1 ± 0.3		
H [a]	3.4 – 5.7	4.1 ± 0.1		
O [b]	31 – 55	26.8 ± 0.3		
N	0.3 – 3.4	4.4 ± 0.1		
S	0.2 – 4.6	-		
P	0 – 0.6	-		
Ash	n.g. [c]	0.11		
Moisture	n.g. [c]	8.4		
Batch		**M145**	**M180A (^{14}C) [d]**	**R2/06A (^{14}C) [d]**
Functional groups / meq/g				
carboxyl [e]	1.5 – 5.7	3.76 ± 0.09	3.76 ± 0.02	4.14 ± 0.07
phenolic [f]	2.1 – 5.7	2.0 ± 0.2	n.a. [g]	n.a. [g]
PEC [h]	n.g. [c]	3.51 ± 0.07	3.34 ± 0.18	3.61 ± 0.3
Specific activity / MBq/g	-	-	23.1 ± 4	8.9 ± 0.6

[a] Corrected for the water content of the HA.

[b] The oxygen content was calculated from the difference to 100 % in consideration of the ash and moisture content of the HA.

[c] n.g. = not given

[d] Personal communication S. Sachs.

[e] Determined by calcium acetate exchange (Schnitzer and Khan, 1972).

[f] Radiometrically determined (Bubner and Heise, 1994; Pompe et al., 2000a).

[g] n.a. = not analyzed

[h] Determined by potentiometric titration.

The batches M180A and R2/06A represent reaction products of second syntheses which were performed to increase the yield of HA after the production of the batches M180 and R2/06. For this, the supernatants of the first reaction mixtures were combined with additional xylose and treated in the same manner as the first syntheses. The resulting HA were separated and purified similar to the batches M180 and R2/06. The structural characterization of the reaction products revealed that batches M180A and R2/06A are comparable to batches M180 and R2/06, respectively.

HA stock solutions of 5 g/L were prepared. For the sorption studies onto kaolinite in dependence on the background electrolyte, 5 mg ^{14}C-labeled synthetic HA (batch M180A) and 45 mg nonlabeled HA (batch M145) were mixed and 1880 µL of 0.1 mol/L NaOH were added. The volume was filled up to 10 mL with Milli-Q water. For the sorption studies in the OPA / OPA pore water system, 5 mg ^{14}C-labeled synthetic HA (batch M180A) and 45 mg nonlabeled HA (batch M145) were mixed and 1880 µL of 0.1 mol/L NaOH were added. The volume was filled up to 10 mL with pore water. The pH-dependent sorption studies with OPA were performed using 0.1 mol/L $NaClO_4$ as background electrolyte. For these studies, a mixture of 16 mg ^{14}C-labeled synthetic HA (batch R2/06A) and 34 mg nonlabeled HA (batch M145) was prepared and 1940 µL of 0.1 mol/L NaOH were added. The volume was filled up to 10 mL with Milli-Q water. For EXAFS measurements, a HA stock solution of nonlabeled HA was prepared by dissolving 50 mg HA (batch M145) in 1.88 mL of 0.1 mol/L NaOH and filling up the volume with Milli-Q water. For the diffusion studies with HA, a HA stock solution was prepared by dissolving 50 mg ^{14}C-labeled synthetic HA (batch M180A) with 1890 µL of 0.1 mol/L NaOH and filling up the volume to 10 mL with pore water.

7.1.7 pH measurements

The pH values were measured using a laboratory pH meter (mod. inoLab pH 720, WTW, Weilheim, Germany) with SenTix® Mic pH microelectrodes (WTW), calibrated using standard buffers (WTW) at pH 1, 4, 7, and 9, equilibrated at 25 or 60 °C depending on the experimental conditions.

7.1.8 E_h determination

The redox potential was determined using a BlueLine 31 Rx redox electrode (Schott, Mainz, Germany) according to a procedure described in literature (Fachgruppe Wasserchemie in der Gesellschaft Deutscher Chemiker and Normenausschuss Wasserwesen im Deutschen Institut für Normung e.V., 1984).

7.1.9 Liquid scintillation counting

The radioactivity of the applied radionuclides ^{3}H, ^{233}U, and ^{14}C was determined by LSC using a TriCarb 3100 TR from Perkin Elmer. A liquid scintillation cocktail was used (Ultima Gold™), which contains diisopropylnaphthalene as solute, 2,5-diphenyloxazole as primary scintillator, and 1,4-bis(5-phenyl-2-oxazolyl)benzene as secondary scintillator (Jähnigen, 2007). For each measurement, a small aliquot of the respective liquid sample solution was added to the scintillation cocktail and a homogeneous mixture was prepared.

The samples can quench the LS counts since they can disturb the energy transfer between the solute and the scintillators of the scintillation cocktail. For instance, the energy can be transformed into heat without emission of photons (chemical quenching), which should be taken into account in particular for the measurement of samples with high volume or high acidity (Jähnigen, 2007). Furthermore, colored samples can absorb photons. This reduces the light output (color quenching). During the measurements in this study, the color quench of the yellow to brown HA samples and the volume quench of the ^{233}U and ^{3}H samples were considered by measuring respective quench curves and including them in the respective LSC protocol.

A typical LSC spectrum of the simultaneous measurement of ^{233}U and ^{14}C-labeled HA is shown in **Fig. 42**.

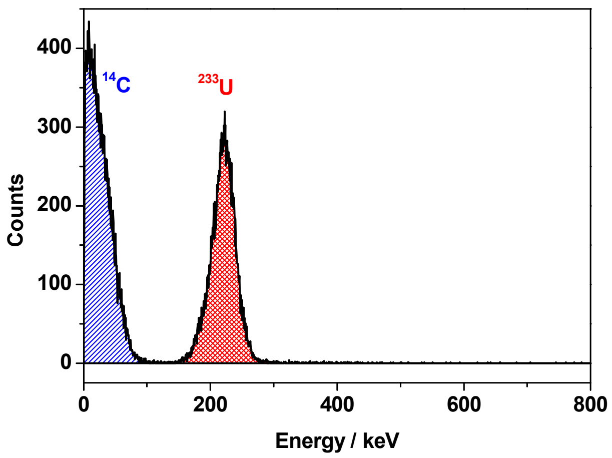

Fig. 42: LSC spectrum of ^{14}C-labeled HA (beta-particle emitter, [HA] = 50 mg/L) and ^{233}U (alpha-particle emitter, [U(VI)] = 1×10^{-6} mol/L) in OPA pore water – simultaneous measurement using TriCarb 3100 TR, Perkin Elmer.

7.2 Clay characterization

7.2.1 Element analysis

The composition of OPA and its suspensions was determined by ICP–MS (mod. ELAN 9000, Perkin Elmer, Boston, USA; error: ± 10 %), atomic absorption spectroscopy (AAS; mod. AAS-4100, Perkin Elmer; error: ± 2 %), and ion chromatography (IC; mod. IC separation center 733, Metrohm, Herisau, Switzerland; error: ± 3 – 10 %). The OPA samples were analyzed after their digestion with HNO_3 (distilled by sub-boiling), HCl, and HF in a microwave oven (mod. multiwave, Anton Paar, Perkin Elmer).

7.2.2 Cation exchange capacity

The CEC was determined by the compulsive exchange method (Sumner and Miller, 1996).

7.2.3 Specific surface area

The specific surface area of OPA was determined with the N_2-BET method (Brunauer et al., 1938) using a surface area and pore size analyzer (mod. Coulter SA 3100, Beckman Coulter, Fullerton, USA). The OPA samples obtained after leaching experiments (cf. section **7.2.7**) were purified by dialysis against pH-adjusted Milli-Q water (pH 4, 7, 10) using dialysis tubes (Thomapor®, exclusion limit MWCO < 1000, Roth). After dialysis, the concentration of $NaClO_4$ in the samples amounted to about 1×10^{-4} mol/L. The samples were lyophilized and N_2-BET was determined. Prior to the measurement the clay samples were heated at 100 °C for 480 min.

7.2.4 Carbon fractions

The TOC and TC contents of OPA were determined by a multi N/C 2100 analyzer (Analytik Jena, Jena, Germany, error: ± 3 %). The TIC content was set to the difference between TC and TOC.

7.2.5 Particle size distribution

The particle size distribution of OPA batch BHE-24/1 was determined by laser diffraction at the Technische Universität Bergakademie Freiberg, Institute of Mechanical Process Engineering and Mineral Processing. For this, the clay was suspended in a wet dispersing unit (mod. QUIXEL, Sympatec GmbH, Clausthal-Zellerfeld, Germany), which was mounted in the measuring zone of a laser diffraction sensor (mod. HELOS H0735, Sympatec). The system allows measurements in the size range of 0.25/0.45 – 87.5 µm. The data were analyzed with the software WINDOX (version 5.4.1.0).

7.2.6 Infrared spectroscopy

The IR spectra were obtained with a FT–IR spectrometer (mod. Spectrum 2000 GX, Perkin Elmer). The clay sample was prepared for measurement by dispersing 2 mg of OPA in 200 mg KBr. From the pressed pellets, spectra were recorded immediately in the region from 4000 to 400 cm^{-1}.

7.2.7 X-ray diffraction

Powder XRD data were collected for the two crushed and homogenized batches of OPA applied for sorption experiments (BHE-24/1, BLT-11/01). Furthermore, XRD was used to investigate a possible alteration of the clay mineral structure of batch BHE-24/1 and formation of secondary mineral phases due to contact with pore water at pH 7.6 or due to contact with 0.1 mol/L $NaClO_4$ at pH 4, 7, and 10. The experiments were performed under ambient atmosphere ($p\mathrm{CO}_2 = 10^{-3.5}$ atm) at room temperature.

The sample in pore water was prepared by weighing 30 g OPA into a 500 mL polypropylene (PP) bottle. Subsequently, 500 mL of pore water were added to reach a S/L ratio of 60 g/L. For pH-dependent investigations in 0.1 mol/L $NaClO_4$, 2 g OPA were weighed into three 500 mL PP bottles each. Subsequently, 500 mL 0.1 mol/L $NaClO_4$ were added in each bottle to reach an S/L ratio of 4 g/L. The pH values were adjusted to pH 4, 7, and 10, respectively. Both the pore water and the 0.1 mol/L $NaClO_4$ solution were prepared in perfluoroalkoxy bottles. The suspensions were continuously shaken for 90 days using an overhead shaker modified for the use of high volume bottles (mod. REAX 20, Heidolph Instruments). The pH values were periodically checked and readjusted. At the end of the experiment, each solid was separated from the aqueous phase and lyophilized.

Powder XRD data were collected for the OPA samples using a Bruker AXS D8 diffractometer (Bruker AXS GmbH, Karlsruhe, Germany) in θ-θ geometry with curved PG-secondary monochromator using CuKα radiation. The scan mode was 'locked-coupled' (Bragg-Brentano geometry). Data were collected from 7 to 70 °2θ using a step size of 0.05 °2θ and a step time of 21 – 54 s. The data were analyzed by phase evaluation using the EVA code (Bruker AXS).

7.2.8 Mössbauer spectroscopy

The OPA samples used for XRD measurements (cf. section **7.2.7**) were studied by Mössbauer spectroscopy to clarify the oxidation state of the iron mineral phases in OPA. ^{57}Fe Mössbauer spectra were recorded by WissEl (Starnberg, Germany) at room temperature in transmission mode using standard instrumental configuration. The ^{57}Co in the rhodium matrix was used as Mössbauer source. A quantitative analysis of the spectra was made using the NORMOS program package of R. A. Brand (University Duisburg) (Brand, 1987).

7.2.9 Leaching experiments in Opalinus Clay pore water at pH 7.6

This experiment was carried out with batch BHE-24/1 after investigating the U(VI) sorption onto OPA in pore water in dependence on S/L ratio (section **7.4.1**). Using the optimal S/L ratio (60 g/L, cf. section **4.4.2**), suspensions of clay in pore water were prepared as described in section **7.2.7.**

In the beginning of the experiment, samples were taken every day; after 8 days three times a week; after 34 days only once a week. After 90 days the sampling was stopped. The pH value was readjusted before each sampling. For sampling, the bottle was removed from the shaker and placed on a magnetic stirrer (mod. Big Squid, IKA, Staufen, Germany). Then, 10 mL of a well-mixed aliquot of the suspension were taken.

The samples were centrifuged for phase separation (30 min, 4000 rpm; mod. Megafuge 1.0, Heraeus Sepatech, Osterode/Harz, Germany). After centrifugation, the supernatants were filtered (450 nm, polyethersulfone, vwr international, Darmstadt, Germany). Prior to filtering, the filters were rinsed with 1 mL sample solution. Filtrates were analyzed for K, Sr, Ba, Al, Si, Fe, and U by ICP–MS, for Mg and Ca by AAS, for F^-, Cl^-, SO_4^{2-}, and PO_4^{3-} by IC, and for TIC content. During the investigations the concentrations of Fe, F^-, and PO_4^{3-} were always below the detection limit of ICP–MS and IC.

7.2.10 Leaching experiments in 0.1 mol/L $NaClO_4$ in dependence on pH

Suspensions of OPA (batch BHE-24/1) in 0.1 mol/L $NaClO_4$ were prepared as a function of pH.

The experiments were performed under ambient atmosphere ($p\text{CO}_2 = 10^{-3.5}$ atm) at room temperature. 40 mg OPA were weighed into 15 mL PP centrifuge tubes (mod. Cellstar, Greiner Bio-One GmbH, Frickenhausen, Germany). Subsequently, 5 mL 0.1 mol/L $NaClO_4$ were added and pH values were adjusted between pH 3 and 10. For pre-equilibration, the samples were continuously shaken on a horizontal shaker (mod. Promax 2020, Heidolph Instruments) and the pH values were periodically checked and readjusted. After one week of pH adjustment (4 – 5 times), the solution was filled up to 10 mL with 0.1 mol/L $NaClO_4$; thus, an S/L ratio of 4 g/L was reached. After that, only small amounts of $HClO_4$ and NaOH had to be added for pH readjustment until the pH values were stable (usually after three weeks). Therefore, the effect of pH adjustment on the S/L ratio was negligible.

Eventually, the final pH values of the samples were determined and the samples were centrifuged and filtered as described in section **7.2.9**. The filtrates of the suspensions were analyzed for Na, K, Sr, Al, Si, P, Fe, and U by ICP–MS, for Mg and Ca by AAS, for F^-, Cl^-, and SO_4^{2-} by IC, and for TIC content. During the investigations the concentration of P was always below the detection limit of ICP–MS (10 µg/L).

7.2.11 Photon correlation spectroscopy

The filtrates of the clay suspensions were investigated for colloids and for the size of the colloidal particles with a BI-90 photon correlation spectroscope (Brookhaven Instruments, USA). A detailed description of the instrument and the PCS procedure is given in (Dreissig et al., 2011).

7.2.12 Zeta potential measurements

Zeta potential measurements of kaolinite and OPA suspensions were performed with laser Doppler velocimetry using a Zetasizer Nano ZS (Malvern Instruments, Malvern, U.K.) with disposable capillary cells. Suspensions of clay in 0.1 mol/L $NaClO_4$ (S/L = 0.1 g/L) were prepared in the pH range from pH 2.5 to 7.5 as described in section **7.2.10**. The zeta potential measurements were repeated 10 times. The temperature was maintained at 25 ± 0.1 °C. Agglomerated particles were re-suspended as flakes by ultrasonic treatment before measurement.

7.3 Characterization of U(VI) and HA solutions

7.3.1 Solvent extraction

Because of the presence of several redox partners in OPA and in solution, the solutions and sorption filtrates were analyzed with respect to a possible reduction of U(VI) to U(IV). For this, solvent extraction was applied using thenoyltrifluoroacetone (TTA; *p.a.*, Fluka/Sigma-Aldrich, Steinheim, Germany) according to Bertrand and Choppin (1982). For TTA extractions, 2 mL of the filtrates were acidified to pH 0.5 using degassed HCl (37 %). After that, 2 mL of freshly prepared 0.5 mol/L TTA solution in degassed xylene (*p.a.*, Fluka) were added and the samples were shaken vigorously for 10 min. The samples were then centrifuged for phase separation (10 min, 4000 rpm). Under these conditions, U(IV) species are extracted by TTA into the organic phase whereas U(VI) remains in the aqueous phase. The resulting U(VI) concentrations in the aqueous phases were analyzed by LSC.

7.3.2 TRLFS measurements under cryogenic conditions

To identify the U(VI) species in OPA pore water in the absence and presence of HA, fluorescence spectroscopy was used. The theoretical background of the method was already described in detail in literature (Albani, 2007; Skoog and Leary, 1996).

In fluorescence spectroscopy, the emission spectra of the excited species are used for qualitative and quantitative analysis. That means, the kind and number of luminescent species as well as stability constants of complexes formed with the excited species can be determined. For luminescence lifetime measurements methods such as time-resolved laser-induced fluorescence spectroscopy (TRLFS) are applied. Thereby, the time dependence of the luminescence signal is recorded and analyzed by fitting the sum of the luminescence intensities over the measured wavelength range by an exponential decay function (**Eq. 10**).

$$I(t) = \sum_i I_{0i} \cdot e^{-t/\tau_i} \qquad \textbf{Eq. 10}$$

$I(t)$ is the total luminescence intensity at time t, I_{0i} the luminescence intensity of the luminescent compound i at $t = 0$, and τ_i the corresponding luminescence lifetime.

Different compounds added to the luminescent system can quench the luminescence signal intensity or / and luminescence lifetime. The quenchers can decrease luminescence by collision with the luminescent molecule (dynamic quenching) or by forming a nonluminescent complex (static quenching) (Albani, 2007). In particular, the effect of static quenching is used to determine stability constants with TRLFS.

In case of uranium, specific changes in its luminescence characteristics – in particular, the luminescence intensity, the position of the emission bands, and lifetime of the luminescence signal – are used to distinguish between different uranium species. In **Fig. 43**, the luminescence of noncomplexed UO_2^{2+} at pH 2.4 is presented as single spectrum (a) and as time-resolved set of spectra (b). Using an excitation wavelength of 410 nm, five main emission bands can be identified at 488, 510, 534, 560, and 585 nm. The luminescence lifetime of the UO_2^{2+} under these conditions amounts to about 1.8 ms (Kremleva et al., 2012).

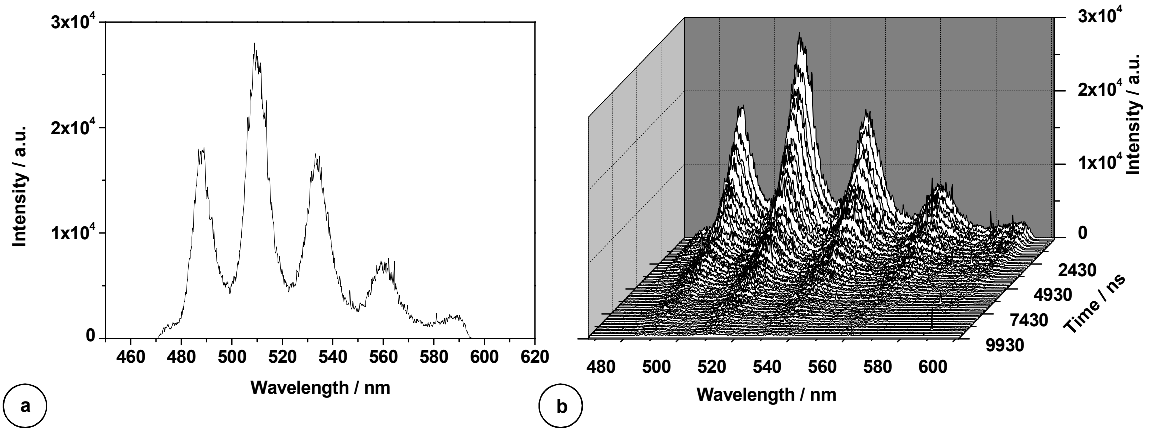

Fig. 43: Luminescence of U(VI) (1×10^{-4} mol/L) in 0.1 mol/L $NaClO_4$ at pH 2.4; (**a**) single spectrum at $t = 0$ ns; (**b**) time-resolved spectra.

In the present study, U(VI) in pore water was investigated using TRLFS under cryogenic conditions at 153 K. TRLFS measurements at room temperature were not suitable, since the U(VI) concentration was too low. Furthermore, as reported by Bernhard et al. (2001) and Wang et al. (2004), the uranyl carbonato species ($(UO_2)_2(OH)_3CO_3^-$; $UO_2CO_3(aq)$; $UO_2(CO_3)_2^{2-}$; $UO_2(CO_3)_3^{4-}$), that are possibly present in solution, show no luminescence properties at room temperature.

Since pore water contains a large amount of chloride, which acts as a strong luminescence quencher, special pore water was prepared for this experiment substituting the chloride salts (cf. **Tab. 20**) by the respective perchlorate salts. Speciation calculations confirmed that these small changes of the background electrolyte do not affect the speciation of U(VI) in solution at pH 7.6. Applying the chloride-free pore water, sorption experiments were performed analogous to those described in **7.4.6**. After sorption experiments, the filtrates were studied and compared to pore water samples with added U(VI) by means of TRLFS.

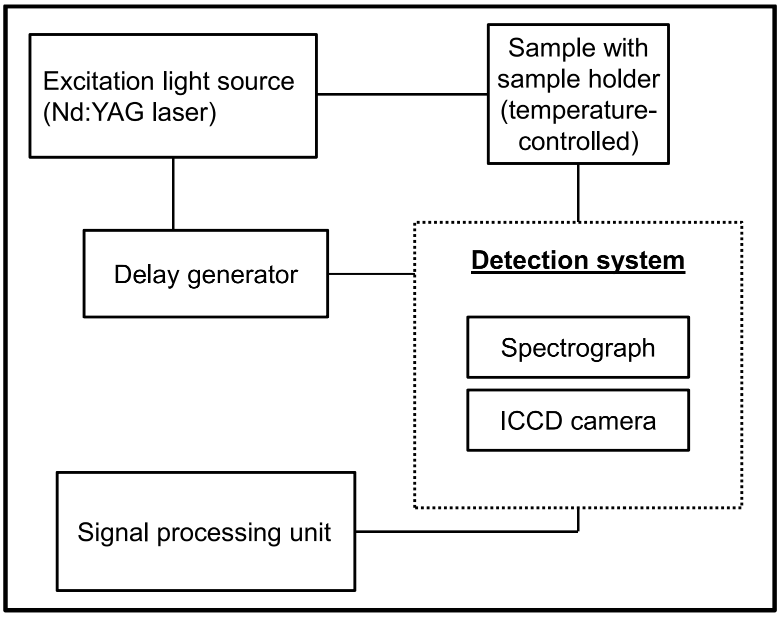
Excitation light source (Nd:YAG laser)
Sample with sample holder (temperature-controlled)
Delay generator
Detection system
Spectrograph
ICCD camera
Signal processing unit

Fig. 44: Schematic illustration of the experimental set-up for the fluorescence spectroscopic measurements.

The experimental set-up for the fluorescence spectroscopic measurements is given in **Fig. 44**. For the measurements, aliquots of pore water and filtrates were filled into plastic cuvettes (mod. BI-SCP, Brookhaven Instruments, Holtsville, NY, USA), placed immediately in a freezer at 255 K and stored for 1 day. For TRLFS measurements, the frozen samples were transferred as ice cubes from the plastic cuvettes into a specifically designed sample holder. The sample holder has one hole to insert the ice cube and windows for laser irradiation. After transfer, the samples were cooled to 153 K via a cryogenic cooling system (mod. TG-KKK, KGW-Isotherm, Karlsruhe, Germany).

TRLFS laser pulses at 410 nm with an average pulse energy of 4 mJ (neodymium-doped yttrium aluminum garnet (Nd:YAG)-MOPO laser system, mod. GCR 230 (20 Hz), Spectra Physics, Mountain View, USA) were used for excitation of the U(VI) luminescence. The emitted luminescence light was detected in a right angle set-up by a Jobin Yvon 270M spectrograph (Jobin Yvon GmbH, Munich, Germany). The spectrograph was equipped with a grating, which had a ruling density of 300 mm^{-1}. The resulting spectra were measured in time-resolved mode using an intensified charge-coupled device (ICCD) camera (512 pixel; mod. Spectrum One, HORIBA Jobin Yvon). The resolution of the spectra was 0.3 nm. The time difference between the trigger of the laser system and the start of the camera was adjusted by a delay generator DG 540

(Stanford Research Instruments, Sunnyvale, USA). The spectra were recorded in the wavelength range from 454 to 604 nm by accumulating 20 to 100 laser pulses using a gate time of the camera of 500 µs. Delay times varied from 50 ns to 4 ms after application of the laser pulse in 10 µs increments. All settings of the camera and the spectrograph were computer controlled with the program SpectraMax (version 3.1, HORIBA Jobin Yvon). The measured time-resolved spectra were analyzed using Origin (version 7.5G, OriginLab Corporation, USA) including the Peak Fitting module (version 1.4) to determine the fluorescence lifetimes and emission bands.

7.3.3 Characterization of the diffusion reservoir solutions at 25 and 60 °C

The source reservoir solutions tracered with ^{233}U(VI) and ^{14}C-HA, used in diffusion experiments with OPA, were analyzed for Na, K, Sr, Ba, Al, Si, P, Mn, Fe, and U by ICP–MS, for Mg and Ca by AAS, and for SO_4^{2-} and Cl^- by IC. The carbon fractions were determined as described in section **7.2.4**. During the diffusion experiments the concentrations of Fe and P were always below the detection limit of ICP–MS.

The pH and E_h values of the source reservoir solutions were measured at the end of the experiments.

The solutions in the source reservoirs were analyzed with respect to a possible reduction of U(VI) to U(IV) by solvent extraction. The detailed procedure is described in section **7.3.1**.

Furthermore, the size distribution of ^{233}U(VI) and ^{14}C-HA in the solutions of the source and receiving reservoirs was determined by ultrafiltration at start and end of diffusion experiments. Ultrafiltration centrifugal devices with molecular weight cutoffs of 1 – 1000 kDa (Microsep^{TM}, Pall Corporation, Port Washington, NY, USA) were used.

To identify the U(VI) species in the pore water at 60 °C, an additional experiment was performed applying laser-induced fluorescence spectroscopy (LIFS). For this, chloride-free pore water was prepared again (cf. section **7.3.2**). 200 mL of the chloride-free pore water were heated to 60 °C and continuously stirred in a closed 250 mL glass bottle (Duran®). After that, $^{238}UO_2(ClO_4)_2$ was added to reach a U(VI) concentration of 1×10^{-4} mol/L. This U(VI) concentration is higher than that used during the diffusion experiments but had to be applied due to the U(VI) detection limit of LIFS at 60 °C (5×10^{-5} mol/L). The solution was equilibrated at 60 °C for three months under anaerobic conditions. The pH was adjusted to pH 7.6 by addition of 1 mol/L Na_2CO_3 (*p.a.*, Merck) at the beginning of the experiment. For the LIFS measurements, aliquots of the solution were taken regularly and filled into a quartz cuvette without further sample preparation. The cuvette was positioned in a temperature-controlled sample holder (cf. **Fig. 44**; mod. FLASH 300 + TC 125, Quantum Northwest, Liberty Lake, WA, USA). The U(VI) luminescence was measured after excitation with laser pulses at 266 nm (Nd:YAG laser, mod. Minilite, Continuum, Santa Clara, CA, USA) with an averaged pulse energy of 300 µJ. The emitted luminescence light of the samples was recorded with a spectrograph (mod. iHR 550, HORIBA Jobin Yvon; grating: 300 mm^{-1}) and an ICCD camera (mod. HORIBA Jobin Yvon) with integrated delay generator in the wavelength range from 371.4 to 664.3 nm by accumulating 250 laser pulses and using a gate time of 2 µs. The resolution of the spectra was 0.45 nm. The settings of the camera and the spectrograph were computer controlled with LabSpec (version 5, HORIBA Jobin Yvon). Data analysis was performed with Origin. Additionally, the sample solutions were investigated for colloids and for the size of the colloidal particles by PCS (cf. section **7.2.11**). After confirmation of the presence of colloids by PCS, samples for SEM–EDX were prepared by filtration of the source reservoir solution through membranes with pore diameters of 0.05 µm (polycarbonate, Nuclepore™ track-etched membranes, Whatman, Maidstone, Kent, UK). After separation, the filters were rinsed with Milli-Q water to remove soluble ingredients and then, dried in a desiccator. The dry filter sections were sputtered with carbon (carbon coater 108 carbon/A, Cressington Scientific Instruments, Watford, UK) to ensure a good conductivity in the EDX microanalysis. SEM investigations were carried out with a high-resolution HitachiS-4800 microscope (Hitachi High-Technologies Canada, Inc., Toronto, Ontario, Canada). The chemical composition of the colloidal particles was determined with an EDX microanalysis system INCA (Oxford Instruments, Tubney Woods, Abingdon, Oxfordshire, UK). This system employed an integrated Si-detector and S-UTW-window.

7.4 Sorption experiments

7.4.1 General procedure

Batch sorption experiments were performed as summarized in **Tab. 22** at room temperature. According to the S/L ratio (cf. **Tab. 22**), a respective amount of clay was weighed into 15 mL PP centrifuge tubes. Subsequently, 10 mL of the background electrolyte (0.1 mol/L $NaClO_4$, 0.39 mol/L NaCl, OPA pore water) were added and the pH value was adjusted. For pre-equilibration, the samples were continuously shaken on a horizontal shaker and the pH values were periodically checked and readjusted. Except for the pH-dependent sorption experiments (pH 3 – 10, all sorption samples were adjusted to pH 7.6.

After pre-equilibration, aliquots of a U(VI) or HA stock solution were added to the clay suspensions to obtain the U(VI) and HA concentrations compiled in **Tab. 22**. The pH values were readjusted immediately. For equilibration, the samples were shaken on

Tab. 22: Experimental conditions applied for batch sorption experiments.

Experiment	Sorbent	Background electrolyte	S/L / g/L	Solute	[U(VI)] / mol/L	[HA] / mg/L
Background electrolyte influence	Kaolinite	0.1 mol/L NaClO$_4$; 0.39 mol/L NaCl; pore water	4	^{233}U(VI) and HA	1×10^{-6}	10, 50
S/L ratio dependence	OPA	Pore water	0.5 – 300	^{238}U(VI)	1×10^{-6}	-
Kinetic sorption studies	OPA	Pore water	60	^{238}U(VI) or HA	1×10^{-6}	10
U(VI) sorption isotherm	OPA	Pore water	60	$^{233/238}$U(VI)	1×10^{-8} – 1×10^{-4}	-
			4	^{233}U(VI)	1×10^{-8} – 5×10^{-7}	-
HA sorption isotherm	OPA	Pore water	60	HA	-	10 – 320
Influence of HA on U(VI) sorption and vice versa	OPA	Pore water	60	^{233}U(VI) and HA	1×10^{-6}	10, 50
Influence of CO$_2$	OPA *	Pore water	60	^{233}U(VI) and HA	1×10^{-6}	10, 50
pH-dependent sorption	OPA	0.1 mol/L NaClO$_4$	4	^{238}U(VI) and HA	1×10^{-6}	50
EXAFS	OPA	Pore water	20	^{238}U(VI) and HA	1×10^{-4}	10

* For batch sorption experiments under ambient conditions OPA batch BHE-24/1 was applied, for experiments under inert gas conditions OPA batch BLT-11/01 was used.

a horizontal shaker for 3 days, whereby the pH was readjusted each day. After 3 days, the final pH values of the samples were determined and the samples were centrifuged for phase separation (30 min, 4000 rpm). After centrifugation, the supernatants were filtered. Prior to filtering, the filters were rinsed with 1 mL sample solution. In a separate experiment, the U(VI) sorption onto the filters was shown as to be insignificant. High performance centrifugation (75600 *g*, 1 h; mod. J-20 XP, Beckman Coulter) was tested as an alternative separation method, but performed less efficiently than the combination of centrifugation and filtration. Therefore, it was not used in the experiments. The filtrates were analyzed for the final U(VI) and HA concentration by ICP–MS and LSC, respectively. For LSC, 1 mL of the filtrate was mixed with 15 mL Ultima Gold™.

Furthermore, blank suspensions of clay in the three different background electrolytes were prepared to determine the amount of naturally contained uranium leached out of the clay. These samples were processed under the same conditions.

Finally, the U(VI) or HA sorption onto vial walls was determined. For this, 7 mL 1 mol/L HNO_3 (U(VI) sorption) or 1 mol/L NaOH (HA sorption) were added to the emptied vials and the vials were shaken for 3 days. The solutions were analyzed by ICP–MS or LSC for U(VI) and / or HA concentration.

The amount of U(VI) / HA sorbed on the mineral surface was calculated as the difference between the initial U(VI) / HA concentration and the concentration of U(VI) / HA in solution after the sorption experiment. The values were corrected by the vial wall sorption and the U(VI) concentration in the blank samples.

Each sorption experiment was carried out as described in this section. Any deviations from this procedure are explained in the specific sections below.

7.4.2 Influence of background electrolyte

Batch sorption experiments under ambient atmosphere ($p\mathrm{CO_2} = 10^{-3.5}$ atm) with kaolinite (batch KGa-1b) were carried out under conditions shown in **Tab. 22**. The samples were prepared in triplicate. The pre-equilibration time was 13 days. For U(VI) sorption, 70 µl ^{233}U(VI) stock solution were added to the suspensions.

7.4.3 S/L ratio dependence

Due to the fact that these experiments were carried out before the pore water leaching experiment (cf. section **7.2.9**), a pre-equilibration and contact time of 3 days each was used according to previous U(VI) sorption studies performed with kaolinite in $NaClO_4$ (Křepelová et al., 2006). The experiments were performed under ambient atmosphere ($p\mathrm{CO_2} = 10^{-3.5}$ atm). The samples were prepared in duplicate.

7.4.4 Kinetic sorption experiments

The experiments were performed under ambient atmosphere ($p\mathrm{CO_2} = 10^{-3.5}$ atm). 12 g OPA were weighed into 250 mL bottles and mixed with 200 mL pore water. Aliquots of a U(VI) or HA stock solution were added and the suspensions were stirred with a magnetic stirrer. After different contact times aliquots of the suspensions were taken and analyzed for their U(VI) or HA concentration.

7.4.5 U(VI) and humic acid sorption isotherms

To determine the U(VI) sorption isotherm, ^{233}U was used to investigate the low U(VI) concentrations ($1\times10^{-8} - 1\times10^{-6}$ mol/L). For U(VI) concentrations of [U(VI)] = $5\times10^{-6} - 1\times10^{-4}$ mol/L, a stock solution of ^{238}U(VI) was tracered with ^{233}U(VI). The experiments were carried out under ambient atmosphere ($p\mathrm{CO_2} = 10^{-3.5}$ atm). The U(VI) sorption isotherm was measured as a function of the U(VI) concentration and of the S/L ratio, whereas the HA sorption isotherm was only measured as a function of HA concentration. The U(VI) and HA concentration in the filtrates was determined by ICP–MS and LSC. All experiments were performed in duplicate.

7.4.6 Influence of humic acid and CO_2 on the U(VI) sorption

The experiments were performed under ambient ($p\mathrm{CO}_2 = 10^{-3.5}$ atm) and inert gas conditions (N_2-box), respectively. After pre-equilibration, HA was added instantly after addition of ^{233}U(VI). For comparison, additional OPA samples with ^{233}U(VI) in the absence of HA and with HA in the absence of ^{233}U(VI) were prepared. The further handling of the samples was as described in section **7.4.1**. Differing from that, the filtrates were analyzed simultaneously for the final U(VI) and HA concentration by LSC. All sorption experiments were performed in triplicate. The redox speciation of uranium after the end of the sorption experiments was studied by solvent extraction (cf. section **7.3.1**).

7.4.7 Influence of pH

After weighing of 40 mg OPA into 15 mL PP centrifuge tubes, 5 mL 0.1 mol/L $NaClO_4$ were added and pH values were adjusted between pH 3 and 10. All sorption samples were prepared in duplicate. After one week of pH adjustment (4 – 5 times), the volume was filled up to 10 mL with 0.1 mol/L $NaClO_4$. After that, only small amounts of $HClO_4$ or NaOH had to be added for pH readjustment until the pH values were stable (usually after three weeks). Therefore, the effect of pH adjustment on the S/L ratio was negligible.

For the investigation of the U(VI) sorption onto OPA in the presence of HA, HA stock solution was added 1 h before addition of U(VI) to allow the interaction of HA with the competing ions that were leached out of the clay. Prior to the determination of the U(VI) concentrations in the samples containing HA, HA was removed by digestion in a microwave oven with HNO_3 in order to avoid any disturbing effects of HA during ICP–MS measurements.

Furthermore, blank solutions containing U(VI) and HA in 0.1 mol/L $NaClO_4$ without clay were prepared as a function of pH to determine the amount of precipitated HA. These samples were processed under the same conditions.

7.4.8 EXAFS measurements

X-ray absorption spectroscopy (XAS) is a method, where X-rays (500 eV to 500 keV) are absorbed by electrons situated close to the atomic core (1s or 2p level). The basic principles of XAS are described elsewhere (Koningsberger and Prins, 1988; Teo, 1986).

During XAS, the intensity of the absorption coefficient μ is measured as a function of energy of the X-ray photon E_x. Thereby, the focus is on energies just above absorption edges. Absorption edges appear in the spectrum, when the X-ray energy is equal to the binding energy of the electron. The energies of the absorption edges are element-specific tabulated values (e.g., uranium L_{III}-edge at 17166 eV (Thompson et al., 2009) corresponding to an electron from the 2p ($^2P_{3/2}$) orbital).

The measurement of the X-ray fluorescence is favored in case of thick samples and low concentrations of the absorbing atom. It is detected in a right angle set-up to the incident beam.

The resulting X-ray absorption spectrum is divided in two parts: X-ray absorption near-edge structure (XANES) and extended X-ray absorption fine-structure (EXAFS) (**Fig. 45**). XANES is strongly sensitive to formal oxidation state and coordination chemistry of the absorbing atom and is investigated typically within 30 eV of the main absorption edge and EXAFS. EXAFS spectroscopy is used to determine the distances, coordination number, and species of the neighbor atoms of the absorbing atom (Newville, 2004) and is used in this study.

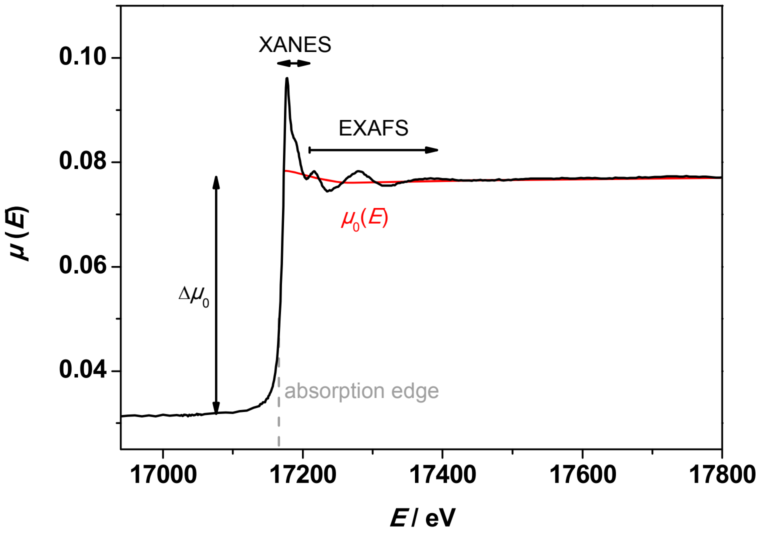

Fig. 45: X-ray absorption spectrum of U(VI) sorbed onto OPA ($[U(VI)]_0 = 1\times10^{-4}$ mol/L) in 0.1 mol/L $NaClO_4$ at pH 6.8 in the presence of 10 mg/L humic acid ($pCO_2 = 10^{-3.5}$ atm). The uranium absorption edge, the XANES and EXAFS regions, the edge-step $\Delta\mu_0(E_0)$, and the smooth background function $\mu_0(E)$ are denoted.

The EXAFS fine-structure function $\chi(E)$ is defined as

$$\chi(E) = \frac{\mu(E) - \mu_0(E)}{\Delta\mu_0(E_0)} \quad \textbf{Eq. 11}$$

where $\mu_0(E)$ represents a smooth background function describing the absorption of an isolated atom without any interference with neighbor atoms and $\Delta\mu_0$ is the jump of the absorption coefficient at the absorption edge with the threshold energy E_0 (cf. **Fig. 45**).

Due to the wave behavior of the emitted photo-electrons, the X-ray energy E is commonly expressed by the wave number of the photo-electron, k, as follows

$$k = \sqrt{\frac{2\,m\,(E - E_0)}{\hbar^2}} \quad \textbf{Eq. 12}$$

where m means the electron mass and $\hbar$ is the reduced Planck constant. The resulting oscillations as a function of wave number $\chi(k)$ are very small, thus they are often k-weighted (multiplied with k^2 or k^3) to intensify them. The frequencies of the oscillations in $\chi(k)$ can be attributed to the various coordination shells of the neighboring atoms and are expressed by the EXAFS equation:

$$\chi(k) = \sum_j \frac{N_j\,S_0^2(k)\,f_j(k)\,e^{-2\,k^2\sigma_j^2}}{k\,R_j^2} \sin\left[2\,k\,R_j + \delta_j(k)\right] \quad \textbf{Eq. 13}$$

thereby S_0^2 represents the amplitude reduction factor, $f(k)$ is the backscattering amplitude, and $\delta(k)$ describes the total phase-shift. $f(k)$ and $\delta(k)$ have to be known to determine the number of neighbor atoms, N, the distance to the neighboring atom, R, and the disorder in the neighbor distance, σ^2, also known as Debye-Waller factor. Furthermore, EXAFS gives information about the atomic species of the neighboring atom, since $f(k)$ and $\delta(k)$ are a function of its atomic number.

By Fourier transformation of the $\chi(k)$ function into R-space the different coordination shells around the absorbing atom can be visualized.

For EXAFS investigations, OPA sorption samples were prepared using an S/L ratio of 20 g/L and a U(VI) concentration of 1×10^{-4} mol/L. This clay / U(VI) ratio guaranteed a U(VI) loading of about 150 ppm (3.6 µg/m^2) on the clay, which represents a sufficient amount of sorbed U(VI) for EXAFS detection.

The EXAFS samples were prepared in the form of a wet paste. The OPA suspensions in pore water were in equilibrium after 13 days. After pre-equilibration of the OPA suspensions U(VI) and HA (nonlabeled HA type M42) were sorbed onto OPA as described in section **7.4.1**. All samples were prepared in duplicate. Furthermore, a leaching sample was processed as described in section **7.2.9**. In the sorption samples, the supernatants were removed and analyzed by ICP–MS. The wet pastes were immediately filled into polytetrafluoroethylene sample holders (SH13A, 16×5×3 mm). These sample holders were sealed with Kapton® polyimide tape and heat-sealed in two layers of polyethylene foil to avoid moisture loss during analysis and to have several layers of shielding of the radioactive sample.

EXAFS data were collected at the Rossendorf Beamline (Funke et al., 2001; Matz et al., 1999; Reich et al., 2000) at the European Synchrotron Radiation Facility, Grenoble, France. A Si(111) double-crystal monochromator was used in channel-cut mode to monochromatize the incoming synchrotron radiation. Uranium L_{III}-edge X-ray absorption spectra were recorded at room temperature in fluorescence mode using a 13-element Ge solid state detector (Canberra). Energy calibration was carried out by the simultaneous yttrium K-edge measurement of a reference yttrium foil (first inflection point at 17038 eV). The threshold energy E_0 of the uranium L_{III}-edge was defined as 17185 eV.

During measurements, 11 and 20 spectra were recorded for the samples U9-40 and U9-41, respectively, and then averaged for each sample. The data of the recorded EXAFS spectra were processed using EXAFSPAK (George and Pickering, 2000) following standard procedures as given in literature (Koningsberger and Prins, 1988; Newville, 2004) including statistical weighting of the 13 fluorescence channels and their dead-time correction. The obtained $\chi(k)$ functions were weighted with k^3. EXAFS structural parameters were calculated by curve fitting both in the *k*-space (EXAFS oscillation spectra) and *R*-space (Fourier transformed spectra). The multishell fitting was always performed in the *k*-range from 3.1 to 10.5 $Å^{-1}$.

Theoretical scattering phases and amplitudes required for curve fitting were calculated with the scattering code FEFF 8.20 (Ankudinov et al., 1998).

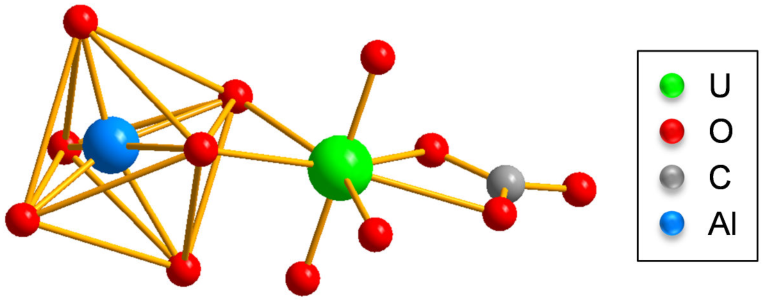

Fig. 46: Ball-and-stick representation of the fit model applied in the present study with bidentate coordination of UO_2^{2+} to an aluminum octahedra and bidentate binding of carbonate to UO_2^{2+}. Hydrogen atoms are omitted for clarity.

In a first approximation for each sample, the FEFF model of $UAlO_6CO_3$ was applied (cf. **Fig. 46**). This describes a hypothetical sorption complex of UO_2^{2+} on an $Al(III)(H_2O)_6$ octahedron. The model was based on the structure of hematite (Blake et al., 1966), whereby iron was substituted with aluminum. Aluminum is one of the main elements present in clay (cf. section **2.1**). The data of Sémon et al. (2001) were used for description of UO_2^{2+}. The carbonate scattering paths were taken from the liebigite structure (Mereiter, 1982), since its aqueous analogue $Ca_2UO_2(CO_3)_3(aq)$ is the dominant species in solution under environmentally relevant conditions (cf. **4.4.8**) and is assumed to sorb onto OPA as uranyl carbonato surface complex in the respective samples.

The structural parameters N, R, and σ^2 were fitted only for the oxygen atoms. With this, contributions of the axial and equatorial oxygen coordination shells of uranyl as well as the multiple scattering path of the axial oxygen atoms U–O$_{ax1}$–U–O$_{ax2}$ (MS$_{U=O}$) (Hudson et al., 1995) were considered. In the fit, MS$_{U=O}$ was constrained to have an effective path length and Debye-Waller factor twice the values of the corresponding U−O$_{ax}$ single-scattering path (Hudson et al., 1995). The shift in the threshold energy, ΔE_0, was linked for all shells. The amplitude reduction factor, S_0^2, was equal to 1.0. To describe the fit quality, the reduced chi-squared value, χ_{red}^2, is given, which is provided by EXAFSPAK after each fit. It is defined as

$$\chi_{red}^2 = \sum \frac{\left(\chi_{exp}(k)\cdot k^3 - \chi_{theo}(k)\cdot k^3\right)^2}{P - F} \qquad \textbf{Eq. 14}$$

with $\chi_{exp}(k)$ being the experimental EXAFS spectrum, $\chi_{theo}(k)$ the fit spectrum, P the number of data points, and F the number of free variables.

7.5 Diffusion experiments

For diffusion experiments, pristine OPA bore core samples (batch BLT-14) were used with a thickness of 11×10^{-3} m and a diameter of 25.5×10^{-3} m. Synthetic OPA pore water (pH 7.6; cf. **Tab. 8**) was used as background electrolyte in all diffusion experiments. To avoid bacterial growth during the experiment, 1×10^{-3} mol/L NaN_3 (*extra pure*, Merck) was added to the pore water.

The experimental set-up of the diffusion experiment is described in section **5.3**. The confining pressure on each sample was 5 MPa. The saturation time of the OPA samples prior to the diffusion experiment amounted to three weeks. After this time the pressure was constant, indicating that the samples were hydrostatically in equilibrium. Subsequently, the reservoir solutions were replaced by fresh ones. The source reservoir contained the tracer and thus tracer diffusion was started. During the duration of the experiment, the pH value in the reservoirs was not readjusted.

After three months, the diffusion experiments were stopped and the clay samples were removed from the cells. With the help of the abrasive peeling technique (Van Loon and Eikenberg, 2005), U(VI) and HA diffusion profiles were determined. The peeled layers were extracted for ^{233}U(VI) content by 1 mol/L HNO_3 (*p.a.*, Roth) and for ^{14}C-HA content by 1 mol/L NaOH. This method was already applied in former experiments (Sachs et al., 2007b). The tracer concentrations in the extracts were determined by LSC.

7.6 Modeling

7.6.1 Speciation calculations with EQ3/6

The aqueous U(VI) speciation was calculated using the speciation code EQ3/6 (Wolery, 1992) and the thermodynamic data for U(VI) compiled in the OECD/NEA data base (Guillaumont et al., 2003), including data for the alkaline earth uranyl carbonato complexes (Bernhard et al., 2001; Dong and Brooks, 2006). Furthermore, this code has been modified (Sachs et al., 2004) to integrate HA complexes by using the CNM (Kim and Czerwinski, 1996) for description. In the EQ3/6 data base, data for the binary complex $UO_2HA(II)$ (Montavon et al., 2000; Pompe et al., 2000a; Pompe et al., 2000b), the ternary complex $UO_2(OH)HA(I)$ (Sachs et al., 2007a), and the carbonato humate complex $UO_2(CO_3)_2HA(II)^{4-}$ (Steudtner et al., 2011a; Steudtner et al., 2011b) were included. Modeling consistency of the complexation data of the three considered U(VI) humate complexes was already checked by Steudtner et al. (2011a). Moreover, the complexation data for the CaHA(II) and SrHA(II) (Paulenová et al., 2000) based on CNM were added.

Knowing the pH-dependence of the loading capacity (LC) of HA (Kim and Czerwinski, 1996) is essential within the CNM framework. LC depends on the cation which is complexed. Due to the fact that in this study several competing ions are present in solution which can be complexed by HA an average pH-dependent LC value was applied for speciation calculations. Literature data show that various divalent cations (e.g., calcium, strontium, lead, copper, cadmium, zinc) exhibit a similar complexation with HA (Beck et al., 2004; Mansel et al., 2003; Paulenová et al., 2000). Their respective LC values and the LC values determined for U(VI) complexation with HA (Montavon et al., 2000; Pompe et al., 1998; Pompe et al., 2000b; Sachs et al., 2007a) were considered. The pH-dependence of LC was obtained by linear regression of LC data (**Eq. 15**) determined at different pH values and used for speciation calculations:

$$LC = 0.1633 \cdot pH - 0.4134. \qquad \textbf{Eq. 15}$$

7.6.2 Modeling of diffusion processes using COMSOL Multiphysics 3.5a

For the determination of the diffusion parameters, a one-dimensional model composed of source reservoir, filter, OPA bore core sample, filter, and receiving reservoir was applied as described by Jakob et al. (2009) using the commercial software COMSOL Multiphysics 3.5a (2008). The OPA sample and the filters were considered as homogeneous with a single value for the transport porosity, ε, each. The general technical details of the filters and the OPA samples are summarized in **Tab. 23**.

Tab. 23: Characteristics of the filters and the OPA samples.

	Parameter	**Value**
Filters	Length	1.55×10^{-3} m
	Diameter	25.5×10^{-3} m
	Transport porosity	0.3
	Bulk density	5000 kg/m^3
OPA	Length	11×10^{-3} m
	Diameter	25.5×10^{-3} m
	Cross-sectional area	5.11×10^{-4} m^2

For HTO, D_e and α were determined by modeling the through-diffusion flux of HTO using the time history of the HTO concentration in the receiving reservoir. For ^{233}U(VI) and ^{14}C-HA, the values for the diffusion parameters (D_e, α, ε, K_d) were determined by fitting the experimental tracer distribution profiles in the clay.

In line with the experiments, the following initial condition was applied:

$$c(x, t \leq 0) = 0, \quad \forall\, x \in \text{transport domain}, \qquad \textbf{Eq. 16}$$

meaning that the clay sample as well as the filters were initially free of tracer. Two alternative descriptions were used in the model as boundary condition for the source reservoir:

$$c(x = 0, t > 0) = f_0(t) \quad \text{and} \qquad \textbf{Eq. 17}$$

$$c(x = 0, t > 0) = c_0 = \text{const.} \qquad \textbf{Eq. 18}$$

The time-dependent change of the source reservoir tracer concentration, cf. **Eq. 17**, was applied for modeling HTO, ^{233}U(VI), and ^{14}C-HA (large colloids) diffusion. The temporal evolution of the concentration of small ^{14}C-HA colloids in the source reservoir was not monitored. However, mass balance consideration showed that the source reservoir concentration of HA did not decrease more than 5 % in maximum by diffusion of small HA colloids into the OPA sample. Hence, a constant concentration boundary condition, cf. **Eq. 18**, was used for modeling diffusion of HA (small colloids). For the boundary conditions of the receiving reservoir two possible descriptions were applied:

$$c(x = L, t > 0) = f_L(t) \quad \text{and} \qquad \textbf{Eq. 19}$$

$$c(x = L, t > 0) = 0, \qquad \textbf{Eq. 20}$$

where L [m] describes the thickness of the system filter / clay / filter. **Eq. 19** was only applied for tracers detected in the receiving reservoir, that means, HTO and small HA colloids. For ^{233}U(VI) and large HA colloids, where no tracer breakthrough could be observed, **Eq. 20** was applied. Continuity regarding tracer flow [mol/s] at the interfaces of filters and clay was considered in the model according to Jakob et al. (2009). In the evaluation of the experiments, the concentration values for the applied radionuclides were decay corrected.

The experimental uncertainty of the determined diffusion parameters was determined differently for each investigated radionuclide.

In the case of HTO diffusion, the uncertainties of the values of the diffusive flux and the accumulated diffused activity in the receiving reservoir resulted from the uncertainty of the parameters required to calculate these values. The main sources of uncertainty are given in Van Loon and Soler (2004). The uncertainty of D_e and ε was estimated by fitting the upper and the lower boundaries covered by the uncertainties of the experimental fluxes. This was done by varying D_e and ε such that 90 % of the experimental values were covered by the envelope curves.

In the case of ^{233}U(VI) and ^{14}C-HA diffusion profiles, the uncertainty of the diffusion distance was given by the combination of the uncertainties of each individual distance measurement. The uncertainties of the D_e and K_d values were estimated by fitting the upper and lower boundaries of the diffusion profile. Both D_e and K_d were varied in such a way that 90 % of the experimental values were covered by the envelope curves.

8 References

Albani, J. R. (2007). *Principles and applications of fluorescence spectroscopy*. Blackwell Publishing, Ames.

Alonso, U., Missana, T., Garcia-Gutierrez, M., Patelli, A., Siitari-Kauppi, M., Rigato, V. (2009). Diffusion coefficient measurements in consolidated clay by RBS micro-scale profiling. *Appl. Clay Sci.* **43**, 477-484.

Altenhein-Haese, C., Bischoff, H., Fu, L., Mao, J., Marx, G. (1994). Adsorption of actinides on cement compounds. *J. Alloys Compd.* **213/214**, 554-556.

Amayri, S., Buda, R. A., Fröhlich, D., Heinrich, J., Klimach, T., Kratz, J. V., Reich, T., Trautmann, N., Wunderlich, T. (2008). Sorption of actinides (Th, U, Np, Pu, Am) on Opalinus Clay in synthetic porewater. *NRC 7*, 24.08.-29.08.2008, Budapest, Hungary. #PB1 (abstr.).

Andersen, F. A., Brečević, L. (1991). Infrared spectra of amorphous and crystalline calcium carbonate. *Acta Chem. Scand.* **45**, 1018-1024.

Ankudinov, A. L., Ravel, B., Rehr, J. J., Conradson, S. D. (1998). Real-space multiple-scattering calculation and interpretation of X-ray-absorption near-edge structure. *Phys. Rev. B* **58**, 7565-7576.

Appelo, C. A. J., Van Loon, L. R., Wersin, P. (2010). Multicomponent diffusion of a suite of tracers (HTO, Cl, Br, I, Na, Sr, Cs) in a single sample of Opalinus Clay. *Geochim. Cosmochim. Acta* **74**, 1201-1219.

Artinger, R., Buckau, G., Geyer, S., Fritz, P., Wolf, M., Kim, J. I. (2000). Characterization of groundwater humic substances: influence of sedimentary organic carbon. *Appl. Geochem.* **15**, 97-116.

Artinger, R., Rabung, T., Kim, J. I., Sachs, S., Schmeide, K., Heise, K. H., Bernhard, G., Nitsche, H. (2002). Humic colloid-borne migration of uranium in sand columns. *J. Contam. Hydrol.* **58**, 1-12.

Bailey, S. W. (1980). Summary of recommendations of AIPEA nomenclature committee on clay minerals. *Am. Mineral.* **65**, 1-7.

Bargar, J. R., Reitmeyer, R., Lenhart, J. J., Davis, J. A. (2000). Characterization of U(VI)-carbonato ternary complexes on hematite: EXAFS and electrophoretic mobility measurements. *Geochim. Cosmochim. Acta* **64**, 2737-2749.

Bauer, A., Fiehn, B., Marquardt, C. M., Klein, M., Römer, J., Schäfer, T., Görtzen, A., Kienzler, B. (2006). Results on the Pu Diffusion in the Opalinus Clay. *6th EC FP - FUNMIG IP*, 21.-23.11.2006, Stockholm, 2nd Annual Workshop Proceedings, 231-237.

Beck, H. P., Wagner, H., Gottfreund, T., Zeitz, M. (2004). Investigations of the behaviour of the heavy elements Cu, Zn, Cd, and Pb in the ternary system metal - humic acid - sand. In: Marquardt, C. M. (Ed.), *Wissenschaftliche Berichte, FZK-6999*. Forschungszentrum Karlsruhe, Karlsruhe.

Beneš, P., Kratzer, K., Vlčková, Š., Šebestová, E. (1998). Adsorption of uranium on clay and the effect of humic substances. *Radiochim. Acta* **82**, 367-373.

Beneš, P. (2009). Radiotracer study of thorium complexation with humic acid at pH 2-11 using free-liquid electrophoresis. *Radiochim. Acta* **97**, 273-281.

Bernhard, G., Geipel, G., Reich, T., Brendler, V., Amayri, S., Nitsche, H. (2001). Uranyl(VI) carbonate complex formation: Validation of the $Ca_2UO_2(CO_3)_3$(aq.) species. *Radiochim. Acta* **89**, 511-518.

Bernhard, G., Geipel, G. (2007). Bestimmung der Bindungsform des Urans in Mineralwässern. *Vom Wasser* **105**, 7-10.

Bertrand, P. A., Choppin, G. R. (1982). Separation of actinides in different oxidation states by solvent extraction. *Radiochim. Acta* **31**, 135-137.

BfS (2012). Sicherheitskriterien für die Endlagerung radioaktiver Abfälle in einem Bergwerk. In: *Handbuch Reaktorsicherheit und Strahlenschutz*. Bundesamt für Strahlenschutz (BfS), Salzgitter.

BGBl (2011). Dreizehntes Gesetz zur Änderung des Atomgesetzes, 31.07.2011. In: Bundesgesetzblatt (BGBl), I, 43, 1704-1705.
Website:
http://www.bgbl.de/Xaver/start.xav?startbk=Bundesanzeiger_BGBl&jumpTo=bgbl111s1704.pdf.

BGR (2007). Endlagerung radioaktiver Abfälle in Deutschland. *Untersuchung und Bewertung von Regionen mit potenziell geeigneten Wirtsgesteinsformationen*. Bundesanstalt für Geowissenschaften und Rohstoffe (BGR), Hannover/Berlin.

Birke, M., Rauch, U., Lorenz, H. (2009). Uranium in stream and mineral water of the Federal Republic of Germany. *Environ. Geochem. Health* **31**, 693-706.

Blake, R. L., Hessevick, R. E., Zoltai, T., Finger, L. W. (1966). Refinement of the hematite structure. *Am. Mineral.* **51**, 123-129.

Blanc, P., Gaucher, E., Sanjuan, B., Crouzet, C., Griffault, L. (2001). Testing a clay/porewater interaction model through a laboratory experiment. *Water-Rock Interaction: Proceedings 10th International Symposium on Water-Rock Interaction - WRI-10*, Villasimius, Italy, Balkema, Lisse, The Netherlands, 243-246.

Bleise, A., Danesi, P. R., Burkart, W. (2003). Properties, use and health effects of depleted uranium (DU): a general overview. *J. Environ. Radioact.* **64**, 93-112.

BMU (2010). Sicherheitsanforderungen an die Endlagerung wärmeentwickelnder radioaktiver Abfälle. Bundesministerium für Umwelt, Naturschutz und Reaktorsicherheit (BMU), Berlin.

Bortiatynski, J. M., Hatcher, P. G., Knicker, H. (1996). NMR techniques (C, N, and H) in studies of humic substances. In: Gaffney, J. S., Marley, N. A., and Clark, S. B. (Eds.), *Humic and fulvic acids - Isolation, structure, and environmental role*. American Chemical Society, Washington, DC.

Bossart, P., Thury, M. (2008). Mont Terri Rock Laboratory. Project, Programme 1996 to 2007 and Results. *Reports of the Swiss Geological Survey No. 3*. Swiss Geological Survey, Wabern.

Brachmann, A. (1997). Zeitaufgelöste laser-induzierte Fluoreszenzspektroskopie zur Charakterisierung der Wechselwirkung des Uranylions mit Huminsäuren und Carboxylatliganden. *Ph.D. thesis*, Technische Universität Dresden.

Bradbury, M., Baeyens, B. (2004). Project Opalinus Clay: Sorption Data Bases for Opalinus Clay Influenced by a high pH Plume. *PSI Bericht 04-07*. PSI, Nuclear Energy and Safety Research Department, Laboratory for Waste Management, Villigen.

Bradbury, M., Baeyens, B., Thoenen, T. (2010). Sorption data bases for generic Swiss argillaceous rock systems. *Technical Report NTB 09-03*. Nagra, Wettingen.

Bradbury, M. H., Baeyens, B. (2006). Modelling sorption data for the actinides Am(III), Np(V) and Pa(V) on montmorillonite. *Radiochim. Acta* **94**, 619-625.

Bradbury, M. H., Baeyens, B. (2009). Sorption modelling on illite. Part II: Actinide sorption and linear free energy relationships. *Geochim. Cosmochim. Acta* **73**, 1004-1013.

Brand, R. A. (1987). Improving the validity of hyperfine field distributions from magnetic alloys. Part I: Unpolarized source. *Nucl. Instrum. Methods Phys. Res., Sect. B* **28**, 398-416.

Brasser, T., Droste, J., Müller-Lyda, I., Neles, J. M., Sailer, M., Schmidt, G., Steinhoff, M. (2008). Endlagerung wärmeentwickelnder radioaktiver Abfälle in Deutschland. *GRS - 247*. Öko-Institut and Gesellschaft für Anlagen- und Reaktorsicherheit (GRS), Braunschweig.

Bräuer, V., Reh, M., Schulz, P., Schuster, P., Sprado, K.-H. (1994). Untersuchung und Bewertung von Regionen in nichtsalinaren Formationen. *Endlagerung stark wärmeentwickelnder radioaktiver Abfälle in tiefen geologischen Formationen Deutschlands*. Bundesanstalt für Geowissenschaften und Rohstoffe (BGR), Berlin/Hannover.

Brečević, L., Nielsen, A. E. (1989). Solubility of amorphous calcium carbonate. *J. Cryst. Growth* **98**, 504-510.

Breivik, H. (2008). Highly enriched uranium and crude nuclear weapons. *FFI-rapport 2008/00490*. Norwegian Defence Research Establishment, Kjeller.

Brooks, S. C., Fredrickson, J. K., Carroll, S. L., Kennedy, D. W., Zachara, J. M., Plymale, A. E., Kelly, S. D., Kemner, K. M., Fendorf, S. (2003). Inhibition of bacterial U(VI) reduction by calcium. *Environ. Sci. Technol.* **37**, 1850-1858.

Brunauer, S., Emmett, P. H., Teller, E. (1938). Adsorption of gases in multimolecular layers. *J. Am. Chem. Soc.* **60**, 309-319.

Bubner, M., Heise, K. H. (1994). Characterization of humic acids. II. Characterization by radioreagent - Derivatization with [^{14}C]diazomethane. *Annual Report 1993, FZR-43.* Forschungszentrum Rossendorf, Institut für Radiochemie, Rossendorf.

Burkart, W. (1991). Uranium, thorium, and decay products. In: Merian, E. (Ed.), *Metals and their compounds in the environment*. VCH, Weinheim.

Burnham, J. U. (2001). Internal dose. In: *Radiation protection*. Point Lepreau Generating Station, New Brunswick Power Corporation, St. Andrews.

Burns, P. C. (1999). The crystal chemistry of uranium. *Rev. Mineral.* **38**, 23-90.

Burns, P. C., Finch, R. J. (1999). Wyartite: Crystallographic evidence for the first pentavalent-uranium mineral. *Am. Mineral.* **84**, 1456-1460.

Busenberg, E., Plummer, L. N., Parker, V. B. (1984). The solubility of strontianite ($SrCO_3$) in CO_2-H_2O solutions between 2 and 91°C, the association constants of $SrHCO_3^+$(aq) and $SrCO_3^0$(aq) between 5 and 80°C, and an evaluation of the thermodynamic properties of Sr^{2+}(aq) and $SrCO_3$(cr) at 25°C and 1 atm total pressure. *Geochim. Cosmochim. Acta* **48**, 2021-2035.

Chapman, D. L. (1913). A contribution to the theory of electrocapillarity. *Philos. Mag.* **25**, 475-481.

Chen, Y., Senesi, N., Schnitzer, M. (1977). Information provided on humic substances by E_4 / E_6 ratios. *Soil Sci. Soc. Am. J.* **41**, 352-358.

Chipera, S. J., Bish, D. L. (2001). Baseline studies of The Clay Minerals Society Source Clays: Powder X-ray diffraction analyses. *Clay Clay Min.* **49**, 398-409.

Chisholm-Brause, C. J., Berg, J. M., Matzner, R. A., Morris, D. E. (2001). Uranium(VI) sorption complexes on montmorillonite as a function of solution chemistry. *J. Colloid Interface Sci.* **233**, 38-49.

Claret, F., Schäfer, T., Bauer, A., Buckau, G. (2003). Generation of humic and fulvic acid from Callovo-Oxfordian Clay under high alkaline conditions. *Sci. Total Environ.* **317**, 189-200.

Cochran, T. B., Paine, C. E. (1995). Nuclear weapons databook: The amount of plutonium and highly-enriched uranium needed for pure fission nuclear weapons. Natural Resources Defense Council, Washington.

COMSOL (2008). Multiphysics 3.5a, Finite-element software package. COMSOL AB, Stockholm. Website: http://www.comsol.com.

Cordfunke, E. H. P. (1969). *The chemistry of uranium*. Elsevier, Amsterdam.

Cornell, R. M., Schwertmann, U. (2003). *The iron oxides - structure, properties, reactions, occurrences and uses*. Wiley VCH, Weinheim.

Courdouan, A., Christl, I., Meylan, S., Wersin, P., Kretzschmar, R. (2007). Characterization of dissolved organic matter in anoxic rock extracts and in situ pore water of the Opalinus Clay. *Appl. Geochem.* **22**, 2926-2939.

Czerwinski, K. R., Buckau, G., Scherbaum, F., Kim, J. I. (1994). Complexation of the uranyl ion with aquatic humic acid. *Radiochim. Acta* **65**, 111-119.

Czerwinski, K. R., Kim, J. I., Rhee, D. S., Buckau, G. (1996). Complexation of trivalent actinide ions (Am^{3+}, Cm^{3+}) with humic acid: The effect of ionic strength. *Radiochim. Acta* **72**, 179-187.

Davies, G., Ghabbour, E. A. (Eds.) (1998). *Humic substances - Structures, properties and uses*. The Royal Society of Chemistry, Cambridge.

Davis, J. A., James, R. O., Leckie, J. O. (1978). Surface ionization and complexation at oxide-water interface. 1. Computation of electrical double-layer properties in simple electrolytes. *J. Colloid Interface Sci.* **63**, 480-499.

Davis, J. A., Coston, J. A., Kent, D. B., Fuller, C. C. (1998). Application of the surface complexation concept to complex mineral assemblages. *Environ. Sci. Technol.* **32**, 2820-2828.

Dong, W. M., Brooks, S. C. (2006). Determination of the formation constants of ternary complexes of uranyl and carbonate with alkaline earth metals (Mg^{2+}, Ca^{2+}, Sr^{2+}, and Ba^{2+}) using anion exchange method. *Environ. Sci. Technol.* **40**, 4689-4695.

Dreissig, I., Weiss, S., Hennig, C., Bernhard, G., Zänker, H. (2011). Formation of uranium(IV)-silica colloids at near-neutral pH. *Geochim. Cosmochim. Acta* **75**, 352-367.

Dzombak, D. A., Morel, F. M. M. (1990). *Surface complexation modeling. Hydrous ferric oxide*. Wiley, New York.

Eisenberg, D., Kauzmann, W. (1969). *The structure and properties of water*. Oxford University Press, Ely House, London.

Fachgruppe Wasserchemie in der Gesellschaft Deutscher Chemiker, Normenausschuss Wasserwesen im Deutschen Institut für Normung e.V. (1984). Physikalische und physikalisch-chemische Kenngrößen: Bestimmung der Redoxspannung (DIN 38 404). In: *Deutsche Einheitsverfahren zur Wasser-, Abwasser- und Schlammuntersuchung: Physikalische, chemische, biologische und bakteriologische Verfahren*. Wiley VCH, Weinheim.

Fauth, H., Hindel, R., Siewers, U., Zinner, J. (1985). *Geochemischer Atlas Bundesrepublik Deutschland: Verteilung von Schwermetallen in Wässern und Bachsedimenten*. Bundesanstalt für Geowissenschaften und Rohstoffe (BGR), Hannover.

Fayek, M., Janeczek, J., Ewing, R. C. (1997). Mineral chemistry and oxygen isotopic analyses of uraninite, pitchblende and uranium alteration minerals from the Cigar Lake deposit, Saskatchewan, Canada. *Appl. Geochem.* **12**, 549-565.

Fernández, A. M., Turrero, M. J., Sánchez, D. M., Yllera, A., Melón, A. M., Sánchez, M., Peña, J., Garralón, A., Rivas, P., Bossart, P., Hernán, P. (2007). On site measurements of the redox and carbonate system parameters in the low-permeability Opalinus Clay formation at the Mont Terri Rock Laboratory. *Phys. Chem. Earth.* **32**, 181-195.

Finch, R., Murakami, T. (1999). Systematics and paragenesis of uranium minerals. *Rev. Mineral.* **38**, 91-179.

Foerstendorf, H., Heim, K., Rossberg, A. (2012). The complexation of uranium(VI) and atmospherically derived CO_2 at the ferrihydrite-water interface probed by time-resolved vibrational spectroscopy. *J. Colloid Interface Sci.* **377**, 299-306.

Fox, P. M., Davis, J. A., Zachara, J. M. (2006). The effect of calcium on aqueous uranium(VI) speciation and adsorption to ferrihydrite and quartz. *Geochim. Cosmochim. Acta* **70**, 1379-1387.

Freundlich, H. (1906). Concerning adsorption in solutions. *Z. Phys. Chem. Stoechiom. Verwandtschafts.* **57**, 385-470.

Fröhlich, D. R., Amayri, S., Drebert, J., Reich, T. (2011). Sorption of neptunium(V) on Opalinus Clay under aerobic / anaerobic conditions. *Radiochim. Acta* **99**, 71-77.

Fröhlich, D. R., Amayri, S., Drebert, J., Reich, T. (2012). Influence of temperature and background electrolyte on the sorption of neptunium(V) on Opalinus Clay. *Appl. Clay Sci.* **69**, 43-49.

Funke, H., Bernhard, G., Claussner, J., Jansen, K., Matz, W., Nitsche, H., Oehme, W., Reich, T., Rollig, D. (2001). Technical description of the radiological safety system for X-ray absorption spectroscopy experiments on radioactive samples at the Rossendorf Beamline. *Kerntechnik* **66**, 195-201.

Gaffney, J. S., Marley, N. A., Clark, S. B. (1996). Humic and fulvic acids and organic colloidal materials in the environment. In: Gaffney, J. S., Marley, N. A., and Clark, S. B. (Eds.), *Humic and fulvic acids - Isolation, structure, and environmental role*. American Chemical Society, Washington, DC.

George, G. N., Pickering, I. J. (2000). EXAFSPAK: A suite of computer programs for analysis of X-ray absorption spectra. Stanford Synchrotron Radiation Laboratory, Stanford Linear Accelerator Center, Menlo Park, CA.

Gillman, G. P., Uehara, G. (1980). Charge characteristics of soils with variable and permanent charge minerals. Part II. Experimental. *Soil Sci. Soc. Am. J.* **44**, 252-255.

Glaus, M. A., Rossé, R., Van Loon, L. R., Yaroshchuk, A. E. (2008). Tracer diffusion in sintered stainless steel filters: measurement of effective diffusion coefficients and implications for diffusion studies with compacted clays. *Clay Clay Min.* **56**, 677-685.

González-Sánchez, F., Van Loon, L. R., Gimmi, T., Jakob, A., Glaus, M. A., Diamond, L. W. (2008). Self-diffusion of water and its dependence on temperature and ionic strength in highly compacted montmorillonite, illite and kaolinite. *Appl. Geochem.* **23**, 3840-3851.

Gouy, L. G. (1910). Constitution of the electric charge at the surface of an electrolyte. *Journal de Physique Théorique et Appliquée, Ser. 4,* **9**, 457-468.

Grenthe, I., Fuger, J., Konings, R. J. M., Lemire, R. J., Muller, A. B., Nguyen-Trung Cregu, C., Wanner, H. (1992). *Chemical Thermodynamics of Uranium (OECD/NEA, ed.)*. Elsevier, Amsterdam.

Guetzloff, T. F., Rice, J. A. (1996). Micellar nature of humic colloids. In: Gaffney, J. S., Marley, N. A., and Clark, S. B. (Eds.), *Humic and fulvic acids - Isolation, structure, and environmental role*. American Chemical Society, Washington, DC.

Guillaumont, R., Fanghänel, T., Neck, V., Fuger, J., Palmer, D. A., Grenthe, I., Rand, M. H. (2003). *Update on the Chemical Thermodynamics of Uranium, Neptunium, Plutonium, Americium and Technetium (OECD/NEA, ed.)*. Elsevier, Amsterdam.

Hart, K. P., Payne, T. E., Robinson, B. J., Vaniseghem, P. (1994). Neptunium uptake on Boom Clay - Time-dependence and association of Np with fine particles. *Radiochim. Acta* **66/67**, 19-22.

Hartmann, E., Geckeis, H., Rabung, T., Lützenkirchen, J., Fanghänel, T. (2008). Sorption of radionuclides onto natural clay rocks. *Radiochim. Acta* **96**, 699-707.

Hayes, M. H. B. (1998). Humic substances: Progress towards more realistic concepts of structures. In: Davies, G. and Ghabbour, E. A. (Eds.), *Humic substances - structures, properties and uses*. The Royal Society of Chemistry, Cambridge.

Henry, W. (1803). Experiments on the quantity of gases absorbed by water, at different temperatures, and under different pressures. *Phil. Trans. R. Soc. Lond.* **93**, 29-274.

Hoth, P., Wirth, H., Reinhold, K., Bräuer, V., Krull, P., Feldrappe, H. (2007). Untersuchung und Bewertung von Tongesteinsformationen. *Endlagerung radioaktiver Abfälle in tiefen geologischen Formationen Deutschlands*. Bundesanstalt für Geowissenschaften und Rohstoffe (BGR), Berlin/Hannover.

Hudson, E. A., Rehr, J. J., Bucher, J. J. (1995). Multiple-scattering calculations of the uranium L_{III}-edge X-ray-absorption near-edge structure. *Phys. Rev. B* **52**, 13815-13826.

Huertas, F. J., Chou, L., Wollast, R. (1998). Mechanism of kaolinite dissolution at room temperature and pressure: Part 1. Surface speciation. *Geochim. Cosmochim. Acta* **62**, 417-431.

Hull, L. C., Grossman, C., Fjeld, R. A., Coates, J. T., Elzerman, A. W. (2004). Hybrid empirical-theoretical approach to modeling uranium adsorption. *Appl. Geochem.* **19**, 721-736.

IAEA (2012). Nuclear power reactors in the world. *Reference data series No. 2*. International Atomic Energy Agency, Vienna. Website: http://www.iaea.org/pris/.

Jähnigen, P. (2007). Simultanbestimmung von Betastrahlern in Nuklidgemischen mittels Flüssigszintillationsspektrometrie. *Diploma thesis*, Technische Universität Dresden.

Jakob, A., Pfingsten, W., Van Loon, L. (2009). Effects of sorption competition on caesium diffusion through compacted argillaceous rock. *Geochim. Cosmochim. Acta* **73**, 2441-2456.

Jasmund, K., Lagaly, G. (Eds.) (1993). *Tone und Tonminerale*. Steinkopff, Darmstadt.

Johnson, L. H., Niemeyer, M., Klubertanz, G., Siegel, P., Gribi, P. (2002). Calculations of the temperature evolution of a repository for spent fuel, vitrified high-level waste and intermediate level waste in Opalinus Clay. *Technical Report NTB 01-04*. Nagra, Wettingen.

Jörg, G., Bühnemann, R., Hollas, S., Kivel, N., Kossert, K., Van Winckel, S., Gostomski, C. L. V. (2010). Preparation of radiochemically pure ^{79}Se and highly precise determination of its half-life. *Appl. Radiat. Isot.* **68**, 2339-2351.

Joseph, C., Schmeide, K., Sachs, S., Brendler, V., Geipel, G., Bernhard, G. (2011). Sorption of uranium(VI) onto Opalinus Clay in the absence and presence of humic acid in Opalinus Clay pore water. *Chem. Geol.* **284**, 240-250.

Joseph, C., Van Loon, L. R., Jakob, A., Steudtner, R., Schmeide, K., Sachs, S., Bernhard, G. (2013). Diffusion of U(VI) in Opalinus Clay: Influence of temperature and humic acid. *Geochim. Cosmochim. Acta* **109**, 74-89.

Joseph, C., Stockmann, M., Schmeide, K., Sachs, S., Brendler, V., Bernhard, G. (2013, accepted). Sorption of U(VI) onto Opalinus Clay: Effects of pH and humic acid. *Appl. Geochem.*

Jung, J., Lee, J. K., Hahn, P. S. (2001). Development and application of a sorption data base for the performance assessment of a radwaste repository. *Waste Manage.* **21**, 363-369.

Katz, J. J., Morss, L. R., Seaborg, G. T. (1986). Summary and comparative aspects of the actinide elements. In: Katz, J. J., Seaborg, G. T., and Morss, L. R. (Eds.), *The chemistry of the actinide elements, 2nd edition*. Chapman and Hall, New York.

Kaufhold, S., Dohrmann, R., Bitzer, C., Pletsch, T., Klosa, D. (2003). Laboratory test results (D 6/2) - Preliminary interpretations: Heater Experiment (HE), Rock and bentonite thermo-hydro-mechanical (THM) processes in the near field. Bundesanstalt für Geowissenschaften und Rohstoffe (BGR), Hanover.

Keeling, P. S. (1958). A simple aid to clay mineral identification. *Clay Miner. Bull.* **3**, 271-275.

Kerisit, S., Liu, C. X. (2010). Molecular simulation of the diffusion of uranyl carbonate species in aqueous solution. *Geochim. Cosmochim. Acta* **74**, 4937-4952.

Khwaja, A. R., Bloom, P. R., Brezonik, P. L. (2006). Binding constants of divalent mercury (Hg^{2+}) in soil humic acids and soil organic matter. *Environ. Sci. Technol.* **40**, 844-849.

Kim, J. I., Buckau, G., Li, G. H., Duschner, H., Psarros, N. (1990). Characterization of humic and fulvic acids from Gorleben groundwater. *Fresenius J. Anal. Chem.* **338**, 245-252.

Kim, J. I., Buckau, G., Klenze, R., Rhee, D. S., Wimmer, H. (1991). Nuclear science and technology: Characterization and complexation of humic acids. *Final report, Part 1 'Complexation'*. Commission of the European Communities, Luxembourg.

Kim, J. I., Czerwinski, K. R. (1996). Complexation of metal ions with humic acid: Metal ion charge neutralization model. *Radiochim. Acta* **73**, 5-10.

Kinniburgh, D. G. (1986). General purpose adsorption isotherms. *Environ. Sci. Technol.* **20**, 895-904.

Kinniburgh, D. G., van Riemsdijk, W. H., Koopal, L. K., Borkovec, M., Benedetti, M. F., Avena, M. J. (1999). Ion binding to natural organic matter: competition, heterogeneity, stoichiometry and thermodynamic consistency. *Colloids Surf., A* **151**, 147-166.

Klaproth, M. H. (1789). Chemische Untersuchung des Uranits, einer neuentdeckten metallischen Substanz. *Chem. Ann. Freunde Naturl.* **2**, 387-403.

Klinge, H., Köthe, A., Ludwig, R.-R., Zwirner, R. (2002). Geologie und Hydrogeologie des Deckgebirges über den Salzstock Gorleben. *Z. Angew. Geol.*, 7-15.

Kockel, F., Krull, P. (1995). Untersuchung und Bewertung von Salzformationen. *Endlagerung stark wärmeentwickelnder radioaktiver Abfälle in tiefen geologischen Formationen Deutschlands*. Bundesanstalt für Geowissenschaften und Rohstoffe (BGR), Berlin/Hannover.

Kolokassidou, C., Pashalidis, I., Costa, C. N., Efstathiou, A. M., Buckau, G. (2007). Thermal stability of solid and aqueous solutions of humic acid. *Thermochim. Acta* **454**, 78-83.

Königsberger, E., Königsberger, L. C., Gamsjäger, H. (1999). Low-temperature thermodynamic model for the system Na_2CO_3-$MgCO_3$-$CaCO_3$-H_2O. *Geochim. Cosmochim. Acta* **63**, 3105-3119.

Koningsberger, D. C., Prins, R. (Eds.) (1988). *X-ray absorption: Principles, applications, techniques of EXAFS, SEXAFS, and XANES*. John Wiley & Sons, New York.

Kornilovich, B., Pshinko, G., Spasenova, L., Kovalchuk, I. (2000). Influence of humic substances on the sorption interactions between lanthanide and actinide ions and clay minerals. *Adsorpt. Sci. Technol.* **18**, 873-880.

Kowal-Fouchard, A., Drot, R., Simoni, E., Ehrhardt, J. J. (2004). Use of spectroscopic techniques for uranium(VI)/montmorillonite interaction modeling. *Environ. Sci. Technol.* **38**, 1399-1407.

Kozai, N., Inada, K., Kozaki, T., Sato, S., Ohashi, H., Banba, T. (2001). Apparent diffusion coefficients and chemical species of neptunium (V) in compacted Na-montmorillonite. *J. Contam. Hydrol.* **47**, 149-158.

Kozaki, T., Sato, H., Fujishima, A., Sato, S., Ohashi, H. (1996). Activation energy for diffusion of cesium in compacted sodium montmorillonite. *J. Nucl. Sci. Technol.* **33**, 522-524.

Kozaki, T., Sato, H., Fujishima, A., Saito, N., Sato, S., Ohashi, H. (1997). Effect of dry density on activation energy for diffusion of strontium in compacted sodium montmorillonite. *Scientific Basis for Nuclear Waste Management XX*, Materials Research Society Conference Proceedings, 893-900.

Kozaki, T., Fujishima, A., Sato, S., Ohashi, H. (1998). Self-diffusion of sodium ions in compacted sodium montmorillonite. *Nucl. Technol.* **121**, 63-69.

Kozaki, T., Inada, K., Sato, S., Ohashi, H. (2001). Diffusion mechanism of chloride ions in sodium montmorillonite. *J. Contam. Hydrol.* **47**, 159-170.

Kremleva, A., Zhang, Y., Shor, A. M., Krüger, S., Joseph, C., Raditzky, B., Schmeide, K., Sachs, S., Bernhard, G., Rösch, N. (2012). Uranyl(VI) complexation by sulfonate ligands: A relativistic density functional and TRLFS study. *Eur. J. Inorg. Chem.* **2012**, 3636-3644.

Křepelová, A., Sachs, S., Bernhard, G. (2006). Uranium(VI) sorption onto kaolinite in the presence and absence of humic acid. *Radiochim. Acta* **94**, 825-833.

Křepelová, A. (2007). Influence of humic acid on the sorption of uranium(VI) and americium(III) onto kaolinite. *Ph.D. thesis*, Technische Universität Dresden.

Křepelová, A., Reich, T., Sachs, S., Drebert, J., Bernhard, G. (2008). Structural characterization of U(VI) surface complexes on kaolinite in the presence of humic acid using EXAFS spectroscopy. *J. Colloid Interface Sci.* **319**, 40-47.

Kretzschmar, R., Hesterberg, D., Sticher, H. (1997). Effects of adsorbed humic acid on surface charge and flocculation of kaolinite. *Soil Sci. Soc. Am. J.* **61**, 101-108.

Kümmel, R., Worch, E. (1990). *Adsorption aus wässrigen Lösungen*. VEB Deutscher Verlag für Grundstoffindustrie, Leipzig.

Langmuir, I. (1918). The adsorption of gases on plane surfaces of glass, mica and platinum. *J. Am. Chem. Soc.* **40**, 1361.

Lehmann, H. P., Fuentes-Arderiu, X., Bertello, L. F. (1996). Glossary of terms in quantities and units in clinical chemistry (IUPAC-IFCC recommendations 1996). *Pure Appl. Chem.* **68**, 957-1000.

Lieser, K. H. (1980). *Einführung in die Kernchemie*. Verlag Chemie, Weinheim.

Lippold, H., Mansel, A., Kupsch, H. (2005). Influence of trivalent electrolytes on the humic colloid-borne transport of contaminant metals: competition and flocculation effects. *J. Contam. Hydrol.* **76**, 337-352.

Lippold, H., Evans, N. D. M., Warwick, P., Kupsch, H. (2007). Competitive effect of iron(III) on metal complexation by humic substances: Characterisation of ageing processes. *Chemosphere* **67**, 1050-1056.

Lippold, H., Lippmann-Pipke, J. (2009). Effect of humic matter on metal adsorption onto clay materials: Testing the linear additive model. *J. Contam. Hydrol.* **109**, 40-48.

Liu, J., Yamada, H., Kozaki, T., Sato, S., Ohashi, H. (2003). Effect of silica sand on activation energy for diffusion of sodium ions in montmorillonite and silica sand mixture. *J. Contam. Hydrol.* **61**, 85-93.

Lu, C., Samper, J., Cormenzana, J. L., Ma, H., Montenegro, L., Cuñado, M. A. (2012). Reactive transport model and apparent K_d of Ni in the near field of a HLW repository in granite. *Comput. Geosci.* **49**, 256-266.

MacCarthy, P., Rice, J. A. (1985). Spectroscopic methods (other than NMR) for determining functionality in humic substances. In: Aiken, G. R., McKnight, D. M., Wershaw, R. L., and MacCarthy, P. (Eds.), *Humic substances in soil, sediment, and water*. John Wiley & Sons, New York.

Madejová, J., Komadel, P. (2001). Baseline studies of The Clay Minerals Society Source Clays: Infrared methods. *Clay Clay Min.* **49**, 410-432.

Magill, J., Pfennig, G., Galy, J. (2006). Karlsruher Nuklidkarte. *Report EUR 22276 EN*. European Commission - DG Joint Research Centre - Institute for Transuranium Elements, Luxembourg.

Mahajan, G. R., Rao, V. K., Natarajan, P. R. (1989). Interaction of humic acid with plutonium(III). *J. Radioanal. Nucl. Chem. Lett.* **137**, 219-227.

Majzik, A., Tombacz, E. (2007). Interaction between humic acid and montmorillonite in the presence of calcium ions I. Interfacial and aqueous phase equilibria: Adsorption and complexation. *Org. Geochem.* **38**, 1319-1329.

Malikova, N., Marry, V., Dufreche, J. F., Simon, C., Turq, P., Giffaut, E. (2004). Temperature effect in a montmorillonite clay at low hydration-microscopic simulation. *Mol. Phys.* **102**, 1965-1977.

Mansel, A., Crustewitz, C., Kupsch, H. (2003). Geochemische Untersuchungen zur Retention von reaktiven Kohlenstoffverbindungen für toxische Schwermetalle. *Abschlussbericht*. Institut für Interdisziplinäre Isotopenforschung, Leipzig.

Marquardt, C. M., Seibert, A., Artinger, R., Denecke, M. A., Kuczewski, B., Schild, D., Fanghänel, T. (2004). The redox behaviour of plutonium in humic rich groundwater. *Radiochim. Acta* **92**, 617-623.

Matz, W., Schell, N., Bernhard, G., Prokert, F., Reich, T., Claussner, J., Oehme, W., Schlenk, R., Dienel, S., Funke, H., Eichhorn, F., Betzl, M., Prohl, D., Strauch, U., Huttig, G., Krug, H., Neumann, W., Brendler, V., Reichel, P., Denecke, M. A., Nitsche, H. (1999). ROBL - a CRG beamline for radiochemistry and materials research at the ESRF. *J. Synchrotron Radiat.* **6**, 1076-1085.

Mazurek, M., Pearson, F. J., Volckaert, G., Bock, H. (2003). Features, events and processes evaluation catalogue for argillaceous media. *NEA4437*. OECD/NEA, Paris.

Meleshyn, A., Azeroual, M., Reeck, T., Houben, G., Riebe, B., Bunnenberg, C. (2009). Influence of (calcium-)uranyl-carbonate complexation on U(VI) sorption on Ca- and Na-bentonites. *Environ. Sci. Technol.* **43**, 4896-4901.

Mell, P., Megyeri, J., Riess, L., Máthé, Z., Csicsák, J., Lázár, K. (2006). Sorption of Co, Cs, Sr and I onto argillaceous rock as studied by radiotracers. *J. Radioanal. Nucl. Chem.* **268**, 405-410.

Mereiter, K. (1982). The crystal structure of liebigite, $Ca_2UO_2(CO_3)_3 \cdot \sim 11\ H_2O$. *Tscher. Miner. Petrog.* **30**, 277-288.

Mibus, J., Sachs, S. (2006). Impact of humic colloids on uranium(VI) migration in clay. *Annual Report 2005, FZR-443*. Forschungszentrum Rossendorf, Dresden.

Mibus, J., Müller, C., Sachs, S., Küchler, R. (2007a). Determination of diffusion coefficients of humic acid in bulk water. *Annual Report 2006, FZD-459*. Forschungszentrum Dresden-Rossendorf, Dresden.

Mibus, J., Sachs, S., Pfingsten, W., Nebelung, C., Bernhard, G. (2007b). Migration of uranium(IV)/(VI) in the presence of humic acids in quartz sand: A laboratory column study. *J. Contam. Hydrol.* **89**, 199-217.

Mincher, B. J., Fox, R. V., Cooper, D. C., Groenewold, G. S. (2003). Neptunium and plutonium sorption to Snake River Plain, Idaho soil. *Radiochim. Acta* **91**, 397-401.

Moll, H., Geipel, G., Reich, T., Bernhard, G., Fanghänel, T., Grenthe, I. (2003). Uranyl(VI) complexes with alpha-substituted carboxylic acids in aqueous solution. *Radiochim. Acta* **91**, 11-20.

Montavon, G., Mansel, A., Seibert, A., Keller, H., Kratz, J. V., Trautmann, N. (2000). Complexation studies of UO_2^{2+} with humic acid at low metal ion concentrations by indirect speciation methods. *Radiochim. Acta* **88**, 17-24.

Moore, W. J., Hummel, D. O., Trafara, G., Holland-Moritz, K. (1986). *Physikalische Chemie*. Walter de Gruyter, Berlin.

Morgenstern, M., Klenze, R., Kim, J. I. (2000). The formation of mixed-hydroxo complexes of Cm(III) and Am(III) with humic acid in the neutral pH range. *Radiochim. Acta* **88**, 7-16.

Morris, K. F., Cutak, B. J., Dixon, A. M., Larive, C. K. (1999). Analysis of diffusion coefficient distributions in humic and fulvic acids by means of diffusion ordered NMR spectroscopy. *Anal. Chem.* **71**, 5315-5321.

Motta, M. M., Miranda, C. F. (1989). Molybdate adsorption on kaolinite, montmorillonite, and illite: Constant capacitance modeling. *Soil Sci. Soc. Am. J.* **53**, 380-385.

Müller, K., Brendler, V., Foerstendorf, H. (2008). Aqueous uranium(VI) hydrolysis species characterized by attenuated total reflection Fourier-transform infrared spectroscopy. *Inorg. Chem.* **47**, 10127-10134.

Murphy, E. M., Zachara, J. M., Smith, S. C., Phillips, J. L. (1992). The sorption of humic acids to mineral surfaces and their role in contaminant binding. *Sci. Total Environ.* **117-118**, 413-423.

Nagra (2002). Projekt Opalinuston, Synthese der geowissenschaftlichen Untersuchungsergebnisse. *Technical Report NTB 02-03*. Nagra, Wettingen.

NEA (2006). *Kernenergie heute*. OECD, Paris.

Nebbioso, A., Piccolo, A. (2009). Molecular rigidity and diffusivity of Al^{3+} and Ca^{2+} humates as revealed by NMR spectroscopy. *Environ. Sci. Technol.* **43**, 2417-2424.

Nebelung, C., Brendler, V. (2010). U(VI) sorption on granite: prediction and experiments. *Radiochim. Acta* **98**, 621-625.

Newville, M. (2004). *Fundamentals of XAFS*. Consortium for Advanced Radiation Sources, University of Chicago, Chicago, IL.

Nitsche, H. (1995). Synchrotron X-ray-absorption spectroscopy: a new tool for actinide and lanthanide speciation in solids and solution. *J. Alloys Compd.* **223**, 274-279.

Niu, Z. W., Fan, Q. H., Wang, W. H., Xu, J. Z., Chen, L., Wu, W. S. (2009). Effect of pH, ionic strength and humic acid on the sorption of uranium(VI) to attapulgite. *Appl. Radiat. Isot.* **67**, 1582-1590.

Noseck, U., Becker, D.-A., Brasser, T., Fahrenholz, C., Flügge, J., Herbert, H.-J., Ionescu, A., Kröhn, K.-P., Kull, H., Meleshyn, A., Mönig, J., Röhlig, K., Rübel, A., Rothfuchs, T., Wolf, J. (2012). Scientific basis for a safety case of deep geological repositories. *GRS-298*. Gesellschaft für Anlagen- und Reaktorsicherheit (GRS), Köln.

OECD/NEA (2006). Physics and safety of transmutation systems - A status report. *NEA No. 6090*. OECD, Paris.

Ościk, J. (1982). *Adsorption*. Ellis Horwood Limited and Polish Scientific Publishers, Chichester and Warsaw.

Pandey, A. K., Pandey, S. D., Misra, V. (2000). Stability constants of metal-humic acid complexes and its role in environmental detoxification. *Ecotoxicol. Environ. Saf.* **47**, 195-200.

Parker, A., Rae, J. E. (Eds.) (1998). *Environmental interactions of clays: Clays in the environment*. Springer, Berlin.

Paulenová, A., Rajec, P., Žemberyová, M., Sasköiová, G., Višacký, V. (2000). Strontium and calcium complexation by humic acid. *J. Radioanal. Nucl. Chem.* **246**, 623-628.

Payne, T. E., Brendler, V., Comarmond, M. J., Nebelung, C. (2011). Assessment of surface area normalisation for interpreting distribution coefficients (K_d) for uranium sorption. *J. Environ. Radioact.* **102**, 888-895.

Pearson, F. J. (1998). Opalinus Clay experimental water: A1Type, Version 980318. *PSI Internal report TM-44-98-07*. Paul Scherrer Institut, Villigen PSI.

Pearson, F. J., Arcos, D., Bath, A., Boisson, J. Y., Fernández, A. M., Gäbler, H. E., Gaucher, E., Gautschi, A., Griffault, L., Hernán, P., Waber, H. N. (2003). Mont Terri Project - Geochemistry of water in the Opalinus Clay formation at the Mont Terri rock laboratory. *Reports of the Federal Office for Water and Geology, Geology Series No. 5*. Federal Office for Water and Geology, Bern.

Pédrot, M., Dia, A., Davranche, M. (2010). Dynamic structure of humic substances: Rare earth elements as a fingerprint. *J. Colloid Interface Sci.* **345**, 206-213.

Phillippi, J. M., Loganathan, V. A., McIndoe, M. J., Barnett, M. O., Clement, T. P., Roden, E. E. (2007). Theoretical solid/solution ratio effects on adsorption and transport: Uranium(VI) and carbonate. *Soil Sci. Soc. Am. J.* **71**, 329-335.

Pompe, S., Bubner, M., Denecke, M. A., Reich, T., Brachmann, A., Geipel, G., Nicolai, R., Heise, K. H., Nitsche, H. (1996). A comparison of natural humic acids with synthetic humic acid model substances: Characterization and interaction with uranium(VI). *Radiochim. Acta* **74**, 135-140.

Pompe, S., Brachmann, A., Bubner, M., Geipel, G., Heise, K. H., Bernhard, G., Nitsche, H. (1998). Determination and comparison of uranyl complexation constants with natural and model humic acids. *Radiochim. Acta* **82**, 89-95.

Pompe, S., Bubner, M., Schmeide, K., Heise, K. H., Bernhard, G., Nitsche, H. (2000a). Influence of humic acids on the migration behavior of radioactive and non-radioactive substances under conditions close to nature. Synthesis, radiometric determination of functional groups, complexation. *Wissenschaftlich-Technische Berichte, FZR-290*. Forschungszentrum Rossendorf, Dresden.

Pompe, S., Schmeide, K., Bubner, M., Geipel, G., Heise, K. H., Bernhard, G., Nitsche, H. (2000b). Investigation of humic acid complexation behavior with uranyl ions using modified synthetic and natural humic acids. *Radiochim. Acta* **88**, 553-558.

Power, W. H., Fabuss, B. M., Satterfield, C. N. (1966). Transient solute concentrations and phase changes of calcium sulfate in aqueous sodium chloride. *J. Chem. Eng. Data* **11**, 149-154.

Pruett, R. J., Webb, H. L. (1993). Sampling and analysis of KGa-1B well-crystallized kaolin source clay. *Clays Clay Miner.* **41**, 514-519.

Raditzky, B., Schmeide, K., Sachs, S., Geipel, G., Bernhard, G. (2010). Interaction of uranium(VI) with nitrogen containing model ligands studied by laser-induced fluorescence spectroscopy. *Polyhedron* **29**, 620-626.

Reardon, E. J., Armstrong, D. K. (1987). Celestite ($SrSO_{4(s)}$) solubility in water, seawater and NaCl solution. *Geochim. Cosmochim. Acta* **51**, 63-72.

Redden, G. D., Jinhe, L., Leckie, J. (1998). Adsorption of U(VI) and citric acid on goethite, gibbsite, and kaolinite: Comparing results for binary and ternary systems. In: Jenne, E. A. (Ed.), *Adsorption of metals by geomedia: Variables, mechanisms, and model applications*. Academic Press, San Diego.

Reich, T., Bernhard, G., Geipel, G., Funke, H., Hennig, C., Rossberg, A., Matz, W., Schell, N., Nitsche, H. (2000). The Rossendorf Beam Line ROBL - a dedicated experimental station for XAFS measurements of actinides and other radionuclides. *Radiochim. Acta* **88**, 633-637.

Reiller, P. (2005). Prognosticating the humic complexation for redox sensitive actinides through analogy, using the charge neutralisation model. *Radiochim. Acta* **93**, 43-55.

Ren, X. M., Wang, S. W., Yang, S. T., Li, J. X. (2010). Influence of contact time, pH, soil humic/fulvic acids, ionic strength and temperature on sorption of U(VI) onto MX-80 bentonite. *J. Radioanal. Nucl. Chem.* **283**, 253-259.

Roehl, K. E. (1997). Experimentelle Untersuchungen zu Retardation und Bindungsformen von Schwermetallen in tonigen Deponiebarrieren. *Ph.D. thesis*, Universität Karlsruhe.

Saada, A., Gaboriau, H., Cornu, S., Bardot, F., Villieras, F., Croue, J. P. (2003). Adsorption of humic acid onto a kaolinitic clay studied by high-resolution argon adsorption volumetry. *Clay Miner.* **38**, 433-443.

Sachs, S., Schmeide, K., Brendler, V., Křepelová, A., Mibus, J., Geipel, G., Heise, K. H., Bernhard, G. (2004). Investigation of the complexation and the migration of actinides and non-radioactive substances with humic acids under geogenic conditions: Complexation of humic acids with actinides in the oxidation state IV Th, U, Np. *Wissenschaftlich-Technische Berichte, FZR-399*. Forschungszentrum Rossendorf, Dresden.

Sachs, S., Brendler, V., Geipel, G. (2007a). Uranium(VI) complexation by humic acid under neutral pH conditions studied by laser-induced fluorescence spectroscopy. *Radiochim. Acta* **95**, 103-110.

Sachs, S., Křepelová, A., Schmeide, K., Koban, A., Günther, A., Mibus, J., Brendler, V., Geipel, G., Bernhard, G. (2007b). Joint Project: Migration of actinides in the system clay, humic substance, aquifer - Migration behavior of actinides (uranium, neptunium) in clays: Characterization and quantification of the influence of humic substances. *Wissenschaftlich-Technische Berichte, FZD-460*. Forschungszentrum Dresden-Rossendorf, Dresden.

Sachs, S., Bernhard, G. (2008). Sorption of U(VI) onto an artificial humic substance-kaolinite-associate. *Chemosphere* **72**, 1441-1447.

Sachs, S., Schmeide, K., Křepelová, A. (2009). Humic substances and their influence on the mobility of actinides in clay formations. *Nuclear safety research: Biennial scientific report 2007-2008, Volume 3, Wissenschaftlich-Technische Berichte, FZD-509*. Forschungszentrum Dresden-Rossendorf, Dresden.

Sachs, S., Reich, T., Bernhard, G. (2010). Study of the role of sulfur functionalities in humic acids for uranium(VI) complexation. *Radiochim. Acta* **98**, 467-477.

Sachs, S., Bernhard, G. (2011). Humic acid model substances with pronounced redox functionality for the study of environmentally relevant interaction processes of metal ions in the presence of humic acid. *Geoderma* **162**, 132-140.

Sakuragi, T., Sawa, S., Sato, S., Kozaki, T., Mitsugashira, T., Hara, M., Suzuki, Y. (2004). Complexation of americium(III) with humic acid by cation exchange and solvent extraction. *J. Radioanal. Nucl. Chem.* **261**, 309-314.

Samper, J., Ma, H., Cormenzana, J. L., Lu, C., Montenegro, L., Cuñado, M. A. (2010). Testing K_d models of Cs^+ in the near field of a HLW repository in granite with a reactive transport model. *Phys. Chem. Earth.* **35**, 278-283.

Sato, H., Yui, M. (1997). Diffusion of Ni in compacted sodium bentonite. *J. Nucl. Sci. Technol.* **34**, 334-336.

Savoye, S., Goutelard, F., Beaucaire, C., Charles, Y., Fayette, A., Herbette, M., Larabi, Y., Coelho, D. (2011). Effect of temperature on the containment properties of argillaceous rocks: The case study of Callovo-Oxfordian claystones. *J. Contam. Hydrol.* **125**, 102-112.

Schäfer, T., Buckau, G., Artinger, R., Kim, J. I., Geyer, S., Wolf, M., Bleam, W. F., Wirick, S., Jacobsen, C. (2005). Origin and mobility of fulvic acids in the Gorleben aquifer system: implications from isotopic data and carbon/sulfur XANES. *Org. Geochem.* **36**, 567-582.

Schimmack, W., Gerstmann, U., Schultz, W., Geipel, G. (2007). Long-term corrosion and leaching of depleted uranium (DU) in soil. *Radiat. Environ. Biophys.* **46**, 221-227.

Schindler, P. W., Gamsjäger, H. (1972). Acid-base reactions of TiO_2 (Anatase) - water interface and point of zero charge of TiO_2 suspensions. *Kolloid Z. Z. Polym.* **250**, 759-763.

Schmeide, K., Pompe, S., Bubner, M., Heise, K. H., Bernhard, G., Nitsche, H. (2000). Uranium(VI) sorption onto phyllite and selected minerals in the presence of humic acid. *Radiochim. Acta* **88**, 723-728.

Schmeide, K., Reich, T., Sachs, S., Brendler, V., Heise, K. H., Bernhard, G. (2005). Neptunium(IV) complexation by humic substances studied by X-ray absorption fine structure spectroscopy. *Radiochim. Acta* **93**, 187-196.

Schmeide, K., Reich, T., Sachs, S., Bernhard, G. (2006). Plutonium(III) complexation by humic substances studied by X-ray absorption fine structure spectroscopy. *Inorg. Chim. Acta* **359**, 237-242.

Schmeide, K., Bernhard, G. (2009). Redox stability of neptunium(V) and neptunium(IV) in the presence of humic substances of varying functionality. *Radiochim. Acta* **97**, 603-611.

Schmeide, K., Bernhard, G. (2010). Sorption of Np(V) and Np(IV) onto kaolinite: Effects of pH, ionic strength, carbonate and humic acid. *Appl. Geochem.* **25**, 1238-1247.

Schmeide, K., Joseph, C. (2012). Influence of organic ligands on U(VI) sorption onto Opalinus Clay between 10 and 50 °C. *Annual Report 2011, HZDR-013*. Helmholtz-Zentrum Dresden-Rossendorf, Dresden.

Schmeide, K., Sachs, S., Bernhard, G. (2012). Np(V) reduction by humic acid: Contribution of reduced sulfur functionalities to the redox behavior of humic acid. *Sci. Total Environ.* **419**, 116-123.

Schnitzer, M., Khan, S. U. (1972). *Humic substances in the environment*. Marcel Dekker, Inc., New York.

Schott, J., Acker, M., Barkleit, A., Brendler, V., Taut, S., Bernhard, G. (2012). The influence of temperature and small organic ligands on the sorption of Eu(III) on Opalinus Clay. *Radiochim. Acta* **100**, 315-324.

Schulten, H. R., Schnitzer, M. (1993). A state of the art structural concept for humic substances. *Naturwissenschaften* **80**, 29-30.

Schulten, H. R., Leinweber, P. (1996). Characterization of humic and soil particles by analytical pyrolysis and computer modeling. *J. Anal. Appl. Pyrol.* **38**, 1-53.

Seibert, A., Mansel, A., Marquardt, C. M., Keller, H., Kratz, J. V., Trautmann, N. (2001). Complexation behaviour of neptunium with humic acid. *Radiochim. Acta* **89**, 505-510.

Seida, Y., Terashima, M., Tachi, Y., Iijima, K., Nakazawa, T., Yamada, M., Yui, M. (2010). Sorption and diffusion of Eu in sedimentary rock in the presence of humic substance. *Radiochim. Acta* **98**, 703-709.

Sémon, L., Boehme, C., Billard, I., Hennig, C., Lützenkirchen, K., Reich, T., Roßberg, A., Rossini, I., Wipff, G. (2001). Do perchlorate and triflate anions bind to the uranyl cation in an acidic aqueous medium? A combined EXAFS and quantum mechanical investigation. *ChemPhysChem* **2**, 591-598.

Silva, R. J., Nitsche, H. (1995). Actinide environmental chemistry. *Radiochim. Acta* **70-1**, 377-396.

Skoog, D. A., Leary, J. J. (1996). *Instrumentelle Analytik: Grundlagen - Geräte - Anwendungen*. Springer-Verlag, Berlin.

Stern, O. (1924). The theory of the electrolytic double shift. *Z. Elktrochem. Angew. P.* **30**, 508-516.

Steudtner, R., Müller, K., Schmeide, K., Sachs, S., Bernhard, G. (2011a). Binary and ternary uranium(VI) humate complexes studied by attenuated total reflection Fourier-transform infrared spectroscopy. *Dalton Trans.* **40**, 11920-11925.

Steudtner, R., Sachs, S., Schmeide, K., Brendler, V., Bernhard, G. (2011b). Ternary uranium(VI) carbonato humate complex studied by cryo-TRLFS. *Radiochim. Acta* **99**, 687-692.

Stevenson, F. J. (1982). *Humus chemistry: Genesis, composition, reactions*. Wiley-Interscience, New York.

Stevenson, F. J. (1985). Geochemistry of soil humic substances. In: Aiken, G. R., McKnight, D. M., Wershaw, R. L., and MacCarthy, P. (Eds.), *Humic substances in soil, sediment, and water*. John Wiley & Sons, New York.

Stumm, W., Huang, C. P., Jenkins, S. R. (1970). Specific chemical interaction affecting stability of dispersed systems. *Croat. Chem. Acta* **42**, 223-245.

Stumm, W., Hohl, H., Dalang, F. (1976). Interaction of metal ions with hydrous oxide surfaces. *Croat. Chem. Acta* **48**, 491-504.

Stumm, W., Kummert, R., Sigg, L. (1980). A ligand exchange model for the adsorption of inorganic and organic ligands at hydrous oxide interfaces. *Croat. Chem. Acta* **53**, 291-312.

Stumm, W. (1992). *Chemistry of the solid-water interface: Processes at the mineral-water and particle-water interface in natural systems*. John Wiley and Sons, New York.

Suffet, I. H., MacCarthy, P. (Eds.) (1989). *Aquatic humic substances - Influence on fate and treatment of pollutants*. American Chemical Society, Washington, DC.

Sumner, M. E., Miller, W. P. (1996). Cation exchange capacity and exchange coefficients. In: Sparks, D. L., Page, A. L., Helmke, P. A., Loeppert, R. H., Soltanpour, P. N., Tabatabai, M. A., Johnston, C. T., and Sumner, M. E. (Eds.), *Methods of Soil Analysis. Part 3: Chemical Methods*. Soil Science Society of America Inc., USA.

Sutton, R., Sposito, G. (2006). Molecular simulation of humic substance-Ca-montmorillonite complexes. *Geochim. Cosmochim. Acta* **70**, 3566-3581.

Suzuki, S., Sato, H., Ishidera, T., Fujii, N. (2004). Study on anisotropy of effective diffusion coefficient and activation energy for deuterated water in compacted sodium bentonite. *J. Contam. Hydrol.* **68**, 23-37.

Szabó, G., Guczi, J., Reiller, P., Miyajima, T., Bulman, R. A. (2010). Effect of ionic strength on complexation of Pu(IV) with humic acid. *Radiochim. Acta* **98**, 13-18.

Szabó, Z., Moll, H., Grenthe, I. (2000). Structure and dynamics in the complex ion $(UO_2)_2(CO_3)(OH)_3^-$. *J. Chem. Soc., Dalton Trans.* **18**, 3158-3161.

Tachi, Y., Suyama, T., Ochs, M., Ganter, C. (2011). Development of JAEA sorption database (JAEA-SDB): Update of data evaluation functions and sorption/QA data. *JAEA-Data/Code 2010-031*. Japan Atomic Energy Agency, Shirakata Shirane. Website: http://migrationdb.jaea.go.jp/english.html.

Teo, B. K. (1986). *EXAFS: Basic principles and data analysis*. Springer, Berlin.

Tertre, E., Berger, G., Castet, S., Loubet, M., Giffaut, E. (2005). Experimental sorption of Ni^{2+}, Cs^+ and Ln^{3+} onto a montmorillonite up to 150°C. *Geochim. Cosmochim. Acta* **69**, 4937-4948.

Tertre, E., Hofmann, A., Berger, G. (2008). Rare earth element sorption by basaltic rock: Experimental data and modeling results using the "Generalised Composite approach". *Geochim. Cosmochim. Acta* **72**, 1043-1056.

Teterin, Y. A., Nefedov, V. I., Nikitin, A. S., Teterin, A. Y., Ivanov, K. E., Maslakov, K. I., Utkin, I. O., Bubner, M., Reich, T., Pompe, S., Heise, K. H., Nitsche, H. (2001). Interaction of UO_2^{2+} and Fe^{3+} ions with natural humic acid. *Russ. J. Inorg. Chem.* **46**, 886-891.

Thompson, A., Lindau, I., Attwood, D., Liu, Y., Gullikson, E., Pianetta, P., Howells, M., Robinson, A., Kim, K.-J., Scofield, J., Kirz, J., Underwood, J., Kortright, J., Williams, G., Winick, H. (2009). *Center for X-ray Optics and Advanced Light Source: X-ray data booklet*. Lawrence Berkeley National Laboratory, University of California, Berkeley, California.

Thompson, H. A., Parks, G. A., Jr. Brown, G. E. (1998). Structure and composition of uranium(VI) complexes at the kaolinite-water interface. In: Jenne, E. A. (Ed.), *Adsorption of metals by geomedia. Variables, mechanisms and model applications*. Academic Press, San Diego.

Tipping, E. (1998). Humic ion-binding model VI: An improved description of the interactions of protons and metal ions with humic substances. *Aquat. Geochem.* **4**, 3-48.

Tipping, E., Rey-Castro, C., Bryan, S. E., Hamilton-Taylor, J. (2002). Al(III) and Fe(III) binding by humic substances in freshwaters, and implications for trace metal speciation. *Geochim. Cosmochim. Acta* **66**, 3211-3224.

Tochiyama, O., Niibori, Y., Tanaka, K., Kubota, T., Yoshino, H., Kirishima, A., Setiawan, B. (2004). Modeling of the complex formation of metal ions with humic acids. *Radiochim. Acta* **92**, 559-565.

Um, W., Serne, R. J., Krupka, K. M. (2007). Surface complexation modeling of U(VI) sorption to hanford sediment with varying geochemical conditions. *Environ. Sci. Technol.* **41**, 3587-3592.

Van Loon, L. R., Soler, J. M., Bradbury, M. H. (2003). Diffusion of HTO, $^{36}Cl^-$ and $^{125}I^-$ in Opalinus Clay samples from Mont Terri - Effect of confining pressure. *J. Contam. Hydrol.* **61**, 73-83.

Van Loon, L. R., Soler, J. M. (2004). Diffusion of HTO, $^{36}Cl^-$, $^{125}I^-$, and $^{22}Na^+$ in Opalinus Clay: Effect of Confining Pressure, Sample Orientation, Sample Depth and Temperature. *PSI-Bericht 04-03*. Paul Scherrer Institut, Villigen PSI.

Van Loon, L. R., Eikenberg, J. (2005). A high-resolution abrasive method for determining diffusion profiles of sorbing radionuclides in dense argillaceous rocks. *Appl. Radiat. Isot.* **63**, 11-21.

Van Loon, L. R., Müller, W., Iijima, K. (2005). Activation energies of the self-diffusion of HTO, $^{22}Na^+$ and $^{36}Cl^-$ in a highly compacted argillaceous rock (Opalinus Clay). *Appl. Geochem.* **20**, 961-972.

Vane, L. M., Zang, G. M. (1997). Effect of aqueous phase properties on clay particle zeta potential and electro-osmotic permeability: Implications for electro-kinetic soil remediation processes. *J. Hazard. Mater.* **55**, 1-22.

Velde, B., Meunier, A. (2008). *The origin of clay minerals in soils and weathered rocks*. Springer-Verlag, Berlin Heidelberg.

Villani, S. (Ed.) (1979). *Uranium enrichment*. Springer-Verlag, Berlin.

Vodrážka, Z. (1979). *Physikalische Chemie für Biologen, Mediziner, Pharmazeuten*. VEB Verlag Volk und Gesundheit, Berlin.

Voegelin, A., Kretzschmar, R. (2002). Stability and mobility of colloids in Opalinus Clay. *Technical Report NTB 02-14*. Nagra, Wettingen.

Volkmer, M. (2007). Kernenergie - Basiswissen. Informationskreis KernEnergie, Berlin.

von Wandruszka, R. (2000). Humic acids: Their detergent qualities and potential uses in pollution remediation. *Geochem. Trans.* **1**, 10-15.

Wang, Z. M., Zachara, J. M., Yantasee, W., Gassman, P. L., Liu, C. X., Joly, A. G. (2004). Cryogenic laser induced fluorescence characterization of U(VI) in hanford vadose zone pore waters. *Environ. Sci. Technol.* **38**, 5591-5597.

Wersin, P., Stroes-Gascoyne, S., Pearson, F. J., Tournassat, C., Leupin, O. X., Schwyn, B. (2010). Part G - Key interpretations and conclusions. Implications for repository safety. *Biogeochemical Processes in a Clay Formation In-situ Experiment*. Nagra, Wettingen.

Wieland, E., Stumm, W. (1992). Dissolution kinetics of kaolinite in acidic aqueous solutions at 25°C. *Geochim. Cosmochim. Acta* **56**, 3339-3355.

WNA (2012). Uranium, from mine to mill. In: *WNA Pocket Guide*. World Nuclear Association (WNA), London.

Wolery, T. J. (1992). *EQ3/6, A software package for the geochemical modeling of aqueous systems, UCRL-MA-110662 Part I*. Lawrence Livermore National Laboratory, Livermore.

Wolf, M., Breitkopf, O., Puk, R. (1989). Solubility of calcite in different electrolytes at temperatures between 10° and 60°C and at CO_2 partial pressures of about 1 kPa. *Chem. Geol.* **76**, 291-301.

Wu, T., Amayri, S., Drebert, J., Van Loon, L. R., Reich, T. (2009). Neptunium(V) sorption and diffusion in Opalinus Clay. *Environ. Sci. Technol.* **43**, 6567-6571.

Zeh, P., Czerwinski, K. R., Kim, J. I. (1997). Speciation of uranium in Gorleben groundwaters. *Radiochim. Acta* **76**, 37-44.

Zheng, Z. P., Tokunaga, T. K., Wan, J. M. (2003). Influence of calcium carbonate on U(VI) sorption to soils. *Environ. Sci. Technol.* **37**, 5603-5608.

Zuo, R., Teng, Y., Wang, J., Hu, Q. (2010). Factors influencing plutonium sorption in shale media. *Radiochim. Acta* **98**, 27-34.

LIST OF FIGURES

Fig. 1: Radiotoxicity evolution in time and its components ((OECD/NEA, 2006); Fig. 1.2). 2

Fig. 2: Multiple barrier system of a nuclear waste repository (based on BfS, 2012). 3

Fig. 3: Clay rock formations in Germany potentially suitable for further investigations as nuclear waste disposal site ((Hoth et al., 2007); Fig. 4.30). 5

Fig. 4: Tetrahedral sheet with hexagonal cavities (a) and trioctahedral sheet (b). Only the oxygen framework is shown, central cations were omitted (based on Jasmund and Lagaly, 1993). 7

Fig. 5: Layer structures of phyllosilicates: 1:1 layer (a) and 2:1 layer (b) (based on Jasmund and Lagaly, 1993). 8

Fig. 6: Zeta potential of kaolinite and Opalinus Clay in 0.1 mol/L $NaClO_4$ (solid-to-liquid ratio (S/L) = 0.1 g/L) as a function of pH. 13

Fig. 7: Shells of *Leioceras opalinum* – index fossil of OPA (picture size: 10 cm; Nagra, 2002). 14

Fig. 8: Particle size distribution of OPA batch BHE-24/1 17

Fig. 9: IR spectra of some mineral components of OPA compared to the IR spectrum of OPA batch BHE-24/1. The spectra are shifted along the y-axis. 18

Fig. 10: IR spectra of OPA batches applied for sorption experiments. 19

Fig. 11: X-ray diffractograms of the OPA batches BHE-24/1 and BLT-11/01. The diffractograms are shifted along the y-axis. 19

Fig. 12: X-ray diffractogram of OPA (BHE-24/1) untreated and leached out with pore water. The diffractograms are shifted along the y-axis. 22

Fig. 13: X-ray diffractograms of untreated OPA (batch BHE-24/1) and OPA leached out with 0.1 mol/L $NaClO_4$ at pH 4, 7, and 10. The diffractograms are shifted along the y-axis for clarity 23

Fig. 14: Concentrations of Ca, Mg, Sr, Si, Al, Fe, and SO_4^{2-} in OPA suspensions contacted with 0.1 mol/L $NaClO_4$ (S/L = 4 g/L) as a function of pH. 25

Fig. 15: Chemical composition of natural uranium (a), low-enriched uranium (b), and spent nuclear fuel (c) (values based on Volkmer, 2007). 28

Fig. 16: Speciation of U(VI) as a function of pH in 0.1 mol/L NaCl ([U(VI)] = 1×10^{-6} mol/L; pCO$_2$ = $10^{-3.5}$ atm). Only species > 5 % are shown. 29

Fig. 17: Hypothetical structure of humic substances adopted from Schulten and Schnitzer (1993); Fig. 1. 31

Fig. 18: Humic acid pseudomicelle (adopted from von Wandruszka (2000); Fig. 2) 33

Fig. 19: The ternary system metal ion / humic substance / clay mineral: (red) metal ions can sorb onto the clay surface; (yellow) sorbed metal ions can serve as bridging compound between clay and humic material; (green) the humic substance can sorb directly on the clay surface; (blue) humic substances can complex metal ions via a variety of functional groups (adopted from Sachs et al., 2009; Fig. 3; based on Stevenson, 1985). 41

Fig. 20: Speciation of U(VI) as a function of pH in 0.1 mol/L $NaClO_4$ (a, b), 0.39 mol/L NaCl (c, d), and OPA pore water (e, f) both in the absence (a, c, e) and presence (b, d, f) of HA ([U(VI)] = 1×10^{-6} mol/L; [HA] = 50 mg/L). Only species > 5 % are shown. 43

Fig. 21: Speciation of U(VI) as a function of pH in pore water in the (a) absence and (b) presence of HA under consideration of the ions leached out from OPA ([U(VI)] = 1×10^{-6} mol/L; [HA] = 50 mg/L). Only species > 5 % are shown. 47

Fig. 22: Speciation of uranium as a function of E_h in pore water in the absence (a) and presence (b) of HA under consideration of the ions leached out from OPA ([U(VI)] = 1×10^{-6} mol/L; [HA] = 50 mg/L, pH 7.6). Only species > 5 % are shown. 48

Fig. 23: U(VI) sorbed onto OPA as a function of S/L ratio ([U(VI)] = 1×10^{-6} mol/L; pore water). 48

Fig. 24: U(VI) and HA sorbed onto OPA as a function of time ([U(VI)] = 1×10^{-6} mol/L; [HA] = 10 mg/L; S/L = 60 g/L; pore water). 49

Fig. 25: Freundlich isotherm of the HA sorption onto OPA with varying HA concentration ([HA] = 10 – 320 mg/L; S/L = 60 g/L; pore water). 50

Fig. 26: Freundlich isotherm of the U(VI) sorption onto OPA with varying U(VI) concentration ([U(VI)] = 1×10^{-8} – 1×10^{-4} mol/L; S/L = 60 g/L; pore water). 50

Fig. 27: K_d values of the U(VI) sorption onto OPA as a function of S/L ratio ([U(VI)] = 1×10^{-6} mol/L; S/L = 4 – 300 g/L; pore water). 52

Fig. 28: Uranium L_{III}-edge k^3-weighted EXAFS spectra and their corresponding Fourier transforms of samples U9-40 and U9-41 for the U(VI) sorption onto OPA in pore water in the presence (U9-40) and absence (U9-41) of HA. The spectra are shifted along the y-axis for clarity. 59

Fig. 29: Speciation of U(VI) as a function of pH in 0.1 mol/L $NaClO_4$ in the (a) absence and (b) presence of HA under consideration of the ions leached out from OPA ([U(VI)] = 1×10^{-6} mol/L; [HA] = 50 mg/L; $pCO_2 = 10^{-3.5}$ atm). Only species > 5 % are shown. 60

Fig. 30: Speciation of HA as a function of pH in 0.1 mol/L $NaClO_4$ in the presence of U(VI) under consideration of the ions leached out from OPA ([U(VI)] = 1×10^{-6} mol/L; [HA] = 50 mg/L; $pCO_2 = 10^{-3.5}$ atm). 61

Fig. 31: U(VI) sorption onto OPA in the absence and presence of HA as a function of pH ([U(VI)] = 1×10^{-6} mol/L; [HA] = 0 or 50 mg/L; S/L = 4 g/L; $I = I_t$; $pCO_2 = 10^{-3.5}$ atm). Error bars: 2σ. 62

Fig. 32: HA sorption onto OPA in the presence of U(VI) as a function of pH ([HA] = 50 mg/L; [U(VI)] = 1×10^{-6} mol/L; S/L = 4 g/L; $I = I_t$; $pCO_2 = 10^{-3.5}$ atm). Error bars: 2σ. 64

Fig. 33: Experimental set-up for the diffusion experiment at 25 °C (based on Van Loon et al. (2003)). 71

Fig. 34: Experimental set-up for the diffusion experiment at 60 °C (based on Van Loon et al. (2003)). 72

Fig. 35: Evolution of flux ($J(L,t)$) and cumulated diffused activity ($A(L,t)$) as a function of time in the HTO through-diffusion experiments at 25 °C (cells 1 and 2, a + b) and 60 °C (cells 3 and 4, c + d). 74

Fig. 36: Particle size distribution of ^{14}C-HA colloids in the presence of ^{233}U(VI) in the source reservoir solutions at 25 °C (cell 2; a + b) and 60 °C (cell 4; c + d) at the beginning (a + c) and the end (b + d) of the diffusion experiments. Percentage distribution refers to the respective concentration of ^{233}U(VI) and ^{14}C-HA in the unfiltered solution at the beginning and the end of the diffusion experiments. ..77

Fig. 37: Luminescence spectra of U(VI) ($[U(VI)]_0 = 1\times10^{-4}$ mol/L) in pore water at 60 °C as a function of equilibration time. For clarity, the spectra were normalized to a maximum intensity of 1 and shifted along the y-axis. As reference, the luminescence spectrum of $Ca_2UO_2(CO_3)_3$(aq) at 65 °C is shown. The spectra were smoothed by Fast Fourier Transform filtering. 79

Fig. 38: (a) SEM image of the separated particles sputtered with carbon, (b, c) EDX spectra measured at the spots indicated by the boxes in (a) ($[U(VI)]_0 = 1\times10^{-4}$ mol/L; pore water). 80

Fig. 39: Concentration profiles of ^{233}U(VI) in the absence (filled symbols) and presence (open symbols) of ^{14}C-HA (a) and of ^{14}C-HA in the presence of ^{233}U(VI) (b) in OPA at 25 °C. 81

Fig. 40: Concentration profiles of ^{233}U(VI) in the absence (filled symbols) and presence (open symbols) of ^{14}C-HA (a) and of ^{14}C-HA in the presence of ^{233}U(VI) (b) in OPA at 60 °C. 84

Fig. 41: Modeled evolution of the ^{233}U(VI) concentration in the receiving reservoir as a function of time at 25 and 60 °C. 88

Fig. 42: LSC spectrum of ^{14}C-labeled HA (beta-particle emitter, [HA] = 50 mg/L) and ^{233}U (alpha-particle emitter, $[U(VI)] = 1\times10^{-6}$ mol/L) in OPA pore water – simultaneous measurement using TriCarb 3100 TR, Perkin Elmer. 97

Fig. 43: Luminescence of U(VI) (1×10^{-4} mol/L) in 0.1 mol/L $NaClO_4$ at pH 2.4; (a) single spectrum at t = 0 ns; (b) time-resolved spectra. 102

Fig. 44: Schematic illustration of the experimental set-up for the fluorescence spectroscopic measurements. 103

Fig. 45: X-ray absorption spectrum of U(VI) sorbed onto OPA ($[U(VI)]_0 = 1\times10^{-4}$ mol/L) in 0.1 mol/L $NaClO_4$ at pH 6.8 in the presence of 10 mg/L humic acid ($pCO_2 = 10^{-3.5}$ atm). The uranium absorption edge, the XANES and EXAFS regions, the edge-step $\Delta\mu_0(E_0)$, and the smooth background function $\mu_0(E)$ are denoted. ..109

Fig. 46: Ball-and-stick representation of the fit model applied in the present study with bidentate coordination of UO_2^{2+} to an aluminum octahedra and bidentate binding of carbonate to UO_2^{2+}. Hydrogen atoms are omitted for clarity. 111

LIST OF TABLES

Tab. 1: Selection of radionuclides with long half-lives contained in high-level nuclear waste (Jörg et al., 2010; Magill et al., 2006). 2

Tab. 2: Overview of phyllosilicates with their corresponding composition (Velde and Meunier, 2008) applied in this work and present in Opalinus Clay. 9

Tab. 3: Composition of kaolinite batch KGa-1b. 12

Tab. 4: Mineralogy of OPA shaly and sandy facies (average of nine and four samples) (Pearson et al., 2003). 15

Tab. 5: Main characteristics of OPA batches BHE-24/1 and BLT-11/01. 16

Tab. 6: Trace elements in OPA batches BHE-24/1 and BLT-11/01 (in ppm). 17

Tab. 7: Assignments of the IR bands of OPA batch BHE-24/1 18

Tab. 8: Composition of pore water: modeled by Pearson (1998) (pore water$_{theor}$), prepared for the experiments (pore water$_{exp}$), and ions leached out from OPA during 7 days contact time with pore water (pore water$_{exp7d}$) (Δleached$_{7d}$ = difference between pore water$_{exp}$ and pore water$_{exp7d}$). 21

Tab. 9: Results of Mössbauer spectroscopy and N_2-BET measurements (error: 2σ). ...24

Tab. 10: U(VI) sorbed onto kaolinite in dependence on background electrolyte in the absence and presence of HA (S/L = 4 g/L, pH 7.6) in comparison to literature data. 45

Tab. 11: HA sorbed onto kaolinite in dependence on background electrolyte in the absence and presence of U(VI) (S/L = 4 g/L, pH 7.6) in comparison to literature data. 46

Tab. 12: U(VI) and HA sorption onto OPA under ambient atmosphere ($p\mathrm{CO}_2$ = $10^{-3.5}$ atm) or inert gas conditions (N_2-box) (S/L = 60 g/L; pore water). 55

Tab. 13: Luminescence properties of the measured U(VI) species (λ_{ex} = 410 nm). 56

Tab. 14: OPA samples prepared for EXAFS measurements with their sorbed amounts of U(VI) and HA, ([U(VI)] = 1×10^{-4} mol/L; [HA] = 10 mg/L; S/L = 20 g/L; pore water; $p\mathrm{CO}_2$ = $10^{-3.5}$ atm) and results of the first fit of the EXAFS spectra. The multiple scattering path $\mathrm{MS}_{U=O}$ was taken into consideration as explained in the text (cf. section 7.4.8). Asymptotic standard deviations are given in parentheses. 57

Tab. 15: Ions leached out from OPA during 13 days contact time with pore water (pore water$_{exp13d}$); S/L = 20 g/L. 58

Tab. 16: Diffusion parameters of HTO in OPA determined by through-diffusion experiments at 25 and 60 °C. 75

Tab. 17: Characterization of the source reservoir solutions at 25 and 60 °C at the end of the ^{233}U(VI) and ^{14}C-HA diffusion experiments as well as U(VI) speciation in the reservoirs calculated for these conditions. 76

Tab. 18: Values for the ^{233}U(VI) and ^{14}C-HA diffusion parameters obtained at 25 °C. 82

Tab. 19: Values for the ^{233}U(VI) and ^{14}C-HA diffusion parameters obtained at 60 °C. 85

Tab. 20: Composition for 1 L of synthetic OPA pore water (Pearson, 1998). 93

Tab. 21: Characteristics of the HA applied in this study (Pompe et al., 1998; Sachs et al., 2004) and from natural HA (Stevenson, 1985; Suffet and MacCarthy, 1989). ...95

Tab. 22: Experimental conditions applied for batch sorption experiments. 106
Tab. 23: Characteristics of the filters and the OPA samples. 114

Danksagung

Zum Gelingen dieser Arbeit haben einige Personen und Institutionen innerhalb und außerhalb von Rossendorf beigetragen.

Hiermit möchte ich mich bei Prof. Dr. Gert Bernhard für die Bereitstellung dieses hochinteressanten und politisch relevanten Themas bedanken und für die Möglichkeit am Institut für Ressourcenökologie im Helmholtz-Zentrum Dresden-Rossendorf zu promovieren.

Mein besonderer Dank gilt meiner Betreuerin Dr. Katja Schmeide sowie Dr. Susanne Sachs, die mir mit hilfreichen Diskussionen und Anregungen zur Seite standen und mit ihrer fortwährenden Unterstützung im Wesentlichen zum Abschluss dieser Arbeit beigetragen haben.

Während meiner Zeit am Institut war ich Mitglied verschiedener Abteilungen. Hiermit möchte ich mich bei Dr. Vinzenz Brendler, Dr. Gerhard Geipel sowie bei Dr. Harald Foerstendorf für die sehr gute Führung, den moralischen Beistand und die Unterstützung bezüglich der Speziationsberechnungen sowie der TRLFS-Messungen bedanken.

Für die Bereitstellung des Opalinustones in verschiedenen Chargen möchte ich mich bei der Bundesanstalt für Geowissenschaften und Rohstoffe sowie beim Karlsruhe Institut für Technologie – Institut für Nukleare Entsorgung (insbesondere Dr. Christian Marquardt) bedanken.

Die Diffusionsversuche stellten einen wichtigen Teil meiner Arbeit dar. Ohne meine hochkompetenten Ansprechpartner am Paul-Scherrer-Institut – Laboratory of Waste Management Dr. Luc R. Van Loon (Diffusion) und Dr. Andreas Jakob (COMSOL-Modellierung) wäre ein erfolgreicher Abschluss der Versuche nicht möglich gewesen. Dafür ein herzliches Dankeschön!

Für die EXAFS-Messungen in Grenoble und die Unterstützung bei der Auswertung der Spektren möchte ich mich bei Dr. Andreas Scheinost, Dr. André Rossberg, Dr. Dipanjan Banerjee, Prof. Dr. Tobias Reich und Dr. Christian Lucks bedanken.

Ein ganz besonderer Dank geht an Christa Müller, Jana Seibt, Stephan Weiß, Sylvia Heller, Sylvia Gürtler, Heidrun Neubert, Christine Fröhlich, Annette Rumpel, Bernd Hiller, Dirk Falkenberg, Angelika Schliephake, Christian Müller, Carlos Fajardo Uribe und Katharina Fritsch für die technische Unterstützung und stete Hilfsbereitschaft im Labor, insbesondere bei der Bewältigung von über 200 Proben pro Tag.

Für die Analyse meiner unzähligen Proben möchte ich mich recht herzlich bei Ursula Schaefer, Aline Ritter und Carola Eckardt bedanken.

Die Flüssigszintillation war eine primäre Analysemethode in meiner Arbeit, daher geht mein Dank an Cordula Nebelung und Dr. Astrid Barkleit für die technische Unterstützung.

Mein Dank geht auch an Dr. Robin Steudtner für die TRLFS-Messungen während meiner Nichtbeschäftigung am Institut.

Für die infrarotspektroskopischen Messungen möchte ich mich bei Karsten Heim bedanken.

Am Institut für Ionenstrahlphysik und Materialforschung konnte ich einige Methoden für die Charakterisierung meiner Proben nutzen, hiermit danke ich insbesondere Andrea Scholz für die XRD-Messungen, Dr. Helfried Reuther für die Mößbauerspektroskopie und Elfi Christalle für die SEM–EDX-Untersuchungen.

Für die Messung der Partikelgrößenverteilung möchte ich mich bei Prof. Dr.-Ing. Urs Peuker und Dr. Bernd Kubier von der Technischen Universität Bergakademie Freiberg, Institut für Mechanische Verfahrenstechnik und Aufbereitungstechnik bedanken.

Ich möchte auch allen nicht namentlich genannten Mitarbeiterinnen und Mitarbeitern des Instituts für Ressourcenökologie für die stets freundliche und familiäre Arbeitsatmosphäre danken. Ganz besonders danke ich den Doktoranden und Post-Docs des Instituts für Ressourcenökologie, die mir gerade bei wissenschaftlichen Rückschlägen mit einem offenen Ohr, aufbauenden Worten, guten Ratschlägen und einer Tasse Kaffee beistanden.

Zum Schluss möchte ich mich bei meiner Familie und meinen Freunden für ihren Rückhalt, ihre Stärke und ihre moralische Unterstützung herzlich bedanken. Dankeschön!

Die vorliegende Arbeit wurde vom Bundesministerium für Wirtschaft und Technologie unter der Projektnummer 02 E 10156 gefördert.

Versicherung

Hiermit versichere ich, dass ich die vorliegende Arbeit ohne unzulässige Hilfe Dritter und ohne Benutzung anderer als der angegebenen Hilfsmittel angefertigt habe; die aus fremden Quellen direkt oder indirekt übernommenen Gedanken sind als solche kenntlich gemacht. Die Arbeit wurde bisher weder im Inland noch im Ausland in gleicher oder ähnlicher Form einer anderen Prüfungsbehörde vorgelegt.

Die vorliegende Arbeit wurde am Helmholtz-Zentrum Dresden-Rossendorf, Institut für Ressourcenökologie in der Zeit von November 2006 bis April 2010 unter der wissenschaftlichen Betreuung von Herrn Prof. Dr. G. Bernhard und Frau Dr. K. Schmeide angefertigt.

Dresden, den 07.06.2013 Claudia Joseph